AFFDL-TR-65-15

HUMAN PILOT DYNAMICS IN COMPENSATORY SYSTEMS

THEORY, MODELS, AND EXPERIMENTS WITH CONTROLLED ELEMENT AND FORCING FUNCTION VARIATIONS

DUANE McRUER
DUNSTAN GRAHAM
SYSTEMS TECHNOLOGY, INC.

EZRA KRENDEL
WILLIAM REISENER, JR.
THE FRANKLIN INSTITUTE

ABSTRACT

The description of human pilot dynamic characteristics in mathematical terms compatible with flight control engineering practice is an essential prerequisite to the analytical treatment of manual vehicular control systems. The enormously adaptive nature of the human pilot makes such a description exceedingly difficult to obtain, although a quasi-linear model with parameters which vary with the system task variables has been successfully applied to many flight situations. The primary purposes of the experimental series reported are the validation of an existing quasi-linear pilot model, and the extension of this model in accuracy and detail.

To this end the influences of controlled-element dynamics and system forcing function characteristics on the pilot's dynamic characteristics are investigated using a five-stage process: (1) Pre-experiment analyses are conducted using the existing model to predict the outcome of experiments which are especially contrived to exercise the model to its limits; (2) controlled-element dynamics which are both crucial task variables (per the pre-experiment analyses) and idealizations of aircraft, booster, and space vehicle dynamics are delineated; (3) describing function and remnant measurements are taken in an extensive experimental program involving eight different controlled element forms and three forcing functions; (4) analytical abstractions of the data are made by curve-fitting procedures; (5) variations in the pilot's characteristics due to controlled element and/or forcing function changes are described in terms of the parameters of the curve fits. The outcome of this process is a substantially refined and extended adaptive and optimalizing model of human pilot dynamic characteristics. Models corresponding to three levels of precision and complexity are developed, the several aspects of pilots' adaptation to controlled element and forcing function changes are detailed, the selective variability nature of human pilot dynamics is presented, key remnant sources are discovered, and many other aspects of human pilot dynamics are treated with a combined experimental-analytical approach.

FOREWORD

The investigations reported here are an element in a U. S. Air Force research program to explore and exploit the concept that vehicle dynamic handling qualities are, to a large extent, dependent on the action of the pilot as a control element in the pilot–vehicle closed-loop system. In this concept, control analysis techniques and pilot dynamic response models are used in the study and optimization of man–vehicle systems. Such procedures promise to greatly enhance the processes involved in the design of manned vehicles.

This report documents an analytical and experimental investigation of human pilot dynamics accomplished under Contract AF 33(616)-7501, Project No. 8219, Task No. 821905, sponsored by the Flight Control Division of the Air Force Flight Dynamics Laboratory. The research was performed by Systems Technology, Inc., at both its Hawthorne, California, and Princeton, New Jersey, offices, and, under subcontract, by The Franklin Institute Laboratories for Research and Development, Philadelphia, Pennsylvania. The project principal investigators were D. T. McRuer and D. Graham, of STI, and E. S. Krendel, of FIL. The Flight Control Division project engineer through most of the program was R. J. Wasicko, succeeded in the last phases by R. H. Smith and P. E. Pietrzak.

As in most team efforts, many have contributed to the results reported here. The major contributors, who all participated in the analytical, planning, experimental execution, data interpretation, and reporting phases, are listed as authors. An indispensable portion of the program, the design and development of analysis apparatus, was accomplished meticulously by R. A. Peters and K. A. Ferrick of STI. Important contributions were also made by R. J. Wasicko in experimental planning, and by R. E. Magdaleno of STI in the interpretation of the results. Special mention and thanks are due: R. P. Harper, Jr., of Cornell Aeronautical Laboratory; G. E. Cooper, of Ames Research Center, NASA; and Lt. Comdrs. M. Johnson and T. Kastner, Capt. B. Baker, and Lts. G. Augustine, F. Hoerner, and J. Tibbs, of the Naval Air Test Center, Patuxent River, Maryland, for their interest and assistance as subjects. The authors would also like to thank their co-workers Diana Fackenthal, S. H. Greene, and M. M. Solow, of FIL, for their contributions to running the experiments, reducing the data and assisting in its analysis; and H. B. Grudberg, A. V. Phatak, and D. B. McElwain, of STI, for their assistance in pre-experiment predictions, and/or postexperiment data analysis and interpretation. Acknowledgment is due to Bolt Beranek and Newman, Inc., of Cambridge, Massachusetts, for the amplitude distribution data processing and some goodness of fit analyses. Finally, the report has been substantially improved by the incorporation of many suggestions due to the extremely careful review by R. O. Anderson, P. E. Pietrzak, and R. J. Woodcock of FDCC.

This technical report has been reviewed and is appro[illegible].

W. A. SLOAN, Jr.
Colonel, USAF
Chief, Flight Control Division
AF Flight Dynamics Laboratory

Contrails

CONTENTS

ILLUSTRATIONS

TABLES

SYMBOLS

a_T	Threshold value of the indifference threshold nonlinearity
A_i	Expected number of observations in a category for a Gaussian distribution
$c(t)$	Operator output time function, limb position
$C(j\omega)$	Fourier transform of operator output
$e(t)$	Error time function
$e_i(t)$	Component of error due to forcing function
$E(j\omega)$	Fourier transform of error
$F(t)$	Limb-applied force
F_s	Stick force/degree stick
G	Total open-loop describing function, Y_pY_c
G_{ie}	Closed-loop describing function, error/forcing function
G_{im}	Closed-loop describing function, system output/forcing function
H	Closed-loop describing function, pilot output/forcing function
$i(t)$	Forcing function time function
$I(j\omega)$	Fourier transform of forcing function
$j\omega$	Imaginary part of the complex variable, $s = \sigma \pm j\omega$
k	Exponent
K	Open-loop gain
K_c	Controlled element gain
K_f	Control sensitivity — inches signal deflection (on display)/stick force
K_p	Human pilot gain
K_s	Control sensitivity — inches (display)/stick motion
K_T	Gain of indifference threshold describing function
m	Integer

$m(t)$	System output time function
M	Integer
$M(j\omega)$	Fourier transform of system output
n	Integer
$\overline{n^2}$	Mean-squared remnant, $\frac{1}{2\pi}\int_0^\infty \Phi_{nn}\, d\omega$
$n_c(t)$	Operator remnant time function
N	Number of subjects
$N_c(j\omega)$	Fourier transform of operator remnant
O_i	Number of observed measurements in a category
$O(\ )$	Order of ( )
p	Significance level
p_c	Output amplitude distribution (first probability density function)
p_e	Error amplitude distribution (first probability density function)
$R_{xx}(\tau)$	Autocorrelation of a general time signal x(t)
s	Complex variable, $s = \sigma + j\omega$; Laplace transform variable
t	Time
T	Time constant
T_I	General lag time constant of human pilot describing function
T_K, T_K'	Lead and lag time constants in precision model of human pilot describing function
T_{lag_i}, T_{lead_i}	General lag and lead time constants
T_L	General lead time constant of human pilot describing function
T_N	First-order lag time constant approximation of the neuromuscular system
T_{N_1}	First-order lag time constant of the neuromuscular system
T_R	Run length
u	Standard score
v	Ratio of standard deviations

$x(t)$	A general time signal
$\overline{x^2}$	Mean-squared value of $x(t)$; $\overline{x^2} = \frac{1}{2\pi}\int_0^\infty \Phi_{xx}\, d\omega = \frac{1}{2}\sum_{m=1}^{M} \varphi_x^2(\omega_m) + \frac{1}{2\pi}\int_0^\infty \varphi_{xx}\, d\omega$
Y	Transfer function
$Y_c(j\omega)$	Controlled element (machine and display) transfer function
Y_p	Pilot describing function
α	Low frequency phase approximation parameter
β	$1/T_I\omega_c$ for $Y_c = K_c$; $1/T_L\omega_c$ for $Y_c = K_c/(j\omega)^2$
δ	Dirac delta function
ζ	Damping ratio
ζ_{CL}	Closed-loop damping ratio
ζ_N	Damping ratio of second-order component of the neuromuscular system
ρ	Correlation coefficient, $\lvert\Phi_{ic}\rvert/\sqrt{\Phi_{ii}\Phi_{cc}}$, $\lvert\Phi_{ie}\rvert/\sqrt{\Phi_{ii}\Phi_{ee}}$, $\lvert\Phi_{im}\rvert/\sqrt{\Phi_{ii}\Phi_{mm}}$
ρ_a	Relative remnant at pilot's output, $\sqrt{1 - \overline{n^2}/\overline{c^2}}$
σ	Standard deviation
σ_c	Standard deviation of pilot output, $c(t)$
σ_e	Standard deviation of error signal, $e(t)$
σ_i	rms value of the forcing function
σ_n	Standard deviation of $\lvert Y_p\rvert_{db}$ or $\measuredangle Y_p$ at ω_n
σ_T	rms value of input to the indifference threshold
σ_x	Standard deviation of the general time signal $x(t)$
τ	Pure time delay
$\Delta\tau$	Incremental time delay
τ_e	Effective time delay

τ_o	Effective time delay for zero forcing function bandwidth, $\tau_o = \pi/2\omega_{c_o}$
$\overline{\tau}_o$	Effective time delay for zero forcing function bandwidth when ω_c is constant, $\overline{\tau}_o = \pi/2\overline{\omega}_c$
φ	Phase angle
$\Delta\varphi_{low}$	Incremental low frequency phase angle
φ_M	Phase margin
$\varphi_c(\omega_n)$	Peak amplitude of a sinusoidal component of c(t) at frequency ω_n
$\varphi_i(\omega_n)$	Peak amplitude of a sinusoidal component of i(t) at frequency ω_n
$\varphi_x(\omega_m)$	Peak amplitude of a sinusoidal component of x(t) at frequency ω_m
φ_{nn}	Closed-loop remnant power spectral density, specifically a continuous density, at pilot's output
φ_{nn_c}	Open-loop remnant power spectral density, specifically a continuous density, at pilot's output
φ_{nn_e}	Open-loop remnant power spectral density, specifically a continuous density, at system error
φ_{xx}	Continuous component of power spectral density of x(t)
$\Phi_{cc}(\omega)$	Pilot's output power spectral density
$\Phi_{ee}(\omega)$	Error power spectral density
Φ_{ec}	Cross power spectral density between e and c
Φ_{ic}	Cross power spectral density between i and c
Φ_{ie}	Cross power spectral density between i and e
$\Phi_{ii}(\omega)$	Forcing function power spectral density
$\Phi_{mm}(\omega)$	System output power spectral density
Φ_{nn}	Closed-loop remnant spectral density, at pilot's output
Φ_{nn_c}	Open-loop remnant spectral density, at pilot's output, $\lvert 1 + Y_pY_c\rvert^2\Phi_{nn}$
Φ_{nn_e}	Open-loop remnant spectral density, at system error, $\lvert 1 + Y_pY_c\rvert^2\Phi_{nn}/\lvert Y_p\rvert^2$

Φ_{xx} Power spectral density of the general time signal x(t) composed of a random component and M sinusoids

$$\Phi_{xx}(\omega) = \varphi_{xx}(\omega) + \pi \sum_{m=1}^{M} \varphi_x^2(\omega_m)\delta(\omega-\omega_m)$$

χ Chi-squared distribution variable

$\overline{\chi}$ Mean value of χ

ψ_m Phase angle

ω Angular frequency, rad/sec

ω_{ba} Undamped natural frequency for a critically damped mode

ω_c System crossover frequency, i.e., frequency at which $|Y_pY_c| = 1$

$\Delta\omega$ Effective bandwidth of the spectral and cross-spectral analyzer (0.141 rad/sec for processing of lower forcing function frequencies; 0.628 rad/sec for high frequencies)

$\Delta\omega_c$ Incremental crossover frequency

$\overline{\omega}_c$ Average crossover frequency

ω_{c_o} System crossover frequency for zero forcing function bandwidth

ω_{CL} A closed-loop inverse time constant

ω_i Forcing function bandwidth

ω_{i_e} Effective bandwidth of forcing function, $\dfrac{\left[\int_o^\infty \Phi_{ii}d\omega\right]^2}{\int_o^\infty (\Phi_{ii})^2 d\omega}$

ω_m Undamped natural frequency

ω_n Frequency of forcing function sinusoidal component

ω_N Undamped natural frequency of second-order part of the neuromuscular system

ω_s Sampler frequency

ω_u Crossover frequency for neutral stability

$\doteq$ Approximately equal to

$\measuredangle$ Angle of

db Decibels; $10 \log_{10}(\ )$ if a power quantity, e.g., spectrum; $20 \log_{10}(\ )$ if an amplitude quantity, e.g., Y_p

$\lvert\ \rvert$	Magnitude
$\lvert\ \rvert_{db}$	Magnitude in db
$(\bar{\ })$	Mean value
*	Complex conjugate
"	Inches
$\mathcal{L}^{-1}$	Inverse Laplace transform

Contrails

CHAPTER I

INTRODUCTION

A. PROJECT BACKGROUND AND PURPOSE

The effective use of manned flight vehicles has always required a satisfactory match of vehicle characteristics (which include vehicle dynamics, control manipulator, display, etc.) with the human pilot's characteristics as a flight controller. An agreeable mating is not inherent in the design process, and the provision of proper vehicle handling qualities has often posed serious problems which the vehicle system designer must solve.

Classically, handling qualities concepts were based on engineering knowledge of vehicle characteristics, leavened by pilot opinion ratings. The opinion ratings were subjective expressions of the over-all suitability of the manual control system consisting of the pilot and the vehicle. A convenient way to express the handling qualities was as catalogs of vehicle dynamic parameters given as functions of pilot ratings. In spite of their reliance on the subtleties of subjective pilot ratings, such catalogs of handling qualities characteristics have been evolved in the past, and will continue to be expanded in the future. But, in a fundamental sense, these catalogs are only reports of specific test results — they fail to adequately explain the mutual interactions between the pilot and the vehicle, and they are difficult, if not impossible, to extrapolate to new situations and novel vehicle characteristics.

To achieve understanding and the capability to extrapolate requires a mathematical theory which can be used to explain old findings and to predict new ones. For handling qualities a theory of this kind has been in the process of construction, refinement, and successful application for some years. It is based on the methods of control engineering, and treats the pilot–vehicle system as a closed-loop (in general, a multi-loop) entity. The sine qua non of the theory is a model of pilot dynamic characteristics in a form suitable for application using relatively

conventional control engineering techniques. Further, the applications to which the theory can, with confidence, be employed is limited fundamentally by the level of pilot-model knowledge.

An adequate description of a pilot's dynamic response characteristics is not easily obtained because of the pilot's inherent adaptability and capacity for learning. Nevertheless, suitable experimental techniques have been devised and employed in the past to provide a limited amount of data. The quality of some of these data, however, has been open to question because of real or imagined deficiencies and uncertainties in the experimental task variables and in the necessary analysis equipment such as spectral and cross-spectral analyzers. In many cases the analyzer calibrations were insufficient to establish fully the accuracy of the data reduction methods (Ref. 51). Furthermore, most experimenters had not made certain measurements which, it turned out, were of crucial importance in the context of pilot-vehicle control system analysis. In spite of such imperfections, the collation of all the existing data, expanded by ultraconservative extrapolations based only on the limited high-reliability data, yielded a data base from which a serviceable, but incomplete, mathematical model was evolved (Refs. 28, 34 - 36). The extensive use of this pilot dynamics model in handling qualities and pilot-vehicle system analysis (Refs. 1 - 4, 8, 11, 12, 17, 27, 33 - 36, 43, 49, 55, 56, and 58) heightened the desire for, and increased the potential importance of, a more complete understanding of the mathematically describable aspects of human dynamics in vehicle control systems. The nature of desired improvements in the model was fundamentally one of degree rather than kind, i.e., increased scope and precision. Such an expanded view could not be evolved from existing data, which had been used in the construction of the model; instead, new data were required. Fortunately, by 1960 enough effort had been devoted to model building and application to give a more definitive notion of how the data were to be used. This, coupled with a very much better appreciation for the data reduction problem, made possible the planning and initial execution of a research program to meet the real needs.

Work on the project was initiated 1 July 1960, and almost two years were spent in the design, construction, and calibration of the data

reduction machines. The results of this effort have been reported elsewhere (Refs. 9, 10, 16, 44–46). Tests with human operators were initiated in May 1962. It is primarily to the task of recording and interpreting the data from some of these experiments that this report is addressed.

The primary results desired from the program from a vehicle control standpoint are, of course, better pilot models to use in handling qualities and manual control system analyses. Although not treated here, the applications of these models are expected to be far-reaching in the future. One reason for this anticipation are the extensive uses of the much less precise and more vague circa 1960 model. For example, in the references cited above this model has been used to:

1. Estimate human pilot and over-all pilot–vehicle system dynamic response, stability, and average performance.
2. Determine barely controllable vehicle dynamics and controllability boundaries.
3. Delineate those features of the vehicle dynamics which are most likely to affect the vehicle handling qualities.
4. Indicate the type of additional system equalization (to be achieved via the display, the manipulator, or by vehicle modifications) desirable to achieve better pilot control—as well as the effects on the pilot characteristics of such modifications.
5. Find the maximum forcing function bandwidth compatible with reasonable control action on the part of the pilot.

The new models developed here are intended to be used for the same sorts of things, but with far greater confidence and considerably better precision. The refined models are expected to be very useful in other ways also. For example, the characteristics of the human pilot's "actuator" and "sensor" dynamics, which were previously lumped into a mid-frequency approximation to lower and higher frequency effects, are distinctly reflected in the new data and models. This new knowledge should have significant impact both on the content and nature of the information displayed to the pilot and on the design of the manipulative devices with which the pilot imparts his desires to the vehicle.

B. OUTLINE OF THE REPORT

As noted above, the major purpose of the experimental program to be discussed here was to provide data for the extension and validation of the existing pilot model. Therefore a necessary preliminary is to consider the status of the mathematical model of the human operator at the time the experiments were planned. This is accomplished in the next chapter, which comprises a statement of the best that was known about human operator behavior in compensatory tracking in 1960 together with a discussion of those areas in which specific knowledge of operator behavior and its measurement was either totally lacking or substantially incomplete. Previous knowledge of human operator behavior in compensatory tracking is summarized in the first section of Chapter II entitled "The Analytical-Verbal Model," while the discussion of what it appeared necessary to find out follows in a treatment entitled "Objects of the Experiments."

A major part of the plan for the model validation aspects was to make analytical predictions of human operator performance in compensatory tracking and then to observe whether or not these predictions could be confirmed with experimental results. To this end the analytical-verbal model, reviewed in Chapter II, is bravely put to use in Chapter III. Although it was recognized that additional data were clearly required to substantiate some of the conjectures on which the model was founded, predictions critical to model validity were made which could later be compared with experimental results. These pre-experiment analyses also provide excellent concrete examples of the techniques involved in applying the human pilot models.

The really essential portion of this program is experimental, for the potential of all existing data as sources for model building and elaboration had been exhausted. Past experimental efforts have seldom been noteworthy examples of precision. In the new experimental series an extremely important desired feature was the provision of supplementary data reduction techniques and methods which would maximize flexibility and minimize the chances of experimental error. The apparatus was designed to make these objectives feasible, but changing feasibility to actuality requires exceptional experimental and data reduction procedures which almost amount to

trade secrets. Some of these are described in Chapter IV, together with a description of the experimental and analytical apparatus.

The experimental objectives of Chapter II plus the pre-experiment analyses of Chapter III lead directly to a desired experimental program plan. An outline of this program is presented in the first section of Chapter V.

Chapters V and VI present the experimental data — describing functions in Chapter V and remnants in Chapter VI. The data are aggregated in various ways to illustrate the gross and detailed effects of changes in the forcing function and controlled element task variables. Other aggregations are used to illustrate the effects of intra- and intersubject variations. The describing function chapter also includes statistical treatments of certain major conclusions. A special feature of the remnant discussion is a presentation of data which indicate the likely major remnant source, as well as data tending to indicate what the remnant is not.

Chapter VII is devoted to detailed analyses of the data and to the development of interpretations and rationalizations. In extending the existing analytical-verbal model it is concluded that, by and large, the hypotheses and extrapolations made from the limited data previously available were generally correct, and reasonably explained. Further, the updated models developed here, which subsume the old model and conform to the new data as well, answer many other questions concerning human behavior. These models are of three levels of precision. The first is relatively crude, and is intended for use in the region of crossover only. The second is sufficiently precise to be suitable for most handling qualities analyses, which primarily emphasize vehicle dynamics, including those involving statically unstable vehicles. Finally, the third is a precision model which is capable of representing the high and very low frequency actuator and sensor dynamic characteristics of the human pilot. Thus, the three models provide a range of complexity and utility which is analogous to the several degrees of model complexity used in ordinary automatic pilot design.

Finally, Chapter VIII summarizes the general conclusions and findings of the study.

C. A GUIDE FOR THE READER

Because this is a very long report, with many involutions, it is appropriate to give some words of advice for readers with various interests. For the casual reader, this introduction and the general summary of Chapter VIII give the gist of the effort. If just a bit more is desired, add Chapter II.

The applications-oriented engineer should start with Chapter II, Section A, for a review of the existing model, followed by Chapter V, Section A for the experimental plan outline and Section D for the grand-average describing function data, and then on to Chapter VIII for the general summary of results. He will then probably wish to absorb more details on the new models, as developed in Chapter VII, and may desire to examine the pre-experimental analyses of Chapter III as concrete examples of applications.

Those who are interested primarily in data can proceed directly to Chapters V and VI, although the experimentalist will also wish to cover Chapter IV.

The model builders can turn directly to Chapter VII, and, if they have models to test against the realities of data, to Chapters V and VI.

Finally, for the reader who is interested in the entire effort the way is directly through the report as laid out, although many of the details can be sloughed over lightly on a first reading. These diligent souls have both the authors' sympathy and blessings!

CHAPTER II

PILOT MODEL SUMMARY AND EXPERIMENTAL OBJECTIVES

A. THE ANALYTICAL-VERBAL MODEL

1. General Nature of the Model

The primary objective of most of the past experimental and analytical programs to develop mathematical descriptions for pilot response characteristics has been to achieve reasonable descriptions of the pilot as a component in engineering systems. Major efforts in model building have thus been placed on the evolution of models which can predict pilot dynamic response characteristics of engineering significance, but which are otherwise of minimum analytical complexity. Such models are conceptual descriptions of the human. They are intended to exhibit analogous cause-and-effect behavior rather than to be analogs in any structural sense. The models are valid to the extent that their behavioral properties resemble the performance of the actual human operator. They gain in scope and descriptive power if certain of their features can also be identified structurally, although they cannot be rejected because of any failure to satisfy this desirable quality.

As a control component the human exhibits a bewildering variety of nonlinear and time-varying behavior. Table I lists some of these. An appropriate type of engineering mathematical description for nonlinear control elements of this nature is some kind of quasi-linear system. This is an equivalent system in which the relationships between some, but not necessarily all, pertinent measures of system input and output signals have "linear-like" features for fixed input conditions in spite of the presence of nonlinear elements.

The quasi-linear system concept originally evolved from the observation that a great many nonlinear systems have responses to specific inputs which appear similar to responses of equivalent linear

TABLE I

HUMAN OPERATOR NONLINEARITIES AND NONSTATIONARITIES

1. Adaptation and Learning

   The adaptive human responds to changes in external environment by modifying characteristics so as to improve performance over that which would be achieved if the characteristics used in the original environment were maintained in the new one.

   The learning human, after operating experience in a given external environment, modifies characteristics to achieve better performance than previously exhibited in the given environment.

2. Set Changes

   "Set" characterizes the temporary operating points or baseline conditions of the human subsystems involved in the control tasks. Changes in these internal conditions facilitate a certain more-or-less specific type of activity or response in the adaptation and learning processes. Set changes include:

   Internal system topography changes, i.e., use of different feedback and feedforward paths

   Variation in steady-state muscle tension

   Variation in force ranges

   Variation in indifference threshold

3. Series Nonlinearities

   Sensory thresholds

   Maximum force and displacement limits

4. Fluctuations in Attention, Motivation, Etc.; General Drifting of Characteristics

systems to the same specific inputs.* For such combinations of specific inputs and nonlinear systems, the response of the nonlinear system can be divided into two parts — one component which corresponds to the response of the equivalent linear element driven by the particular input, and an additional quantity which represents the difference between the output of the actual nonlinear system and the equivalent linear element. This second component is called the "remnant" because it is left over from the portion of the system response representable by a linear element. Quasi-linear equivalents to the nonlinear system, for the specific input of interest, are characterized mathematically by a describing function (which is the equivalent linear element) and the remnant. An essential feature is that the quasi-linear system has a response to the input in question identical to that of the original nonlinear system, so the quasi-linear system is an exact cause–effect representation of the nonlinear system for the specific kinds of inputs and responses considered. When the inputs are changed, the quasi-linear model also changes. If the device were such that its quasi-linear system remained the same for all kinds of forcing functions, and if, further, the remnant were zero, then the system would have a constant-coefficient linear nature.

The most common quasi-linear system element in engineering use is the sinusoidal-input describing function, which is of such great value in stability studies of nonlinear servomechanisms. Here the action of the describing function on a sinusoidal input results in an output which is the fundamental of the output of the actual nonlinear system. The remnant, which must be added to the output fundamental to achieve equivalence with the nonlinear system, is made up of all the higher harmonics resulting from the passage of the sinusoid through the nonlinearity. Describing functions can also be defined for transient inputs, such as step functions, and for random inputs. In principle the systems can be time-varying as well as nonlinear. Random-input quasi-linear systems representing the human operator for certain conditions are the type pertinent to the operator data treated here.

*Many texts on nonlinear control theory treat aspects of quasi-linear systems. Chapters 3–6 of Ref. 21 are especially pertinent as background in the context of this report.

2. Review of Existing Quasi-Linear System Describing Function Plus Remnant Model for Single-Loop Tasks

In terms of idealizations, the simplest manual control system is that shown in the block diagram of Fig. 1. This is also the most commonly occurring system structure in practical manual control systems — either as a total system by itself or as a component part of a more complex multiloop system. To control engineers, this is a single-loop feedback system (except for feedbacks internal to the operator); to engineering psychologists, it is a compensatory system. The important single-loop features are the solitary stimulus (the error) and the random-appearing nature of the forcing function (the system input). If either of these is changed, the whole complexion of the task also changes. For instance, if the pilot is shown the system's input and output directly (a pursuit display) instead of their differences, he is often able to take advantage of the additional information and thereby to improve over-all system performance. Also, if the forcing function is not random-appearing, but perhaps periodic over relatively short time intervals, the pilot can often detect and anticipate the repetitive or deterministic nature of the input and adjust his response accordingly. Both of these higher order types of behavior amount to the presence in the system of further signal paths and a more complex than single-loop structure.

For the system shown in Fig. 1 there are three task variables that have a major effect on the pilot's dynamics — the forcing function characteristics, the controlled-element dynamics, and the manipulator. Many other factors are implicitly involved. These include operator-centered variables such as training, fatigue, and motivation, and external environmental characteristics such as ambient illumination and temperature. Ideally, all of these implicit (or "procedural") variables should be taken into account, and someday perhaps they will.* But for the present

*Chapter VII of Ref. 34 presents a preliminary discussion of the effects of a few implicit variables on pilot response measures. Reference 48 provides an excellent detailed example of pilot describing function changes accompanying changes in a typical environmental variable — in this case, the pilot's effective "g" field.

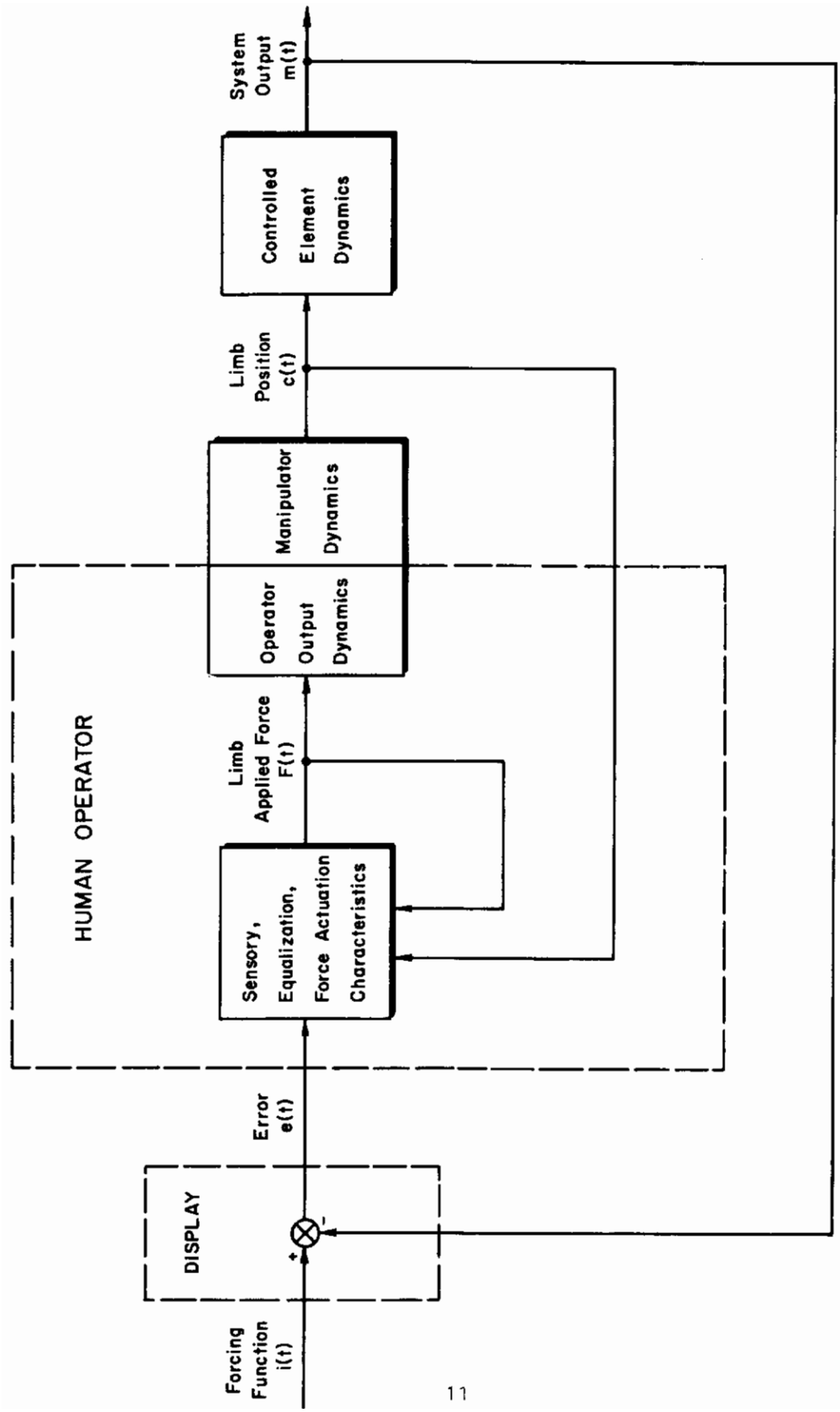

Figure 1. Single-Loop Manual Control System

the central aim is to explore operator dynamics in specialized situations wherein the vast majority of these procedural variables are held constant. This is simple enough to do for the external environmental factors, but for the operator-centered factors the best that can be hoped for is the establishment of reasonably stable levels of stationarity. Stationarity in the over-all experimental situation is enhanced by confining the forcing functions to signals possessing stationary characteristics, and by using highly trained and motivated subjects drawn from a narrowly limited population for which high-grade skill in manual control is an essential feature.

Tustin (Ref. 59) first noted, in a formal way, that operators in manual control systems, responding to random-appearing visual forcing functions, exhibit a type of behavior which is analogous to the behavior of equalizing elements inserted into a servo system to improve the over-all dynamic performance. Since then, a number of measurements of human response to visual inputs have been made in situations such as the one illustrated by the control system block diagram of Fig. 1. For the actual measurement situations the human being is represented by his quasi-linear model, that is, as a describing function plus a remnant. The dynamics of the display and other system elements are lumped into a "controlled element," and the system forcing function is modified (if necessary) into an equivalent forcing function. The equivalent block diagram then takes the form shown in Fig. 2. The control loop signals are represented as time functions and their Fourier transforms, e.g., $e(t)$ and $E(j\omega)$, and also as power spectra or power spectral densities, e.g., $\Phi_{ee}(\omega)$. The linear constant-coefficient controlled element is totally defined by its transfer function, $Y_c(j\omega)$, whereas the nonlinear time-varying human requires the describing function, Y_p, and the remnant power spectrum, Φ_{nn_c}, to provide an adequate dynamic description in the sense that the power spectral densities of the signals in the actual and the quasi-linear equivalent system are the same.

The number of conditions studied by the principal investigators of human operator describing functions, through the year 1960, are summarized in Table II. The table is organized with respect to task variables. The most influential of these turned out to be the forcing function and

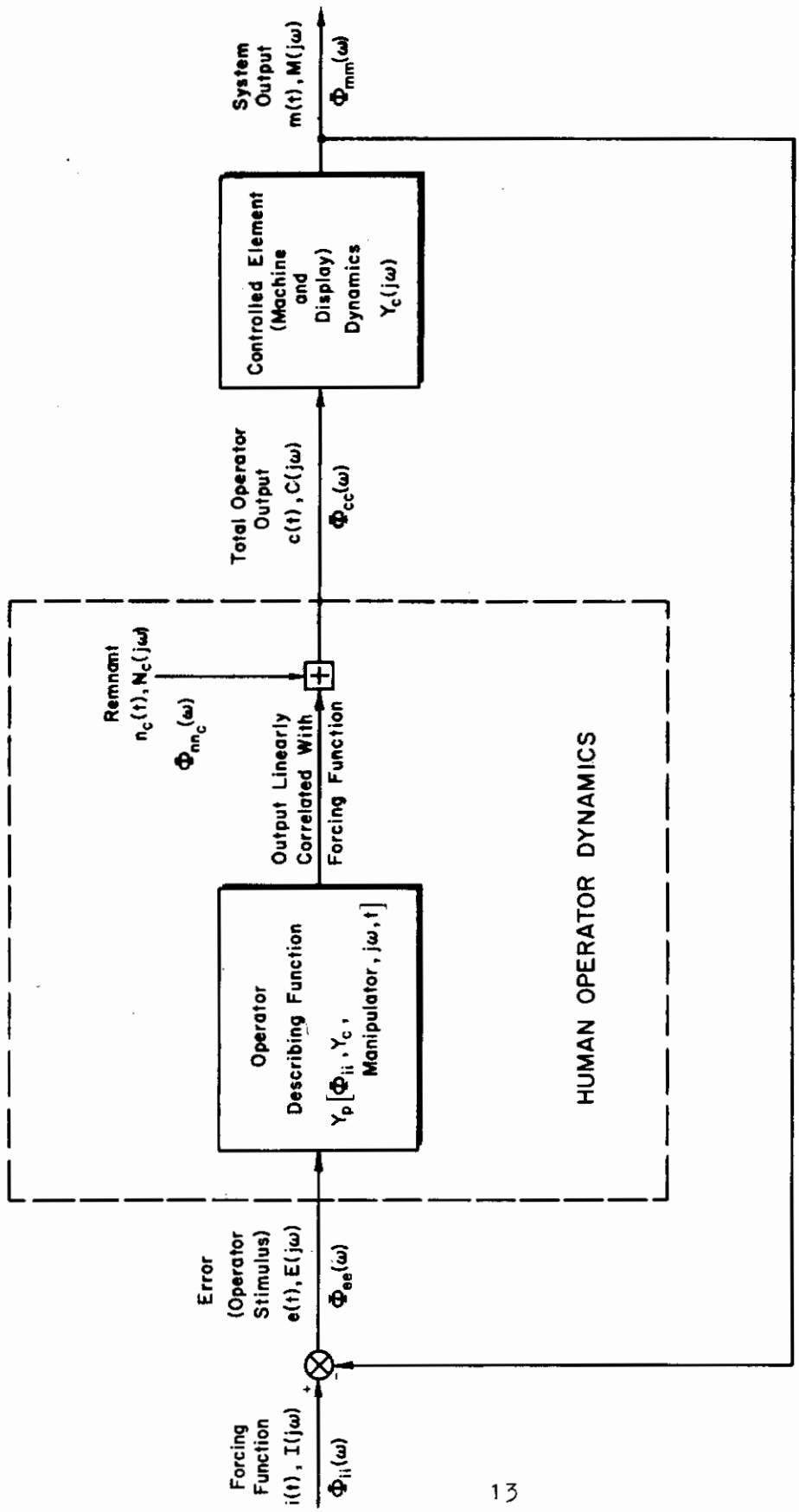

Figure 2. Equivalent Block Diagram of the Human Operator in a Compensatory Tracking Task

TABLE II

SUMMARY OF EXPERIMENTS IN HUMAN RESPONSE FOR STATIONARY SITUATIONS

INVESTIGATOR	NO. OF RANDOM-APPEARING FORC. FUNC. TYPES INVEST.	NO. OF CONTROLLED ELEMENT TYPES INVESTIGATED	MANIPULATOR	NO. OF CROSSOVER REGION MEASUREMENTS	REMARKS
Tustin (Ref. 59)	2	2	Spade grip, spring restraint	0	Simulated tank gun turret tracking. Single-dimensional input.
Russell (Ref. 47)	2	11	Handwheel, no restraint	6	Single-dimensional input.
Goodyear (Refs. 18, 19)	2	2	Aircraft control stick	0	Simulated control of aircraft pitch axis in both stationary and pitching simulator. Single-dimensional input.
Krendel, et al (Refs. 29, 34)	3	3	Aircraft control stick	0	Simulated control of aircraft lateral and longitudinal axes in tail-chase, with and without airframe dynamics. Two-dimensional input.
Elkind (Ref. 13)	20	1	Pencil-like stylus, no restraint	6	Single-dimensional input.
Seckel, et al (Ref. 50)	2	2	Aircraft control stick	2	Stabilization of aircraft lateral and longitudinal axes in both flight and fixed-base simulator. Two-dimensional input.
Hall (Refs. 24, 25)	1	20	Aircraft control wheel	19	Stabilization of various aircraft longitudinal dynamics while also controlling a fixed set of lateral characteristics. Two-dimensional input.

the dynamics of the controlled element. By comparing the results from all these experiments, the influence of the manipulator was shown to be unimportant for the ranges of frequency measured and manipulators tested.

The dependence of the human operator describing function on forcing function and controlled element dynamics has tended, in the actual experimental situations, to be obscured by the limited frequency range (bandwidth) and the run-to-run variability of the measurements. Reference 34, however, shows how, by considering averaged data, it is possible to formulate a fairly simple analytical describing function form which can be adjusted to describe the main features of human behavior. Although the Hall data (Refs. 24 and 25) were not available at the time Ref. 34 was written, Ref. 36 represents an effort to bring these data into consonance with the results considered earlier, and the circa 1960 statement of the model below takes account of those results. Thus, when the describing function data for all the experiments represented in Table II are considered as a whole, they serve as the data base for evolution of a servo model describing human operation and adaptation for compensatory tracking with a visually presented, random-appearing forcing function. This model is the key element in a dynamic description of the human operator's capabilities in such tasks (the other element being the remnant). It characterizes the predominant majority of all the experimental results.

The model comprises two elements:

a. A generalized describing function form

b. A series of "adjustment rules" which specify how to "set" the parameters in the generalized describing function so that it becomes an approximate model of human behavior for the particular situation of interest

The most extensive and generalized describing function form for one- and two-dimensional compensatory control tasks developed in Ref. 34 is:

$$Y_p \doteq K_p e^{-j\omega\tau} \frac{(T_L j\omega + 1)}{(T_I j\omega + 1)} \frac{K_T \left[\frac{a_T}{\sigma_T}\right]}{\left[\left(\frac{j\omega}{\omega_N}\right)^2 + \frac{2\zeta_N j\omega}{\omega_N} + 1\right](T_{N_1} j\omega + 1)} \qquad (1)$$

where

K_p = gain

τ = reaction time delay (transport lag)

$\frac{(T_L j\omega + 1)}{(T_I j\omega + 1)}$ = equalization characteristic

$K_T\left[\frac{a_T}{\sigma_T}\right]$ = indifference threshold describing function ($1 - \sqrt{2/\pi}\, a_T/\sigma_T$ when $a_T/\sigma_T \ll 1$)

$\frac{1}{\left[\left(\frac{j\omega}{\omega_N}\right)^2 + \frac{2\zeta_N j\omega}{\omega_N} + 1\right](T_{N_1} j\omega + 1)}$ = neuromuscular system characteristic

The describing function is written in terms of the frequency operator, $j\omega$, instead of the Laplace transform variable, s, to emphasize that this describing function is only valid in the frequency domain and only exists under essentially stationary conditions. For instance it cannot be used to compute the system response to a discrete input, e.g., a step response.

The indifference threshold effect was derived as a serial member in the operator's characteristics in the Goodyear studies (Refs. 18 and 19), and was shown (Ref. 34) to be compatible with Elkind's variable amplitude results (Ref. 13). However the ratio of threshold to its input, a_T/σ_T, is quite small relative to one for input signal levels conventionally used in tracking tests, so the describing function K_T is near unity. The indifference threshold is, therefore, a second-order effect that can be ignored here (although it can be of importance in other applications).

The third-order neuromuscular system description shown in Eq 1 is based primarily on high frequency data available from step function inputs. None of the describing function measurements referred to in Table II give a direct indication of the complete third-order representation because there is no forcing function power at the high frequencies about ω_N. The describing function data do, however, reflect the low frequency effects of the neuromuscular system. In fact, these data support a first approximation to the neuromuscular system consisting of a first-order lag. Thus the usual version of the describing function model

developed in Ref. 34 has only a first-order neuromuscular lag term, $(T_N j\omega + 1)^{-1}$, where $T_N \doteq T_{N_1} + (2\zeta_N/\omega_N)$.

With the simplification discussed above, the general low frequency describing function of Eq 1 becomes approximately

$$Y_p \doteq \frac{K_p e^{-j\omega\tau}(T_L j\omega + 1)}{(T_I j\omega + 1)(T_N j\omega + 1)} \qquad (2)$$

While Eq 2 can be shown to have a very considerable range of validity for a variety of operators, forcing functions, controlled elements, and manipulators, only the <u>form</u> of the describing function has this over-all validity. Most of the parameters in the describing function are adjustable as needed to make the system output follow the forcing function — i.e., the parameters as adjusted reflect the pilot's efforts to make the over-all system (including himself) stable and the error small.

The pure time delay represented by the $e^{-j\omega\tau}$ term is due to sensor excitation (the retina in the visual case), nerve conduction, computational lags, and other data processing activities in the central nervous system. It is closely related to, but not identical with, certain kinds of classical reaction times. τ is currently taken to be a constant because it appears to be essentially invariant with forcing function and controlled element dynamics for either single or dual random-appearing input tasks. However both inter- and intra-subject τ variations occur. Observed τ's run as low as about 0.1 sec and as high as 0.2 sec.

The neuromuscular lag, T_N, is partially adjustable for the task. The nature of the adjustment is somewhat obscure due to the lack of high frequency data, although the general trend is a monotonic decrease in T_N with increasing forcing function bandwidth (see Table 13, Ref. 34). The observed variation of T_N with forcing function bandwidth ranges from less than 0.1 sec to somewhat greater than 0.6 sec. Because the details of the T_N variation with forcing function bandwidth are not known, this important variation has often been ignored in applications and typical values of T_N near 0.1 sec have been used.

The equalizing characteristics, $(T_L j\omega + 1)/(T_I j\omega + 1)$, coupled with the gain, K_p, are the major elements in that adaptive capability of the

human which allows him to control many differing dynamic devices. Their function is the modification of the stimulus signal into a suitable neuromuscular command which is properly scaled and phased for suitable over-all man-machine system operation. For given input and controlled element characteristics, the form of the equalizer is adapted to compensate for the controlled element dynamics and the pilot's reaction time delay.

The describing function adjustment rules are not simply stated since they depend intimately on interactions of the elements in the man-machine system. In general, the adjustments can artificially be divided into two categories — adaptation and optimalization. Broadly speaking, adaptation is the selection by the operator of a specific form (lag-lead, lead-lag, pure lead, pure lag, or pure gain) for the equalization characteristics; and optimalization is the adjustment of the parameters of the selected form to satisfy some internally generated criteria. The result of the adaptation process is fairly well understood, since the form selected is one compatible with good low frequency, closed-loop response and the absolute stability of the system. The internal optimalizing criteria are not known, although they appear to be generally compatible with the minimization of the rms error (Refs. 31 and 34).

The known adjustment rules for the human operator's describing function, in decreasing order of their certainty, can be summarized as follows (Refs. 34, 36, and 37):

1. **Stability:** The human adapts the form of his equalizing characteristics to achieve stable control.

2. **Form Selection — Low Frequency:** The human adapts the form of his equalizing characteristics to achieve good low frequency closed-loop system response to the forcing function. A low frequency lag, T_I, is generated when both of the following conditions apply:

   a. The lag would improve the system low frequency characteristics.

   b. The controlled element characteristics are such that the introduction of the low frequency lag will not result in destabilizing effects at higher frequencies which cannot be overcome by a single first-order lead, T_L, of somewhat indefinite but modest size.

3. Form Selection — Lead: After good low frequency characteristics are assured, within the above conditions, lead is generated when the controlled element characteristics together with the reaction time delay are such that a lead term would be essential to retain or improve high frequency system stability.

4. Parameter Adjustment: After adaptation of the equalizing form, the describing function parameters are adjusted so that:

a. Closed-loop low frequency performance in operating on the forcing function is optimum in some sense analogous to that of minimum mean-squared tracking error.

b. System phase margin, φ_M, lies somewhere between 0° and 50° when the forcing function bandwidth, ω_i, is much less than the system crossover frequency, ω_c; and from 50° to 110° when ω_i is near ω_c.* This strong effect of forcing function bandwidth on the phase margin is associated with the variation of T_N with the same task variable.**

5. ω_c Invariance Properties

a. ω_c — K_c Independence: After initial adjustment, changes in controlled element gain, K_c, are offset by changes in pilot gain, K_p; i.e., system crossover frequency, ω_c, is invariant with K_c.

b. ω_c — ω_i Independence: System crossover frequency does not depend on forcing function bandwidth for $\omega_i < \omega_{c_o}$. (ω_{c_o} is that value of ω_c adopted for $\omega_i \ll \omega_c$.)

c. ω_c Regression: When ω_i nears or becomes greater than ω_{c_o}, the crossover frequency regresses to values much lower than ω_{c_o}.

---

*"Forcing function bandwidth" is a vague term unless the forcing function spectrum is rectangular. For other spectral shapes an effective rectangular forcing function bandwidth must be defined. Several possible bases for this exist, but recent results by Elkind (Ref. 14) can be used to support the selection of "effective degrees of freedom" as the basis for defining a rectangular bandwidth equivalent for a nonrectangular spectrum, i.e.,

$$\omega_{i_e} = \frac{\left[\int_0^\infty \Phi_{ii}\, d\omega\right]^2}{\int_0^\infty (\Phi_{ii})^2\, d\omega} \qquad (3)$$

**The phase margin adjustment rule noted here has undergone many changes in the course of time. Initially (Ref. 34) a range of $0-30^\circ$ was suggested; this was based almost entirely on extrapolation of low frequency data to crossover. Subsequent re-examination of some of the Elkind data having forcing function power in the crossover region led to extension of the upper value to about 60°. The Hall data almost all spanned the crossover region (see Table II). Phase margins extracted from these (Ref. 36) were highly variable, but ranged from 50° to 110°. The criterion will again be modified in this report!

It turns out that the operator describing function adapted for a given task is very similar to the one that a control engineer would select if he were given an element to control together with a controller "black box," having within it elements making up the describing function given by Eq 2, and knobs on the outside for the adjustment of T_I, T_L, and K_p. Thus, the adaptation of equalization form covered by Adjustment Rules 2 and 3 may be foreign to the reader who is not thoroughly grounded in control theory since it is analogous to operations which have an artistic flavor even in conventional control system synthesis. Examples often help, so Table III is presented to illustrate the equalizer form taken for several simple controlled elements.

TABLE III

EQUALIZER FORMS FOR DIFFERENT CONTROLLED ELEMENTS

WHEN THE CONTROLLED ELEMENT TRANSFER FUNCTION, Y_c, IS	THE OPERATOR'S EQUALIZER FORM ADAPTED IS
$\frac{K_c}{j\omega}$	Pure gain, K_p
K_c	Lag-lead, $T_I \gg T_L$
$\frac{K_c}{(j\omega)^2}$	Lead-lag, $T_L \gg T_I$
$\frac{K_c}{(j\omega)^2 + 2\zeta\omega_m(j\omega) + \omega_m^2}$	Lead-lag (if $\omega_m \ll 2/\tau$) Lag-lead (if $\omega_m \gg 2/\tau$)

This, then, is the analytical-verbal describing function model of the human operator which existed prior to the current study. The analytical portion of the model is the expression of Eq 2, and the verbal portion comprises the adjustment rules given in the numbered statements above.

While the describing function is the critical factor in determining operator-system stability, the uncorrelated — in a linear sense — portion of the operator's output, the remnant, can be important for estimates of

system performance, such as mean-squared error. This situation arises because the remnant, represented as a power spectral density, $\Phi_{nn}(\omega)$, is one of two additive terms in the expression for the spectral density of the operator's output.

Considering that no disturbances are present, the mean-squared error is

$$\overline{e^2} = \frac{1}{2\pi}\int_0^\infty \left|\frac{E(j\omega)}{I(j\omega)}\right|^2 \Phi_{ii}(\omega)\,d\omega + \frac{1}{2\pi}\int_0^\infty \left|\frac{Y_c(j\omega)}{1 + Y_pY_c(j\omega)}\right|^2 \Phi_{nn_c}(\omega)\,d\omega \tag{4}$$

where

$\frac{E(j\omega)}{I(j\omega)} = \frac{1}{1 + Y_pY_c(j\omega)}$ = the error/input describing function

and

$\Phi_{ii}(\omega)$ = the power spectral density of the input

$\Phi_{nn_c}(\omega)$ = the power spectral density of the remnant expressed as an "equivalent" open-loop input applied at the pilot's output

The first term in Eq 4 derives from the describing function portion of the pilot model operating on the forcing function. At the operator's output this component can be represented by a power spectral density $|H|^2\Phi_{ii}(\omega)$, where $H = Y_p/(1 + Y_pY_c)$ is the closed-loop describing function relating pilot's output to the system forcing function. The power spectral density of the remnant can also be expressed in closed-loop form as $\Phi_{nn} = |1/(1 + Y_pY_c)|^2\Phi_{nn_c}$. Then the total power spectral density of the operator's output is

$$\Phi_{cc}(\omega) = |H|^2\Phi_{ii}(\omega) + \Phi_{nn}(\omega) \tag{5}$$

The ratio of the linearly correlated pilot-output power to the total pilot-output power is the square of the "correlation coefficient," ρ:

$$\rho^2 = \frac{|H|^2\Phi_{ii}}{\Phi_{cc}} = 1 - \frac{\Phi_{nn}}{\Phi_{cc}} \tag{6}$$

The meaning of ρ in a specific instance is dependent on the data analysis apparatus and on the nature of the system forcing function.

For our experiments ρ is found using an analyzer which mechanizes spectral and cross-spectral measurements using multiplications and very low pass filters (Chapter IV). If the forcing function is a sum of sinusoids, Φ_{ii} will be a sum of delta functions (i.e., a series of line spectra which exist only at the frequencies of the individual forcing function sinusoidal components). Then, in general, the output, Φ_{cc}, will be a sum of delta functions at the same frequencies as those in Φ_{ii}, plus delta functions at other discrete frequencies (if nonlinearities or constant rate sampling are present), plus a continuous power spectral density component representing random fluctuations in the output. At the frequencies for which they exist the delta function components will generally overpower the random component, and the ρ measured at forcing function frequencies will generally be 1.0 unless low frequency time variations in H result in additional power within the measurement filter bandwidth. In fact, ρ will be 1.0 even in the presence of many kinds of system nonlinearities. At other frequencies ρ will be undefined since Φ_{ii} is zero.

For forcing functions which are samples of random processes, the power spectral densities in Eq 6 are all continuous. The meaning of ρ for this case is quite different; its value relative to 1.0 becomes primarily a measure of the relative importance of the remnant. Near-unity ρ values indicate a linear constant-coefficient system, whereas lesser values imply nonlinearity and/or nonstationarity and/or "noise" injection (Ref. 34). Thus ρ for the random-input case is not as discriminating a measure as when the input is made up of simple sinusoids.

All past human operator data for which ρ values exist used forcing functions which were samples of random processes (Refs. 24, 29, 34, and 50), or very many, closely spaced in frequency, sinusoids (Ref. 13) which were not separable in the analysis technique used. Therefore past ρ data fall into the random-input category. Much of the existing data show correlation coefficients near 1.0, although considerably lower values were not uncommon. In general, the larger the correlation coefficient, the smaller was the remnant and the mean-squared tracking errors. The smallest observed remnants occurred in connection with controlled elements which had the least energy storage, i.e., $Y_c \doteq K_c$. Here

the form of the operator's equalizer characteristic is either a low frequency lag or a pure gain. Finally, the least remnant is associated with forcing functions having the least bandwidth or high frequency components.

Unfortunately, mechanisms for the description of the remnant are not nearly as well "understood" in an equivalent mathematical model form as those for the describing function. Observed remnants in one-dimensional control tasks have, however, been "explained" in three possibly equally likely ways (Ref. 34):

a. Random "noise," with a mean-squared value proportional to mean-squared linear output, superimposed on the operator's linear output

b. Nonsteady operator behavior, that is, variation of the operator's describing function during the course of a measurement run

c. Nonlinear anticipation or relay-like operation, superimposed on the operator's linear output

Remnant data are far more sparse than describing function information; and the data available are not especially reliable. Consequently, the summary statements above are about all that should be said in connection with the circa 1960 model.

3. Rationale for the Existing Model

It may be well to remark that the analytical-verbal model is in part a hypothesis which derives from what, after all, can only be described as limited data. The rationale of the model, however, does not rest exclusively on observation. The adjustment rules are partly an expression of practical synthesis procedures for inanimate servomechanisms (Refs. 7, 22, and 26).

Desirable properties of a "good" feedback control system are to:

a. Provide specified command-response relationships

b. Suppress unwanted inputs and disturbances

c. Reduce effects of variations and uncertainties in elements of the control loop

It can be shown (Ref. 7, for example) that these three functions are accomplished in a single-loop manual or automatic feedback control system by making the complex gain of the open-loop system, Y_pY_c, very large over the range of frequencies in which the command input and load disturbances have substantial components, and very small outside this range.

For the unity feedback system of Fig. 2, the desired closed-loop transfer function is the transfer function of a low pass filter. The entire range of positive real frequencies may then be divided into three regions of principal interest in terms of the magnitude of the open-loop system transfer function. These are displayed in Table IV.

TABLE IV

OPEN- AND CLOSED-LOOP TRANSFER FUNCTIONS
OF A "GOOD" SERVOMECHANISM

FREQUENCY	OPEN-LOOP TRANSFER FUNCTION	CLOSED-LOOP TRANSFER FUNCTION
$\frac{\omega}{\omega_c} \ll 1$	$\lvert Y_pY_c \rvert \gg 1$	$\frac{Y_pY_c}{1+Y_pY_c} \doteq 1$
$\frac{\omega}{\omega_c} \doteq 1$	$Y_pY_c \doteq \frac{1}{j(\omega/\omega_c)}$	
$\frac{\omega}{\omega_c} \gg 1$	$\lvert Y_pY_c \rvert \ll 1$	$\frac{Y_pY_c}{1+Y_pY_c} \doteq Y_pY_c$

The region near the crossover frequency, ω_c, (where $|Y_pY_c| \doteq 1$) has a surpassing importance in the synthesis of feedback systems. First, for "good" performance the crossover frequency must exceed the largest frequency, ω_i, at which there are appreciable components of the commands or external disturbances. ω_c is, in this sense, somewhat greater than an upper bound on the frequency region wherein $|Y_pY_c| \gg 1$, a condition which provides good following of the system input by the output and suppression of disturbance effects. Second, the shape of Y_pY_c at and

near crossover frequency determines the dynamics of the dominant modes of system response. The condition for neutral oscillatory stability is

$$|Y_pY_c| = 1 \text{ and } \angle Y_pY_c = -\pi \text{ when } \operatorname{sgn} Y_pY_c(0) = + \qquad (7)$$

Hence, neutrally stable or unstable dominant modes are most often avoided by adjusting the system so that

$$\text{and} \quad \begin{array}{llll} |Y_pY_c| < 1 & \text{when} & \angle Y_pY_c = -\pi \\ \angle Y_pY_c > -\pi & \text{when} & |Y_pY_c| = 1 \end{array} \qquad (8)$$

These are the often quoted conditions of positive gain margin and phase margin (e.g., Ref. 22). They are an expression for simple minimum phase or minimum phase plus transport lag systems of the Nyquist stability criterion. Since stability is quite literally the sine qua non of a feedback control system, these requirements for gain and phase margin may severely restrict the choice of the crossover frequency.

The phase angle at a frequency ω_c of a transfer function, Y_pY_c, which contains a transport lag, τ, but which is otherwise minimum phase, in terms of amplitude ratio slopes is (Refs. 7 and 26)

$$\varphi(\omega_c) = -\tau\omega_c + \frac{\pi}{40}\left[\frac{d|Y_pY_c(\omega)|}{d\left(\ln\frac{\omega}{\omega_c}\right)}\right]_{\omega=\omega_c} + \frac{1}{20\pi}\int_{-\infty}^{\infty}\left\{\frac{d|Y_pY_c(\omega)|}{d\left(\ln\frac{\omega}{\omega_c}\right)} - \left[\frac{d|Y_pY_c(\omega)|}{d\left(\ln\frac{\omega}{\omega_c}\right)}\right]_{\omega=\omega_c}\right\} \ln\coth\frac{\left|\ln\frac{\omega}{\omega_c}\right|}{2}\, d\left(\ln\frac{\omega}{\omega_c}\right) \qquad (9)$$

where the slopes, $d|Y_pY_c|/d\left[\ln(\omega/\omega_c)\right]$, are expressed in db/decade. As illustrated by Fig. 3, the $\ln\coth(1/2)|\ln(\omega/\omega_c)|$ term in the integral applies a large weighting to slope changes in the immediate vicinity of ω_c and greatly attenuates the effects of the integrand of slope changes elsewhere. Consequently, the phase at ω_c is affected primarily by $\tau\omega_c$, by the local db amplitude ratio slope (the second term in the expression), and by

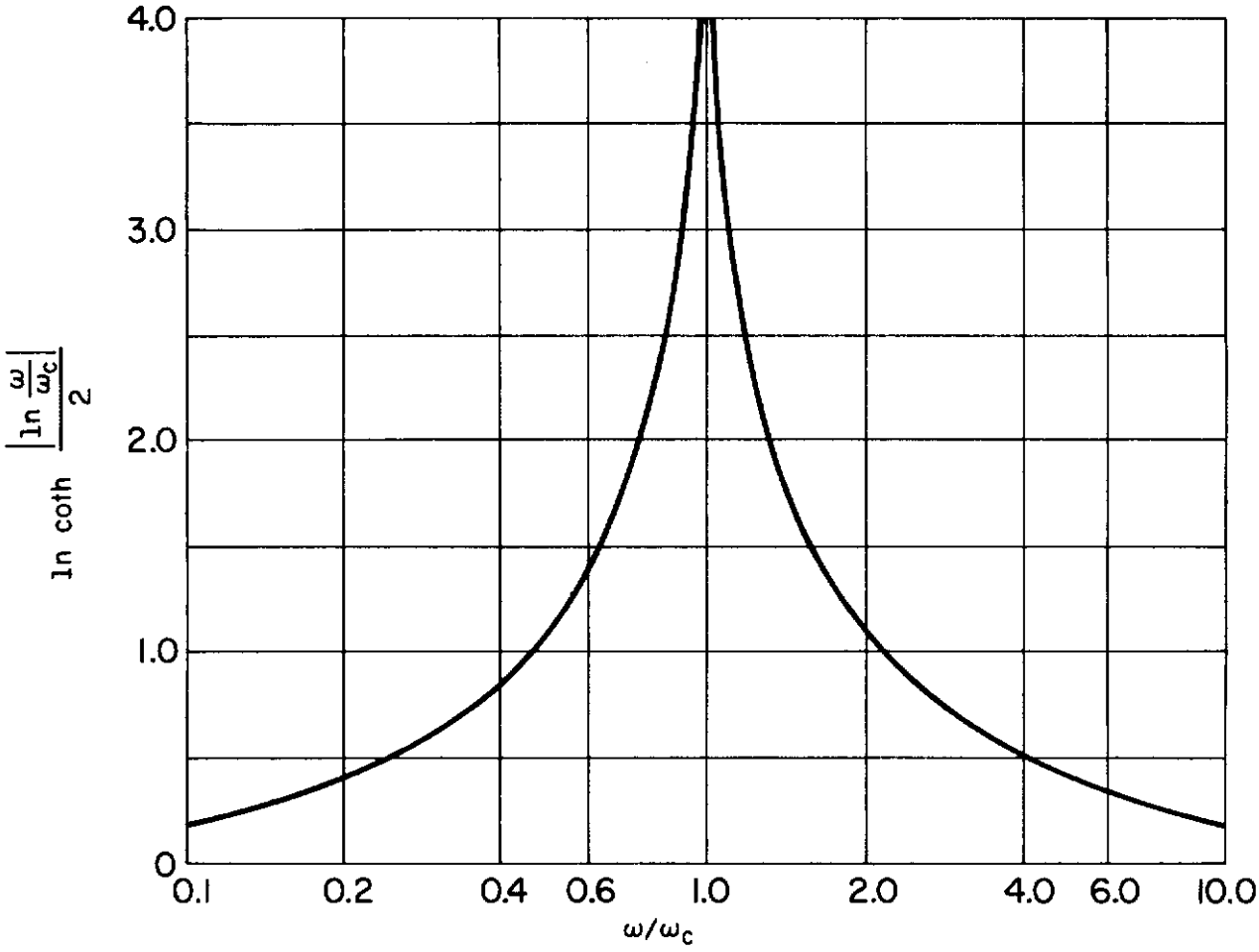

Figure 3. Weighting Function for Bode's Amplitude Ratio Slope: Phase Relationship

local changes in this slope (the integral term). If the db amplitude ratio slope is essentially constant over a wide region about ω_c, the expression reduces approximately to the second term alone plus the transport lag's contribution. In this event the phase associated with a constant amplitude ratio slope of $-20n$ db/decade will be simply $-\tau\omega_c - n\pi/2$ rad.

For low pass open-loop transfer functions the amplitude ratio slope at gain crossover is negative, so a positive phase margin can usually exist only when $d\left[Y_p Y_c\right]_{db}/d\left[\ln\left(\omega/\omega_c\right)\right]$ in the immediate vicinity of crossover is less (numerically) than -40 db/decade, the local changes in slope are moderate, and the $\tau\omega_c$ contribution is minor. The available crossover regions for most transfer functions are, therefore, confined to areas where the local amplitude ratio slope fulfills these conditions, and the choice of crossover frequency is delimited accordingly.

These considerations are embodied in the Primary Rule of Thumb of frequency response synthesis: "Find or create a fair stretch of −20 db/decade slope for the amplitude ratio, and then make it the crossover region by putting the 0 db line through it" [i.e., make the gain such that $|Y_pY_c(j\omega)| = 1$ where $Y_pY_c(j\omega) \doteq 1/j(\omega/\omega_c)$]. This crude prescription for stability and good response is generally adequate for minimum phase systems. It can be extended directly to the transport lag case by adding a prescription for a positive phase margin. Typically, the phase margin, Φ_M, for a well-adjusted regulator is approximately $30-40^\circ$; a somewhat higher value is customarily used for servomechanisms, which must follow commands as well as suppress disturbances. The human has his own ideas (Adjustment Rule 4b):

Finally, then, for a "good" feedback control system the operator's describing function, $Y_p(j\omega)$, must be adjusted so that the crossover frequency, ω_c, exceeds the highest important frequency in the input, ω_i; and so that $Y_pY_c(j\omega)$ conforms at low frequencies, high frequencies, and crossover frequency to the requirements noted in Table IV.

Many of the above remarks about the rationale of equalization adopted by the pilot can be made more concrete and understandable by the definition of an approximate "crossover model" for manual control systems. This has been done in Ref. 38, where it is pointed out that consideration of the requirements of "good" feedback system performance leads directly to the conclusion that the pilot adjusts his describing function so that the open-loop function, Y_pY_c, in the vicinity of the gain crossover frequency, ω_c, is closely approximated by

$$Y_pY_c \doteq \frac{\omega_c e^{-j\omega\tau_e}}{j\omega} \qquad (10)$$

This crossover model is not a replacement for the analytical–verbal model, but is instead a convenient approximation suitable for many engineering purposes. While it is a better description of amplitude ratio characteristics than of phase characteristics, it often describes the most significant features of operator behavior adequately. This is because the actual shape of the open-loop function away from the gain crossover

frequency is usually almost irrelevant to the closed-loop performance. It is, therefore, often unnecessary to retain terms in the describing function whose influence is not felt in the immediate vicinity of gain crossover.

Table V shows the application of the adjustment rules to the prediction of a pilot's describing function and to the formulation of the crossover model for several simple limiting-case controlled elements.*

TABLE V

OPERATOR DESCRIBING FUNCTION AND CROSSOVER MODEL

WHEN THE CONTROLLED ELEMENT TRANSFER FUNCTION IS (Y_c)	THE OPERATOR'S DESCRIBING FUNCTION IS (Y_p)	THE CROSSOVER MODEL (ω about ω_c) IS Y_pY_c
$\frac{K_c}{j\omega}$	$K_p e^{-j\omega\tau_e}$	$\frac{K_pK_c e^{-j\omega\tau_e}}{j\omega}$
K_c	$\frac{K_p e^{-j\omega\tau_e}}{(T_I j\omega + 1)}$; $\frac{1}{T_I} \ll \omega_c$	$\frac{K_pK_c}{T_I}\frac{e^{-j\omega\tau_e}}{j\omega}$
$\frac{K_c}{(j\omega)^2}$	$K_p e^{-j\omega\tau_e}(T_L j\omega + 1)$; $\frac{1}{T_L} \ll \omega_c$	$\frac{K_pK_cT_L e^{-j\omega\tau_e}}{j\omega}$

In many instances more complicated controlled elements can be satisfactorily approximated in the vicinity of gain crossover by these simple limiting cases. Thus, for example, a damped second-order controlled element, $Y_c = K_c/\left[(j\omega/\omega_m)^2 + (2\zeta/\omega_m)j\omega + 1\right]$, with a natural frequency, $\omega_m \ll \omega_c$, is closely approximated near $\omega = \omega_c$ by a double integrator, $Y_c = K_c\omega_m^2/(j\omega)^2$. The operator's describing function would then include a lead equalization (see also the last entry in Table III).

*Note that the neuromuscular lag, which has an important influence at and near crossover frequencies, is subsumed in a larger effective reaction time delay, $\tau_e \doteq \tau + T_N$ for $K_c/(j\omega)^2$. For the other two controlled elements the lead equalization can occur at high frequencies, so for these $\tau_e \doteq \tau + T_N - T_L$. Actually, τ_e is a catchall term which serves to incorporate into the describing function the phase effects near crossover of pure transport lags and poles and zeros with breakpoints much greater than ω_c.

B. OBJECTS OF THE EXPERIMENTS

The primary purposes of the experimental series are the validation of the existing analytical–verbal model and the extension of this model in accuracy and detail.

1. Model Validation

In the sense in which it is used here, "validation" is intended to mean the confirmation of the extrapolations based on limited data. The delineation of crucial experiments designed to test the validity of the model involve the following preliminary predictions:

a. Describing function form adjustment. For a variety of controlled elements the adjustment rules should be used to predict the operator's describing function form. These controlled elements should be such as to require a complete range of operator equalization form adaptation; and they should be "new" in that they have not previously been examined experimentally in detail.

b. Mean-squared error minimization and variation. Estimates of mean-squared error due to system forcing function, and its variation with forcing function characteristics, should be derived. Special control situations should be selected which most concretely illuminate the experimental consequences of describing function adjustment for minimum mean-squared tracking error, and the variation of this quantity with forcing function modifications.

With these preliminary analyses and predictions in hand, an experimental series can readily be delineated to provide data which either confirm or deny the predictions of the model.

As already indicated in Table III, the simple controlled elements $Y_c = K_c$, $K_c/j\omega$, and $K_c/(j\omega)^2$ evoke a complete range of equalizer form adjustment, so these become prime candidates for critical validation experiments. Presuming that Elkind's experiments (Ref. 13) with a variety of forcing functions for the simple controlled element $Y_c = K_c$ could be repeated, in part, in the current series, then his data as a whole could be considered in direct context with our own. The crucial controlled element form for model validation would then be $Y_c = K_c/j\omega$

and $K_c/(j\omega)^2$. Limited tests have been accomplished for the first of these (Refs. 24 and 47), but no data are available for the second. These controlled element forms are further attractive in that they represent, in the vicinity of crossover, limiting cases of a great variety of other possible controlled elements of far greater complexity.

As another aspect of validation, it is necessary to distinguish between those features of the model in any particular situation which must be evidenced, and which therefore would tend to be invariant with different operators, and those features which might be, to an extent, a matter of indifference. It will become apparent later that individual operators may display what can only be described as a particular tracking style. The style of one operator may be somewhat different from the style of another operator, and this is reflected in changes in the describing function model in those regions where the form of the model is not critical to good tracking performance. On the other hand, where the describing function form is critical to good tracking performance, most particularly in the vicinity of the crossover frequency, it is to be expected that the operator will not exercise a choice and that the tracking performance will be tightly constrained. The three controlled elements mentioned above are not particularly constraining except in the region of crossover. However, certain unstable controlled elements tend to require a more uniform behavior.

2. Model Extension

The primary limitations to the existing model are due to limitations in the experimental data on which the model is based. In essence, the model is about as sophisticated as it can be without further empirical knowledge. So, the question becomes "Where are the existing data deficient?"

a. The vast majority of the data are based on forcing function bandwidths which were very low in frequency relative to ω_c. Hence, most of the important crossover features of the model are based on extrapolations and the doctrine of compatibility between data sources.

b. These low frequency forcing-function bandwidth data do not disclose any differences between manipulators.

c. To achieve random-appearing forcing functions, noise generators or their equivalent were used. This choice of forcing function, while satisfying the random-appearing criterion, introduced other problems:

(1) Sampling variability (i.e., effects of finite run length) introduced several uncertainties.

(2) Data processing equipment was complex and often notoriously unreliable.

(3) The remnant, of course, came out as a continuous power spectral density. Consequently it was of such form that it was not possible to discriminate among the several possible remnant sources (i.e., remnant can be due to sampling, nonlinearities, nonstationary behavior, actual random noise injection, etc., but the distinctive features corresponding to each of these tended to be lost in a general smoothed-over slush). Also, precious little remnant data were available.

d. With the notable exception of Elkind's results, the effects of variation in forcing function bandwidth were not systematically explored. Also, the consequences of changes in forcing function amplitude on open-loop describing function data were not known in detail.

Many other data deficiencies exist, in both scope and kind, but the four major items listed above were the most influential in the program planning phases of the experiments to be reported here. A major correction of these data deficiencies was desired, at least in the areas most significant for man-machine system analysis. Thus, beyond the critical experiments for the validation of the analytical-verbal model, it was expected that experimental phases of the program would yield additional data which would permit:

a. The refinement of statements concerning the adjustment rules and the form of the describing function in the vicinity of the crossover frequency. Such data might include:

(1) Phase margin data (and gain margin data where this parameter is pertinent)

(2) Closed-loop dominant mode characteristics, such as closed-loop damping ratio, ζ_{CL}

(3) Tighter limits on values of τ and/or $\tau + T_N$

(4) Better understanding of and limits on the ω_c regression condition

(5) Better limits on the maximum value of lead time constant, T_L, and lag time constant, T_I

b. An improved understanding of the general effects of forcing function amplitude and bandwidth.

c. An improved understanding of the possible effects on the pilot's describing function of changes in the manipulator.

d. An extension of the population over which the operator's describing function was measured. (It would, of course, enlarge confidence in the model if it could be shown that not just a few subjects, but many, could be described in the same way.)

A natural result of an experimental program carried out for these purposes would be a set of definitive data measured over a wide range of frequencies for elementary and limiting-case controlled elements.

In addition to all the purposes described above, it was hoped that the experimental results would yield the information which would permit a variety of questions concerning human operator performance in tracking tasks to be answered. Some of the questions which have arisen time after time in connection with previous investigations are suggested by the following phrases:

* a. Motor response models: Few, if any, investigators using random-input describing function techniques have carried their measurements to frequencies high enough to reveal any but the crudest facts concerning the motor response (neuromuscular lags) of the human operator.

b. Stationarity during runs: Data reduction performed in the frequency domain requires fairly long averaging times. The describing function which is measured is then an average describing function for the period of the test. It may be postulated that the operator's performance is far from invariant over a period of minutes, and that, for example, his describing function might be appreciably different at the end of a long run than at the beginning. If this were the case, there would be good reason to doubt the validity of the mathematical description under any circumstances other than as an expression of the average performance in a particular experimental

situation. The nature of cross-spectral data reduction techniques and the forcing function frequencies of interest preclude the explicit examination of variations in the operator's describing function for any period shorter than approximately 2 min, but evidence for or against rapid fluctuations in the description of the operator could be indicated by considering ρ values in context with other measurements. Also, the question of whether or not the description would be appreciably different for the first 2 min and the last 2 min of the 10-min run could quite easily be examined.

* c. Pulsing control as an expression of lead: It is a matter of fairly common experience that in control tasks which are very difficult, either because of potential instability of the controlled element or because of a very wide bandwidth of the input forcing function, the operator will tend to exercise control with a series of discrete pulses. The reasons why he does this are not clear, but it may be that he can in this fashion arrange more lead or phase advance. This behavior, however, has some nonlinear properties and is a possible source of remnant.

* d. Sampling effects: Some authors have suggested (Refs. 5, 6, and 60) that the human may behave as a sampled-data system with a reasonably constant sampling rate for otherwise stationary conditions. Physical evidence for or against this hypothesis is very sparse. If the human operator approximates a constant-sampling-period, sampled-data subsystem, the effect of sampling would be a directly testable physical source of the remnant.

* e. Nonlinear effects: There is evidence of nonlinear behavior in both the perceptual and actuation mechanisms of the operator. For example, there are rate thresholds below which the perception of motion is not possible. Further, in attempting to make predictions of future motion at rates above the threshold, the operator will overestimate slow rates and underestimate fast ones. Some such nonlinear effects might well be a suitable source of the remnant.

* f. Other sources of remnant: In addition to Items a – e above, a variety of mechanisms might possibly be the source of the remnant.

It was not thought desirable to attempt to resolve all of these questions within the framework of the present program, but certain experiments were planned, to be carried out more or less explicitly, to resolve some of them. (Those which are treated, to some extent, in this

report are marked with an asterisk in the margin.) All the questions and data deficiencies listed were carefully considered in evolving the final experimental plans, and where at all possible attempts were included to attack such questions within the main framework of the planned experiments.

CHAPTER III

PRE-EXPERIMENT ANALYSES

Pragmatically, the most compelling justification of any model is its capacity to subsume past experimental results and to predict the outcome of future experiments especially contrived to exercise the model to its limits. The existing human pilot model, discussed in the last chapter, was constructed on the basis of compatibility with past results, so it performed the first function noted prior to the initiation of the current program. Its next test was in forecast of extended situations. These predictions were the basis of much of the planning of the experiments and choice of particular experimental situations.

Three kinds of predictions are summarized here. The first is, fundamentally, application of the adjustment rules and rationale to three simple controlled elements. Although one of these, $Y_c = K_c$, has been extensively studied, it is treated again here with the model to provide the basis for comparative statements between this and the other two systems. The second kind of forecast is also concerned with describing function adjustment, but in a rather special way. The intent was to find special controlled element forms which would tend to tightly constrain the operator's choice of characteristics. To this end the model is used to explore possible control situations which will tend to confirm or deny conjectures about variability. Finally, the third type of prediction uses the model to make mean-squared-error estimates for subsequent experimental validation. In pursuing this objective, unexpected results were obtained which provide the raison d'etre for two adjustment rules which previously lacked a theoretical basis.

A. EQUALIZATION ADJUSTMENT

A series of controlled elements which require the pilot's equalization selection to range from lag-lead to essentially pure gain to lead-lag have

already been discussed in the last chapter. From there it will be recalled that these pilot-adapted forms correspond to $Y_c(j\omega)$ forms of K_c, $K_c/j\omega$, and $K_c/(j\omega)^2$, respectively. Detailed analyses of man-machine systems involving these controlled elements will be summarized below.

1. $Y_c = K_c$

This simplest possible controlled element is also the most extensively studied, since it was included as one of the controlled elements in three of the programs listed in Table II. The most definitive investigation was that conducted by Elkind (Ref. 13). Yet some characteristics remained ill defined (e.g., phase margins) or not too well understood (e.g., ω_c regression).

The operator-adapted describing function for control of the pure gain controlled element will be

$$Y_p(j\omega) \doteq \frac{K_p e^{-j\omega\tau}\,(T_L j\omega + 1)}{(T_I j\omega + 1)(T_N j\omega + 1)} \tag{11}$$

The phase margin of this system will be

$$\begin{aligned}\varphi_M &= \pi + \angle Y_p Y_c(j\omega_c) \\ &= \pi - \tan^{-1} T_I\omega_c - \tau\omega_c - \tan^{-1} T_N\omega_c + \tan^{-1} T_L\omega_c\end{aligned} \tag{12}$$

The lag time constant, T_I, will be much greater than either the lead time constant, T_L, or the neuromuscular lag, T_N, to achieve good low frequency closed-loop system response. In fact, the lead and the neuromuscular lag will occur at relatively high frequencies and they will tend to cancel. Therefore, at frequencies in the crossover region and below, the primary effect of these two terms will be seen in their contribution to the phase, which will be approximately

$$\tan^{-1} T_L\omega - \tan^{-1} T_N\omega \doteq (T_L - T_N)\omega \quad , \quad \omega \leq O(\omega_c)$$

where O( ) means "of the order of."

The net effect is thus indistinguishable at low frequencies from a modified "effective" reaction time delay, τ_e, given by

$$\tau_e \doteq \tau + T_N - T_L \tag{13}$$

Using this approximation, the open-loop system characteristics become

$$Y_p Y_c \doteq \frac{K_p K_c e^{-j\omega\tau_e}}{T_I j\omega + 1} \quad , \quad \omega \leq O(\omega_c) \tag{14}$$

A generic $j\omega$ Bode plot showing the open-loop characteristics of Eq 14 is given in Fig. 4. Also illustrated there is the crossover model approximation obtained by noting that $1/T_I\omega_c \ll 1$, so that $K_p K_c/T_I \doteq \omega_c$. The crossover model version of Eq 14 is then

$$Y_p Y_c\Big]_{\text{crossover}} \doteq \frac{\omega_c e^{-j\omega\tau_e}}{j\omega} \quad , \quad \omega = O(\omega_c) \tag{15}$$

Because $\omega_c \gg 1/T_I$ for good low frequency closed-loop response, the phase margin expression (Eq 12) as modified by Eq 13 becomes approximately

$$\begin{aligned} \Phi_M &\doteq \pi - \left(\frac{\pi}{2} - \frac{1}{T_I\omega_c}\right) - \tau_e\omega_c \\ &\doteq \frac{\pi}{2} + \beta - \tau_e\omega_c \end{aligned} \tag{16}$$

where $\beta = 1/T_I\omega_c$. The crossover model phase margin will be the same as that given by Eq 16 when β is set equal to zero.

In this system the most important parameter is the crossover frequency. Unfortunately ω_c is also one of the more difficult things to estimate accurately using the existing model because of the absence of extensive phase margin data. Consequently an estimate of a likely crossover frequency range is usually the best that can be done. In the present

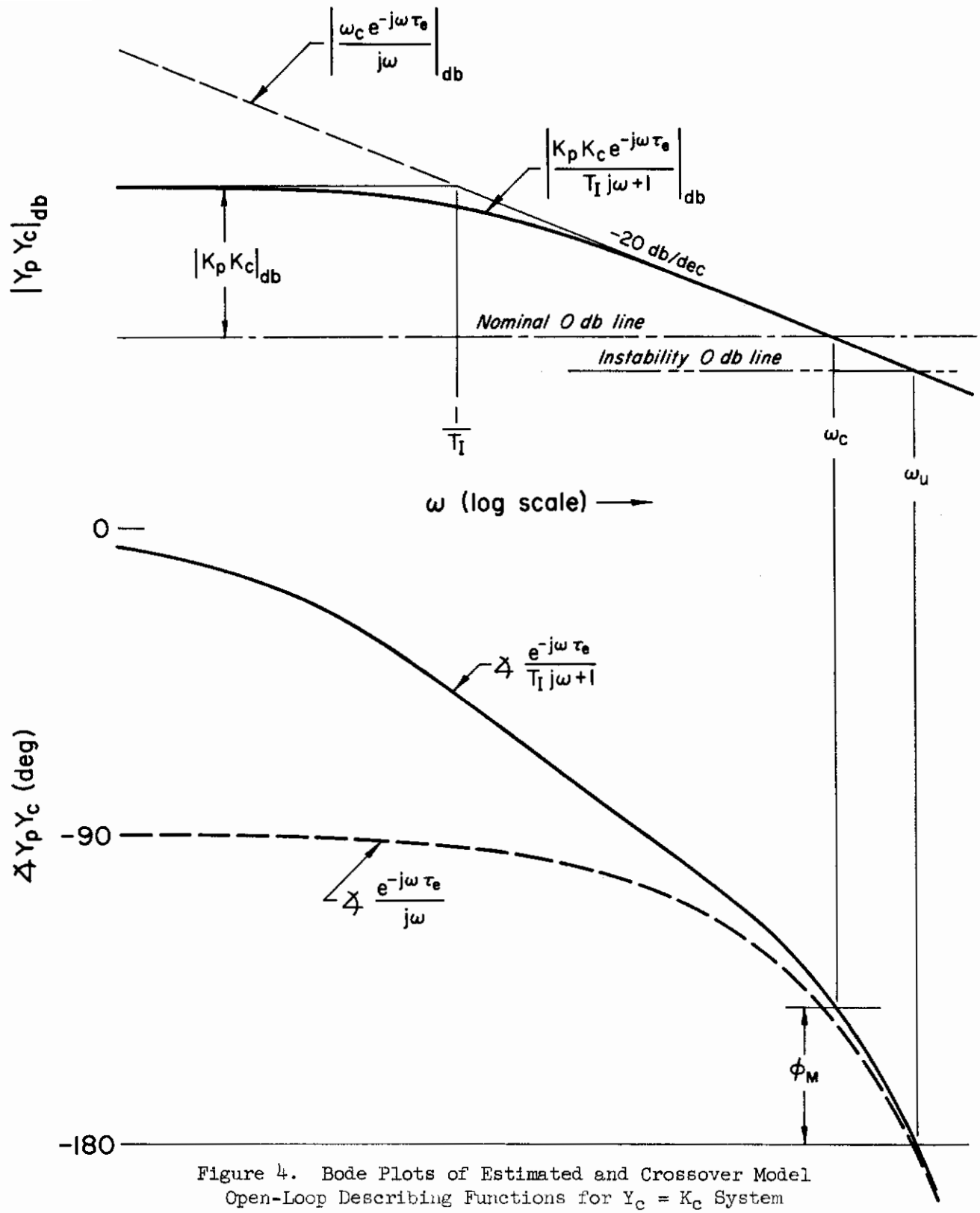

Figure 4. Bode Plots of Estimated and Crossover Model Open-Loop Describing Functions for $Y_c = K_c$ System

case this can be approached as follows. Solving for the crossover frequency from Eq 16,

$$\omega_c \doteq \frac{1}{\tau_e}\left(\frac{\pi}{2} + \beta - \varphi_M\right) \tag{17}$$

Because T_N and T_L approximately cancel for this case, τ_e will approach τ. A reasonable value for τ_e is then about 0.20 sec, which corresponds to the higher side of the τ range given in Chapter II. With a value for τ_e selected, a series of bounds on ω_c can be established using various values of β and φ_M in Eq 17. Any value of β less than 0.1 is compatible with good closed-loop system response, so a $\beta = 0.1$ line provides one boundary. The system will be unstable if the phase margin is less than zero degrees, so an upper bound is established by the line

$$\omega_{c_{max}} \doteq \frac{1}{\tau_e}\left(\frac{\pi}{2} + \beta\right) \tag{18}$$

Finally, an upper limit for the phase margin will be taken as 40°. (This estimate is based on the very limited Elkind data in the crossover region.) The $\omega_{c_{40}}$ line,

$$\omega_{c_{40}} \doteq \frac{1}{\tau_e}\left(\frac{5\pi}{18} + \beta\right) \tag{19}$$

established a lower boundary on the region of likely crossover frequencies.

The boundaries developed above are illustrated in Fig. 5. Using the middle of the region, an estimated crossover frequency will be about 6.5 rad/sec.

Boundaries similar to those shown in Fig. 5 can be developed using a constant phase margin and a variable τ_e (see Ref. 37). Uncertainties exist in both τ_e and the phase margin (which are <u>not</u> independent quantities—see Adjustment Rule 4b), so the bounded region can be considered to take into reasonable account nominal variations in both quantities.

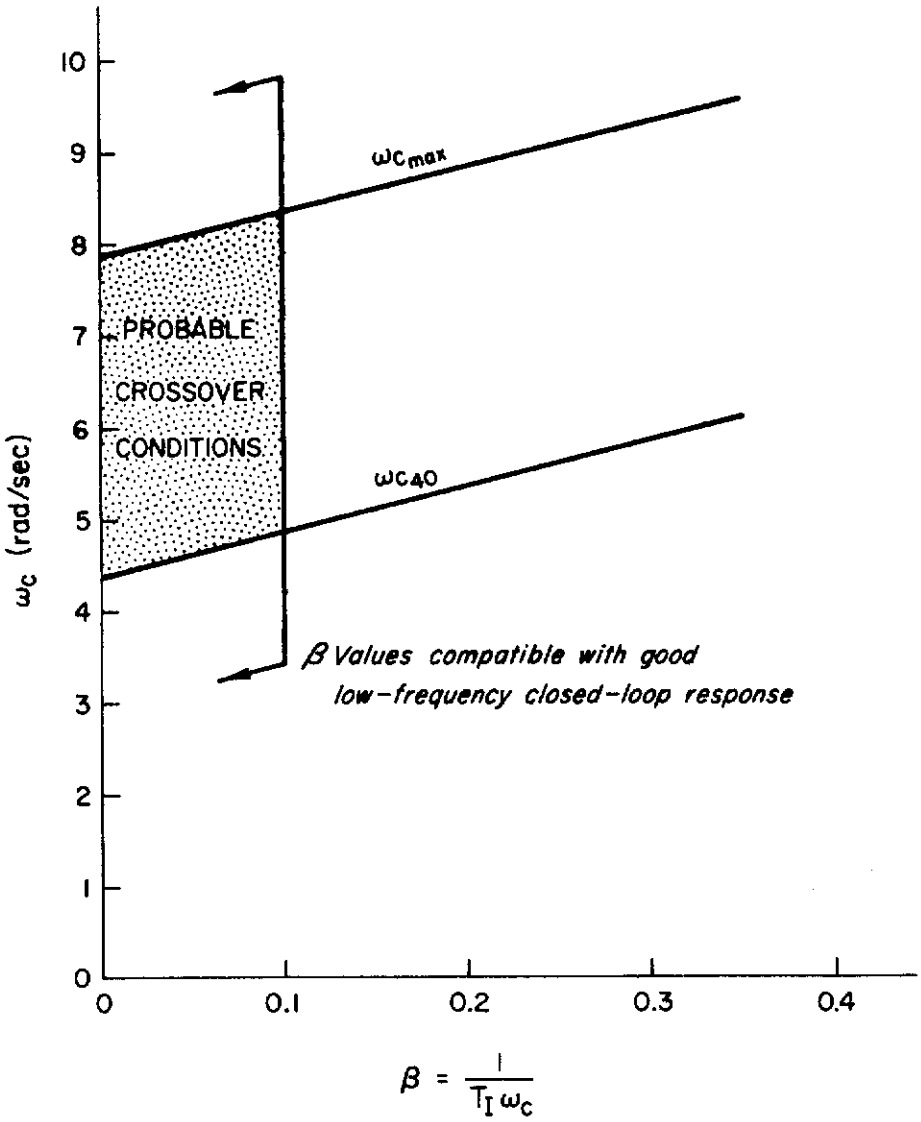

Figure 5. Crossover Frequency Estimation for $Y_c = K_c$

According to Adjustment Rules 5a, b, and c, the crossover frequency estimated above will be essentially independent of variations in K_c, and will also be constant in the presence of increases in forcing function bandwidth until ω_{i_e} (Eq 3) approaches or exceeds 6.5 rad/sec or so. When ω_{i_e} exceeds the estimated ω_c, the observed crossover frequency will exhibit a substantial decrease (ω_c regression).

2. $Y_c = K_c/j\omega$

This single-integrator controlled element is an idealized rate control, i.e., an operator-applied step function input to the machine results in an output rate proportional to the step input. Because of the free s, there is no requirement for low frequency equalization, so the adjustment rules indicate $T_I = 0$. At high frequencies the operator lead can be used to compensate for the neuromuscular lag. Thus the appropriate open-loop system model is

$$Y_p Y_c \doteq \frac{K_p K_c e^{-j\omega\tau_e}}{j\omega} \doteq \frac{\omega_c e^{-j\omega\tau_e}}{j\omega} \tag{20}$$

where $\tau_e = \tau + T_N - T_L$. This complete open-loop system model is identical to the crossover model (compare with Table V). The open-loop system Bode diagram is essentially the same as that for the crossover model Bode diagram for the $Y_c = K_c$ case (dashed curves in Fig. 4).

Because conditions in the region of crossover are so similar to those for the $Y_c = K_c$ situation, the best estimate of ω_c possible using the circa 1960 model is based on that given in the last article presuming β does not appear in Eq 16. Because β is thus effectively zero, the estimated mean ω_c might be dropped to about 6 rad/sec or so by using the average of the $\omega_{c_{max}}$ and $\omega_{c_{40}}$ bounds evaluated for zero β. [A few higher phase margins have been observed (Ref. 24) for some $Y_c = K_c/j\omega$ data, so the lower bound should also, perhaps, be reduced.] As far as the numerical values are concerned (6.5 and 6 rad/sec), this is a refinement that is probably not warranted because of the basic uncertainties present in both estimates. But the relative magnitudes of ω_c for $Y_c = K_c$ and $K_c/j\omega$ are expected to exhibit this ordering.

The application of Adjustment Rule 5 to this case is the same as noted for the $Y_c = K_c$ situation.

3. $Y_c = K_c/(j\omega)^2$

The double-integrator controlled element provides a crucial test for the validation of the analytical–verbal model since experimental data had never been obtained prior to the current program. Thus the application of the adjustment rules represents pure extrapolation of the adaptation principles believed relevant to human operator description.

The operator describing function adapted for the control of the $K_c/(j\omega)^2$ controlled element needs no low frequency equalization ($T_I = 0$), but does require the use of some lead equalization to meet the simple and primary requirement of stability. Thus, in the complete open-loop describing function

$$Y_pY_c \doteq \frac{K_pK_ce^{-j\omega\tau}\ (T_Lj\omega + 1)}{(j\omega)^2\ (T_Nj\omega + 1)} \tag{21}$$

it is immediately apparent that $T_L > \tau + T_N$ is a necessary condition for stability. A low frequency approximation to Eq 21 is

$$Y_pY_c \doteq \frac{K_pK_ce^{-j\omega\tau_e}\ (T_Lj\omega + 1)}{(j\omega)^2}\ ,\quad \omega \leq 0(\omega_c) \tag{22}$$

where $\tau_e = \tau + T_N$. This approximate expression is suitable for the low frequency range up to and somewhat beyond crossover. Note especially that, because the equalizing lead is needed at much lower frequencies to obtain stability, τ_e here does <u>not</u> contain the compensating effect of a high frequency lead tending to offset the neuromuscular lag. Consequently, τ_e for the $Y_c = K_c/(j\omega)^2$ case will be considerably larger than those values estimated for the $Y_c = K_c$ and $Y_c = K_c/j\omega$ systems. Note also that Eq 22 approaches the crossover model (Table V) only when $T_L\omega_c \gg 1$.

To gain a better appreciation for the likely position of $1/T_L$, consider the detailed unified servo analysis (Ref. 39) presentation shown in Fig. 6. Here $1/T_L$ is located at a frequency which is considerably

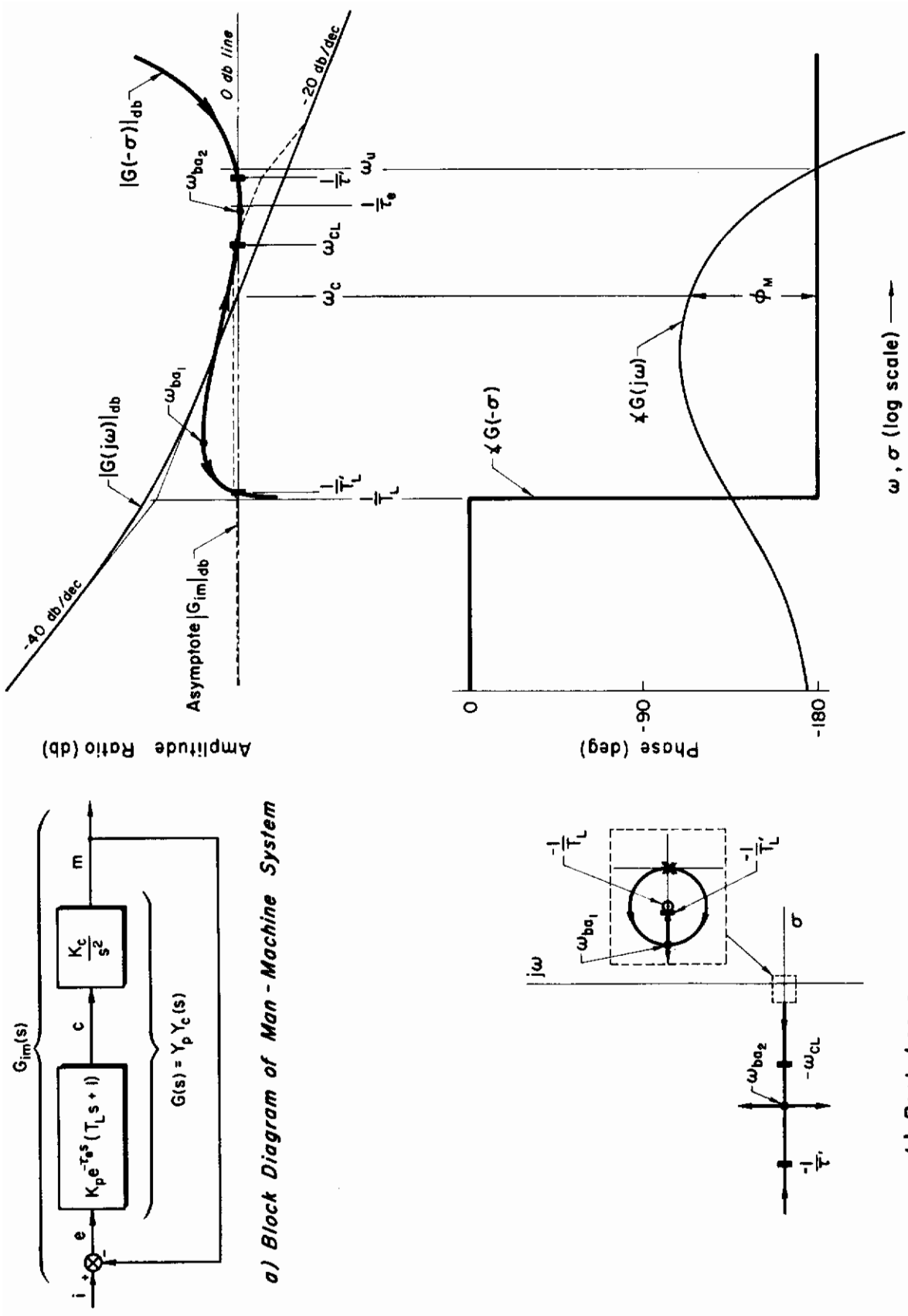

Figure 6. Detail Analysis of $Y_c = K_c/s^2$ Man-Machine System for $1/T_I \omega_c << 1$

less than the crossover frequency. The closed-loop system in this case will have a low frequency characteristic given by

$$G_{im}(j\omega) = \frac{G(j\omega)}{1 + G(j\omega)}$$

$$\doteq \frac{(T_L j\omega + 1)}{(T'_L j\omega + 1)(\frac{j\omega}{\omega_{CL}} + 1)(\tau' j\omega + 1)} \quad , \quad \omega < O(\omega_c) \qquad (23)$$

$$\doteq \frac{1}{(\frac{j\omega}{\omega_{CL}} + 1)(\tau' j\omega + 1)} \quad , \quad \omega < O(\omega_c) \qquad (24)$$

The approximate cancellation of the low frequency closed-loop lag, T'_L, by the lead equalization time constant, T_L, indicated in Eq 24 results in an excellent low frequency closed-loop response characteristic.

Now, by way of contrast, imagine that the lead break point is much closer to $1/\tau_e$ and the crossover frequency. The dipole pair in Eq 23 will then no longer nearly cancel. Also, for separations between $1/T_L$ and $1/\tau_e$ of about 6 $\left(T_L/\tau_e = 3 + \sqrt{8} = 5.83\right.$, obtained from the requirement that two real values of $\left.d[Y_p Y_c(-\sigma)]/d\sigma = 0\right)$, the two poles starting at the origin can never reach the real axis. Further, the closed-loop characteristics become increasingly sensitive to variations in T_L and τ_e as their separation becomes less. Consequently, it is clear that $1/T_L$ should, ideally, be located at values much less than ω_c. This completes the prediction of the detailed form of Y_p for this case.

The next problem is to estimate the approximate crossover frequency. This will be accomplished in a fashion similar to that used for $Y_c = K_c$. The phase margin corresponding to Eq 22 is

$$\varphi_M = \tan^{-1} T_L\omega_c - \tau_e\omega_c \qquad (25)$$

which, if $1/T_L\omega_c \ll 1$, becomes approximately

$$\varphi_M \doteq \frac{\pi}{2} - \frac{1}{T_L\omega_c} - \tau_e\omega_c$$

$$\doteq \frac{\pi}{2} - \beta - \tau_e\omega_c \qquad (26)$$

where $\beta = 1/T_L\omega_c$. Rearranging Eq 26, an expression for the crossover frequency is obtained:

$$\omega_c = \frac{1}{\tau_e}\left(\frac{\pi}{2} - \beta - \varphi_M\right) \qquad (27)$$

This equation is similar to Eq 17 for the $Y_c = K_c$ controlled element, and the likely range for ω_c values will be determined in the same general way. The pertinent boundaries in this case are:

$$\beta < 0.1 \quad , \text{ for good low frequency response}$$

$$\omega_{c_{max}} = \frac{1}{\tau_e}\left(\frac{\pi}{2} - \beta\right) , \text{ for the } \varphi_M = 0^\circ \text{ bound}$$

$$\omega_{c_{40}} = \frac{1}{\tau_e}\left(\frac{5\pi}{18} - \beta\right) , \text{ for the } \varphi_M = 40^\circ \text{ bound}$$

Before these boundaries can actually be drawn, a value for τ_e must be estimated. A well-established and representative number for τ is 0.2 sec, to which must be added an estimate for T_N. As noted in Chapter II, T_N is variable over a fairly wide range, but a typical value of 0.1 is often used as representative of the order of magnitude. This will be the procedure used here. With $\tau_e \doteq 0.3$ sec, the boundaries appear as shown in Fig. 7. The center of the probable crossover region is $\omega_c \doteq 4$ rad/sec. Just as in the $Y_c = K_c$ and $Y_c = K_c/j\omega$ cases, one should not make too much of the exact numerical value. Instead, the important estimates are the general range of values, i.e., $2.5 \leq \omega_c \leq 5$ rad/sec, and the order of the ω_c values for the various controlled elements, i.e., $\omega_c]_{K_c} > \omega_c]_{K_c/j\omega} > \omega_c]_{K_c/(j\omega)^2}$. Finally, here again it can be anticipated that reductions in controlled element gain will be offset by increases in the operator's gain and vice versa; and that ω_c regression will occur for forcing function bandwidths of about 4 rad/sec.

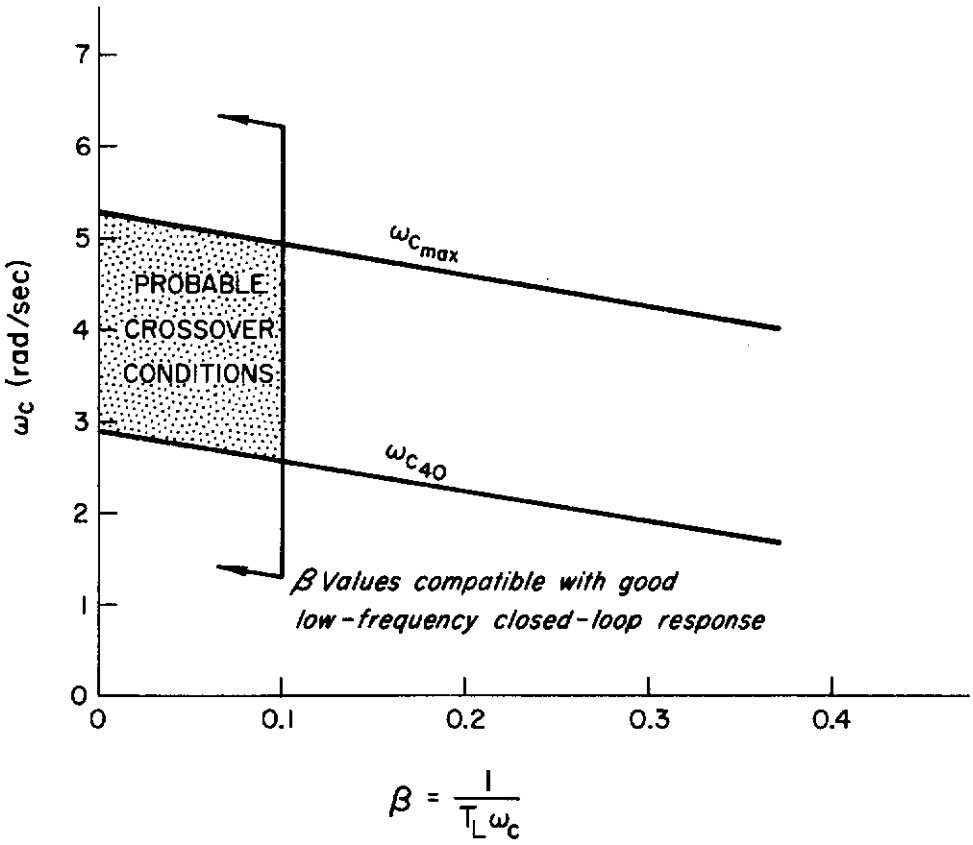

Figure 7. Crossover Frequency Estimation for $Y_c = K_c/(j\omega)^2$

B. EQUALIZATION ADJUSTMENT FOR CONDITIONALLY STABLE SYSTEMS

The three controlled elements considered above can all be stabilized easily by the human without any fundamental conflict between stability and low frequency response. The operator is under some constraint at frequencies in the region of crossover, but elsewhere his transfer properties can conceivably vary a great deal without causing difficulty. For instance, at very low frequencies the open-loop describing function Y_pY_c is large relative to one for all three controlled elements, so over the low frequency range the resulting closed-loop systems all exhibit nearly unity input-output relationships; the effect on this property of minor reductions or increases in the low frequency portion of the operator's describing function will be insignificant practically. In other words, the systems treated thus far have not been equally sensitive over the entire frequency range of interest to changes in the operator's characteristics, but have, instead, been far more critically affected by Y_p changes in some ranges than in others. One could conjecture that the operator might be able to take some advantage of this situation by being relatively haphazard over frequency regions where such behavior makes little difference, while being far more precise where it really counts.

There are controlled elements of great practical importance which tend to be far less forgiving of variations in the controller characteristics. The most common of these are vehicles which have various kinds of instabilities over which control must be exerted to create a stable man-machine system. The resulting system is conditionally stable, because either too high or too low a gain will result in instability.

Idealizations of two controlled elements which result in conditionally stable closed-loop systems have been selected for further examination. These are:

$$Y_c = \frac{K_c}{j\omega - \frac{1}{T}}$$

$$Y_c = \frac{K_c}{j\omega\left(j\omega - \frac{1}{T}\right)}$$

The first can be thought of as a generalization of the $Y_c = K_c/j\omega$ controlled element (wherein $1/T = 0$), and the second as a similar generalization of the $Y_c = K_c/(j\omega)^2$ configuration. Just as in their special $1/T = 0$ cases, the major difference between these two controlled elements derives from the necessity of using low frequency lead in the second to attain stability, whereas lead is not required for stability in the first, so any lead generated can be used to improve the high frequency response.

1. $$Y_c = \frac{K_c}{j\omega - \frac{1}{T}}$$

This simple divergence controlled element has been studied analytically previously in Ref. 1, and certain facets have been examined experimentally in Ref. 11.

Figure 8 presents a detailed analysis of a system composed of the unstable divergence and a pure time delay, τ_e. As might be expected, when $1/T$ is very small relative to $1/\tau_e$ the system characteristics appear very similar to those for $Y_c = K_c/j\omega$. For this limiting case it will be recalled that the lead equalization was used primarily to offset high frequency neuromuscular system effects. Consequently, for small values of $1/T$, at least, the operator describing function for control of this controlled element will be

$$Y_p \doteq K_p e^{-j\omega\tau_e} \qquad (28)$$

where $\tau_e \doteq \tau + T_N - T_L$. This operator describing function will probably be retained as $1/T$ increases toward $1/\tau_e$ since neither lead nor lag modifications are capable of improving the system significantly. As can be appreciated from Fig. 8, the value of $1/\tau_e$ provides an upper limit on the operator's control capacity, so T_L will play an important role indeed in reducing τ_e to its lowest effective value. An experimental issue of great interest here is the extent to which the operator may possibly be able to reduce the neuromuscular lag and reaction time delay when the pressure to do so is extreme.

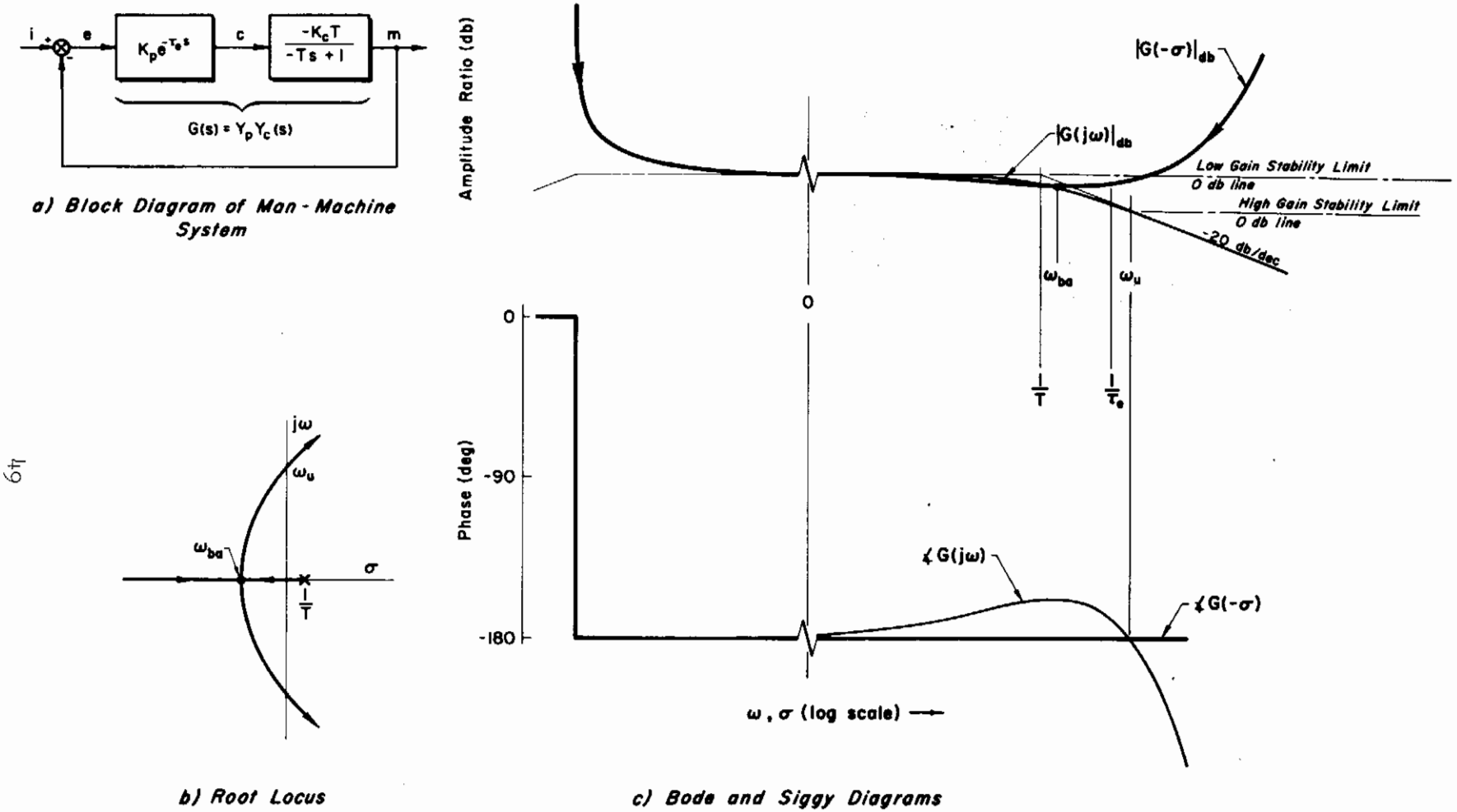

Figure 8. Detail Analysis of $Y_c = K_c/(s - 1/T)$ Man–Machine System

The conditionally stable nature of this system is revealed by the low and high gain stability limit zero-db lines shown in Fig. 8c. The operator's gain characteristics must be such as to establish and maintain the actual system zero-db line somewhere between these two extremes. Deviation from this policy at low frequencies results in an aperiodic divergence, whereas at high frequencies an oscillation is the penalty incurred for exceeding the stability limit.

The tolerances on operator gain adjustments can be made extremely small by proper adjustment of $1/T$. As the divergence time constant decreases, the spread between $1/T$ and $1/\tau_e$ also decreases. Maximum phase margin becomes smaller and, most important of all, the range of stable gain levels becomes smaller. This range is theoretically reduced to a single value of gain when the real axis breakaway (ω_{ba}) coincides with the origin on the root locus. The position of the breakaway is easily determined since it coincides with the point of zero slope on the $G(-\sigma)$ amplitude plot. Thus, the breakaway point is that value of σ for which $dG/d\sigma$ is zero. Since $G(-\sigma)$ is

$$G(-\sigma) = \frac{-(K_p K_c T) e^{\tau_e \sigma}}{T\sigma + 1} \tag{29}$$

then the slope of the Siggy plot will be

$$\frac{dG(-\sigma)}{d\sigma} = \frac{T\tau_e G(-\sigma)}{T\sigma + 1}\left[\sigma + \frac{\tau_e - T}{T\tau_e}\right] \tag{30}$$

which is zero when

$$\sigma = \omega_{ba} = \frac{T - \tau_e}{T\tau_e} = \frac{1}{\tau_e} - \frac{1}{T} \tag{31}$$

The breakaway will coincide with the origin when the divergence time constant, T, is equal to τ_e. Since the low frequency effects of the

neuromuscular system can be largely canceled by the lead equalization, τ_e is essentially τ. Hence, operator control of divergences having time constants of the order of 0.15 sec are theoretically possible. Early experimental evidence on the control of such divergences tends to support this conclusion (see Ref. 1, p. 45), and subsequent experiments (Ref. 11) amount to conclusive demonstration.

For the experimental program contemplated here, the main objective is to explore the effects of system constraints on operator variability. To obtain the precision desired in describing function measurements, relatively long tracking runs are required, some with large forcing function bandwidths. Under these conditions, divergence time constants near the stability limit are likely to be too extreme, tending to induce fatigue and frustration in both operator and experimenter. Much smaller values of $1/T$, say 1 to 2 rad/sec, impose significant constraints on operator variability while being compatible with a more relaxed experimental procedure. For example, with $\tau_e = 0.2$ sec and $T = 0.5$ sec, the breakaway frequency, ω_{ba}, is 3 rad/sec and the total stable gain region is 10 db.

2. $Y_c = \dfrac{K_c}{j\omega\left(j\omega - \dfrac{1}{T}\right)}$

Just as for its double-integrator special case ($1/T = 0$) this controlled element requires low frequency lead equalization for stability. Because of the divergence, some minimum gain level is required, thereby leading to the conditionally stable nature of this system. The appropriate operator describing function is

$$Y_p \doteq K_p e^{-j\omega\tau_e} (T_L j\omega + 1) \qquad (32)$$

where τ_e here is approximately $\tau + T_N$, just as for $Y_c = K_c/(j\omega)^2$. Figure 9 presents a detailed unified servo analysis of this system. There the $1/T_L$ lead break point occurs before the $1/T$ divergence. This relative position is appropriate for the moderate to large values

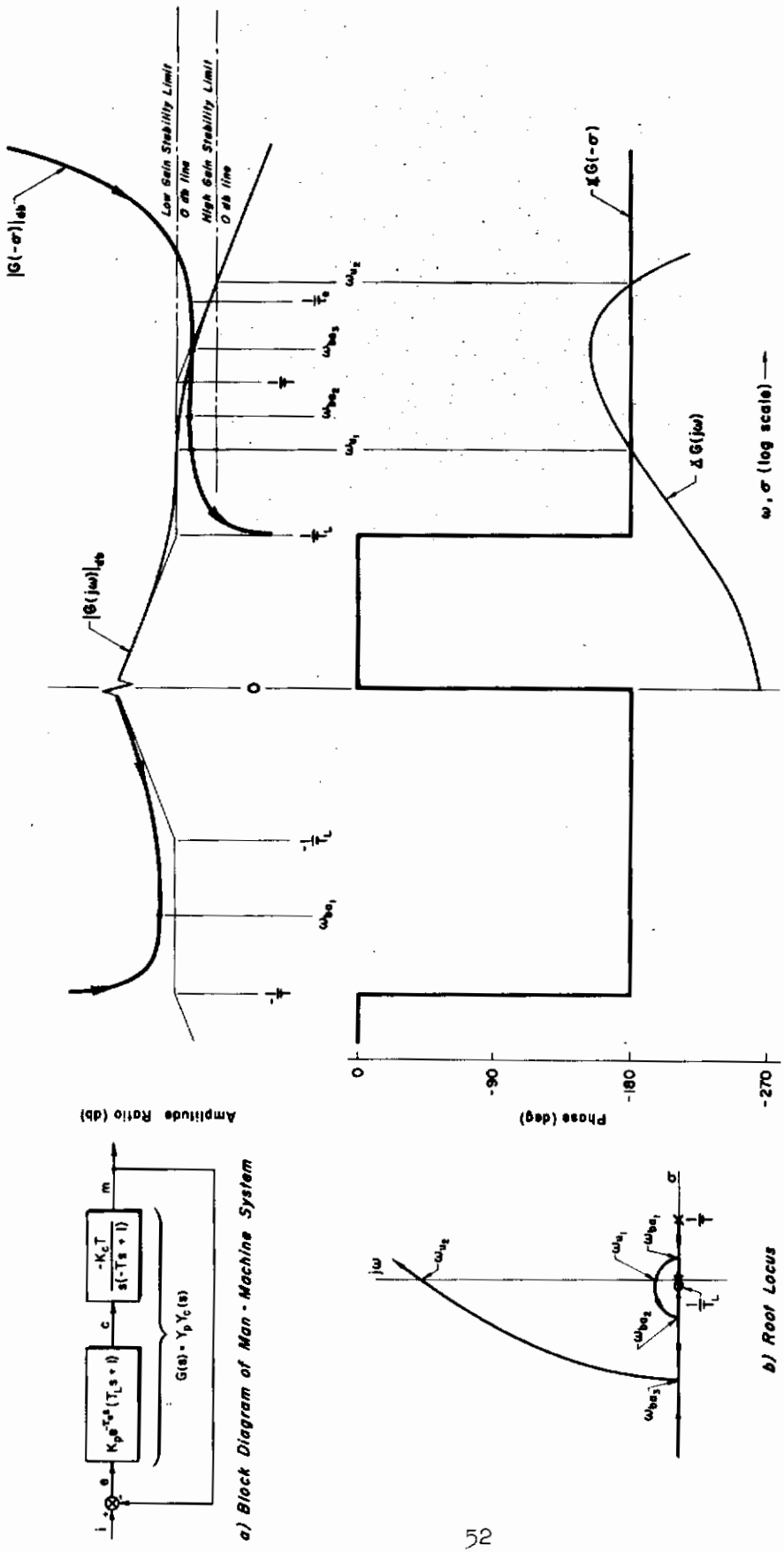

Figure 9. Detail Analysis of $Y_c = K_c/s(s - 1/T)$ Man-Machine System

of $1/T$ which are of primary interest here; for very small values of $1/T$, however, the relative position of these break points will be reversed. That this relative order of $1/T_L$ and $1/T$ is pertinent can be readily appreciated by considering the alternative.

In the limit, as $1/T_L$ approaches zero, this man-machine system tends to approach in form that for the simpler first-order divergence considered above. In such a limiting circumstance the controllability limit would occur when $T = \tau_e$. Because the lead equalization is not, in this case, tending to cancel neuromuscular lags, τ_e is substantially larger than that for the simple divergence.

Although the root loci for the simple divergence of Fig. 8 differs drastically from that shown in Fig. 9, the essential character of these systems in the region of crossover is similar. This is most easily seen by comparing Figs. 8c and 9c. The differences so prominent on the root loci occur at gains which are lower than those of direct concern. The key similarity in both circumstances is that as $1/T$ is increased, the tolerances on available gain variations decrease. The central differences between the two constraining situations, already mentioned above, are the necessity for low frequency lead generation in one instance and the differences in τ_e.

C. PERFORMANCE MEASURES AND MINIMIZATION ADJUSTMENTS

The mean-squared error generated in a man-machine system with stationary forcing functions has significance from at least three points of view. First, mean-squared error or any closely related error functional, such as $\overline{|e|}$, is often used for the relative assessment of competing man-machine systems. Second, the stationarity of mean-squared error values gives a direct and easily obtained indication of over-all system stationarity. Learning curves, for example, usually consist of a record of mean-squared error or similar quantity versus time, with stationary conditions being presumed for the system as well as the performance measure when it has achieved what appears to be a constant minimum value. Third, there is some reason to believe that the operator's

describing function parameters are finally adjusted so that closed-loop low frequency performance in operating on the forcing function minimizes or nearly minimizes the mean-squared tracking error. This is, in fact, Adjustment Rule 4a.

Because of the importance of mean-squared error, it was desirable to develop some simplified relationships, using the pilot model, that can be used to make predictions which can subsequently be tested by experiment. Unfortunately, not enough was known about remnant to include it in any mean-squared error formulations. However, it is not difficult to separate the mean-squared error into two components — that due to remnant and that due to forcing function. Attention here will be devoted to the mean-squared error component due to forcing function, i.e., the first term in Eq 4.

The mean-squared error component due to forcing function is given by

$$\begin{aligned} \overline{e_i^2} &= \frac{1}{2\pi}\int_0^\infty \left|\frac{E(j\omega)}{I(j\omega)}\right|^2 \Phi_{ii}(\omega)\,d\omega \\ &= \frac{1}{2\pi}\int_0^\infty \Phi_{ee_i}(\omega)\,d\omega \end{aligned} \tag{33}$$

where Φ_{ee_i} is the error power spectral density due to Φ_{ii}. An extremely simple yet remarkably universal open-loop system describing function model is the crossover model of Eq 10, which is repeated below.

$$Y_p Y_c \doteq \frac{\omega_c e^{-j\omega\tau_e}}{j\omega} \tag{10}$$

This model has a high degree of validity for the $Y_c = K_c/j\omega$ system and is also quite good for most $Y_c = K_c$ systems. It can have some validity for special cases in other systems also, such as the $Y_c = K_c/(j\omega - 1/T)$ system when $1/T$ is small. Although this open-loop describing function also has merit as an approximation to describing functions for $Y_c = K_c/(j\omega)^2$ in the crossover region, its description of the phase at frequencies not

too far below ω_c is inaccurate. Still, mean-squared error calculations based on this simple form will have a measure of applicability to many of the situations to be examined experimentally.

The simplified systems for which mean-squared error calculations will be made are shown in Fig. 10. The crossover model system, Fig. 10a, leads to integrals which cannot be evaluated without making simplifying approximations, although it can easily be evaluated numerically. Both of these approaches will be used below. For all the calculations the forcing function spectral density will be taken as the rectangular spectrum given by Fig. 10b.

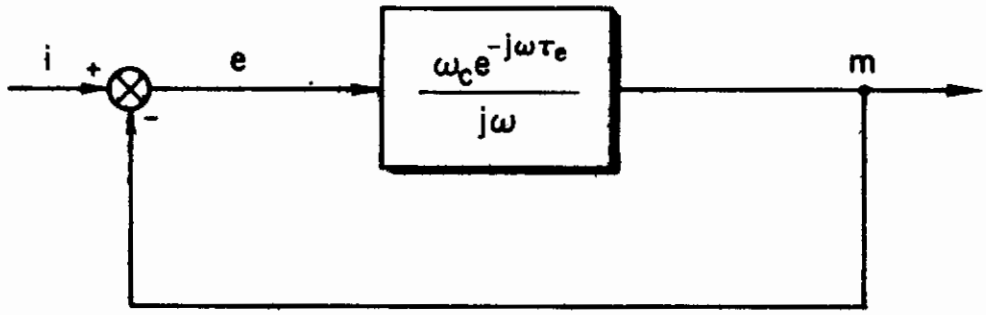

a) Crossover Model System

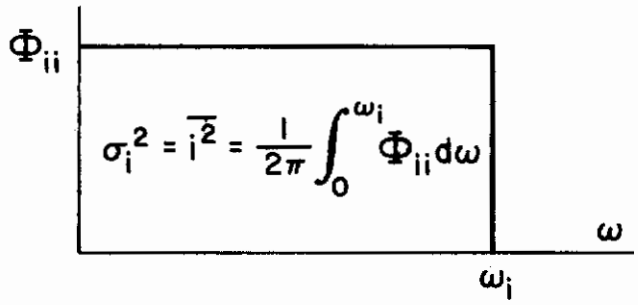

b) Forcing Function Power - Spectral Density

Figure 10. Elements of $\overline{e_I^2}$ Calculations

The error-to-input describing function for the crossover model is given by

$$\frac{E(j\omega)}{I(j\omega)} = G_{ie}(j\omega) = \frac{j\omega}{j\omega + \omega_c e^{-j\omega\tau_e}} \tag{34}$$

When Eq 34 is inserted into Eq 33

$$\overline{e_i^2} = \frac{\Phi_{ii}}{2\pi} \int_0^{\omega_i} \frac{\omega^2}{\omega^2 - 2\omega\omega_c \sin \omega\tau_e + \omega_c^2} d\omega \tag{35}$$

This integral is not readily evaluated. However, if $\sin \omega\tau_e$ is replaced by its argument (a good approximation for systems wherein ω_i is such that $\omega_i\tau_e \ll 1$) the integral is easily found. The result is

$$\frac{\overline{e_i^2}}{\sigma_i^2} \doteq \frac{1}{(2\omega_c\tau_e - 1)} \left[1 - \frac{\omega_c/\omega_i}{\sqrt{2\omega_c\tau_e - 1}} \tanh^{-1} \frac{\omega_i}{\omega_c} \sqrt{2\omega_c\tau_e - 1} \right] \tag{36}$$

or

$$\frac{\overline{e_i^2}}{\sigma_i^2} \doteq \frac{1}{3}\left(\frac{\omega_i}{\omega_c}\right)^2 \tag{37}$$

if the hyperbolic arctangent is carried only to the second term in its expansion. The exceptionally simple result (Ref. 37) given by Eq 37 is often referred to as the "one-third law." It will later be seen to hold remarkably well as long as ω_i/ω_c is somewhat less than 1.

Equation 35 can also be integrated numerically. The result of such an operation is shown in Fig. 11. In this plot τ_e serves as a normalizing parameter, so the figure is essentially relative mean-squared error versus crossover frequency, with forcing function bandwidth as a parameter. These results are of very great interest indeed, for they imply much about operator adjustment! It will be noted that the minimum values of mean-squared error for the smaller ω_i conditions occur at the stability limit. This implies that crossover frequency should be adjusted at or near this value and be kept there, i.e., $\omega_c \doteq$ constant. This is a highly enlightening analytical justification for Adjustment Rules 5a

and 5b, which were based on extrapolations of experimental observations. But Fig. 11 contains still more information. Notice that at a value of $\tau_e\omega_i$ lying between 1.2 and 1.4 the minimum mean-squared error will no longer be along the stability limit. Instead, smaller values of mean-squared error can be obtained by a drastic reduction in the crossover frequency. This phenomenon is, of course, the ω_c regression noted in Adjustment Rule 5c. Judging from Fig. 11, such regressions should occur when ω_i/ω_c becomes greater than about 0.8, which is completely compatible with the experimental data on which the order of magnitude condition, $\omega_i/\omega_c \doteq 1$, was based.

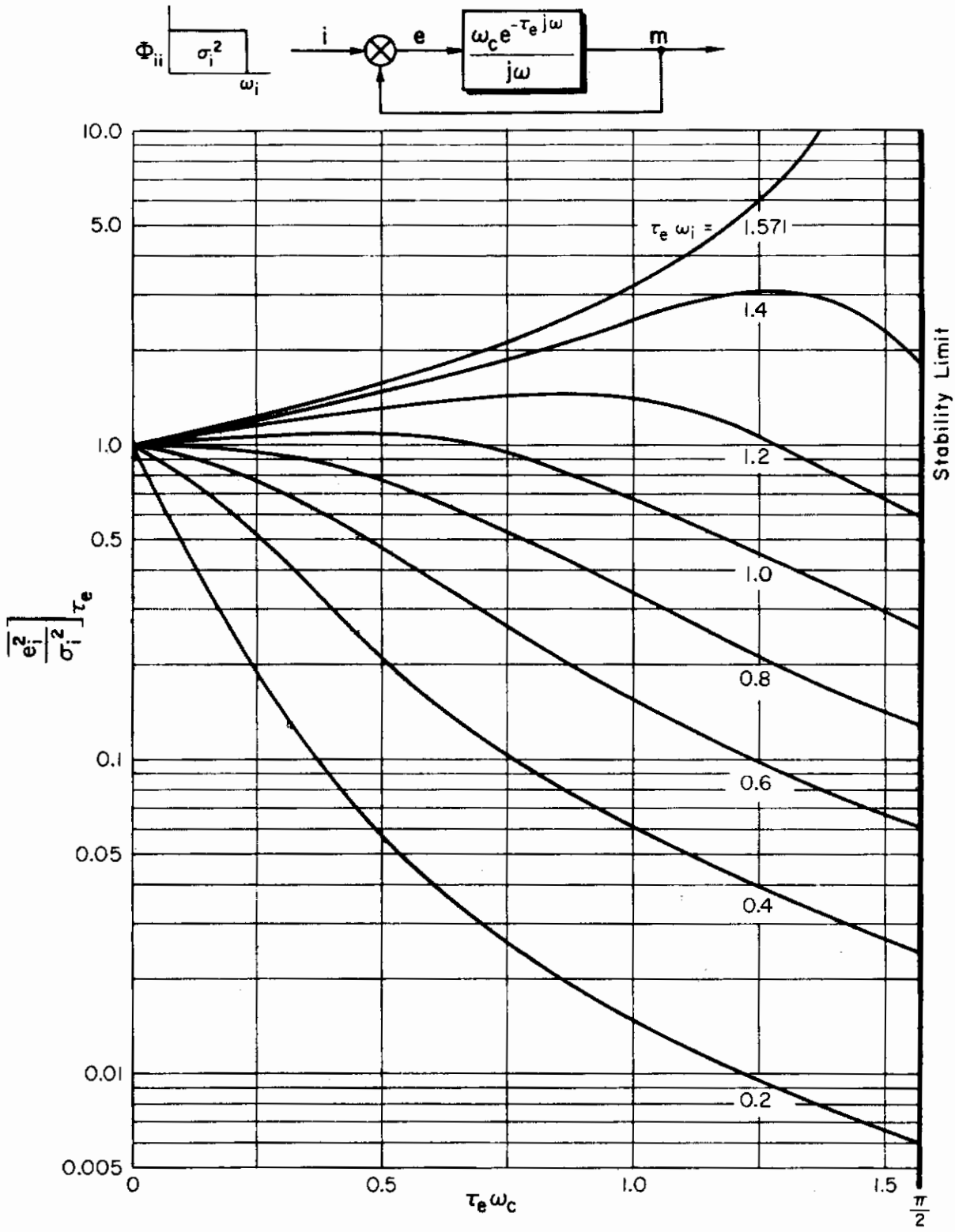

Figure 11. Mean-Squared Error Based on Crossover Model

CHAPTER IV

MEASUREMENT CONDITIONS, FORCING FUNCTIONS, AND TECHNIQUES FOR EQUIPMENT USAGE

The experimental portions of this study were intended to make explicit and to quantify those aspects of human adaptive behavior which can be demonstrated in essentially stationary experimental situations. Great emphasis was placed on the isolation and, wherever feasible, control of sources of variability so that the experimental findings could be presented, insofar as possible, in a deterministic rather than statistical fashion. This was accomplished by precise measurements, sometimes on two independent analysis machines; by using specially contrived experimental and measurement procedures; and by paying meticulous attention to details. These means have been successful enough to allow definitive results to be obtained using a restricted number of experimental runs.

The general measurements and task variables involved in the experiments are summarized in Fig. 12. The task variables under the experimenter's control are enclosed in dashed boxes; those actually controlled in this experimental series were the forcing function and controlled element. For the data to be discussed here, Y_c was set equal to K_c, $K_c/j\omega$, $K_c/(j\omega-1/T)$, $K_c/(j\omega)^2$, and $K_c/j\omega(j\omega-1/T)$. The basis for the selection of all these controlled elements has been laid in the previous chapter. The selection of i(t) will be discussed subsequently in this chapter.

The measurable signals in the control loop are characterized by power spectra such as Φ_{ee}, mean-squared values such as $\overline{e^2}$, and amplitude probability distributions such as p_e. The operator is characterized by the describing function Y_p and the remnant Φ_{nn}. These quantities are sufficient to completely define the man-machine system in spectral, average, and amplitude distribution terms. The key analyses necessary are those pertinent to determination of power spectra and cross spectra.

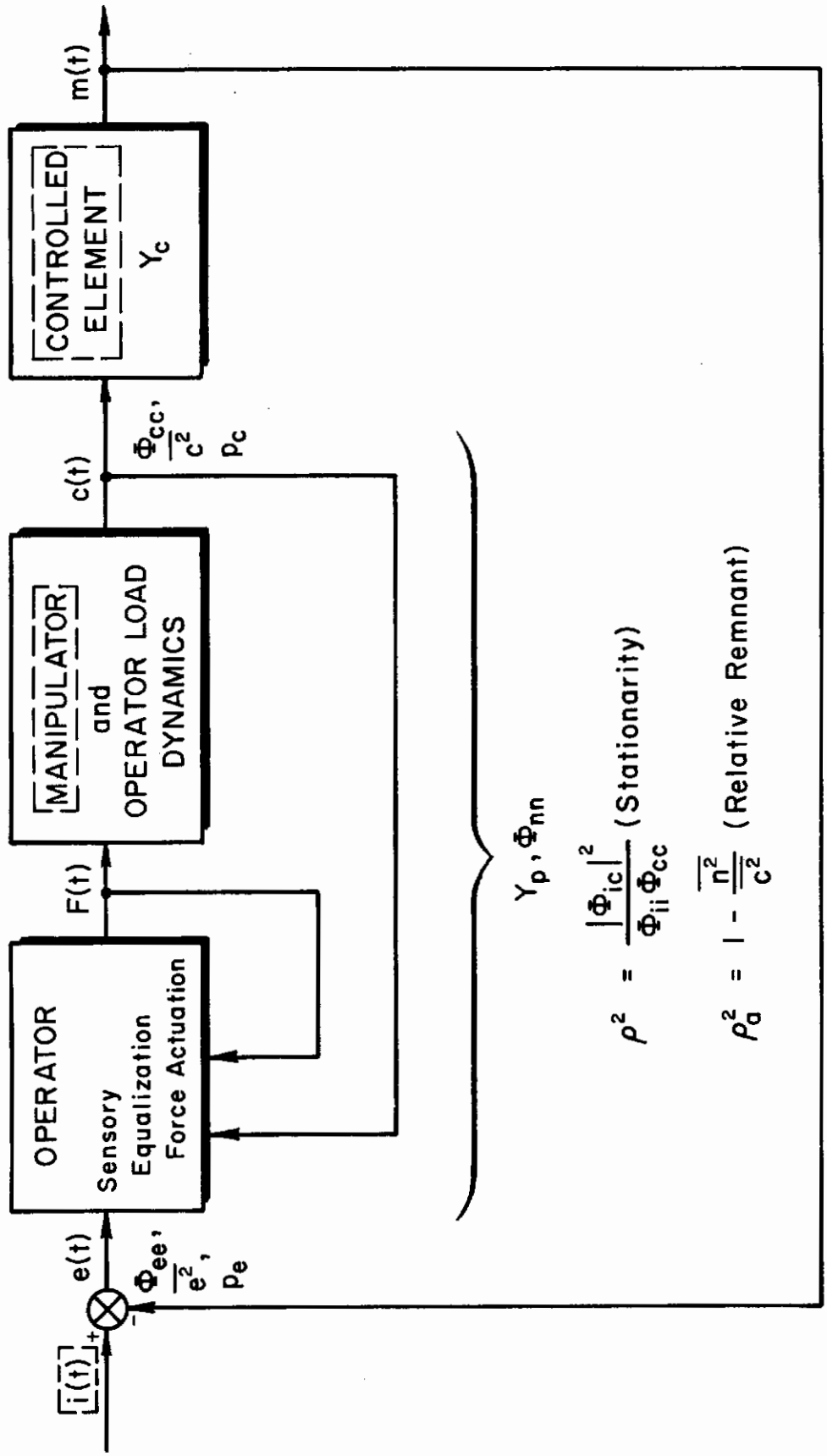

Figure 12. General Measurements and Task Variables

The analytical details involved in proceeding from the spectral quantities to describing function, remnant, etc., are so well known and documented (e.g., Refs. 13, 21, 24, 29, 34, 35, 50, 51, etc.) as to make detailed repetition here unnecessary. However, it is worth mentioning again that the correlation coefficient, ρ, as used in these experiments has been made especially sensitive to operator time variations by virtue of the forcing function type selected and the analyzer used. Also, another dimensionless quantity, ρ_a, has been defined to indicate the relative amount of remnant in the total output. Finally, because both periodic and random time functions are present in the experimental systems, the power spectra may have two different natures, line and continuous. Terminology and definitions which are consistent with both possibilities are, therefore, needed. These are given below.

In general the symbol $\Phi_{xx}(\omega)$ will be used to denote the power spectral density of a time signal $x(t)$. In more compact style the power spectral density is also referred to as the power spectrum or, even more simply, as the spectrum. The autocorrelation function, $R_{xx}(\tau)$, of the same signal is defined to be

$$R_{xx}(\tau) = \lim_{T \to \infty} \frac{1}{2T} \int_{-T}^{T} x(t)x(t+\tau)\, dt$$

$$= \overline{x(t)x(t+\tau)} \qquad (38)$$

The power spectral density is proportional to the Fourier cosine transform of the autocorrelation function, $R_{xx}(\tau)$, i.e.,

$$\Phi_{xx}(\omega) = 4 \int_{0}^{\infty} R_{xx}(\tau) \cos \omega\tau \, d\tau \qquad (39)$$

The mean-squared value of the time signal will be

$$\overline{x^2} = \frac{1}{2\pi} \int_{0}^{\infty} \Phi_{xx}(\omega)\, d\omega$$

$$= R_{xx}(0) \qquad (40)$$

The definition used above for the Fourier Transform is:

$$X(\omega) = \int_{-T}^{T} x(t) e^{-j\omega t}\, dt = 2 \int_{t_0}^{t_0+T} x(t) e^{-j\omega t}$$

$x(t) = 0$ except for $-T \le t \le T$

If x(t) is a periodic function,

$$x(t) = \sum_{m=1}^{M} \varphi_x(\omega_m) \sin(\omega_m t + \psi_m) \tag{41}$$

then the autocorrelation function is

$$R_{xx}(\tau) = \sum_{m=1}^{M} \frac{\varphi_x^2(\omega_m)}{2} \cos \omega_m \tau \tag{42}$$

and the power spectral density, considering only positive frequencies, will be

$$\Phi_{xx}(\omega) = \pi \sum_{m=1}^{M} \varphi_x^2(\omega_m)\delta(\omega - \omega_m) \tag{43}$$

The magnitudes of the delta function spectral lines in Φ_{xx} are π times the square of the peak amplitudes of the sinusoidal components in x(t). When plots representing the line spectra are made, the actual quantities used are $\varphi_x^2(\omega_m)$, expressed in power db, i.e., 10 $\log_{10} \varphi_x^2$. The mean square of x(t), following Eq 40, is

$$\overline{x^2} = \frac{1}{2\pi} \int_0^\infty \pi \sum_{m=1}^{M} \varphi_x^2(\omega_m)\delta(\omega - \omega_m)\, d\omega$$

$$= \frac{1}{2} \sum_{m=1}^{M} \varphi_x^2(\omega_m) \tag{44}$$

When x(t) is a stationary random function the autocorrelation function definition remains unchanged, and the power spectral density definition based on the autocorrelation, Eq 39, and the mean-squared value expression, Eq 40, are also unmodified. The form of the power spectral density will, however, be entirely different from the sum of delta functions occurring for the periodic case, i.e., the power spectral density will be continuous. If, for one reason or another, the component

of the power spectral density which is due to a random component in x(t) is required to be specifically identified, then the notation φ_{xx} is used. Thus, if both periodic and random components appear in x(t), the power spectral density will be

$$\Phi_{xx}(\omega) = \varphi_{xx}(\omega) + \pi \sum_{m=1}^{M} \varphi_x^2(\omega_m)\delta(\omega - \omega_m) \qquad (45)$$

Power db are also used for plots of $\varphi_{xx}(\omega)$, i.e., 10 $\log_{10}$ $\varphi_{xx}(\omega)$.

The experimental measurement of the quantities summarized above is critically dependent on the manner in which the measurements are executed and on the apparatus associated with the control tasks and signal analysis. This chapter is therefore devoted to descriptions of the physical layout and equipment, the task variables (forcing function and controlled element), the measurement situations and data presentation conventions, and other empirical aspects. Particular attention is given to the description of special procedures evolved in the course of the program to avoid pitfalls or to increase the reliability of the data.

A. PHYSICAL LAYOUT AND EQUIPMENT

The experiments were performed in a laboratory area consisting of two connected rooms. The larger of the two rooms contains all of the electronic equipment for performing and analyzing the experiments. The smaller room contains the manipulator and display. In this way, the operator is isolated from the measuring equipment and other disturbances. An intercom is used for communication between operator and experimenter.

The experimental equipment consists mainly of three basic systems. The first is the watt-hour meter analyzer shown in Figs. 13 and 14. This is an analog device capable of computing the cross spectra between the forcing function and two other functions at each of the ten frequencies contained in the input, in real time. This device is more extensive than, but is otherwise similar to, apparatus originally used by Russell (Ref. 47) to obtain human response measurements. It contains ten sinusoidal function generators, Fig. 13, from which the forcing function is

synthesized. Since a separate signal is available at each of these frequencies (both sine and cosine components), the calculation of the cross spectrum between the forcing function and another signal is relatively simple (see Refs. 44 and 51). At each of the input frequencies, a multiplier and an integrator are required for the real and imaginary parts. These functions are provided by watt-hour meters, Fig. 14. The use of these devices makes possible simultaneous computation of cross spectra at all input frequencies. The limitations of this equipment are that measurements are restricted to input frequencies and it is not possible to measure power spectra. The major use of this equipment is to calculate the describing function during the actual experiment, so that the results are immediately available. Mean-squared error, $\overline{e^2}$, and operator output, $\overline{c^2}$, are also measured by other watt-hour meters in the same gear.

The second system is the magnetic tape recording equipment, Fig. 15. During an experiment the forcing function, i(t); error signal (input to operator), e(t); operator's output, c(t); and controlled element output (system output), m(t), are recorded on tape. These signals are later transcribed onto a continuous tape loop which provides repetitive data for further processing.

The third basic component of the data reduction equipment is the spectral and cross-spectral analyzer (Ref. 57). Besides providing an alternative means for cross-spectrum measurement, this equipment (Fig. 16) fills the need for the additional measurements of power spectra needed for remnant calculations. It is capable of computing the cross spectrum between any two signals without necessarily requiring the forcing function to be made up of sinusoids. However, because of its sequential operation, the input data must be repeated once for each frequency for which a value is desired, so that on-line operation is not possible. Input data for this analyzer are obtained from the magnetic tape recordings. From these tapes are obtained the correlation coefficient, the describing function calculations for corroboration of the watt-hour meter analyzer results, and remnant spectra as print-outs on a paper tape.

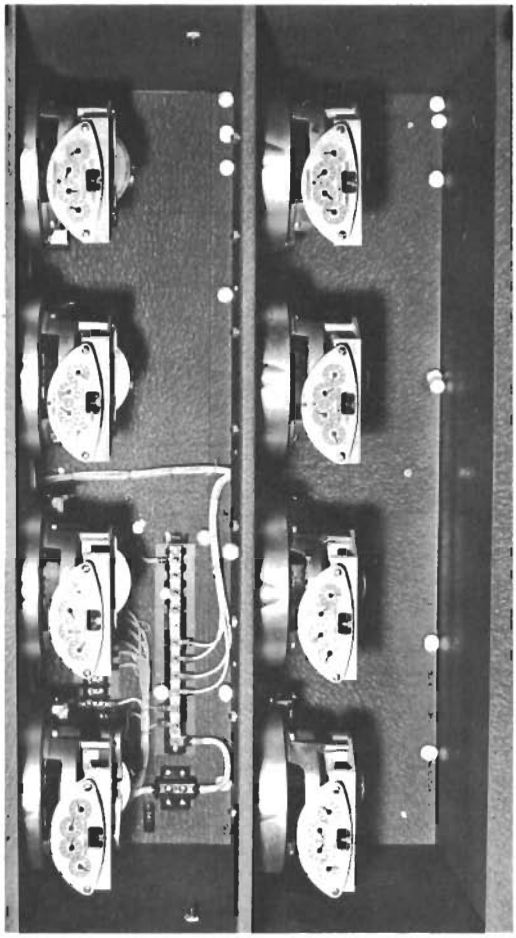

FIGURE 14. WATT HOUR METER BOX

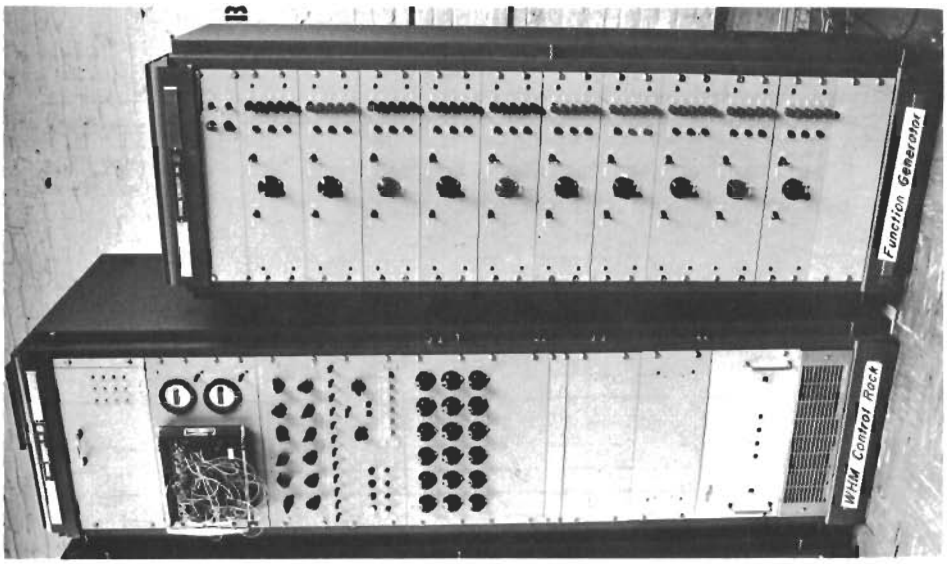

FIGURE 13. WATT HOUR METER ANALYZER CONTROL RACK AND FUNCTION GENERATOR

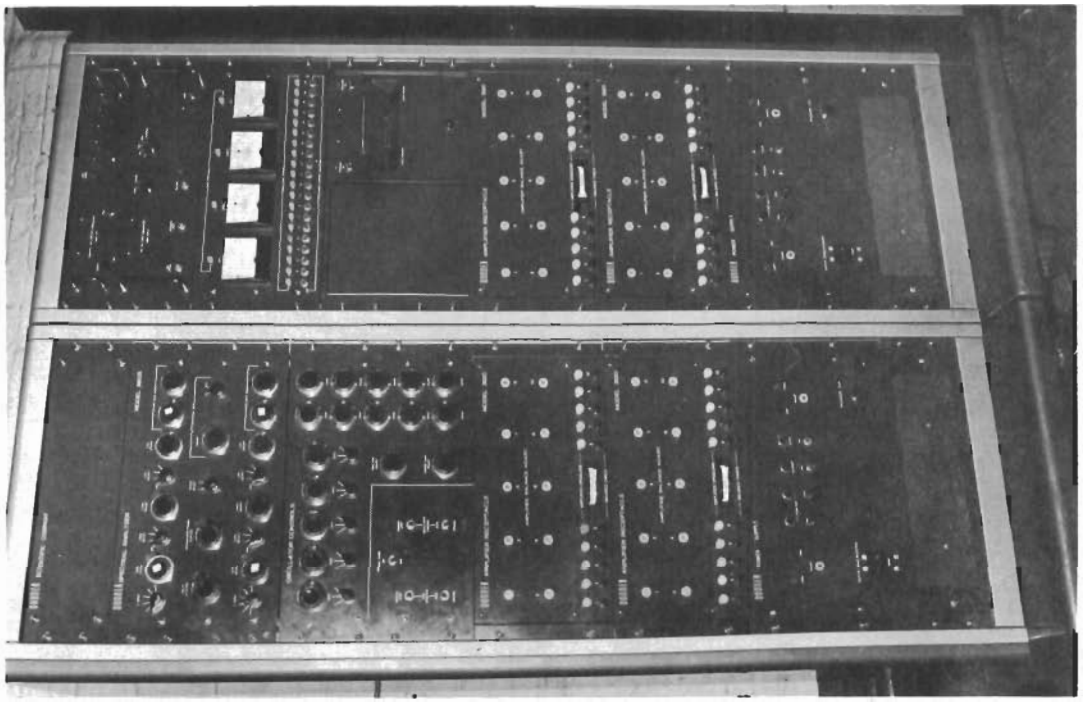

FIGURE 16. CROSS SPECTRAL ANALYZER

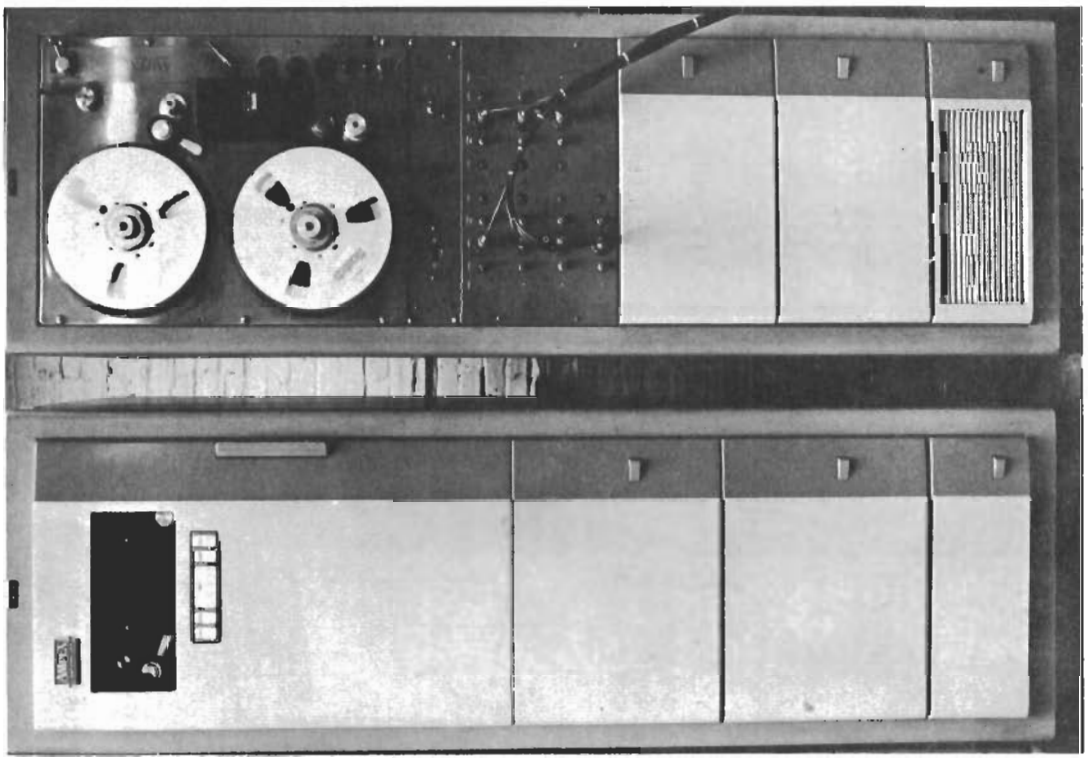

FIGURE 15. TAPE RECORDING EQUIPMENT

The controlled element is generated with an analog circuit. This circuitry is contained in a separate rack (Fig. 17). By switching feedback components, a variety of response characteristics can be obtained. These include the limiting cases used for the majority of experiments, K_c, $K_c/j\omega$, and $K_c/(j\omega)^2$, and the unstable cases which approach $K_c/j\omega$ and $K_c/(j\omega)^2$ as $1/T$ approaches zero, $K_c/(j\omega - 1/T)$ and $K_c/j\omega(j\omega - 1/T)$.

The manipulator used for these experiments (Fig. 18) was designed to exhibit the minimum possible inertia and damping, so that it behaved essentially as a spring restraint. Only the lateral degree of freedom (for transverse or roll control) was used in this experimental series. The stick was manipulated to minimize the error, displayed on a 6" oscilloscope face as the horizontal distance of a spot from the center.

In order to estimate the accuracy with which describing functions can be measured using this equipment, an extensive series of tests were performed (Refs. 44–46). The results of these tests indicate an accuracy for both the watt-hour meter analyzer and the spectral and cross-spectral analyzer of about 0.5 db in amplitude and 4^o in phase angle over a dynamic range of 40 db in amplitude and a frequency range of 2 decades (0.14 to 14 rad/sec). Typical measurements are shown in Fig. 19. For these, the tracking loop contained only the controlled element, which was set to give the indicated transfer functions. Excellent agreement was obtained between the two analyzers and the theoretical response for the known controlled elements.

B. DESCRIPTION OF THE FORCING FUNCTION

Since the watt-hour meter analyzer can measure only at the forcing function frequencies, the selection of these frequencies and the forcing function spectral shape is of great importance in minimizing measurement variability. In Refs. 21, 40, 41, and 54 conditions pertinent to the use of deterministic signals to simulate random-appearing signals having Gaussian amplitude distributions are presented. Requirements for independence of sine waves and appropriate choice of run lengths for minimizing the measurement error are discussed in detail. In Ref. 54

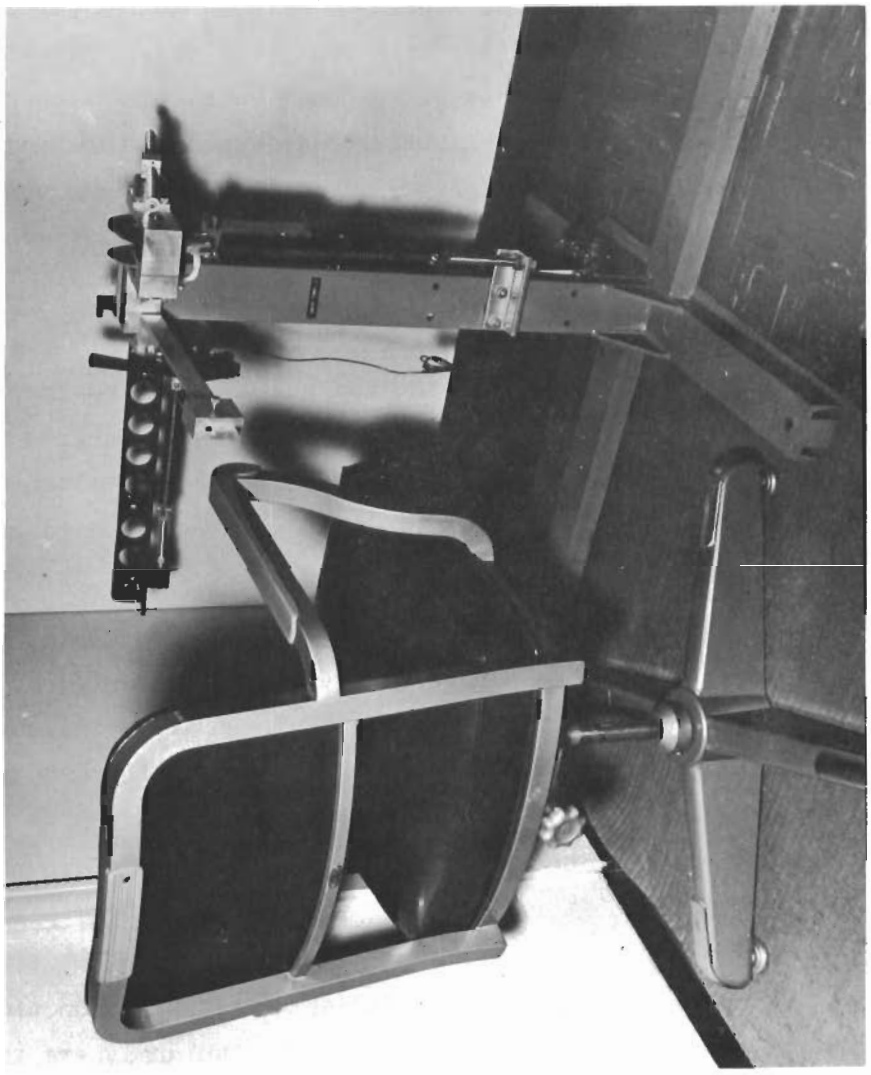

FIGURE 18. MANIPULATOR

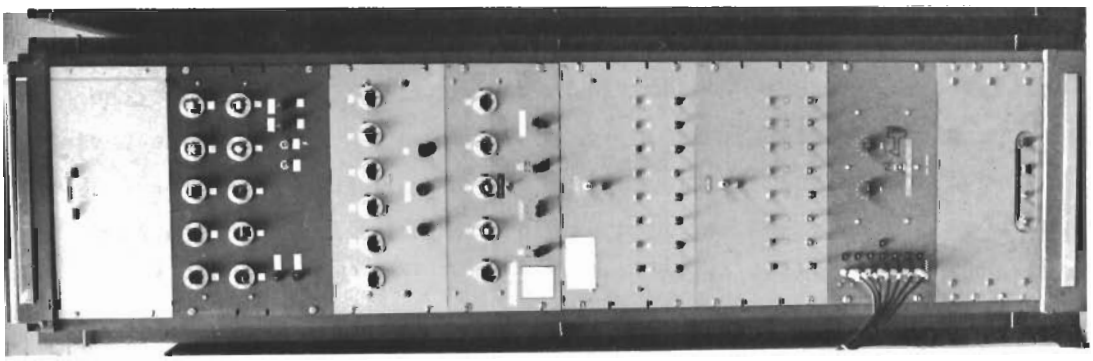

FIGURE 17. CONTROLLED ELEMENT SIMULATOR

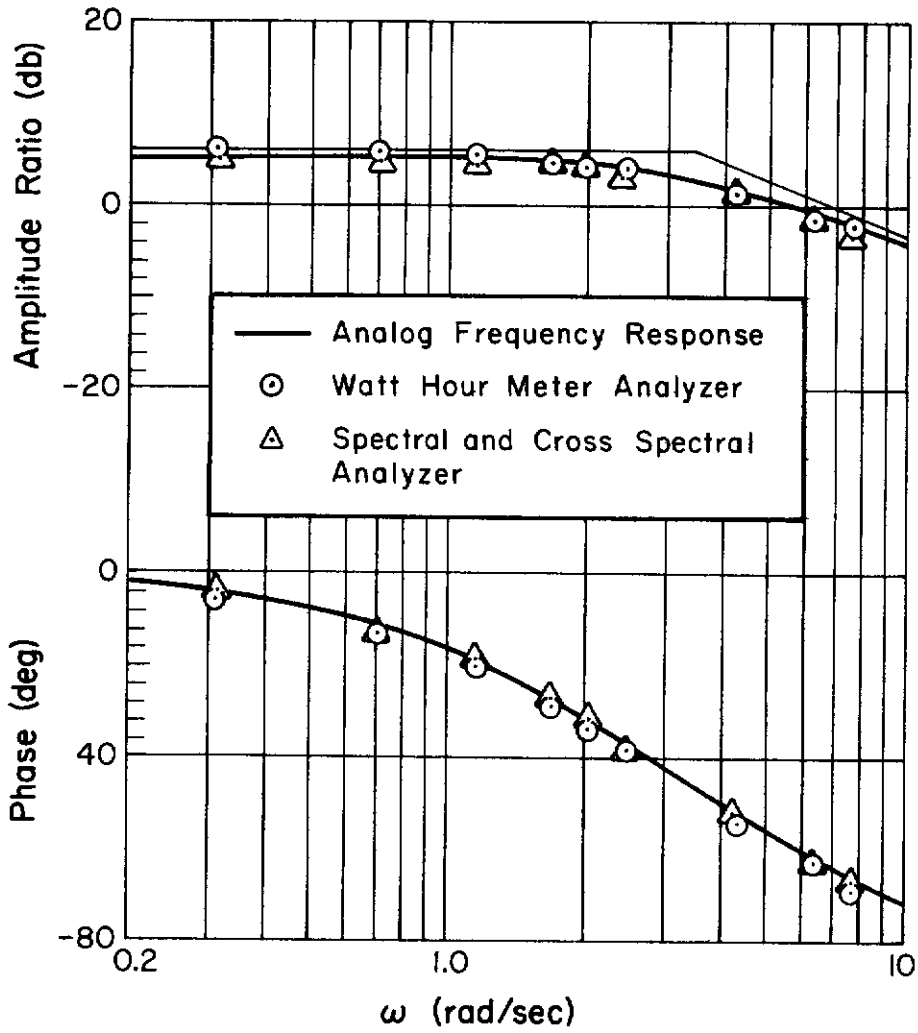

Figure 19. Accuracy and Compatibility of Analyzers

it is shown that a close approximation to a Gaussian amplitude distribution can be achieved when as few as five properly chosen independent sine waves are summed. Therefore the ten independent signals available are more than adequate, and even allow some flexibility.

The desirable characteristics of a forcing function composed of independent sine waves, and to be used for human response studies, can be specified as:

1. Random-appearing, so that the operator cannot detect any internal coherence in the forcing function and thereby adopt a higher level of behavior

2. Having a Gaussian amplitude distribution, so that Gaussian-input describing function theory may be used
3. Extending over about 2 decades, including low frequencies below 0.5 rad/sec
4. Having a simply definable cutoff frequency
5. Providing energy in the crossover range without disturbing the operator's low frequency performance
6. Being composed of low frequency sine waves which are integral multiples of the run length to minimize averaging error

The forcing function, i(t), selected for the set of experiments described in this report — the so-called augmented rectangular input spectrum — conforms to these requirements. This input is designated ω_i, σ_i where ω_i is the cutoff frequency in radians/second and σ_i is the rms amplitude of this input as measured on the pilot's display. Ordinarily, σ_i was 1/2", so σ_i is specified in our notation only when it differs from 1/2". The frequency setting, ω_n, and the number of periods for each component in the fixed 240-sec run length, T_R, are as follows:

ω_n	$n = T_R\omega_n/2\pi$
0.157	6
0.262	10
0.393	15
0.602	23
0.969	37
1.49	57
2.54	97
4.03	154
7.57	289
13.8	527

Three ω_i values were used — 1.5, 2.5, and 4.0 rad/sec. For the ω_i, 1/2" forcing function, ω_i alone characterizes i(t). To define these three inputs, the amplitudes at the lowest six, seven, or eight frequencies were set equal, for cutoff frequencies of 1.5, 2.5, or 4.0 rad/sec,

respectively. The amplitudes of the remaining frequencies were set to one tenth of the low frequency amplitudes (20 db attentuation). The logarithmic spacing (which facilitates fitting theoretical curves to the measured values) was selected to insure the effective independence of the sine wave components over the run length of interest.

Figure 20 shows measurements of the three forcing functions which illustrate the augmentation of the well-defined rectangular cutoff frequency spectral shape by a series of very low energy signals extending up to 13.8 rad/sec. Specific tests were performed to assure that

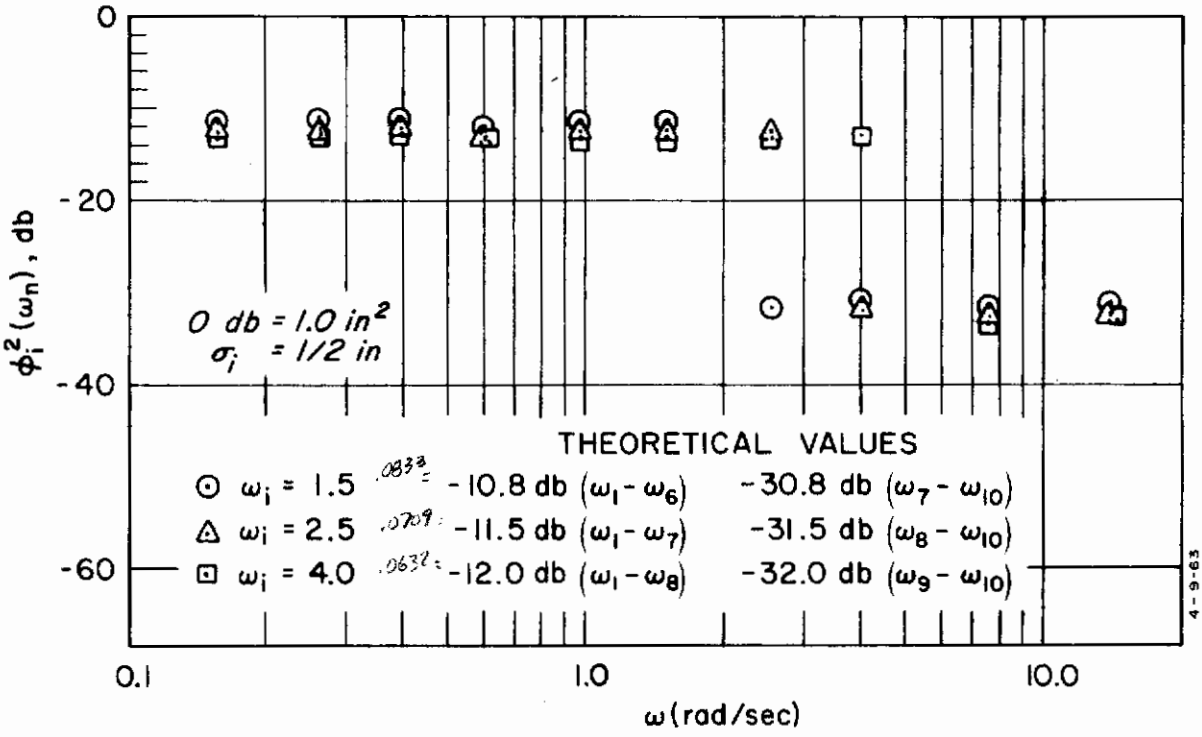

CAUTION! $(\phi_i^2(\omega_n))_{db} = 10 \log_{10}(\phi_i^2(\omega_n))$ - Power db. Figure is correct!

Figure 20. Measured Input Power Spectra Magnitudes

these forcing function spectra were indeed nearly Gaussian. Figure 21, which is representative of the data for $\omega_i = 1.5$ and $\omega_i = 4.0$ as well, is a plot on probability paper of the cumulative probability distributions for seven $\omega_i = 2.5$ inputs. A straight line is produced by a Gaussian distribution. Amplitude distribution analyses were also made

for these three inputs using a chi-squared test (e.g., Ref. 23). These indicate that the inputs are all Gaussian at the 0.05 level.

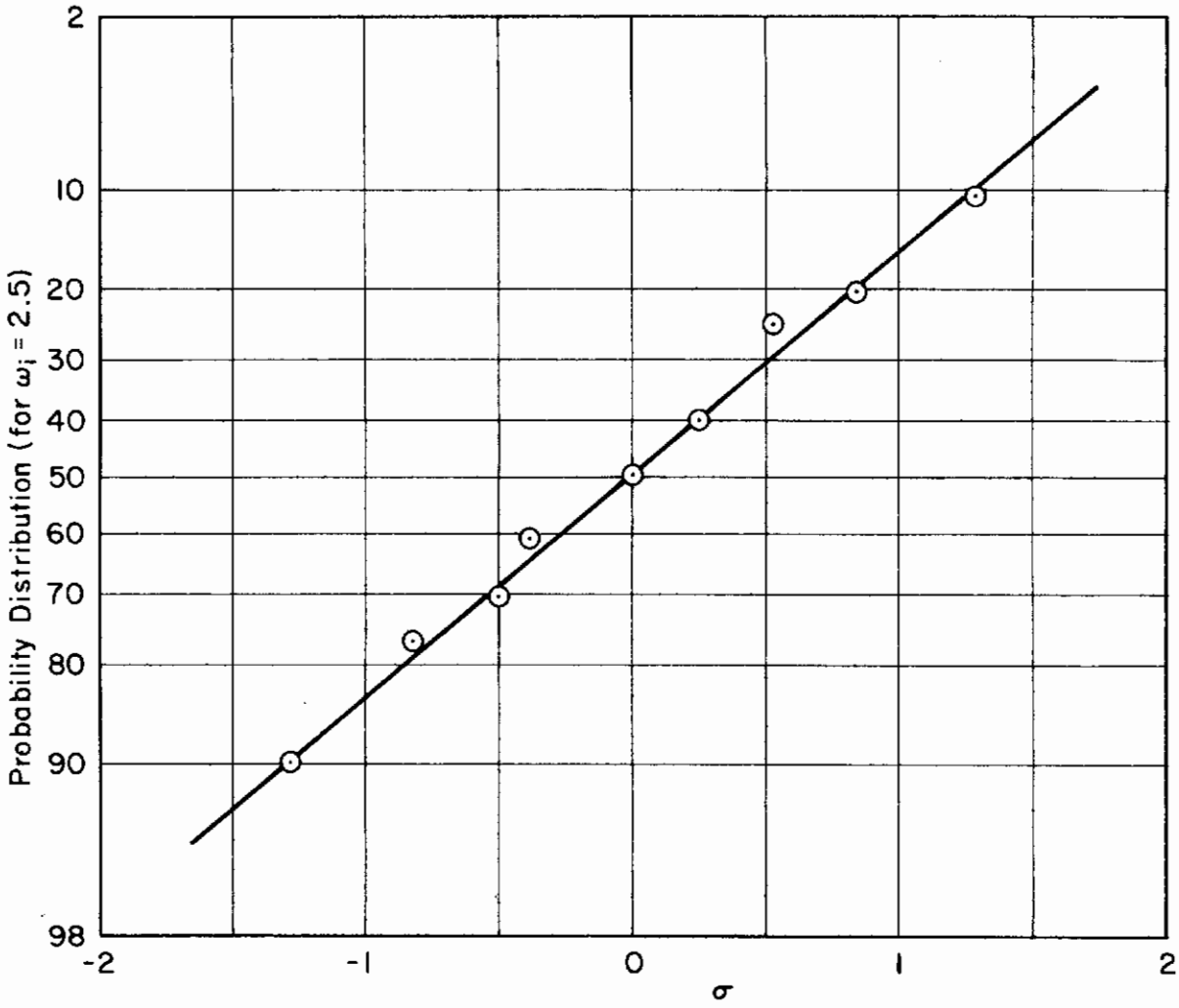

Figure 21. Measured Cumulative Probability Distribution of Forcing Function Amplitude

For each of the forcing functions, the chi-squared test for goodness of fit to a Gaussian distribution used, as a null hypothesis, the hypothesis that any difference between the observed distributions and the Gaussian distribution was the result of chance forces. For this test,

$$\chi^2 = \sum_{i=1}^{k} \frac{(O_i - A_i)^2}{A_i} \qquad (46)$$

where O_i represents the observed measurements in a given category, which is a decile here, and A_i is the number of observations expected in a decile if the distribution is Gaussian with the measured mean and variance. Because the categories used were deciles, k = 10. Since the Gaussian distribution has two parameters and these parameters are unknowns in this case, there are seven degrees of freedom. Using this hypothesis as the test hypothesis, any difference between the observed distributions and the Gaussian distribution which turned out to be significant, i.e., not Gaussian at, say, the 0.05 level of significance, could be expected to occur only one time in twenty (5 percent) or less if solely chance forces caused that difference. All of the chi-squared tests for individual inputs, i.e., five 1.5, seven 2.5, and three 4.0 forcing function samples, failed to reject the null hypothesis. The chi-squared values were then averaged, and these averages are plotted, together with the ranges, in Fig. 22.

The augmented rectangular forcing function shape was, of course, intended to overcome the past deficiencies in human response data due to their limited frequency range and to the lack of precise measurements in the critical crossover region. Hopefully, the tiny high frequency forcing function components greater than ω_i do little to disturb the operator's low frequency performance. Ideally, the low frequency characteristics should be substantially the same as those measured with a pure rectangular forcing function spectra, i.e., without the augmentation frequencies.

In order to demonstrate the relative lack of influence of the low energy higher frequency signals on the low frequency describing function behavior, we refer to Elkind's definitive set of data for $Y_c = 1$ (Ref. 13). Figure 23 shows Y_p for Elkind's R.40 forcing function—a pure rectangular forcing function spectra consisting of 40 equally spaced equal-amplitude sine waves up to $\omega_i = 2.5$ rad/sec and of 1.0 inches rms magnitude—and Y_p for Elkind's B-6 forcing function

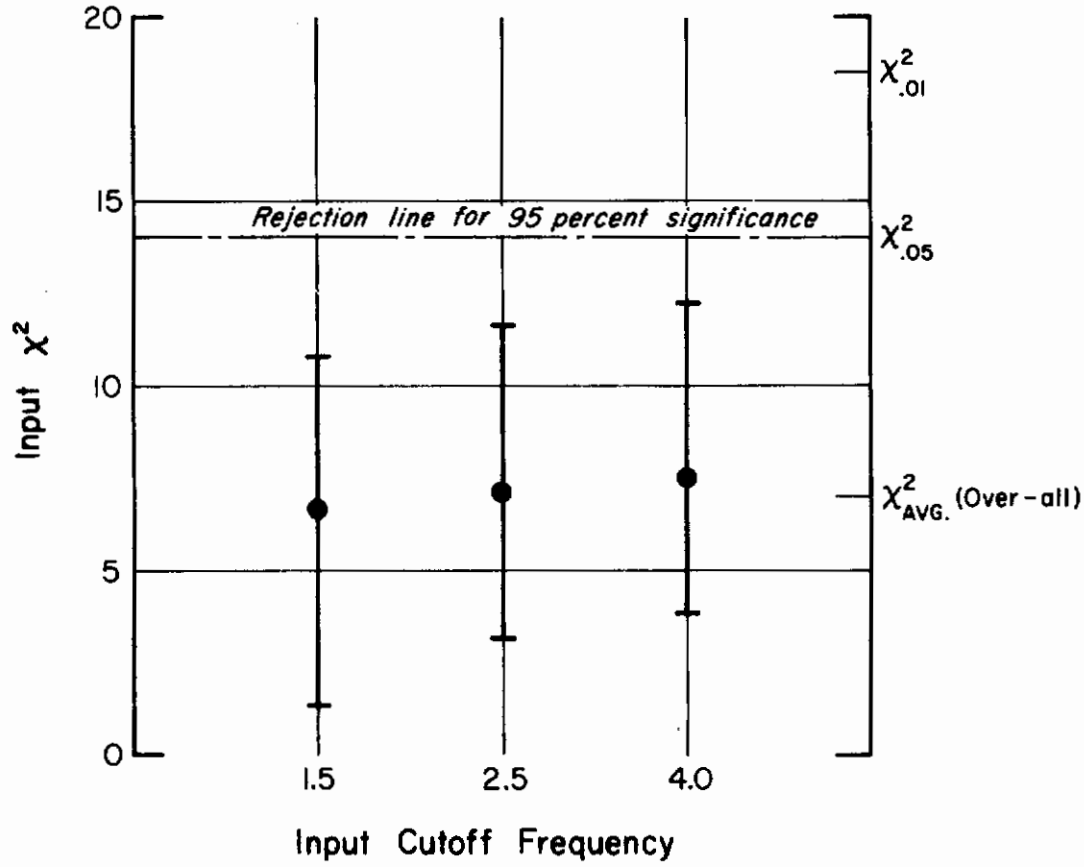

Figure 22. Average χ^2 Values for Augmented 1.5, 2.5, and 4.0

which was an augmented rectangular forcing function spectra composed of 144 sinusoids and equivalent to ω_i = 3.0, 1" in our notation. It will be noted that the B-6 data provide a convincing extrapolation of the R.40 data to the crossover frequency. Subsequently we shall demonstrate that the $Y_c = K_c$ data developed in the current program are compatible with Elkind's data. It therefore follows that the augmented rectangular forcing functions used here provide a reasonable extrapolation of low frequency measurements to and beyond the crossover frequency and that the high frequency shelf does not materially affect the operator's behavior.

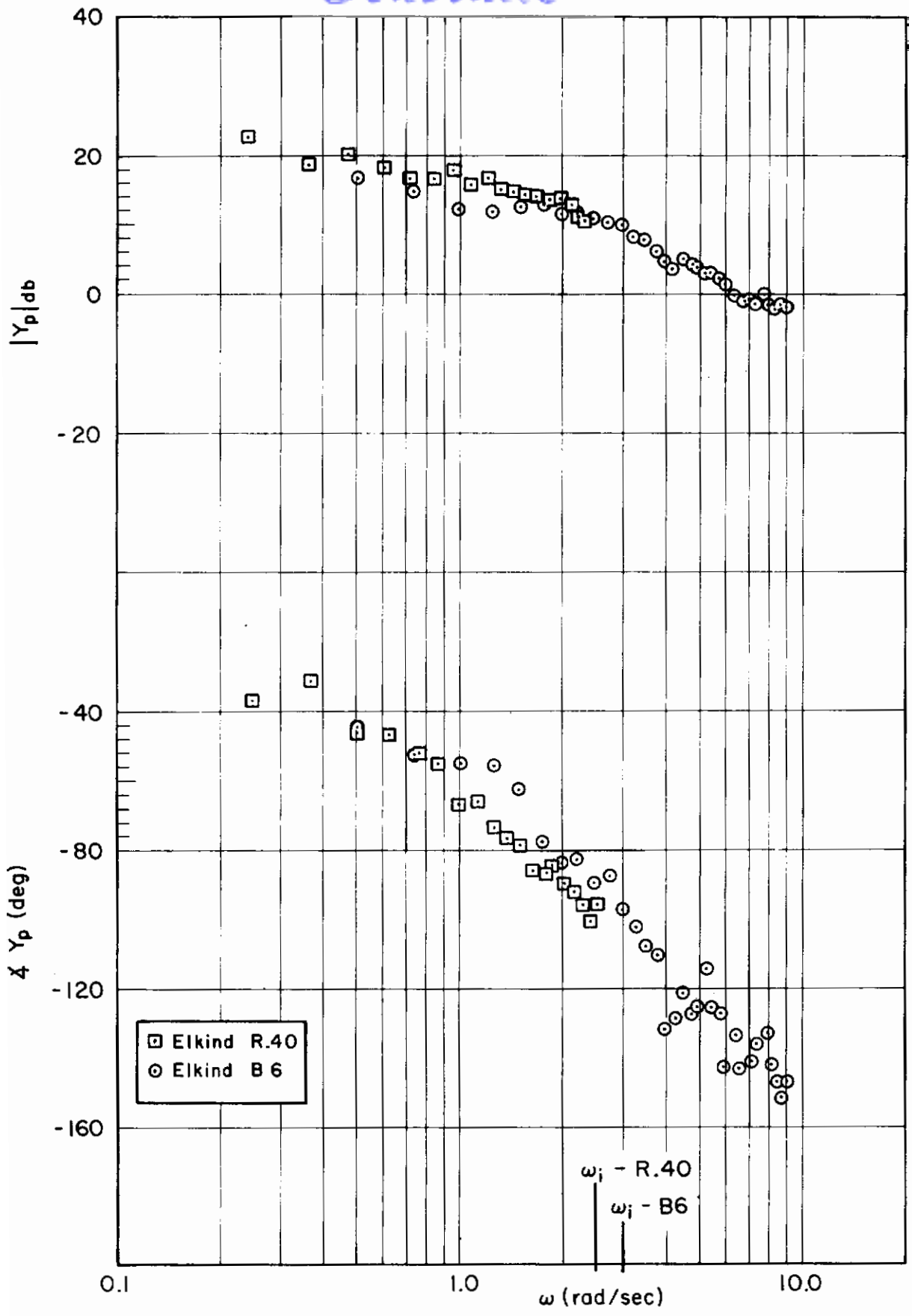

Figure 23. Comparison of Elkind's Data
for Rectangular (R.40) and Augmented (B-6) Forcing Functions

C. MEASUREMENT SITUATION AND DATA PRESENTATION CONVENTIONS

The measurement situation was as follows. The pilot manipulated a stick (Fig. 24) which produced, as an electrical output signal, the pilot's output, c(t), which was fed to the controlled element, Y_c (refer to Fig. 12). The damping and inertia of this stick were made as low as possible.

The circuit gains were set to give the following deflection sensitivities on the display for a pure gain controlled element of unity:

K_s = 1 inch (display)/6 deg (stick)

F_s = 2.21 oz/deg stick (applied with a 4 inch moment arm)

With the 4 inch moment arm, lateral motion of the operator's hand amounts to about 0.07 inches (stick) per degree of stick rotation. Accordingly, the sensitivity can be expressed in terms of the linear motion of the operator's hand by dividing the angular sensitivity (in inches per radian) by the moment arm, i.e.,

$$K_s = 1 \text{ inch}/6 \text{ deg} \times 57.3 \text{ deg/rad} \times 0.25 \text{ inch}^{-1} = 2.38 \text{ inches/inch}$$

For a pure gain controlled element with gains other than unity, the actual displacement on the display as a result of a stick displacement was the value given above, K_s, multiplied by the controlled element gain, K_c. In summary, for pure gain controlled elements:

$K_c = 1$: $K_s = 0.167$ inches/deg
or $K_s = 2.38$ inches/inch (4 inch moment arm)
$K_f = 0.0754$ inches/oz

$K_c \neq 1$: $K_s = 0.167 K_c$ inches/deg
or $K_s = 2.38\ K_c$ inches/inch
$K_f = 0.0754 K_c$ inches/oz

For frequency-dependent controlled elements the dynamics of the controlled element intervene between the stick output and the display. The

deflection sensitivities, when referred to the display as a commpon point, then become dynamic entities. So, for a unit step displacement of 1 deg applied to the stick the deflection on the scope will be $0.167\,\mathcal{L}^{-1}[Y_c/s]$ if this convention is used.

For convenience and simplicity it is much easier to think of the deflection sensitivities in terms of the steady-state characteristics which are ultimately approached after a unit stick deflection. For this type of description the appropriate expressions are

$$K_s = 0.167\,\left[s^k Y_c(s)\right]_{s=0} \quad \text{inches/deg}$$
$$K_s = 2.38\,\left[s^k Y_c(s)\right]_{s=0} \quad \text{inches/inch}$$
$$K_f = 0.0754\,\left[s^k Y_c(s)\right]_{s=0} \quad \text{inches/oz}$$

where k is the order of the free s term in Y_c

For example, if $Y_c = K_c/s$ the deflection sensitivity will be $0.167 K_c$ inches/sec (display)/deg (stick). The expressions above are adequate to characterize system gains even when the controlled element is unstable, for although a "steady-state" never occurs there is still a definable "steady-state" component in the response.

Further conversion factors can be defined based on the operator's eye to scope distance of about 29 inches.

Roll axis control using the stick was accomplished by grasping the control handle and exerting lateral force on it, as illustrated in Fig. 24.

The output of the controlled element (system output), m, was subtracted from the input forcing function to produce the error signal, e. This function was displayed to the operator on the oscilloscope. Because the watt-hour meters must operate at 60 cps, part of the control loop used a 60 cps carrier. The signals from the d-c portion of the loop were fed to the tape recorder for future processing. The error and pilot's output signals were passed through pre-emphasis networks before recording in order to increase the signal-to-noise ratio on the tape at high frequencies.

The computation time for the experiment was accurately controlled, equal to an integral number of periods of the input frequencies. Prior

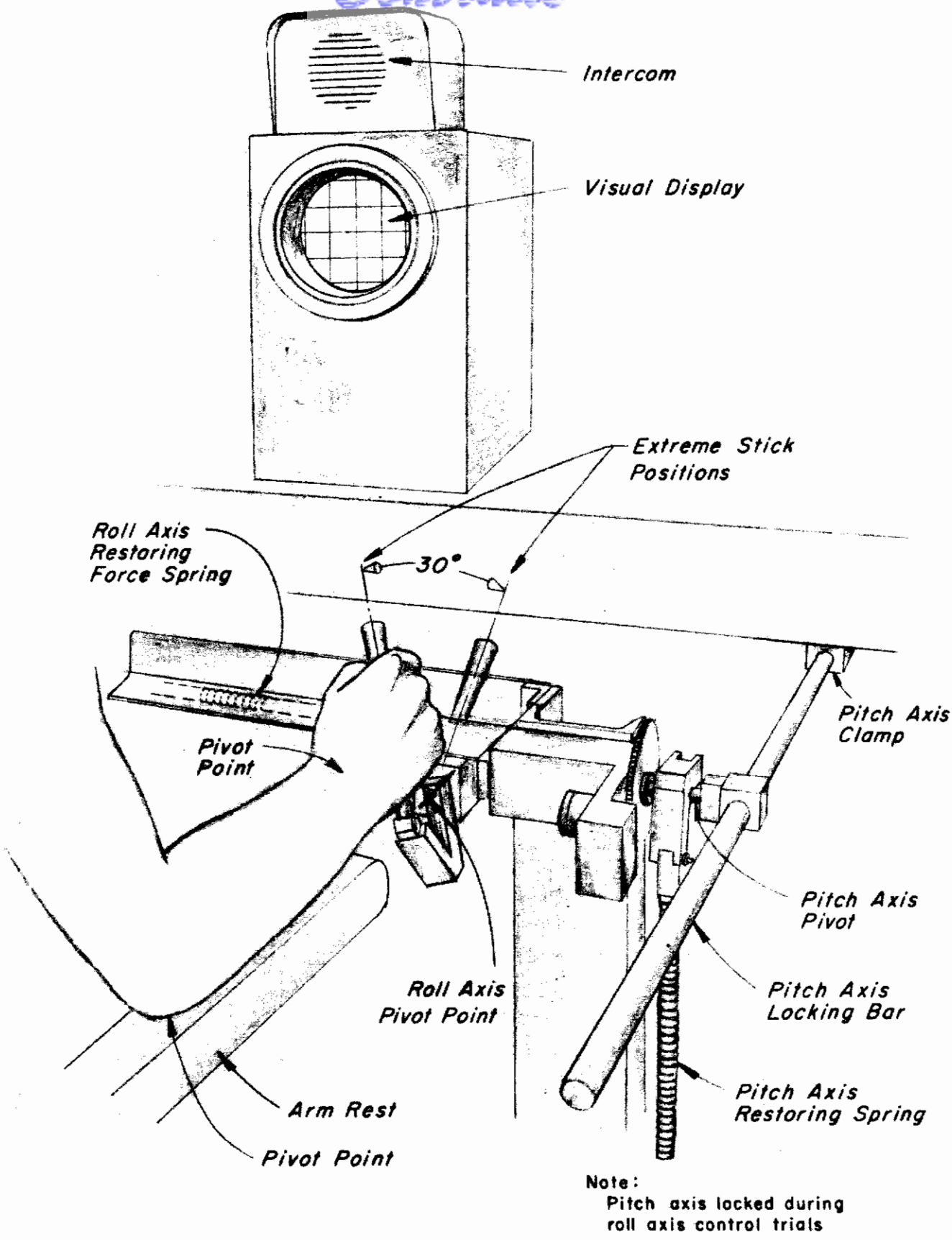

FIGURE 24. STICK MANIPULATOR

to the beginning of the computation, 10 to 15 sec were allowed for the operator to reach a stable tracking condition. Before and after each experiment, the readings of the watt-hour meters were recorded. From these, the operator's describing function was calculated at each of the input frequencies.

The Y_p data have generally been presented as dimensionless quantities. To do this, the describing function has been defined in terms of the pilot's output and error signals, referred to deflection on the display (in inches). Similarly, the power spectral densities are referred to the display and are expressed in units of square inches per radian per second.

In cases where the power spectral density has both a continuous portion and discrete lines, the line components are plotted as if the total power in the line were distributed over the bandwidth of the measuring equipment. In this way the integrated spectrum still gives the total power, but the peak amplitude shown for the line has no significance.

D. MEASUREMENT TECHNIQUES

In processing the data, cross spectra have been computed between the input function and the signal to be analyzed. From these it is possible to compute the describing function:

$$Y_p = \frac{\Phi_{ic}(\omega_n)}{\Phi_{ie}(\omega_n)} \qquad (47)$$

Using this technique, the effects of signal components at other frequencies or of a random nature are minimized, since these are uncorrelated with the input and tend to average out. It is possible that the describing function may not be stationary but may exhibit a low frequency time dependence. In these cases the computed value of Y_p is an average value for the length of the experiment.

A slight modification has been made to the Y_p calculation for the results from the spectral and cross-spectral analyzer. Since the frequency at which the measurement is made is set independently of the input function generator, a slight error in the setting will affect the results.

To eliminate this, the ratio of the cross spectrum to the input power spectrum was calculated for each signal, and these ratios were then used to calculate Y_p:

$$Y_p = \frac{\Phi_{ic}(\omega_n)/\Phi_{ii}(\omega_n)}{\Phi_{ie}(\omega_n)/\Phi_{ii}(\omega_n)} \qquad (48)$$

The bulk of the describing function data presented in this report has been calculated from the watt-hour meter results. In certain cases the spectral and cross-spectral analyzer results have been used; mainly where the watt-hour meter results were inaccurate due to small signal levels. Generally, the describing function was calculated from watt-hour meter measurements of the error signal, e, and pilot's output, c. However, for many of the controlled elements that were used, this results in relatively inaccurate data at the lowest frequencies. For $Y_c = K_c/j\omega$ or $K_c/(j\omega)^2$ the controlled element gain is very large at low frequencies and very small at high frequencies. As a result, the operator is required to produce only small control deflections at low frequencies to obtain large system outputs, m(t). However, at high frequencies he must produce large output deflections in order to obtain reasonable system outputs. The power spectrum of the pilot's output, Φ_{cc}, then increases with frequency, with the major portion of his total output appearing near the input cutoff frequency. Conversely, the system output, Φ_{mm}, will be relatively flat at low frequencies and will decrease rapidly above crossover. Since it is necessary to adjust the analyzer gains to avoid saturation due to the large frequency components present, the very small components at low frequencies in the pilot's output do not produce sufficient deflections on the watt-hour meters to obtain accurate results. However, if the system output is used, correspondingly poor data will be obtained at high frequencies. For most of the measurements it was desired to obtain the best possible results near crossover, and for this reason the pilot's output was used in the analysis.

In certain cases, however, to clear up questions which arose about the low frequency behavior, the analysis was based on the system output. In particular, there was a strong indication that large phase delays

exist at low frequencies. These have been noted before and generally ignored (Ref. 34, Fig. 4-24C, for example). Measurement of Φ_{ic} resulted in too low an accuracy to determine if these delays actually existed or if they were due to measurement errors. The use of Φ_{im}, on the other hand, provided sufficient accuracy to verify their existence.

A similar problem was encountered when measuring the remnant with the spectral and cross-spectral analyzer. In this case, the existence of tape background noise and extraneous noise (such as that from the playback amplifiers) was sufficiently large to cause large errors at low frequencies for Φ_{cc} and at high frequencies for Φ_{mm}. Therefore, the measurements of Φ_{nn} and ρ were based on Φ_{mm} at low frequencies and Φ_{cc} at high frequencies.

The inputs used made it necessary to include pre-emphasis of the error and pilot's output signals before recording to increase the amplitude of the high frequency components (above 4-6 rad/sec) by 20 db. Without it, the tape noise made it impossible to obtain good accuracy at input frequencies above cutoff, due to the 20-db drop in input amplitudes above this frequency. In addition, the pre-emphasis also increased the accuracy of the remnant measurements at high frequencies, since it effectively increased the signal-to-noise ratio at the input to the spectral and cross-spectral analyzer.

what effect does this have on the data presented in this 1947?

A large portion of the measurement program was based on calculations of the correlation coefficient, ρ, which can be measured with the spectral and cross-spectral analyzer. This value provides a means for estimating the degree of time variation in the operator's transfer function. However, the bandwidth of the measuring equipment must be considered in determining the precise meaning of a particular ρ value. For the spectral and cross-spectral analyzer two different bandwidths were used, depending on the spacing of the input frequencies and the stability of the equipment. Generally, for low frequencies the narrow bandwidth ($\Delta\omega_1$ = 0.141 rad/sec between 3-db points) was used, while for high frequencies the wide bandwidth ($\Delta\omega_2$ = 0.628 rad/sec) was used. Since the pilot's or system's output is approximately the sum of a line spectrum (linearly correlated with the input) and a random continuous spectrum, the correlated power measured by the spectral and cross-spectral

analyzer is independent of bandwidth, while the uncorrelated power is roughly proportional to bandwidth. Thus, the measured value of ρ for high frequencies (where the wide bandwidth is used) would appear to be smaller than those for low frequencies (where the narrow bandwidth is used). To avoid this discrepancy the high frequency values were corrected to be equal to the values that would have been measured if the narrow bandwidth had been used, even though they were actually measured with the wide bandwidth. To make this correction, the signal-to-noise ratio (correlated to uncorrelated power) at a frequency ω_n can be expressed as

$$\frac{\rho_1^2}{(1-\rho_1^2)} = \frac{\pi\varphi_c^2(\omega_n)}{\varphi_{nn}(\omega_n)\Delta\omega_1} \quad \text{for the narrow bandwidth} \tag{49}$$

$$\frac{\rho_2^2}{(1-\rho_2^2)} = \frac{\pi\varphi_c^2(\omega_n)}{\varphi_{nn}(\omega_n)\Delta\omega_2} \quad \text{for the wide bandwidth} \tag{50}$$

However, the ratio φ_c^2/φ_{nn} is independent of the measuring equipment, and can be eliminated between the two equations. This gives

$$\frac{\Delta\omega_1\rho_1^2}{(1-\rho_1^2)} = \frac{\Delta\omega_2\rho_2^2}{(1-\rho_2^2)} \tag{51}$$

or by rearranging

$$\rho_1^2 = \frac{1}{\left[1+\left(\frac{\Delta\omega_1}{\Delta\omega_2}\right)\frac{(1-\rho_2^2)}{\rho_2^2}\right]} \tag{52}$$

This equation can be used to calculate the value of ρ that would be measured with the narrow bandwidth, $\Delta\omega_1$, from the value, ρ_2, measured with the wide bandwidth, $\Delta\omega_2$. As a check, several values were actually measured with both bandwidths. The results were as follows:

ω_n	4.29	6.17
ρ_2 (wide bandwidth).....	0.906	0.910
ρ_1 (narrow bandwidth).....	0.973	0.972
ρ_1 (calculated from ρ_2)...	0.975	0.977

The close agreement between measured and calculated values of ρ_1 indicates the validity of the method.

Several methods were used to check the computing process — computing the transfer function of the known controlled element from measured data and computing the describing function by two different methods. The controlled element transfer function can be computed either from

$$Y_c = \frac{\Phi_{im}}{\Phi_{ic}} \tag{53}$$

or from

$$Y_c = \begin{cases} \dfrac{\Phi_{mm}}{\Phi_{mc}} & \text{at low frequencies} \\ \dfrac{\Phi_{cm}}{\Phi_{cc}} & \text{at high frequencies} \end{cases} \tag{54}$$

For the types of controlled elements of interest, neither of these gives very good results at the extremely low or high frequencies because of the signal levels discussed earlier. Similarly, the operator's describing function can be found from

$$Y_p = \begin{cases} \dfrac{1}{Y_c}\dfrac{\Phi_{im}}{\Phi_{ie}} & \text{at low frequencies} \\ \dfrac{\Phi_{ic}}{\Phi_{ie}} & \text{at high frequencies} \end{cases} \tag{55}$$

or from

$$Y_p = \frac{\Phi_{ec}}{\Phi_{ee}}\left\{\frac{1 + \left(\dfrac{1-\rho^2}{\rho^2}\right)|Y_pY_c|^2}{1 - \left(\dfrac{1-\rho^2}{\rho^2}\right)Y_p^*Y_c^*}\right\} \tag{56}$$

This second method is not convenient for calculating Y_p, but it serves as a computational check. The values of Y_p and Y_pY_c are found from the first method of computing Y_p and the theoretical value of Y_c. Using computed values of ρ and Y_pY_c and Eq 56, the ratio Φ_{ec}/Φ_{ee} can be calculated from

$$\frac{\Phi_{ec}}{\Phi_{ee}} = Y_p \left\{ \frac{1 - \left(\frac{1-\rho^2}{\rho^2}\right) Y_p^* Y_c^*}{1 + \left(\frac{1-\rho^2}{\rho^2}\right) |Y_pY_c|^2} \right\} \qquad (57)$$

This ratio can also be measured, and should agree with the calculated value. Extensive measurements of this type were made for one of the runs using $\omega_i = 1.5$, 1/4" with a $Y_c = K_c/(j\omega)^2$. The results are shown in Figs. 25 and 26.

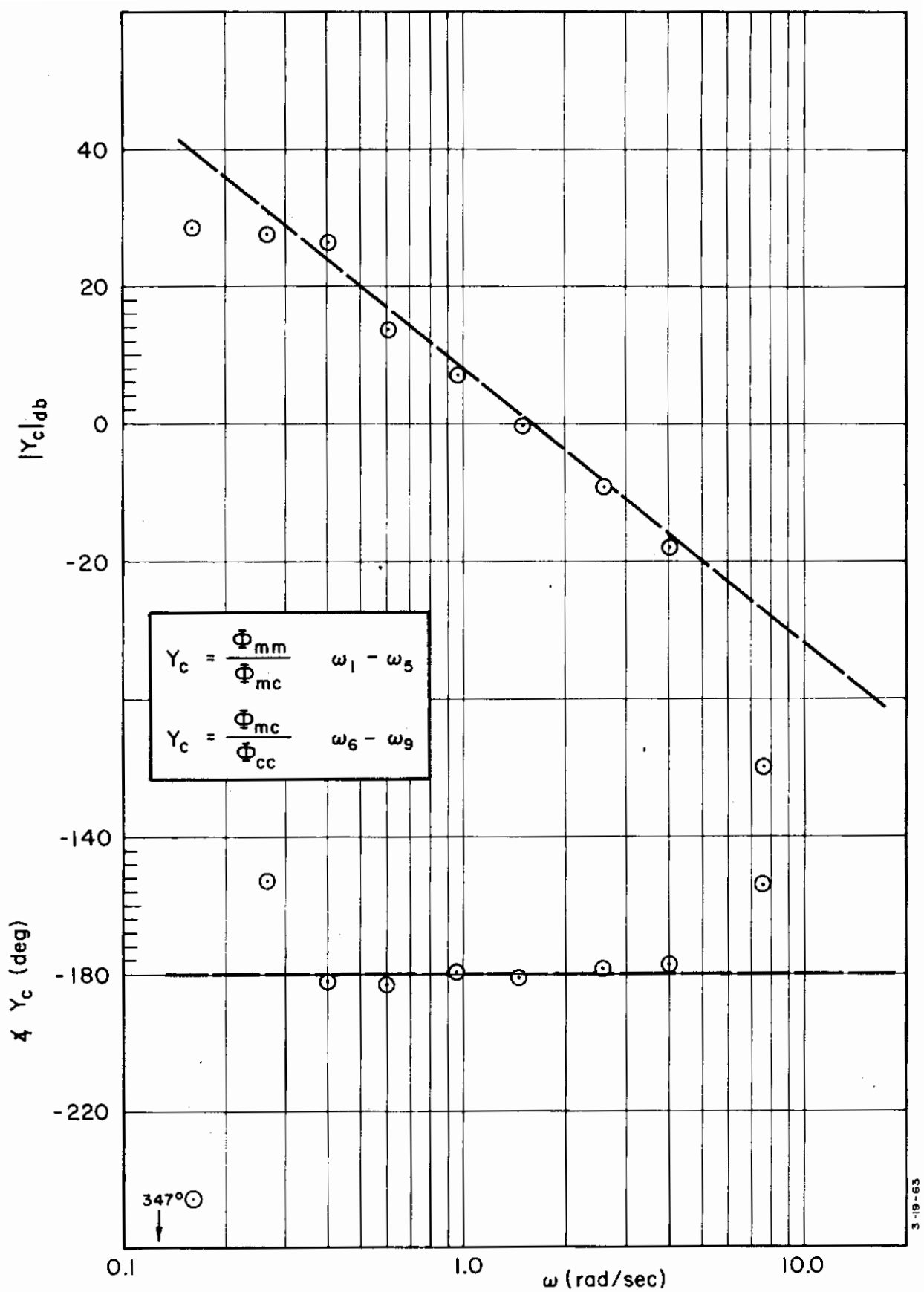

Figure 25. Internal Consistency Check, Y_c Amplitude and Phase

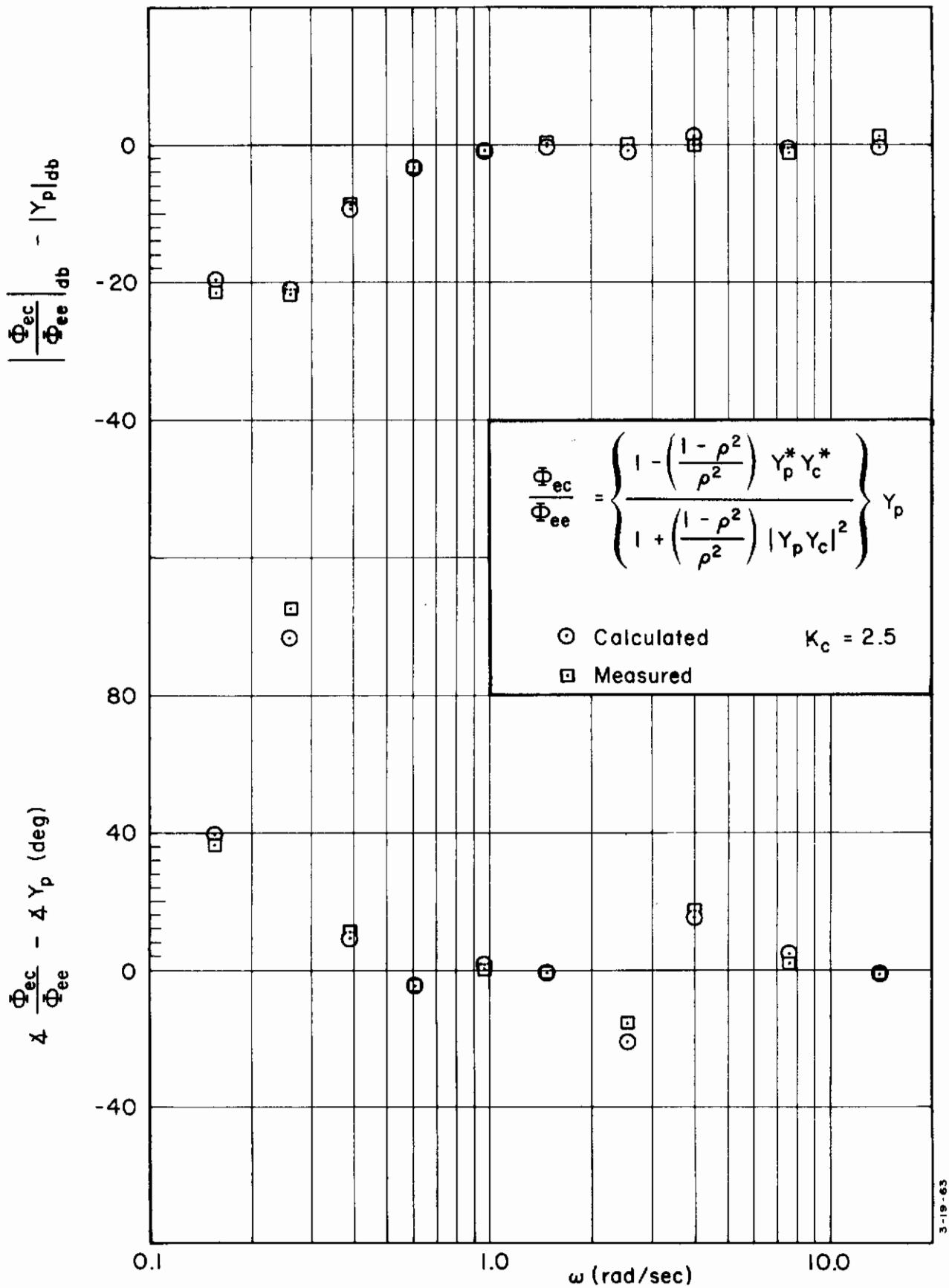

Figure 26. Internal Consistency Check, Y_p Amplitude and Phase

CHAPTER V

EXPERIMENTAL DESCRIBING FUNCTION DATA

A. EXPERIMENTAL PLAN

This chapter presents the experimental describing function data obtained to serve as a data base for the validation and elaboration of the analytical-verbal model. The data will be presented in various aggregations designed to illustrate and illuminate the findings. Each set of data taken was an element in a grand design conceived to fulfill the experimental objectives discussed in Chapter II. These objectives were sharpened and made concrete as specific experimental conditions by the pre-experimental analyses of Chapter III. The resulting experimental matrix is shown in Fig. 27a.

In the experiment a total of nine subjects were used. It is obvious that filling the boxes in Fig. 27a for K_c variation, ω_i variation, Φ_{ii} amplitude variation, and degree of training for each of nine pilots is clearly both overly ambitious and not particularly useful. Instead, the matrix, as indicated in Fig. 27b, has been selectively filled in those particular blocks where the findings would shed the most light on the over-all model for the pilot. The numbers in the blocks indicate runs by that pilot for the condition noted.

Besides using judicious selection to decrease the magnitude of the experimental task, major reductions in the amount of data required can be accomplished without decreasing the total scope by making maximum use of available data. Since an extensive amount of data is available for $Y_c = K_c$ (Ref. 13), it was important to establish consistency with these data. Then the sets of data generated in the program would be closely enough related to past work to avoid expensive and time consuming repetition. Similarly, since the range of realistic input amplitudes was small and past evidence indicated amplitude independence of the measured describing function over a factor of ten in σ_i, a linearity

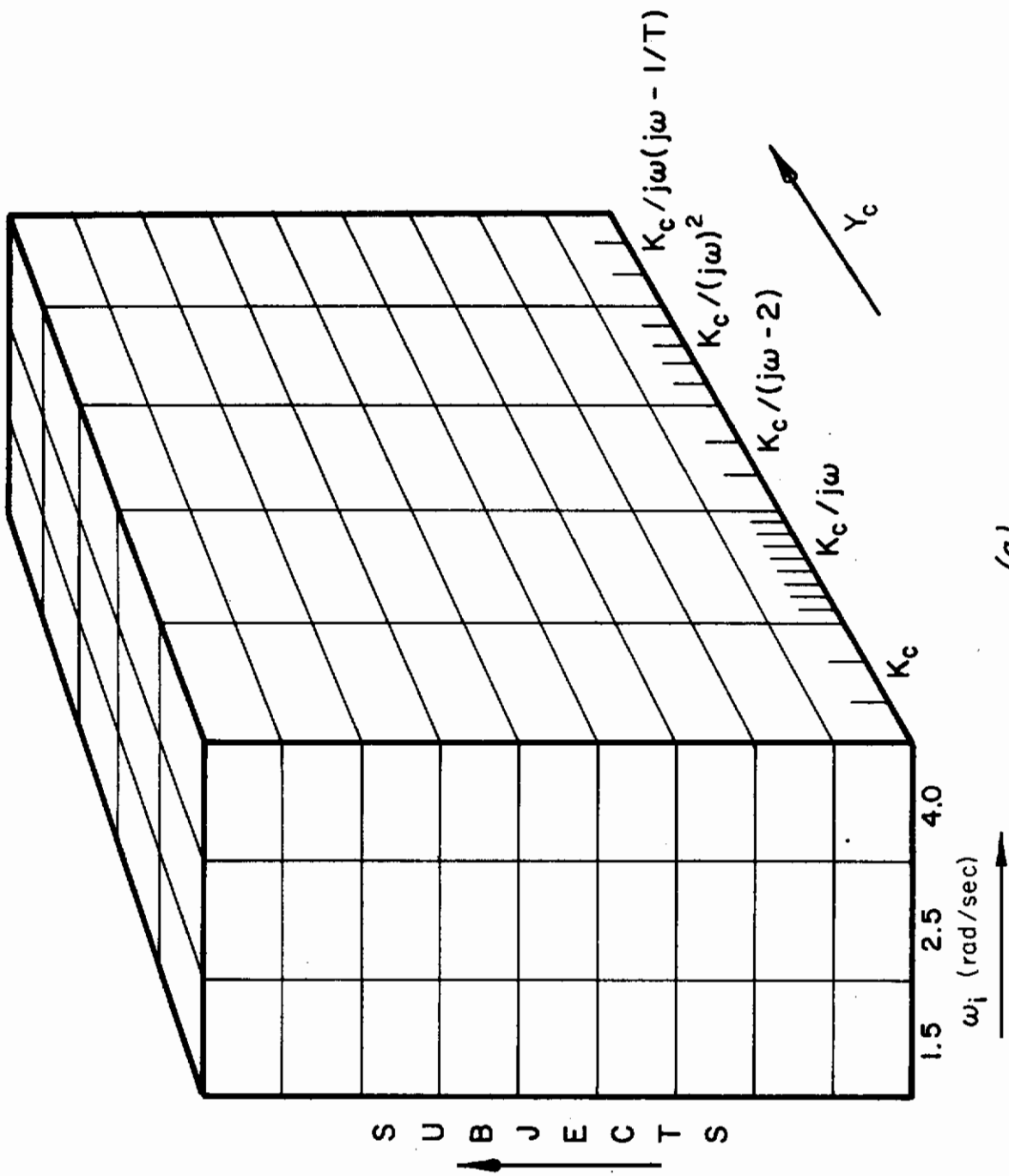

Figure 27. Experimental Plan

Controlled Elements Y_c	Forcing Function Amplitude σ_i	Controlled Element Gain K_c	Forcing Function Bandwidth ω_i (rad/sec)																											
			1.5									2.5									4.0									
			Subjects									Subjects									Subjects									
			▽ 1	□ 2	○ 3	△ 4	◇ 5	⌂ 6	⌂ 7	◿ 8	◊ 9	▽ 1	□ 2	○ 3	△ 4	◇ 5	⌂ 6	⌂ 7	◿ 8	◊ 9	▽ 1	□ 2	○ 3	△ 4	◇ 5	⌂ 6	⌂ 7	◿ 8	◊ 9
K_c	1"	5						2									2									2				
		2				2									2									2						
		1		2									2									2								
$\frac{K_c}{j\omega}$	1/2"	50																	3											
		20				2									2				3					2						
		15							2									2	3							2				
		10							2				1					2	3							2				
		7	2	2					2	3		2	2					2	3		3	2				2	3			
		6							2									2								2				
		5	2		2		2	2	1		2	1		2		2	2		3	2			2		2	2			2	
		2																	3											
		1																	3											
$\frac{K_c}{j\omega - 2}$	1/2"	20				2									2								2							
		7	2	2								2	2								2	2								
		5			2			2						2			2						2			2				
$\frac{K_c}{(j\omega)^2}$	1/2"	50																	3											
		20																	3											
		10			2	2				3				2	2				3				2	2					3		
		5	2	2				2	2		2	2	2				2	2	3	2	2	2				2	2			2
		2																	3											
$\frac{K_c}{j\omega(j\omega - 1/T)^*}$	1/4"	10							2	3																				
		5						2			2	2																		
		2.5	2				1		2																					

*1/T ≡ 0, 0.5, 1.0, 1.5

(b)

Figure 27 (contd)

check was made and thereafter rms input amplitudes were standardized at a magnitude that was both realistic and trackable for most conditions — $\sigma_i = 1/2"$.

The subjects were two highly experienced civilian engineering test pilots, six naval test pilots, and one light-aircraft-qualified civilian pilot subjected to extensive training. Thus, by dint of professional experience and special training the subjects were select members of an unusually homogeneous group which exhibited high grade skills in tasks similar to those performed in the experiments. The subjects were briefed on the purposes of the experiments, including the anticipated ultimate use of the data obtained in vehicle handling qualities studies. Their level of interest and cooperation was extremely high. Consequently, by subject selection and thorough briefing, variability and performance differences due to population inhomogeneities or lack of motivation were minimized.

To minimize variability due to practice effects, each pilot was trained to a stable level of performance as measured by $\overline{e^2}/\sigma_i^2$. In general, this means that at least ten and often twenty trial runs of two minutes duration with each different controlled element were carried out before recorded runs were made with a given controlled element. Figure 28 is a representative proficiency curve.

The remaining sections of this chapter are devoted to the describing function data presentations. The next section covers the establishment of connections with existing data, and considers the effect of forcing function amplitude on the describing function for a critical condition. The third section treats the variability of describing function data by examining selected data sets which illustrate intra- and intersubject effects. Finally, the fourth section of the chapter presents grand-average describing functions which exhibit the central variations examined in this study— those caused by controlled element and forcing function changes. This section also subjects some important qualitative conclusions to statistical examination.

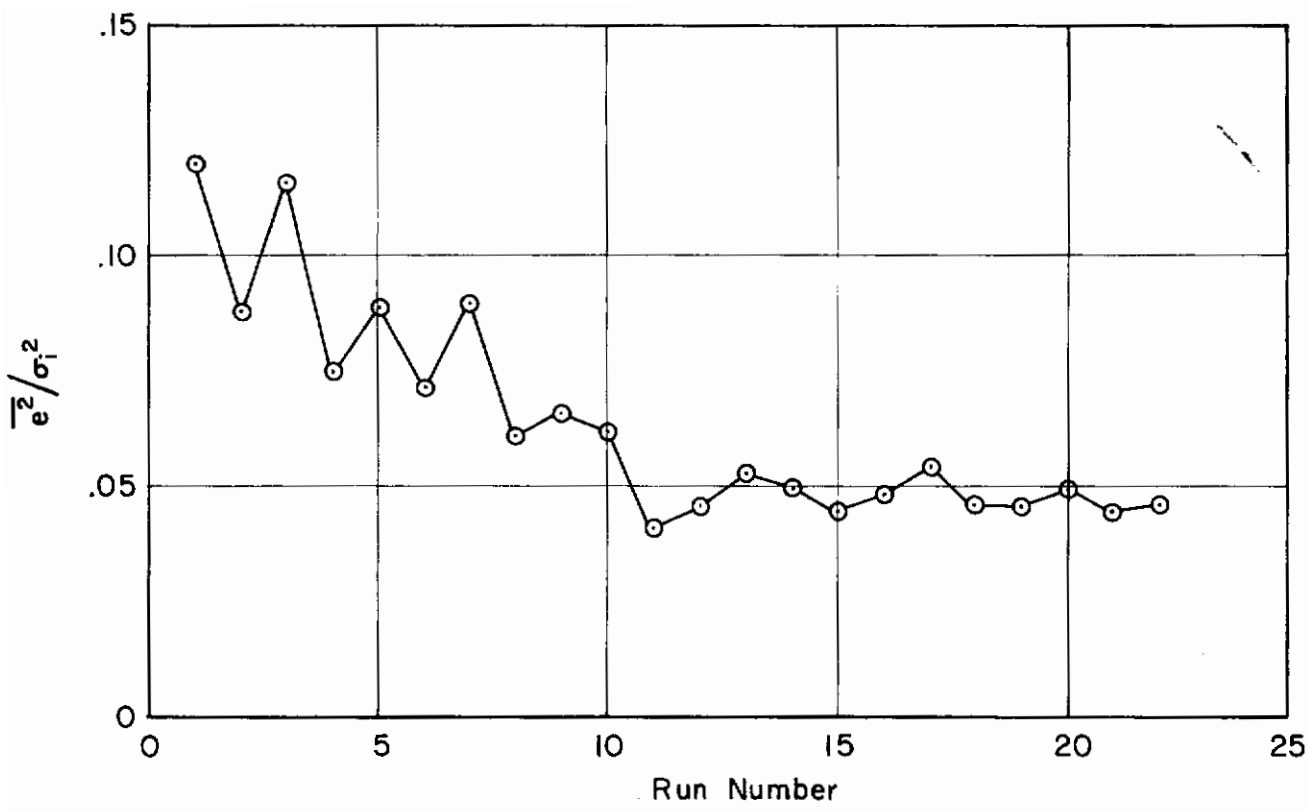

Figure 28. Typical Proficiency Curve

B. PURE GAIN CONTROLLED ELEMENT AND INPUT AMPLITUDE

In order to tie in with the body of data generated from $Y_c = K_c = 1$ in Ref. 13, a tracking situation as similar as feasible to Elkind's had to be considered. Ideally, the tie-in experiments should be conducted with forcing functions and manipulator similar to those to be used in our other experiments, yet also similar enough to Elkind's to effect a reasonable connection. Fortunately Elkind's B6 forcing function amounts, in our notation, to $\omega_1 = 3.0$, 1", so the $\omega_1 = 2.5$, 1" forcing function was thought to provide reasonably close approximation. The lightly restrained stick manipulator used in our series differs substantially in form from Elkind's freely moving pencil-like pip tracker, although the movements in both cases were generally lateral (with more rotation involved in our series). Yet, in our past work we had been able to show reasonable connections with Elkind's data even using an aircraft center stick (Ref. 34), so any differences due to the manipulators were expected to be slight. Consequently a series based on the use of an $\omega_1 = 2.5$, 1" forcing function was planned.

Three highly trained pilots, Nos. 2, 4, and 6, tracked two runs each for $Y_c = K_c = 1$, 2, and 5, respectively. The differences between Y_p measurements for successive runs for each pilot were very slight, and the two runs were averaged. These data were, in turn, averaged in the Y_pY_c form to make them comparable across Y_c values. These averages are shown in Fig. 29, with the hash marks indicating the range of the data, i.e., the location of the high and low pilot averages used in the three pilot grand averages. Elkind's comparable data for $\omega_1 = 3.0$, 1" are shown for comparison in Fig. 29. These data are averages of four four-minute runs, two from one subject and one run from each of two other subjects. It is clear from Fig. 29 that the STI-FIL results are remarkably compatible with the Elkind data. In fact, this extremely close correspondence between data taken years apart, by different experimenters at different locations, with different subjects, different analysis apparatus, and slightly different forcing functions and manipulators, etc., is very satisfying. On the basis of this most compelling

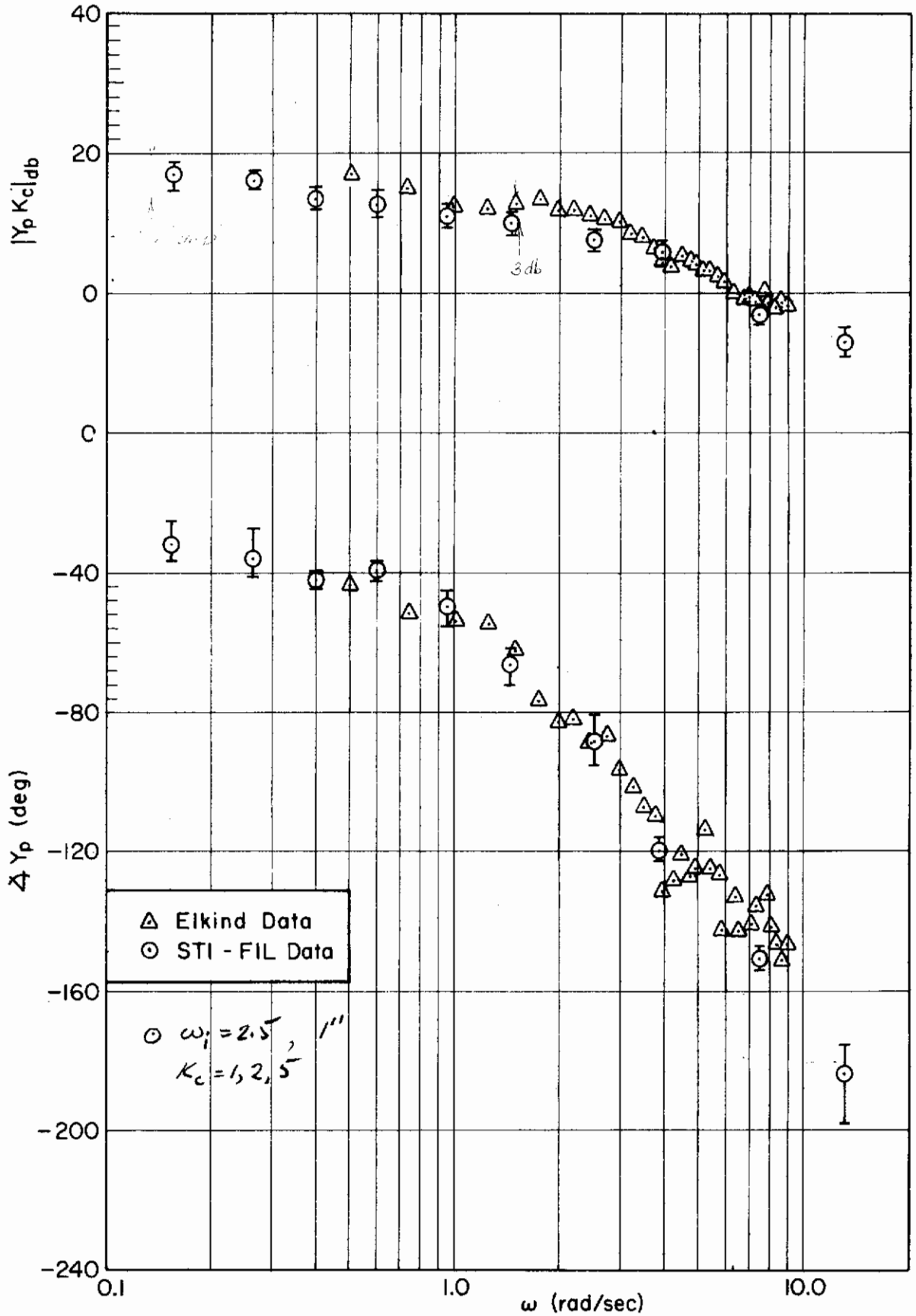

Figure 29. Comparison of $Y_c = K_c$ Data with Elkind Data

evidence it was concluded that extensive measurements with $Y_c = K_c$ were unnecessary and that Elkind's data could and should reasonably be considered a subset of ours to the extent required in model building and verification.

Another important item preliminary to the major experimental series relates to the effect of forcing function amplitude. Elkind had demonstrated (Ref. 13), by means of comparisons at two low frequencies (less than ω_c) of the closed-loop describing function, $Y_p/(1 + Y_p)$, that these closed-loop measurements are independent of forcing function amplitude over the range from 0.1 to 1 inch rms. This result is, of course, totally in keeping with what would be expected in a good closed-loop system. Of much greater interest is the general effect of forcing function amplitude on Y_p. For reasons of experimental economy one might hope that any such effect would be small over a reasonable range, although on other grounds (e.g., see Table I) it is certain that some amplitude-sensitive effects are present. Consequently, in order to examine the appropriateness of the restricted forcing function amplitude values in Fig. 27b, a check of linearity was made for a controlled element, $Y_c = K_c/(j\omega)^2$, which is difficult to control and which, on an à priori basis, may possibly result in significant nonlinear controller action. A typical comparison for one pilot controlling $Y_c = 10/(j\omega)^2$ is presented in Fig. 30, in which the averages for three runs for $\omega_i = 1.5$, 1/4" and $\omega_i = 1.5$, 1/2" are presented for Pilot 8. The comparison was made with an individual pilot rather than an average over pilots so as to accentuate any possible differences rather than obscure them by averaging additional pilots. An examination of these data in Fig. 30 makes it clear that there is no evidence of nonlinear behavior in the sense of a describing function variation with σ_i. This point will be examined further subsequently when the output spectrum, $\Phi_{cc}(\omega)$, is examined in fine detail.

C. VARIABILITY OF DESCRIBING FUNCTION DATA

The condition under which the measurements of the pilot's describing function and associated characteristics of human control behavior were made was that of a highly skilled and highly motivated operator performing

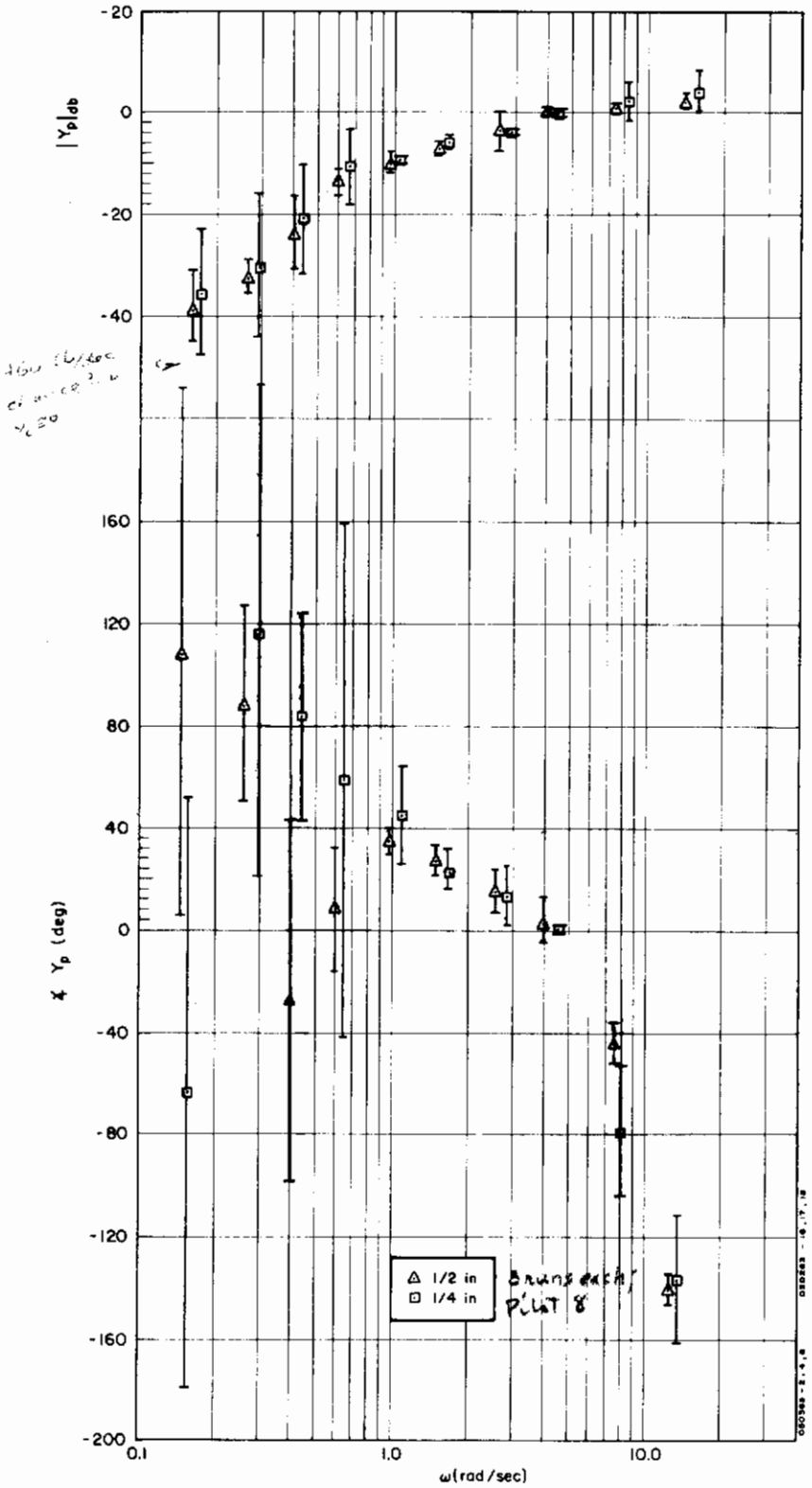

Figure 30. Comparison of Y_p for Different Forcing Function Amplitudes; $Y_c = K_c/(j\omega)^2$, $\omega_i = 1.5$

a carefully and tightly defined task. The pilots were told that although the control and display were only idealizations of flying situations, there were similarities in that the controlled elements could be thought of as being representative of certain aircraft-like dynamics in the case of $Y_c = K_c/j\omega$, of space-vehicle-like dynamics in the case of $Y_c = K_c/(j\omega)^2$, and of an unstable vehicle in the cases of $Y_c = K_c/(j\omega - 1/T)$ and $Y_c = K_c/j\omega(j\omega - 1/T)$. The instructions were to minimize the error and to attempt to do this in the context of their flying experience.

By confining the tests to this highly motivated, highly skilled, carefully selected sample of the population the intent was to reduce the effects of population inhomogeneities on the data. Still, sources of both intra- and intersubject variability exist over and above the expected variations due to changes in controlled element dynamics and forcing function characteristics. The nature of the subject-centered variations, for describing functions, will be examined below.

1. Intrapilot Variability — Run-to-Run and Differential K_c Effects

a. Run-to-run variability. The first intrapilot variability of interest is of a run-to-run nature — a pilot compared with himself when he tracks the same input successively.

The representative individual run data and the four controlled elements used to examine the repeatability of successive runs by the same pilot may be characterized as follows:

Fig. No.	Pilot	Controlled Element
31	8	$K/j\omega$: Easiest to control
32	6	$K/(j\omega-2)$: Unstable, but is easy to control if the pilot is attentive
33	8	$K/(j\omega)^2$: Difficult to control and requires considerable practice to do well
34	8	$K/j\omega(j\omega-1.5)$: Very difficult to control; momentary lapses of attention will cause a loss of control

On examining Figs. 31 – 34 we observe that all four controlled elements indicate considerable run-to-run variation at low frequencies. There is much less variation in the mid-band, which is in the region of crossover, and then a bit more at the higher frequencies beyond crossover. This kind of variation is particularly well displayed in Figs. 31 and 33. As discussed in Chapter III, this behavior is consistent with the demands of the closed-loop system. The influence of Y_p variations on closed-loop system behavior is relatively small at low frequencies, but the behavior of Y_p in the region of crossover has a large influence on closed-loop performance, which is, after all, what the pilot observed.

For the unstable elements, $K_c/(j\omega-2)$ and $K_c/j\omega(j\omega-1.5)$, there is evidence of constrained behavior throughout the entire measurement range. This is particularly apparent for both amplitude ratio and phase for $K_c/(j\omega-2)$, Fig. 32. With the very difficult task of Fig. 34, successful tracking forced a restricted form of gain variation behavior on the pilot, although the phase variations appear quite large. These occurred because the task was difficult enough to induce brief periods of loss of control due to inappropriate variations in temporal action — literally time-varying phase shifts. These are reflected by phase variability in the measurements.

In summary, pilots are capable of extremely high repeatability where it is necessary, e.g., at crossover or in the control of an unstable Y_c where Y_p is rigidly constrained. The extent to which this repeatability can be maintained is a function of frequency (relative to ω_c) determined by the form of the controlled element and, near the limits of control $\left[\text{e.g., } K_c/j\omega(j\omega-1.5)\right]$, a function of the task difficulty.

b. Effect of K_c variation. We have indicated previously that the form of the controlled element exerts a large influence on the amount of variability exhibited by the pilot. Now we can proceed to vary the parameters of the form to determine whether these are the source of the variation. This was done for Pilot 8 for a gain range of 50 to 1 in $K_c/j\omega$ and a range of 25 to 1 in $K_c/(j\omega)^2$, as shown in Figs. 35 and 36. In general, these data indicate that changes in controlled element gain are offset by the pilot, thereby constituting further verification of Adjustment

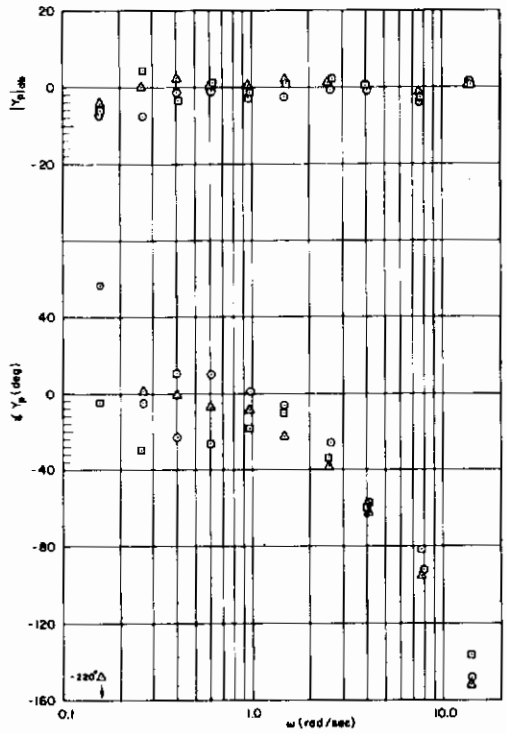

Figure 31. Run-to-Run Variability; $Y_c = 5/j\omega$, $\omega_i = 2.5$

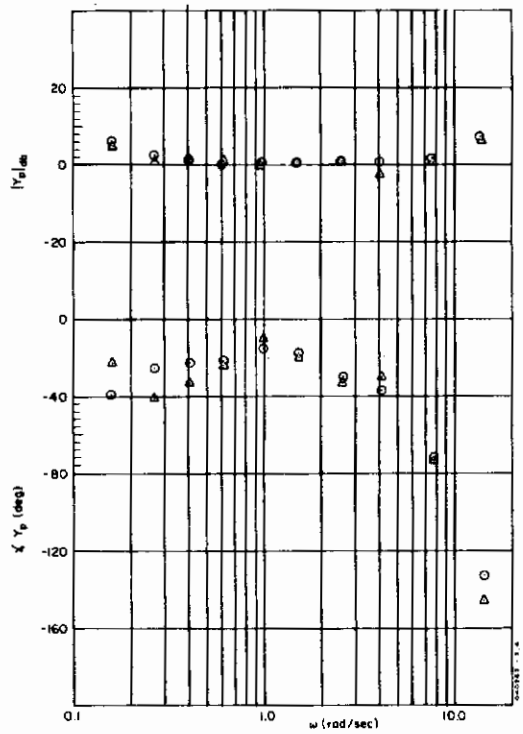

Figure 32. Run-to-Run Variability; $Y_c = 5/(j\omega - 2)$, $\omega_i = 2.5$

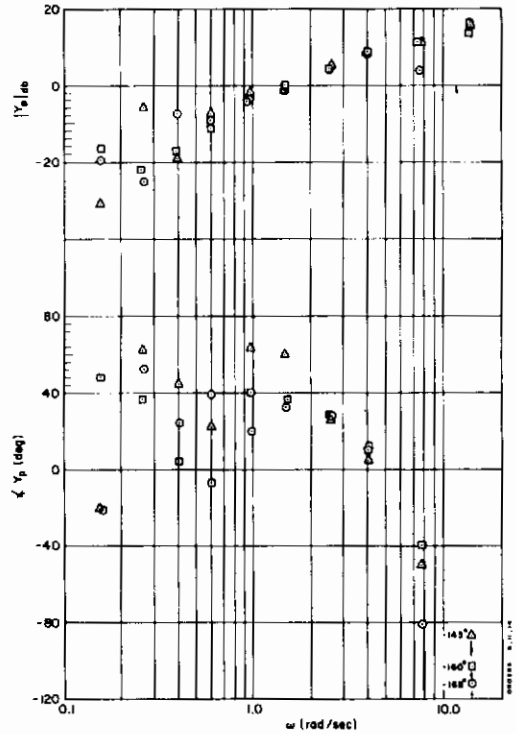

Figure 33. Run-to-Run Variability; $Y_c = 5/(j\omega)^2$, $\omega_i = 2.5$

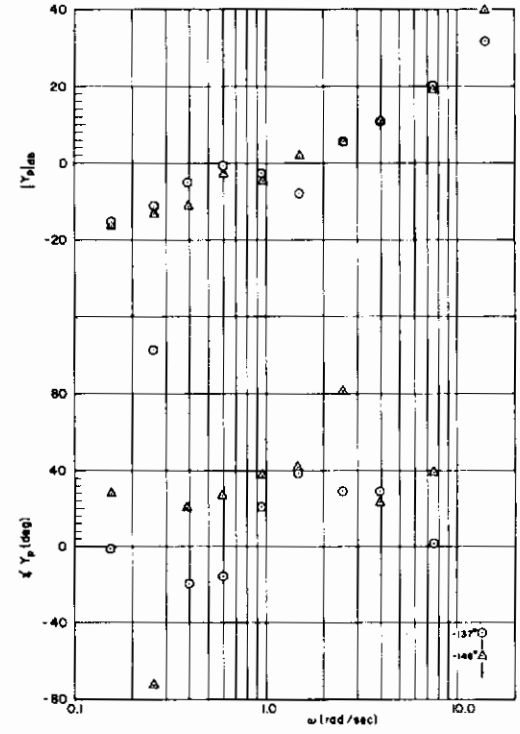

Figure 34. Run-to-Run Variability; $Y_c = 5/j\omega(j\omega - 1.5)$, $\omega_i = 1.5$, 1/4"

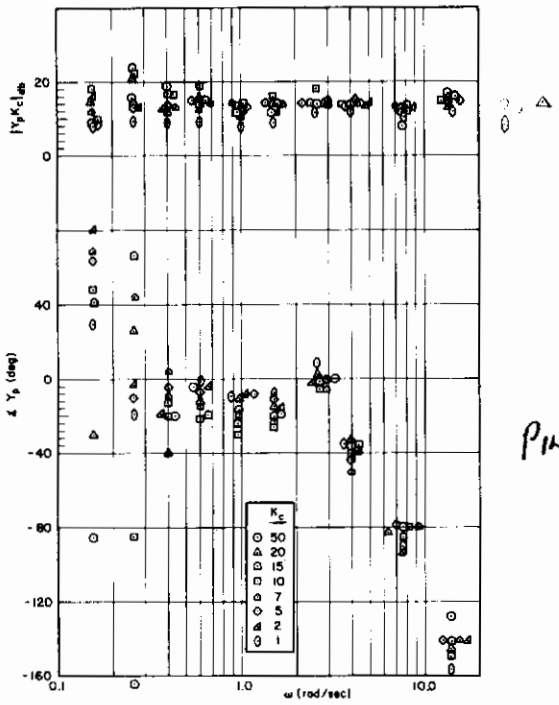

Figure 35. Effect of K_c Variation; $Y_c = K_c/j\omega$, $\omega_1 = 2.5$

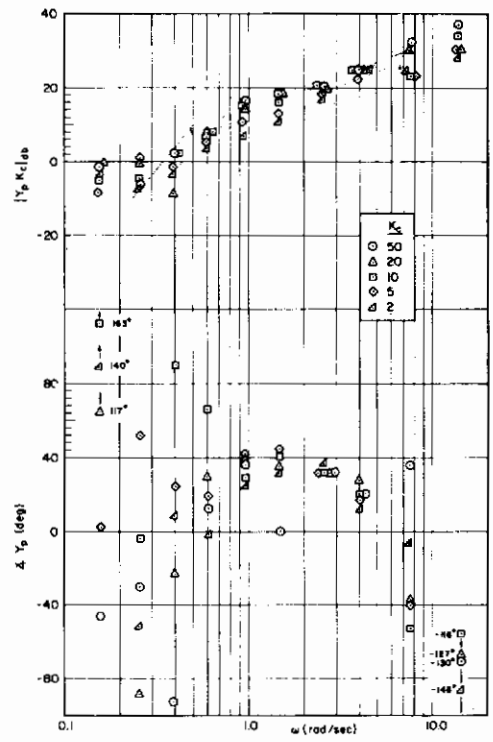

Figure 36. Effect of K_c Variation; $Y_c = K_c/(j\omega)^2$, $\omega_1 = 2.5$

Rule 5 (Chapter II). There are variations with K_c, but these are more or less random and appear to amount to the same thing as the run-to-run variations discussed above. That is, if the data are considered only to be representative of successive runs, then the general trends of variability with frequency indicated in Figs. 35 and 36 are very similar to those present in Figs. 31 and 33. On this basis the conclusion noted above that repeatability is a function of Y_c form can be refined to the statement that the run-to-run variability is dependent on Y_c/K_c.

2. Intersubject Variability

By compiling data for the most numerous subject situations the impact of subjects on the variability of the describing functions can be examined. This is done in Figs. 37 – 40, where data similar to those in Figs. 31 – 34 are shown but with subjects replacing runs as the key variables. The data presented in these figures are obtained by averaging two successive runs for each pilot, save for Pilot 8 for whom three runs were averaged. Also, the data base is made larger for the two unstable controlled elements by using all K_c's (Figs. 38 and 40). This procedure is unlikely to introduce much more variation because the effect of K_c changes are largely offset by the pilot; but even more dramatic evidence to this end are the extremely low ranges apparent in the phase data of Fig. 38, and also in the amplitude ratio data when the different K_c values are taken into account.

Again we notice the same general trends as already observed for the run-to-run and K_c intrasubject changes. That is:

a. For $K_c/(j\omega)$ and $K_c/(j\omega)^2$ fairly wide ranges of variation at frequencies much smaller than or much greater than ω_c, and tighter limits on the range in the crossover region.

b. For the unstable controlled elements the range of variation in amplitude ratio across the entire frequency range is generally small.

c. There is a rather wide variation in the phase for the case involving the critically difficult controlled element $K_c/j\omega(j\omega-1.5)$. Again this is attributed to the time variations in behavior implicit in the brief periods in which control was nearly lost.

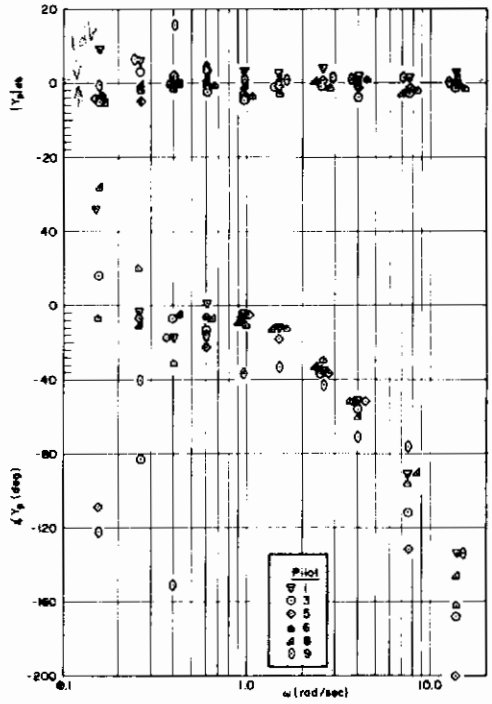

Figure 37. Pilot-to-Pilot Variability; $Y_c = 5/j\omega$, $\omega_1 = 2.5$

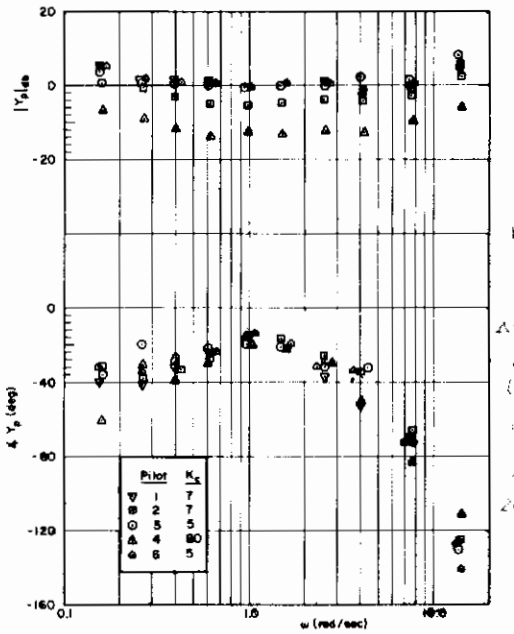

Figure 38. Pilot-to-Pilot Variability; $Y_c = K_c/(j\omega - 2)$, $\omega_1 = 2.5$

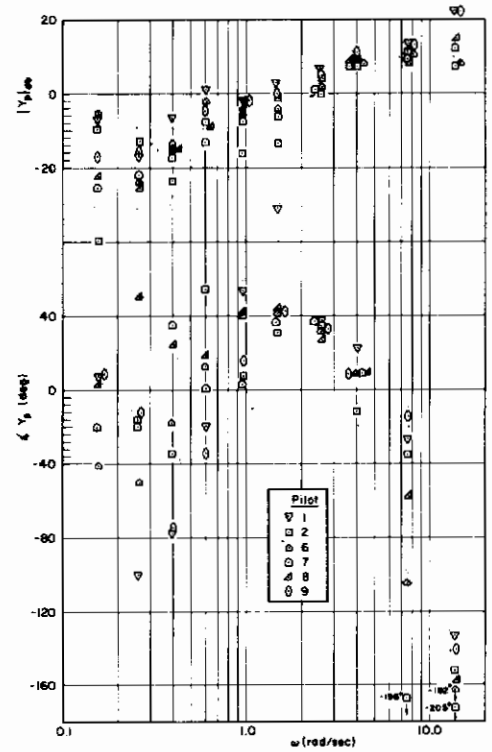

Figure 39. Pilot-to-Pilot Variability; $Y_c = 5/(j\omega)^2$, $\omega_1 = 2.5$

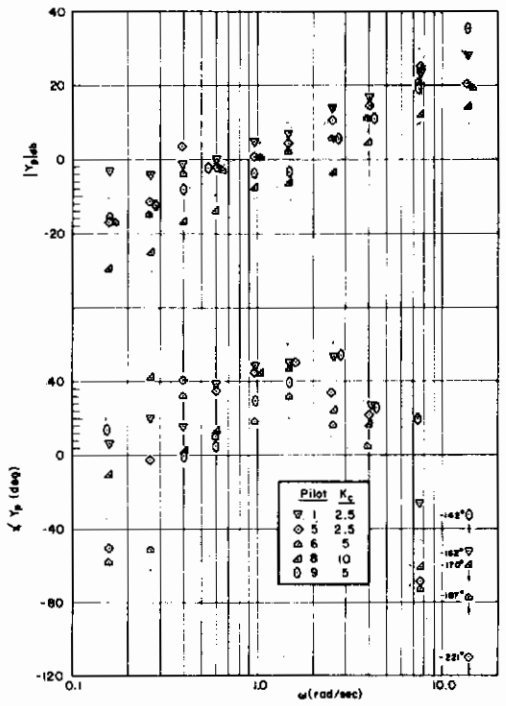

Figure 40. Pilot-to-Pilot Variability; $Y_c = K_c/j\omega(j\omega - 1.5)$, $\omega_1 = 1.5$, 1/4"

An additional fact, which is most easily seen in Fig. 39, should also be noted. There is a great deal of indifferent behavior before and after crossover, but each pilot appears to be indifferent in his own way. Thus individual pilots may express their tracking style where it isn't critical for closed-loop performance, but everyone behaves nearly identically under the constrained conditions.

D. GRAND-AVERAGE DESCRIBING FUNCTIONS AND STATISTICAL ANALYSIS

1. Describing Function Averages

The central aspects of manual control in this study are the nature of pilot adaptation and optimalization induced by controlled element and/or forcing function changes. The most vital data to show these effects are averages of $|Y_pY_c|_{db}$ for fixed forcing function conditions. Averages of this nature, together with $\pm 1\sigma$ bands, are given in Figs. 41, 42, and 43 for $Y_c = K_c/j\omega$, $K_c/(j\omega-2)$, and $K_c/(j\omega)^2$, respectively. Parts a, b, and c of these figures correspond to values of ω_i = 1.5, 2.5, and 4.0 rad/sec, respectively. Figure 44 shows a similar set for $Y_c = K_c/j\omega(j\omega-1/T)$, ω_i = 1.5, 1/4"; these are segregated as Parts a, b, c, and d corresponding to values of 1/T = 0.0, 0.5, 1.0, and 1.5 rad/sec, respectively.

The data in Figs. 41 -44 constitute major findings of the study. In Chapter VII they will be extensively analyzed and interpreted. Here it is appropriate only to summarize certain salient features of these figures as data per se in the context of the analytical-verbal model.

One of the most interesting general aspects of the describing function data is the tendency for the amplitude ratios to approximate -20 db/decade slopes throughout the measurement range. This tendency is adhered to quite well for the $Y_c = K_c/j\omega$ and $K_c/(j\omega)^2$ data (Figs. 41 and 44), whereas for the unstable controlled elements the tendency is most prevalent only in the immediate region of crossover. In fact, near the controllability limits the slope becomes considerably shallower than -20 db/decade. All of this is in general agreement with the pre-experiment predictions.

Another general feature of great interest is the universal presence of low frequency phase lags. In almost all cases these lagging phases are not associated with amplitude ratio break points within the measurement band. Such break points must accordingly occur at frequencies somewhat lower than those in the forcing function. The analytical-verbal model makes no provision whatsoever for the low frequency phase lags, and consequently should be modified to account for their presence.

Summary open-loop describing function data of supreme importance are crossover frequencies and phase margins. Figure 45a presents crossover frequency as a function of forcing function bandwidth for the three controlled elements for which ω_i was a variable, and Fig. 45b provides the same information for the variable divergence Y_c, ω_i = 1.5, 1/4". Considering the data and curve reading tolerances, the crossover frequencies for the three variable-ω_i controlled elements (Fig. 45a) each appear to be essentially constant. A fair case can be made for a slight increase in ω_c as ω_i increases, but the maximum deviation from the mean value is less than 5 percent. The most significant deviation from a constant crossover occurs for $Y_c = K_c/(j\omega)^2$ where the ω_i = 4 point has regressed. All of these data are in substantial accord with two of the ω_c invariance properties, Adjustment Rules 5b and c, and hence offer direct verification and validation for the analytical-verbal model.

The average crossover frequencies shown in Fig. 45a for $K_c/j\omega$ and $K_c/(j\omega)^2$ occur in the relative order and have values within the probable ranges predicted in the pre-experiment analyses. The experimental ω_c's are, however, about 20 percent lower than the estimates of the center of the probable crossover range (see, e.g., Fig. 7).

Phase margin data derived from Figs. 41 – 44 are summarized in Fig. 46. In general, it appears that phase margin increases directly with forcing function bandwidth. Initially, for small ω_i's the trend is linear, rounding off as ω_i increases. As promised previously, these phase margin data will result in significant improvements in Adjustment Rule 4b. The phase margins for $Y_c = K_c/j\omega(j\omega - 1/T)$ shown in Fig. 46b are all very low. This is due to the small ω_i (1.5 rad/sec) used for these cases and, for the higher 1/T values, the marginal controllability. The phase margin and

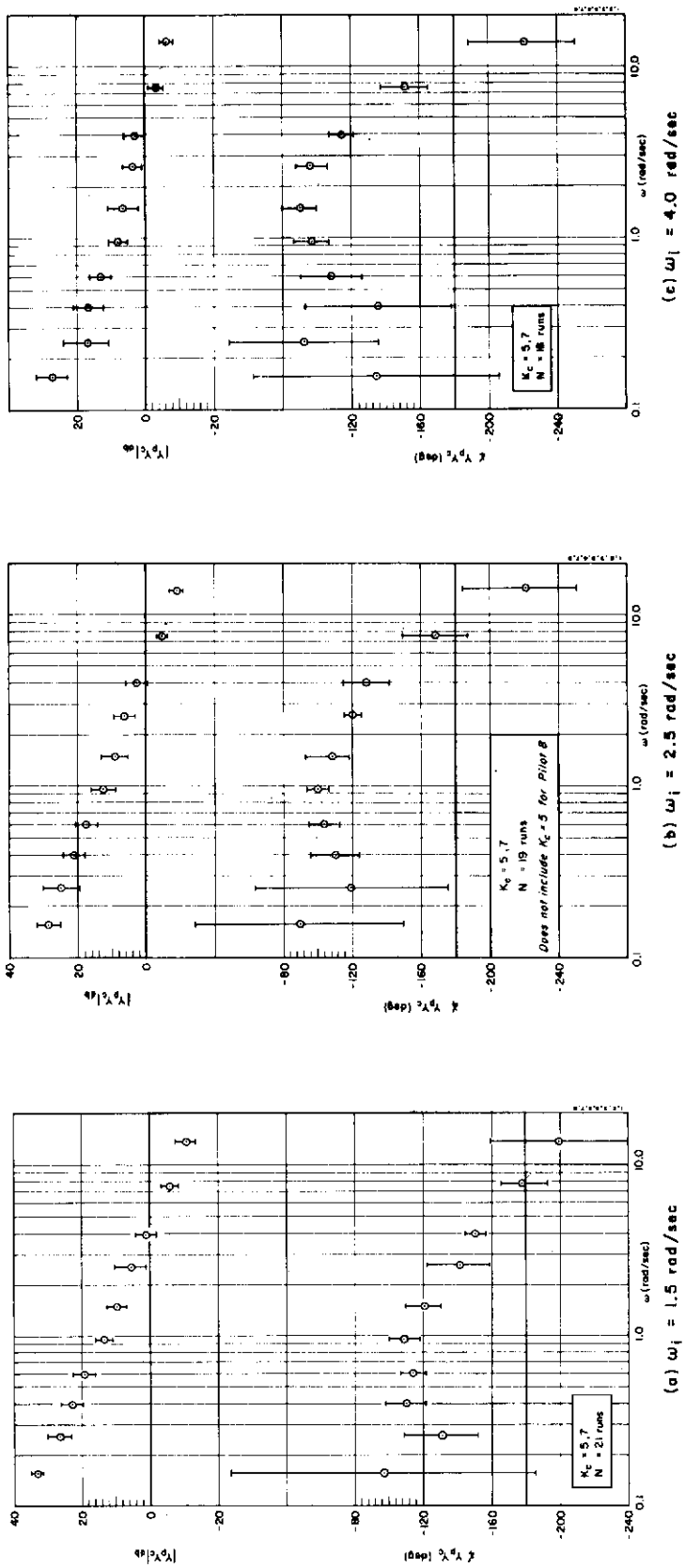

Figure 41. Open-Loop Describing Functions for $Y_c = K_c/j\omega$

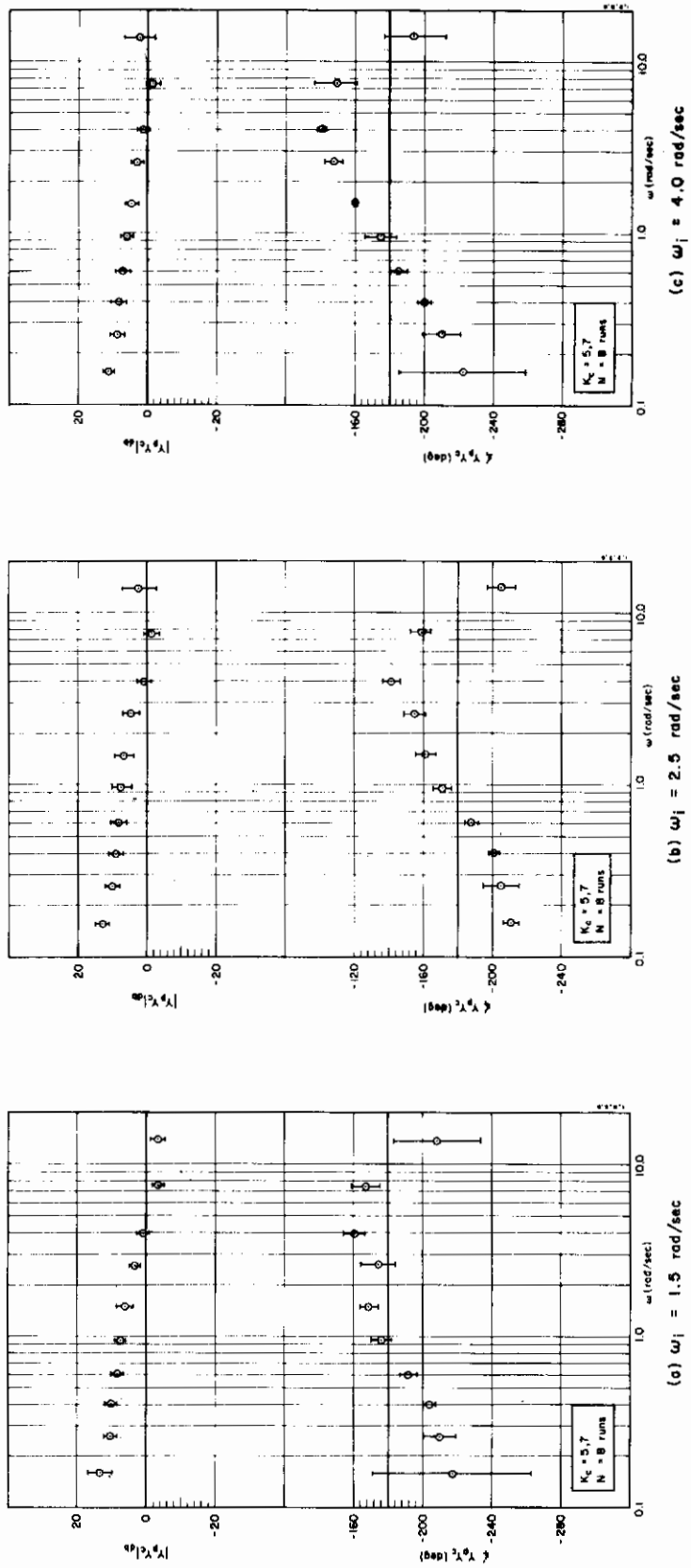

Figure 42. Open-Loop Describing Functions for $Y_c = K_c/(j\omega - 2)$

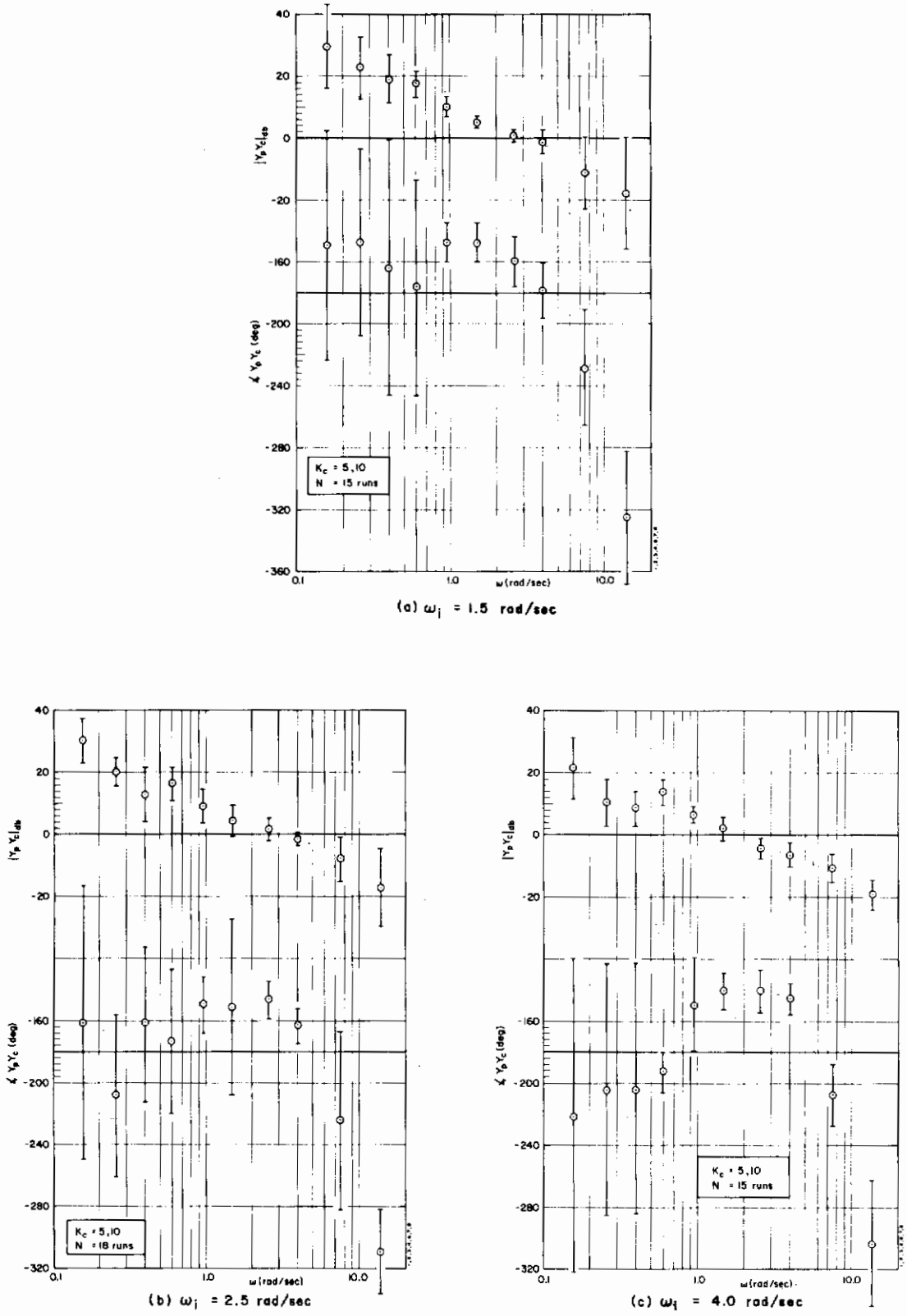

Figure 43. Open-Loop Describing Functions for $Y_c = K_c/(j\omega)^2$

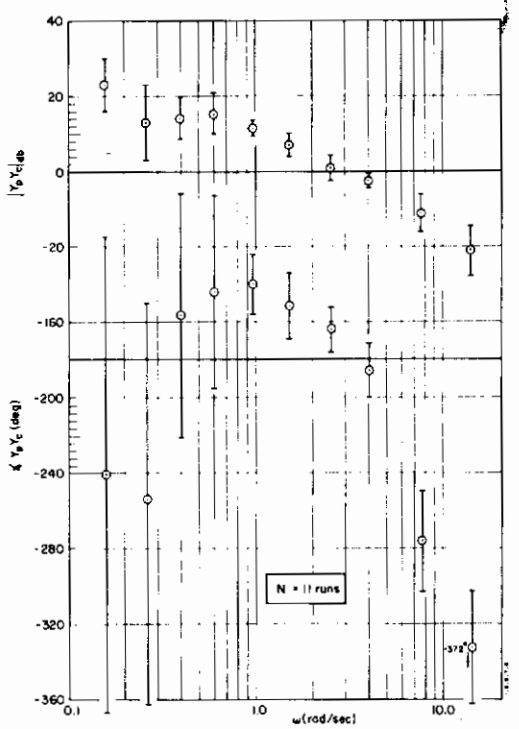

(a) 1/T = 0 POR = 6 - 6.5

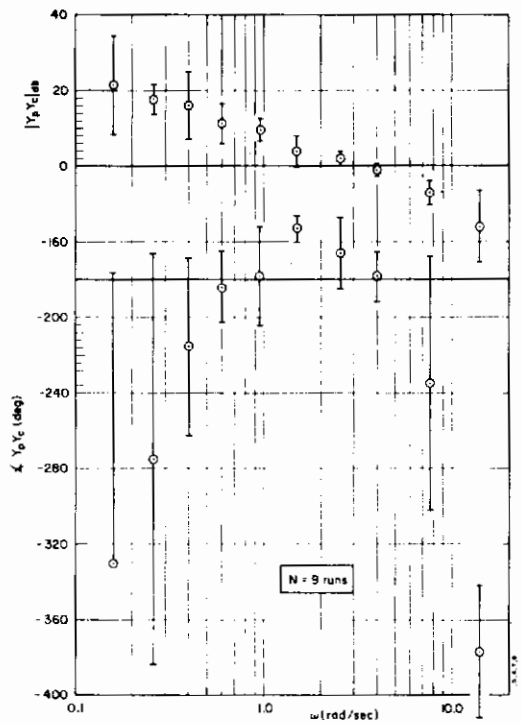

(b) 1/T = 0.5 POR = 6 - 7

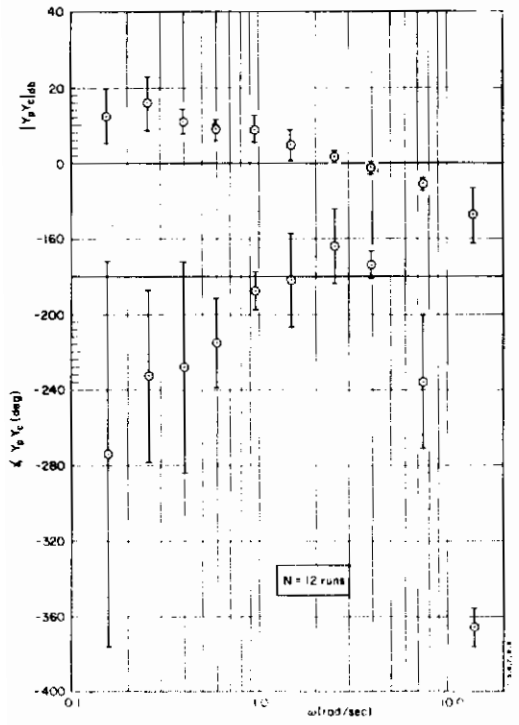

(c) 1/T = 1.0 POR = 8 - 8.5

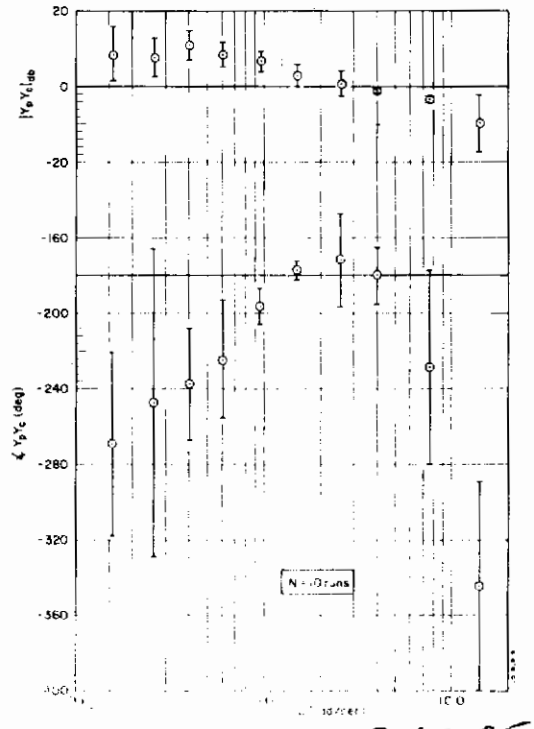

(d) 1/T = 1.5 POR = 8.5 - 9

Figure 44. Open-Loop Describing Functions for $Y_c = K_c/(s(\omega_1 s + 1)^2)$
$\omega_1 = 1.5, 1/4$"

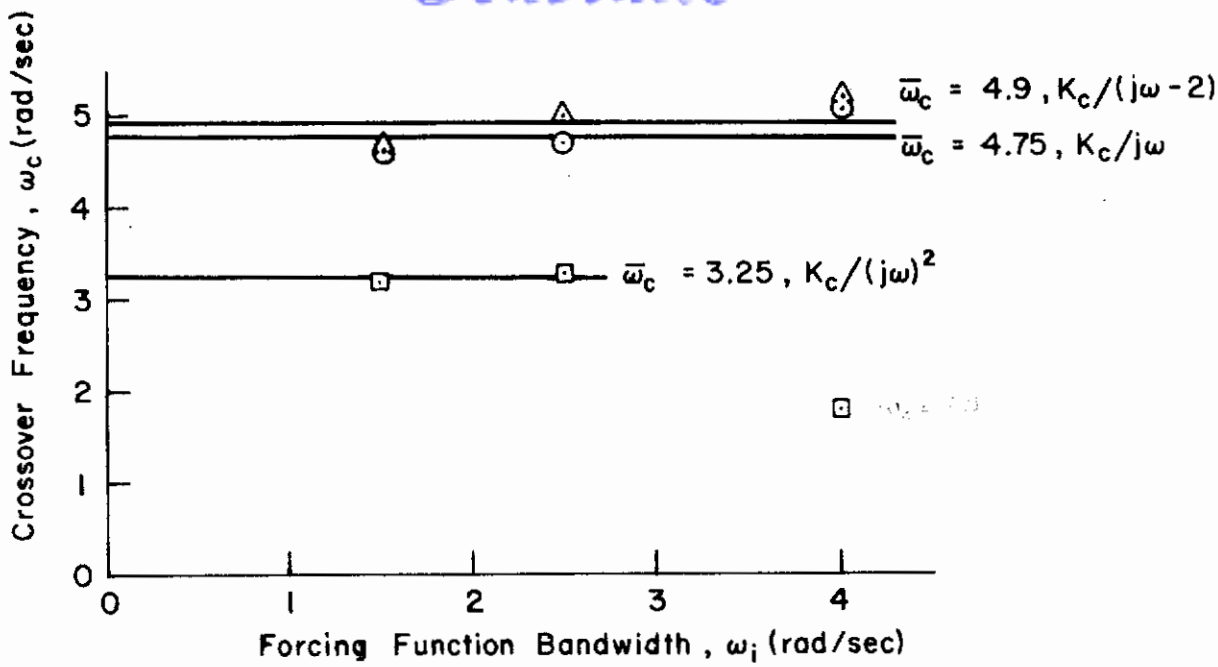

(a) Crossover Frequency Variation with Forcing Function Bandwidth for $Y_c = K_c/j\omega$, $K_c/(j\omega)^2$, and $K_c/(j\omega - 2)$

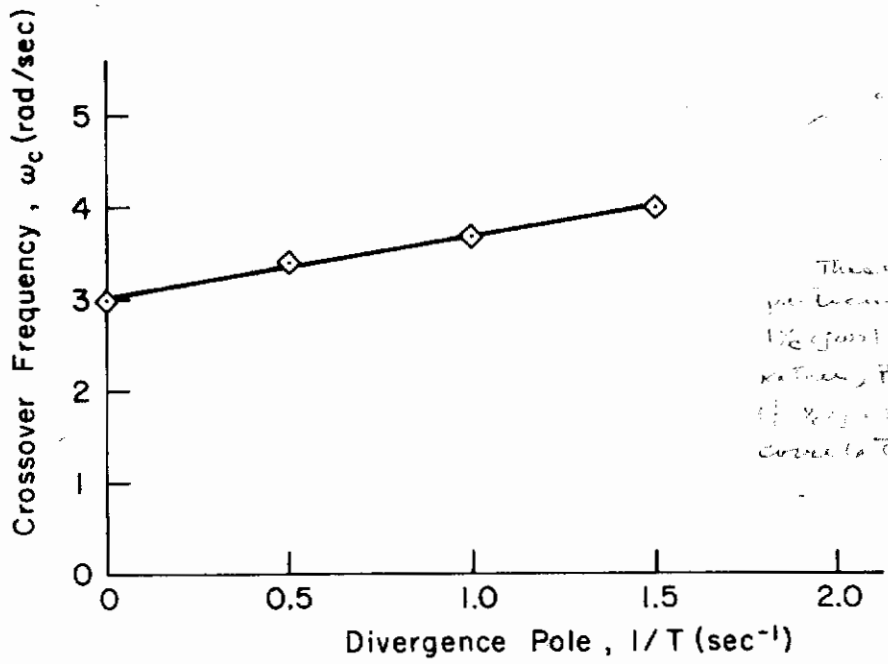

(b) Crossover Frequency Variation with 1/T for $Y_c = K_c/j\omega(j\omega - 1/T)$, ω_i = 1.5, 1/4"

Figure 45. Crossover Frequency Variations

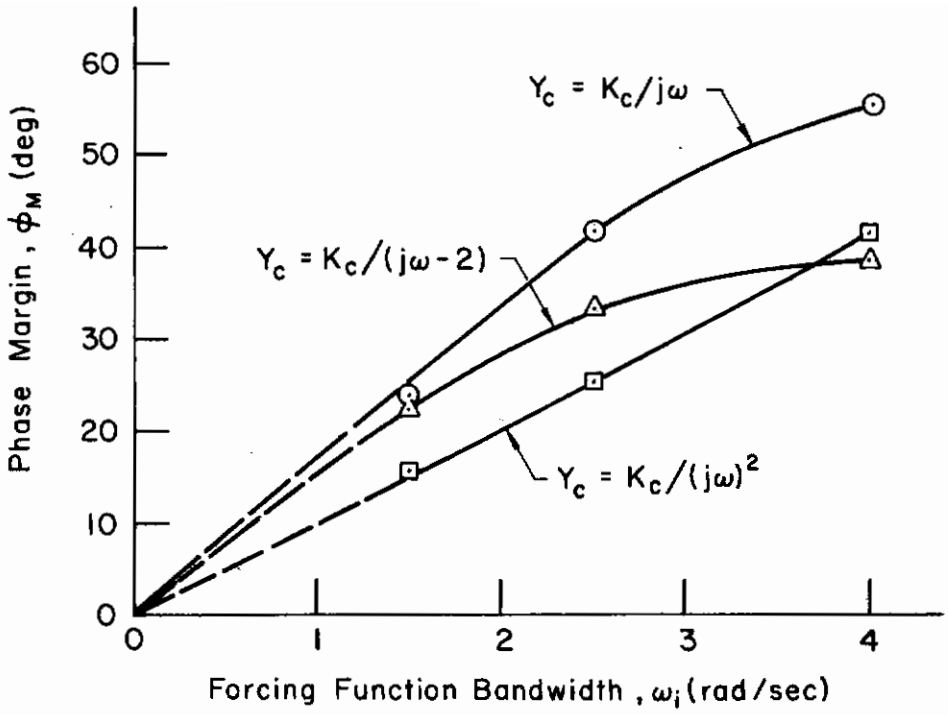

(a) Phase Margin Variation with Forcing Function Bandwidth for $Y_c = K_c/j\omega$, $K_c/(j\omega)^2$, and $K_c/(j\omega - 2)$

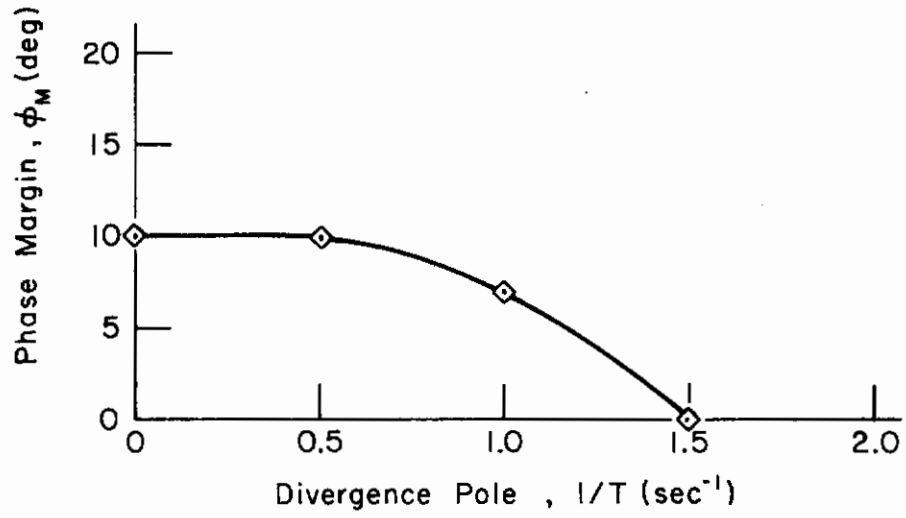

(b) Phase Margin Variation with 1/T for $Y_c = K_c/j\omega(j\omega - 1/T)$ $\omega_i = 1.5$, 1/4"

Figure 46. Phase Margin Variations

crossover (in Fig. 45) shown for this Y_c with 1/T = 0 differs slightly from those for $Y_c = K_c/(j\omega)^2$ because different populations were used (see Fig. 27).

2. Statistical Comparisons of the Data

Although the nature of this investigation was such that detailed statistical comparisons of data were not indicated in general, aggregations such as those shown in Figs. 41 and 43 for $Y_p = K_c/j\omega$ and $Y_p = K_c/(j\omega)^2$ containing between 15 and 21 individual runs make some simple statistical comparisons feasible. While the numbers in the sample are such as to be on the ragged edge for the applicability of small sample statistics, the following assessments can be made for the aggregated data:

a. Are the phase and db amplitude data for Y_pY_c normally distributed? If they are normal, and past experience indicates that they will be (Refs. 15 and 50), the statistical comparisons of the means can be made more easily.

b. Is the selective variability characteristic of Y_p, which is obscured somewhat in the averaged Y_pY_c data, a statistically significant observation?

c. Are the mean values of Y_pY_c in fact different for different forcing function ω_i values?

These questions are examined, in the order stated, below.

The small number of data points made it inadvisable to use a chi-squared goodness of fit test to determine whether the distributions of $\angle Y_pY_c$ and $|Y_pY_c|_{db}$ were Gaussian. Instead, the data were converted to standard scores, i.e., $u = (\chi - \bar{\chi})/\sigma$ so that they could be expressed in terms of a Gaussian distribution of zero mean and unity standard deviation. These standard values were then aggregated by intervals which were constant for any one set of runs, and cumulative percentages computed. The cumulative values were then plotted against the standard scores on cumulative probability paper. To put the scatter about the desired straight line in perspective, 95 percent limits for random variations about the desired straight line were calculated for the various sample sizes used (Ref. 23, Chap. 6). This test of the distribution of $|Y_pY_c|_{db}$ was carried out for averaged $|Y_pY_c|_{db}$ data generated with $Y_c = K_c/j\omega$ and

$Y_c = K_c/(j\omega)^2$. Because of the large amount of effort involved, the plots were calculated at a limited number of input frequencies which bracketed the crossover frequency range. These were ω_n = 0.969, 2.54, and 13.8 rad/sec. All of the 36 distributions studied were close to Gaussian as defined by the 95 percent limits. A typical plot is shown in Fig. 47. This plot is for ω_i = 2.5, $Y_c = K_c/(j\omega)^2$, ω_n = 2.54 rad/sec, for both $|Y_p|_{db}$ and $\angle Y_p$.

The second question raised above deals with the extent to which the different variabilities shown in the averaged data as functions of ω (specifically, the ω_n's in the forcing function) were statistically significant effects. To obtain a better appreciation for this, successive comparisons were made of σ_n^2 and of selected frequencies at either side of the crossover frequency with σ_n^2 values at frequencies bracketing the crossover frequency $\left[\sigma_n = \sigma_{|Y_p|_{db}}(\omega_n) \text{ or } \sigma_{\angle Y_p}(\omega_n)\right]$. These variances were compared with each other by the ratio of variances $\sigma_1^2/\sigma_2^2 = v^2$, also known as the F-test (Ref. 23). The ratio of the larger variance, σ_1^2, to the smaller, σ_2^2, was always used. Tables for this test dependent on N_1 and N_2 for various p levels are readily available. The p level, which indicates the probability of exceeding the tabulated v^2 values by chance, was arbitrarily set at or below the 5 percent level. Table VI presents the results of comparing the variances for $|Y_p|_{db}$ and $\angle Y_p$, for both $Y_c = K_c/j\omega$ and $K_c/(j\omega)^2$, at input frequencies 0.157, 7.57, and 13.8 rad/sec with the variances at each of the six frequencies from 0.969 to 13.8 rad/sec. Note that each comparison box is divided into six segments — three for $|Y_p|$ and three for $\angle Y_p$ for each of the three ω_i values 1.5, 2.5, and 4.0 rad/sec.

In the comparisons we note that for the controlled element $K/(j\omega)^2$ in Table VI-b there is significantly more variability in Y_p, for both amplitude ratio and phase, at the lower and higher frequencies (ω_n = 0.969, 7.57, and 13.8 rad/sec), than there is at the frequencies ω_n = 2.54 and 4.03 rad/sec which bracket the crossover region. Thus, as we depart from the region of crossover in either direction, the funnel pattern of increasing variability which appears in Figs. 43a, b, and c becomes evident in the statistical analysis of Table VI-b as well.

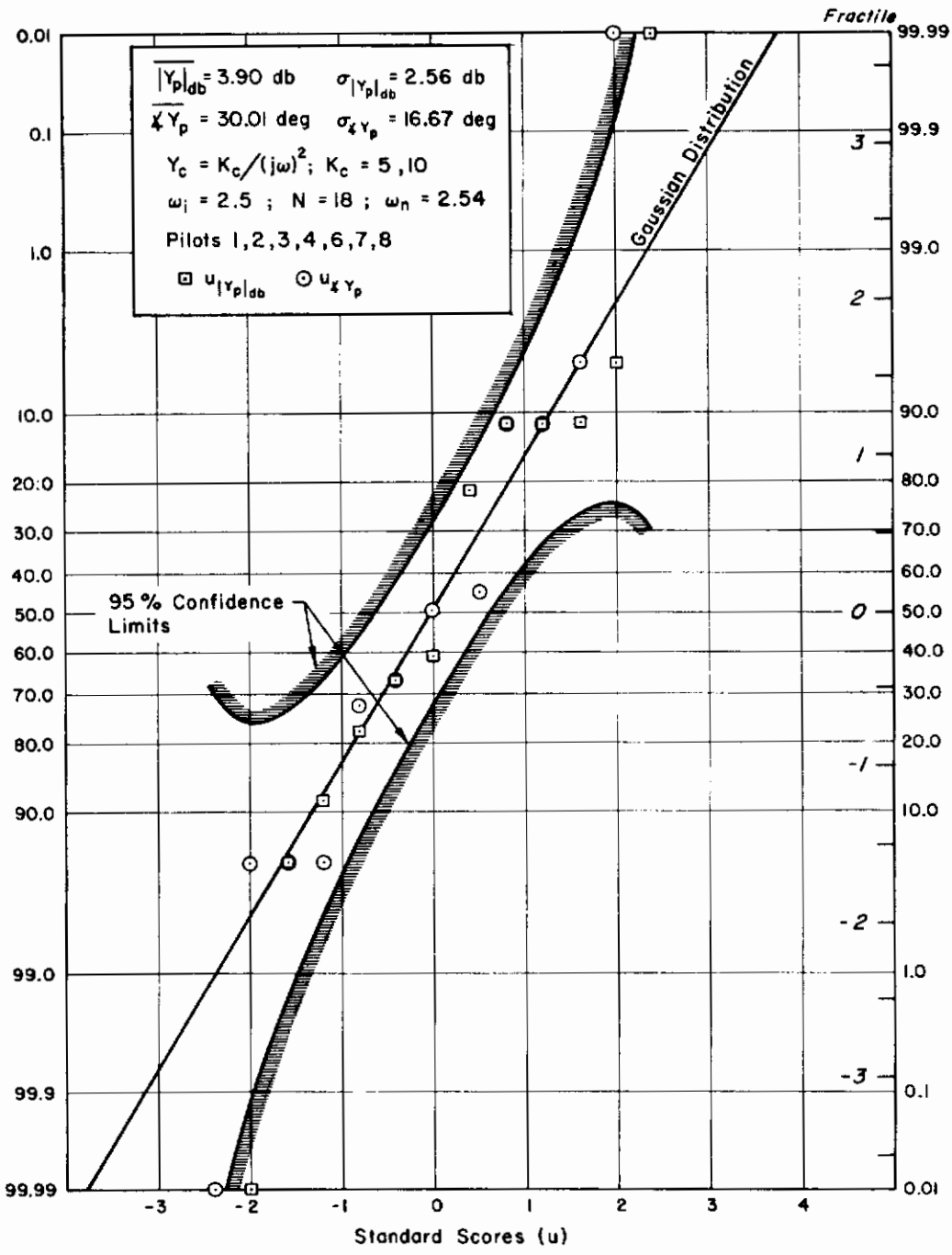

Figure 47. Typical Cumulative Distributions of Amplitude Ratio and Phase

TABLE VI

STATISTICAL ASSESSMENT OF SELECTIVE VARIABILITY PROPERTY

$Y_c = \frac{K_c}{j\omega}$	ω_n	0.969			1.49			2.54			4.03			7.57			13.8		
ω_n	ω_i →	1.5	2.5	4.0	1.5	2.5	4.0	1.5	2.5	4.0	1.5	2.5	4.0	1.5	2.5	4.0	1.5	2.5	4.0
0.157	$\lvert Y_p \rvert_{db}$	▒		▒	▒		▒			▒	▒	▒	▒	▒	▒	▒			▒
	$\measuredangle Y_p$	▒	▒	▒	▒	▒	▒	▒	▒	▒	▒	▒	▒	▒	▒	▒		▒	▒
7.57	$\lvert Y_p \rvert_{db}$													X	X	X			
	$\measuredangle Y_p$	▒	▒			▒			▒	▒	▒		▒	X	X	X			
13.8	$\lvert Y_p \rvert_{db}$										▒						X	X	X
	$\measuredangle Y_p$	▒	▒	▒	▒	▒	▒	▒	▒	▒	▒	▒	▒	▒	▒	▒	X	X	X

(a)

▒ Indicates that the variance for $\lvert Y_p \rvert_{db}$ or $\measuredangle Y_p$ at the frequency ω_n indicated in the column is significantly smaller than the variance for $\lvert Y_p \rvert_{db}$ or $\measuredangle Y_p$ at the frequency ω_n indicated in the row.

$Y_c = \frac{K_c}{(j\omega)^2}$	ω_n	0.969			1.49			2.54			4.03			7.57			13.8		
ω_n	ω_i →	1.5	2.5	4.0	1.5	2.5	4.0	1.5	2.5	4.0	1.5	2.5	4.0	1.5	2.5	4.0	1.5	2.5	4.0
0.157	$\lvert Y_p \rvert_{db}$		▒	▒	▒	▒	▒	▒	▒	▒	▒	▒	▒	▒	▒	▒	▒	▒	▒
	$\measuredangle Y_p$					▒	▒	▒	▒	▒	▒	▒	▒	▒		▒	▒	▒	▒
7.57	$\lvert Y_p \rvert_{db}$				▒			▒	▒	▒	▒	▒	▒	X	X	X			
	$\measuredangle Y_p$	▒	▒		▒	▒	▒	▒	▒	▒	▒	▒	▒	X	X	X		▒	
13.8	$\lvert Y_p \rvert_{db}$				▒			▒	▒	▒	▒	▒	▒				X	X	X
	$\measuredangle Y_p$	▒	▒		▒		▒	▒	▒	▒	▒	▒	▒				X	X	X

(b)

The picture for Table VI-a is not as clear-cut. There is statistical evidence of more variability at the extremes than in the vicinity of crossover, which for Fig. 41a, b, and c is from 4 to 5 rad/sec. This evidence is strong for the phase of Y_p and somewhat spotty for the magnitude. This finding, of course, reflects the visual impression one gets from examining Fig. 41a, b, and c.

The third question relates to the describing function difference as a function of forcing function bandwidth, ω_i. Figures 48-50 present the Y_pY_c data for $Y_c = K_c/j\omega$, $K_c/(j\omega-2)$, and $K_c/(j\omega)^2$ plotted with ω_i as a parameter. The $Y_c = K_c/j\omega$ and $K_c/(j\omega)^2$ data show some minor differences in the amplitude ratio outside the crossover region, and major differences in the phase throughout the frequency range. The $K_c/(j\omega-2)$ data show only the phase differences, and even these are much less than those for the other two controlled elements. A "t" test, using bilateral confidence limits since the direction of differences was not assumed, was performed to determine the statistical significance of apparent differences in the Y_pY_c means for $Y_c = K_c/j\omega$ and $K_c/(j\omega)^2$ at $\omega = 0.969$, 2.54, and 13.8 rad/sec (Ref. 23, Chap. 15). In essence, these test results indicate that the reasonably large differences between the curves are, in fact, real effects, whereas the smaller differences are not.

Finally, the data for $Y_c = K_c/j\omega(j\omega-1/T)$ are presented in one plot with $1/T$ as a parameter in Fig. 51.

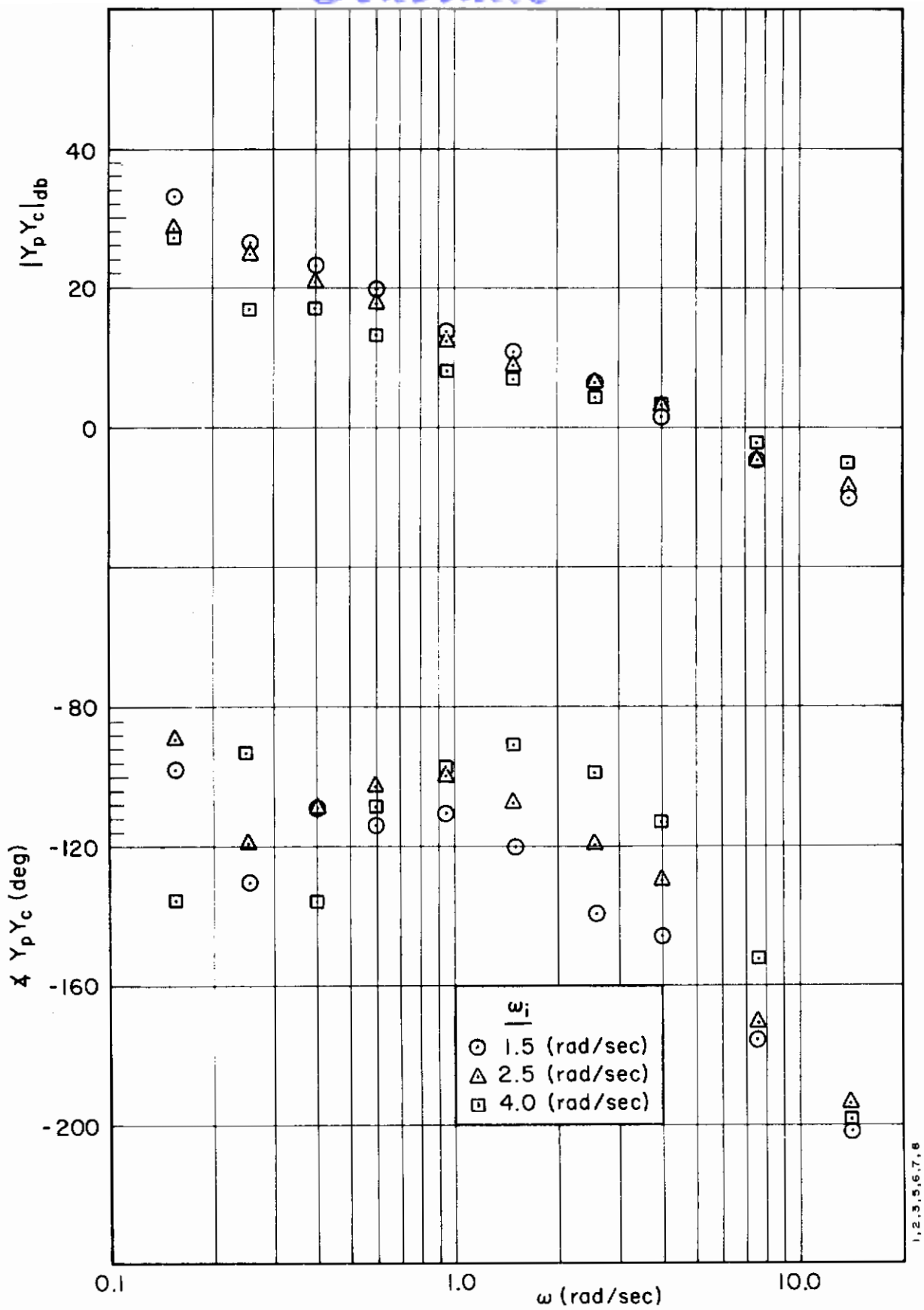

Figure 48. Averaged Open-Loop Describing Functions for $Y_c = K_c/j\omega$ with ω_i as Parameter

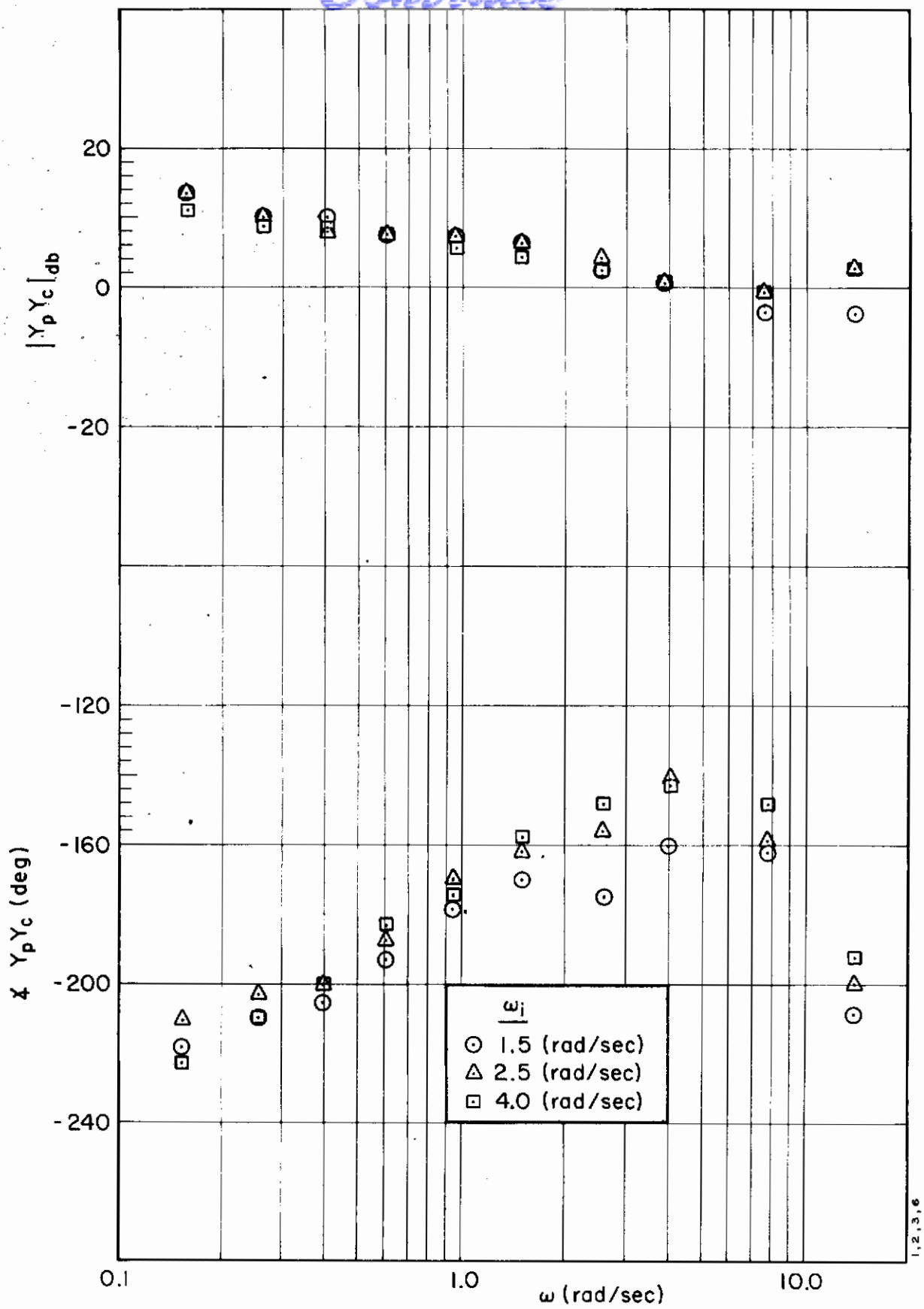

Figure 49. Averaged Open-Loop Describing Functions for $Y_c = K_c/(j\omega - 2)$ with ω_i as Parameter

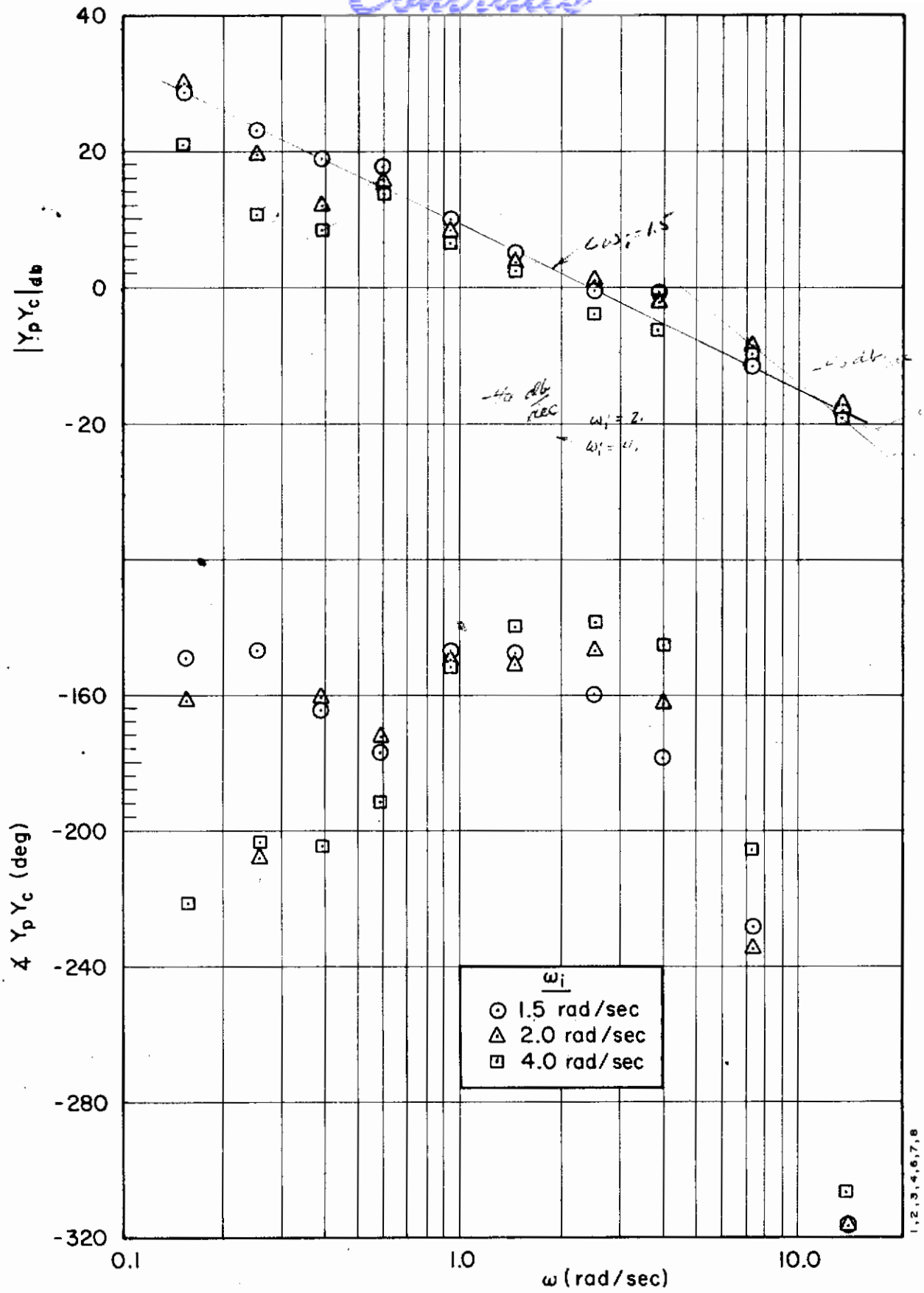

Figure 50. Averaged Open-Loop Describing Functions for $Y_c = K_c/(j\omega)^2$ with ω_i as Parameter

$K_c = 5, 10$ (from p. 106)
(no distinction possible between data corresponding).

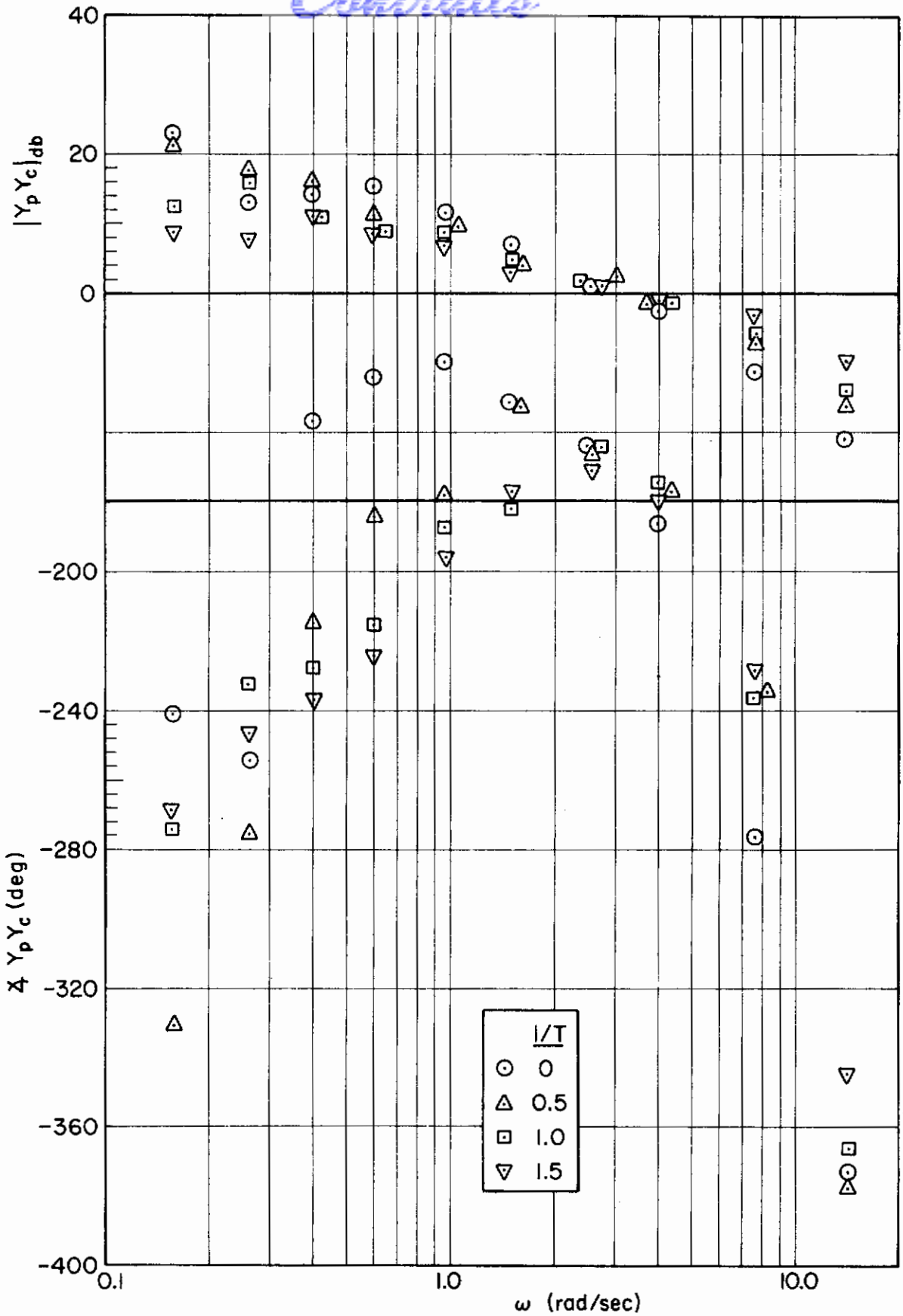

Figure 51. Averaged Open-Loop Describing Functions for $Y_c = K_c/j\omega(j\omega - 1/T)$, $\omega_i = 1.5$, 1/4" with 1/T as Parameter

CHAPTER VI

EXPERIMENTAL REMNANT DATA

A. GENERAL

The describing function, Y_p, comprises only one part of the quasi-linear system; the remnant is an equally important component. Both the magnitude and the form of $\Phi_{nn}(\omega)$ are of interest — the magnitude for its influence on $\overline{c^2}$ and $\overline{e^2}$, and the form because of the insights it may provide into the detailed nature and sources of the remnant.

The remnant, $\Phi_{nn}(\omega)$, can be measured directly by making determinations of $\Phi_{cc}(\omega)$ at other than forcing function frequencies and over such intervals that the energy in Φ_{cc} at the input frequencies does not contaminate the measurement. $\Phi_{nn}(\omega)$ can also be found at forcing function frequencies by using measurements of ρ and Φ_{cc} in connection with Eq 6, i.e.,

$$\Phi_{nn}(\omega) = \left[1 - \rho^2(\omega)\right]\Phi_{cc}(\omega) \tag{58}$$

These methods are compatible and complementary.

Considered as a noise injection signal, the point of application of the remnant can be moved from the pilot's output to other locations in the loop as long as no nonlinear elements are passed in the process. In other words, the remnant may be considered to be injected at the pilot's output, input, or someplace in between if such pilot nonlinearities as the indifference threshold are ignored. Referring to Fig. 12 and denoting open-loop remnant at e and c injected into the closed-loop as Φ_{nn_e} and Φ_{nn_c}, respectively, the remnant forms are related by

$$\frac{\Phi_{nn_c}}{|1 + Y_pY_c|^2} = \frac{\Phi_{nn_e}|Y_p|^2}{|1 + Y_pY_c|^2} = \Phi_{nn} \tag{59}$$

In principle, remnant data could be computed for all the elements in the experimental plan shown in Fig. 27. However, these computations are both time consuming and expensive, so only a relatively few runs were completely reduced. The selection was based on limiting values of the relative remnant, ρ_a, and on desired trend-establishing controlled element and forcing function combinations. ρ_a data are presented in the second section and the results of the selection process are given in the third section of this chapter.

The major contents of the third section are remnant and correlation coefficient data. The effects of controlled element, controlled element gain, and forcing function on the remnant data are explored and some features indicating nonstationary behavior as a likely remnant source are revealed. The fourth and fifth sections present additional information tending to isolate the remnant sources. Amplitude distributions of signals in the loop are given in the fourth section, with particular emphasis on those of a non-Gaussian nature. The fifth section presents fine-grained output power spectral density measurements intended to reveal the presence or absence of nonlinear or sampling behavior.

B. RELATIVE REMNANT DATA, ρ_a

The relative remnant, ρ_a, is a measure of the ratio of coherent output to total output of the pilot. The value of ρ_a can range from nearly zero to nearly one. It grossly reflects nonlinearities, nonstationary behavior, and effective noise injection, although it is not a measure of any one of these unless the others are negligible. Thus low values of ρ_a do not necessarily imply nonlinearity, or nonstationarity, or noise injection — although they do imply that at least one of these effects is present in significant amounts. ρ_a is defined by

$$\rho_a^2 = 1 - \frac{\overline{n^2}}{\overline{c^2}} = \frac{\int_0^\infty (\Phi_{cc} - \Phi_{nn})\, d\omega}{\int_0^\infty \Phi_{cc}\, d\omega} \qquad (60)$$

Presuming forcing functions made up of sinusoids, this becomes

$$\rho_a^2 = \frac{\sum_{n=1}^{N} \varphi_c^2(\omega_n)}{\left[\sum_{n=1}^{N} \varphi_c^2(\omega_n) + \frac{1}{\pi}\int_o^\infty \Phi_{nn}(\omega)\, d\omega\right]} \qquad (61)$$

where $\pi\varphi_c^2(\omega_n)$ is the amplitude of that portion of the output power spectra linearly correlated with the forcing function at frequency ω_n. ρ_a can be computed readily from data derived using either the watt-hour meter analyzer or the spectral and cross-spectral analyzer. For data from the watt-hour meter analyzer,

$$\rho_a^2 = \frac{\overline{c^2} - \overline{n^2}}{\overline{c^2}} = \frac{\frac{1}{2}\sum_{n=1}^{N} \frac{|Y_p|^2}{|1 + Y_pY_c|^2}\varphi_i^2(\omega_n)}{\overline{c^2}} \qquad (62)$$

or, since $$\Phi_{ic}(\omega_n) = \frac{Y_p}{(1 + Y_pY_c)}\Phi_{ii}(\omega_n) \qquad (63)$$

$$\rho_a^2 = \frac{\frac{1}{2}\sum_{n=1}^{N} \left|\frac{\Phi_{ic}(\omega_n)}{\Phi_{ii}(\omega_n)}\right|^2 \varphi_i^2(\omega_n)}{\overline{c^2}} \qquad (64)$$

When the spectral and cross-spectral density analyzer is used, the appropriate formula is

$$\rho_a^2 = \frac{\sum_{n=1}^{N} \frac{|\Phi_{ic}|^2}{\Phi_{ii}}}{\sum_{n=1}^{N} \frac{|\Phi_{ic}|^2}{\Phi_{ii}} + \frac{1}{\pi}\int_o^\infty \Phi_{nn}(\omega)\, d\omega} \qquad (65)$$

Using various of these formulas the relative remnant measure, ρ_a^2, was computed for almost all of the data. The results are presented in Figs. 52 –57 and are discussed below.

It will be recalled from the detailed experimental matrix, Fig. 27b, that Pilot 8 was used in an extensive exploration of controlled element gain effects for $K_c/j\omega$ and $K_c/(j\omega)^2$. Averaged data (three runs for each K_c) for this series are shown in Figs. 52 and 53. Pilot 7 was used to investigate at least four controlled element gains for $Y_c = K_c/j\omega$ for all forcing function bandwidths. Averages (two runs) from this series are also presented in Fig. 52. In general, Figs. 52 and 53 indicate a decrease in ρ_a^2 as controlled element gain is increased. In fact, Pilot 8 demonstrated one of the very largest ($\rho_a^2 = 0.81$) and one of the smallest ($\rho_a^2 = 0.065$) values of relative remnant in the entire experimental program in this $K_c/j\omega$ series.

Figures 54 – 56 present individual pilot ρ_a^2 values as functions of forcing function bandwidth for $Y_c = K_c/j\omega$, $K_c/(j\omega-2)$, and $K_c/(j\omega)^2$, respectively. All of these values are averaged over two runs except those for Pilot 8 for whom three runs were used. It is interesting to note that, across the figures, Pilot 6 generally exhibits the highest ρ_a values, whereas Pilot 4 sturdily maintains his position on the lower side. The exceptionally high values of ρ_a exhibited by Pilot 6 for many of the conditions noted indicate a close correspondence between his actions and those of an equivalent constant-coefficient linear system. Finally, Fig. 57 presents averaged ρ_a^2 data for five pilots in control of $Y_c = K_c/j\omega(j\omega-1/T)$, $\omega_i = 1.5, 1/4"$. For Figs. 54 – 57 the values of K_c for the various cases can be found by reference to Fig. 27.

C. REMNANT POWER SPECTRAL DENSITIES AND CORRELATION COEFFICIENTS

From Figs. 52 – 57, high, low, and typical conditions as defined by the average ρ_a^2 were picked out for further examination. These data were culled to find compatible sets which could exhibit the ranges of Y_c, K_c, and ω_i of interest in determining the effects of these variables on remnant. The conditions surviving the selection process are shown flagged in Figs. 52 – 57. Typical single runs were then selected from the data represented by the flagged points. These runs are listed in Table VII, where each ρ_a^2 shown is for a specific run.

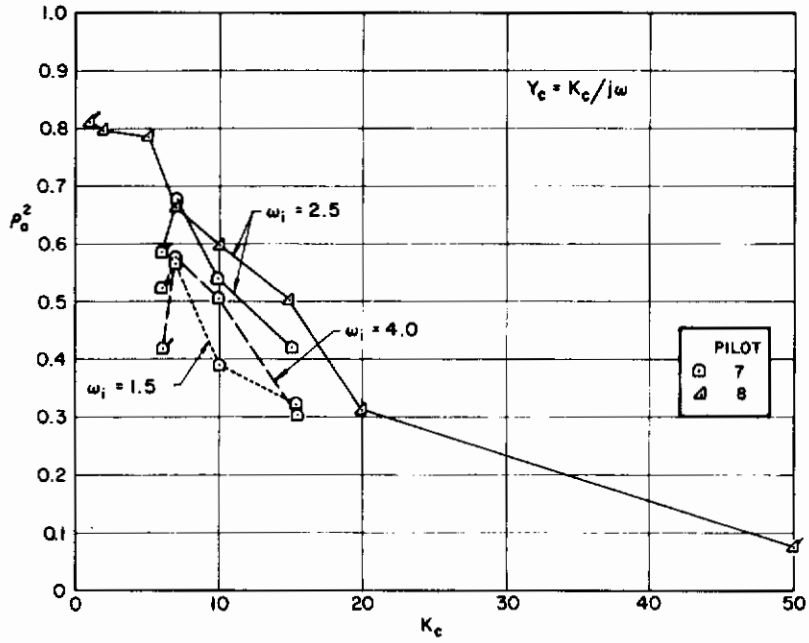

Figure 52. Relative Remnant Versus K_c for $Y_c = K_c/j\omega$

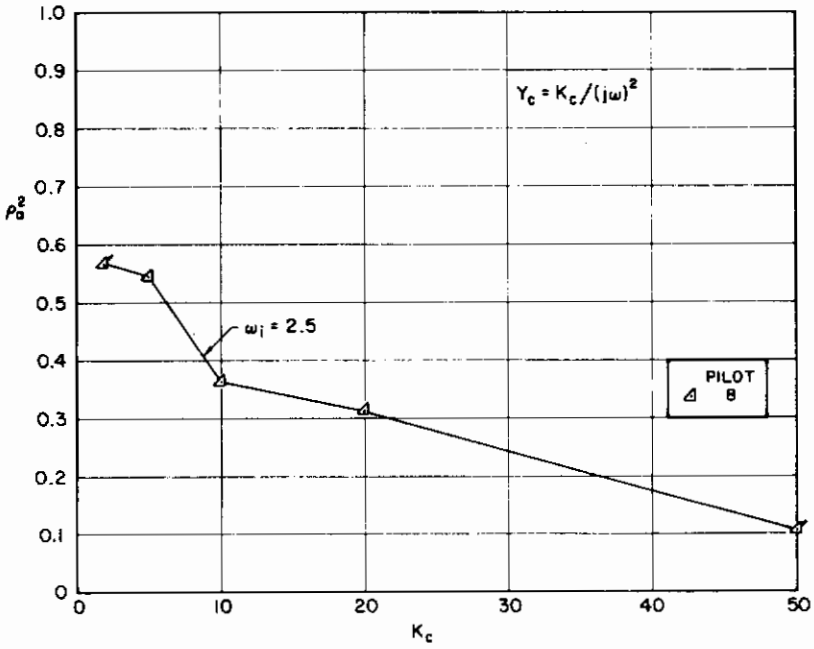

Figure 53. Relative Remnant Versus K_c for $Y_c = K_c/(j\omega)^2$

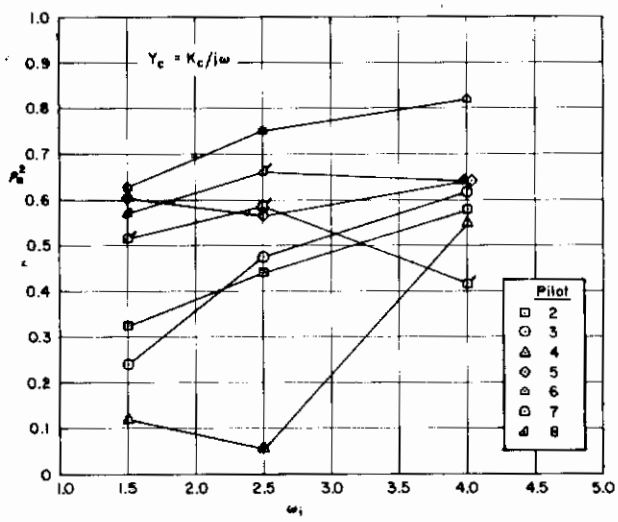

Figure 54. Relative Remnant Versus Forcing Function Bandwidth; $Y_c = K_c/j\omega$

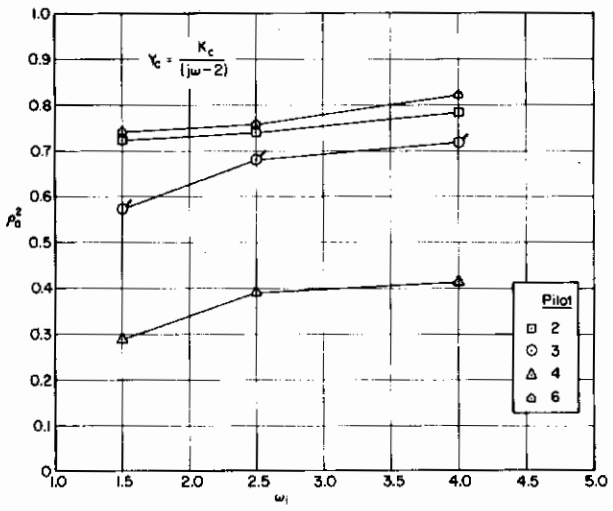

Figure 55. Relative Remnant Versus Forcing Function Bandwidth; $Y_c = K_c/(j\omega - 2)$

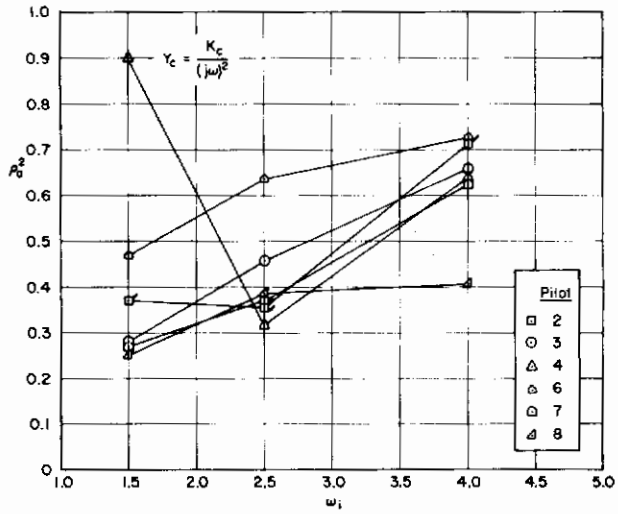

Figure 56. Relative Remnant Versus Forcing Function Bandwidth; $Y_c = K_c/(j\omega)^2$

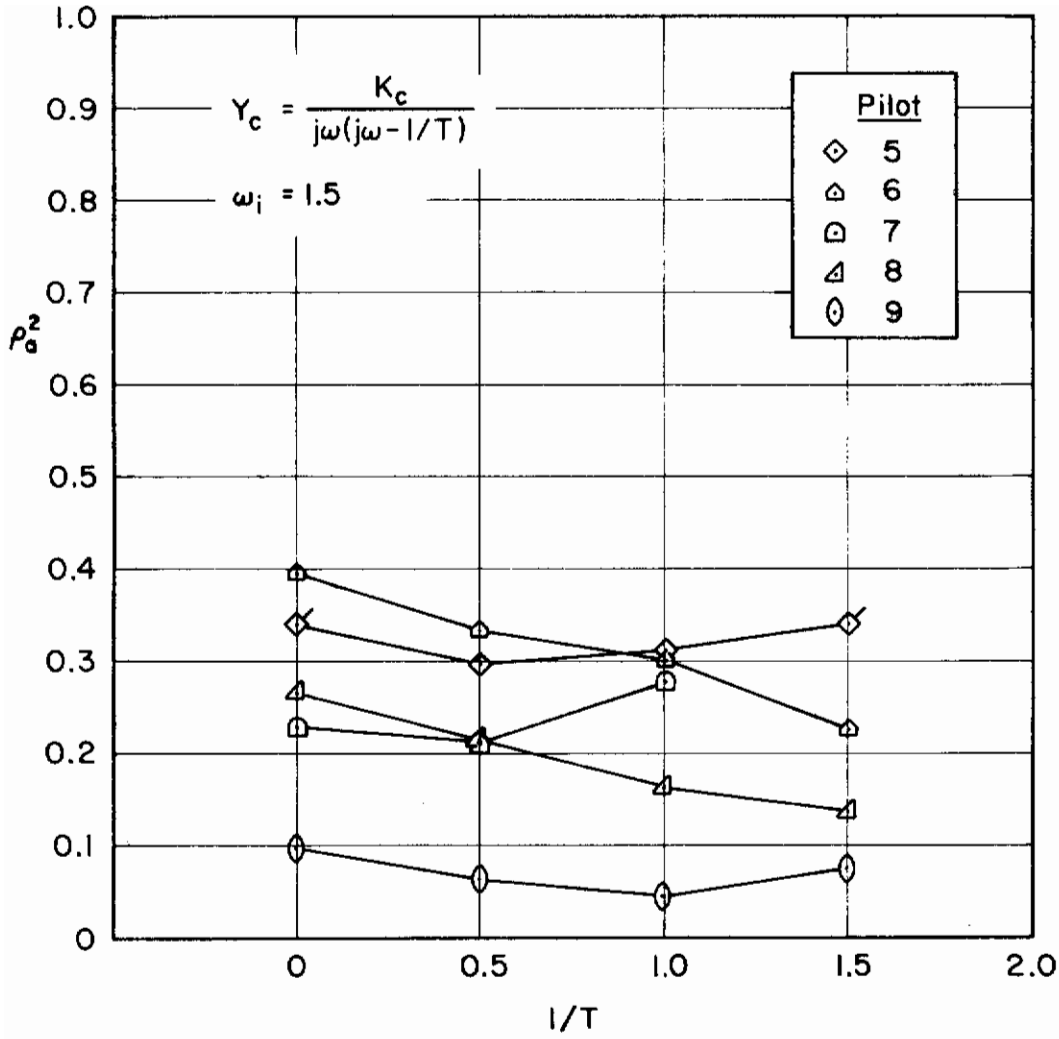

Too bad pilot 4 data wasn't obtained. Suspect; pilot 4 would have shown much larger ρ_a^2 for all $\frac{1}{T}$ than those data shown above. He appears to be much more rate sensitive based on his small ρ_a^2 for $\frac{K_c}{s^2} \neq \frac{K_c}{s-\frac{1}{T}}$

Figure 57. Relative Remnant Versus 1/T for $Y_c = K_c/j\omega(j\omega - 1/T)$, $\omega_i = 1.5$, 1/4"

There is no logical reason why the 1/T = 0 case should necessarily be better. The pilot 6 data suggests it is not.

TABLE VII

CONDITIONS SELECTED FOR DETAILED ANALYSIS

ρ_a^2	Y_c	INPUT ω_i	OPERATOR
0.11	$50/(j\omega)^2$	2.5	8
0.65	$2/(j\omega)^2$	2.5	8
0.81	$1/j\omega$	2.5	8
0.065	$50/j\omega$	2.5	8
0.55	$6/j\omega$	1.5	7
0.59	$6/j\omega$	2.5	7
0.39	$6/j\omega$	4.0	7
0.34	$2.5/(j\omega)^2$	1.5, 1/4"	5
0.34	$2.5/j\omega(j\omega - 1.5)$	1.5, 1/4"	5
0.56	$5/(j\omega - 2)$	1.5	3
0.67	$5/(j\omega - 2)$	2.5	3
0.72	$5/(j\omega - 2)$	4.0	3
0.35	$5/(j\omega)^2$	1.5	2
0.50	$5/(j\omega)^2$	2.5	2
0.69	$5/(j\omega)^2$	4.0	2

The remnants for these selected runs were measured with the spectral and cross-spectral analyzer. To obtain the best accuracy, the power spectrum was measured at the pilot's output, Φ_{cc}, at high frequencies, and at the controlled element output, Φ_{mm}, at low frequencies. The uncorrelated part of the power spectrum was found by multiplying the total power spectrum by $(1-\rho^2)$. To relate the remnant as measured at the controlled element output to the pilot's output, these values were divided by the squared magnitude of the controlled element amplitude ratio,

$$\Phi_{nn} = \frac{1}{|Y_c|^2}(1-\rho^2)\Phi_{mm} \quad \text{at low frequencies} \tag{66}$$

Otherwise Eq 58 applies (e.g., at high frequencies).

Φ_{nn} is the closed-loop remnant referred to the pilot's output. If the measurement frequency was set to one of the input frequencies, a relatively high value of ρ was generally obtained, due to the large contribution of the correlated portion (essentially a line spectrum). At frequencies other than the input frequencies, the value of ρ is very nearly zero, so that the remnant is measured directly. Values of the remnant computed at the input frequencies generally fit a smooth curve through those measured between input frequencies, indicating the generally continuous, power spectral density-like (i.e., significant line spectra absent) nature of the remnant. To indicate the continuous nature of the remnant power spectral density, it will hereafter be denoted as φ_{nn}, following our previously established convention.

After examining the remnant data in its closed-loop form as φ_{nn}, and in the open-loop forms, φ_{nn_c} and φ_{nn_e}, which result in equivalent closed-loop effects, it was found that the highest degree of similarity among remants for the Table VII conditions exists if the remnant is viewed as an open-loop quantity injected at the operator's input, i.e., as φ_{nn_e}. This is related to φ_{nn} by Eq 59, or

$$\varphi_{nn_e} = \frac{|1 + Y_p Y_c|^2}{|Y_p|^2} \varphi_{nn} \qquad (67)$$

The values can be further normalized by dividing by the mean-squared value of the input, σ_i^2, so that the result has the dimensions of one over frequency, $(\text{rad/sec})^{-1}$. Zero db is taken as 1.0 $(\text{rad/sec})^{-1}$.

The open-loop remnants referred to the pilot's input, for the cases noted in Table VII, constitute the basic data base for considering the effects of controlled element gain, forcing function bandwidth, and controlled element form on the remnant. These data are presented in Figs. 58-65. Associated with each remnant plot are the corresponding correlation coefficient, ρ, values. It will be recalled that values of this parameter less than one indicate time-varying behavior over the measurement run length.

1. Effect of K_c Variation

Two sets of data, for $Y_c = K_c/j\omega$ in Fig. 58 and for $K_c/(j\omega)^2$ in Fig. 59, illustrate the general dependence of open-loop remnant referred to pilot's input on controlled element gain. Remnant increases with controlled element gain, but the variation is not as extreme as that of the gain. There are also substantial differences in ρ between the two controlled elements considered, indicating that the pilot is fluctuating more in the course of a measurement run for $Y_c = K_c/(j\omega)^2$ than for $Y_c = K_c/j\omega$.

2. Effect of Forcing Function Bandwidth

The effect of forcing function bandwidth on remnant spectral density and the associated linear correlation is examined for three different controlled elements, $Y_c = 6/j\omega$, $5/(j\omega)^2$, and $5/(j\omega-2)$, in Figs. 60, 61, and 62, respectively. The $Y_c = 6/j\omega$ data (Fig. 60) indicate an increase in remnant with increase in forcing function bandwidth. A correlation coefficient decrease with ω_1 increase is also present in this instance. The close correspondence of these trends and their direct connection, if time variation is presumed to be the dominant cause of remnant, is a strong indication that just such time-varying remnant causes are indeed dominant here.

The remnants and ρ values for Pilot 2 in control of $Y_c = 5/(j\omega)^2$ are somewhat different for the three forcing function bandwidths, although no orderly variation appears to be present (Fig. 61). The spread present is probably as indicative of run-to-run variability as it is of any φ_{nn_e} dependence on the forcing function bandwidth.

Finally, Fig. 62 shows both the open-loop remnant and the correlation coefficient for the unstable-divergence controlled element, $Y_c = 5/(j\omega-2)$, to be invariant with forcing function bandwidth.

In summary, the data examined above indicate that the effect of forcing function bandwidth on the remnant can vary from minor to none.

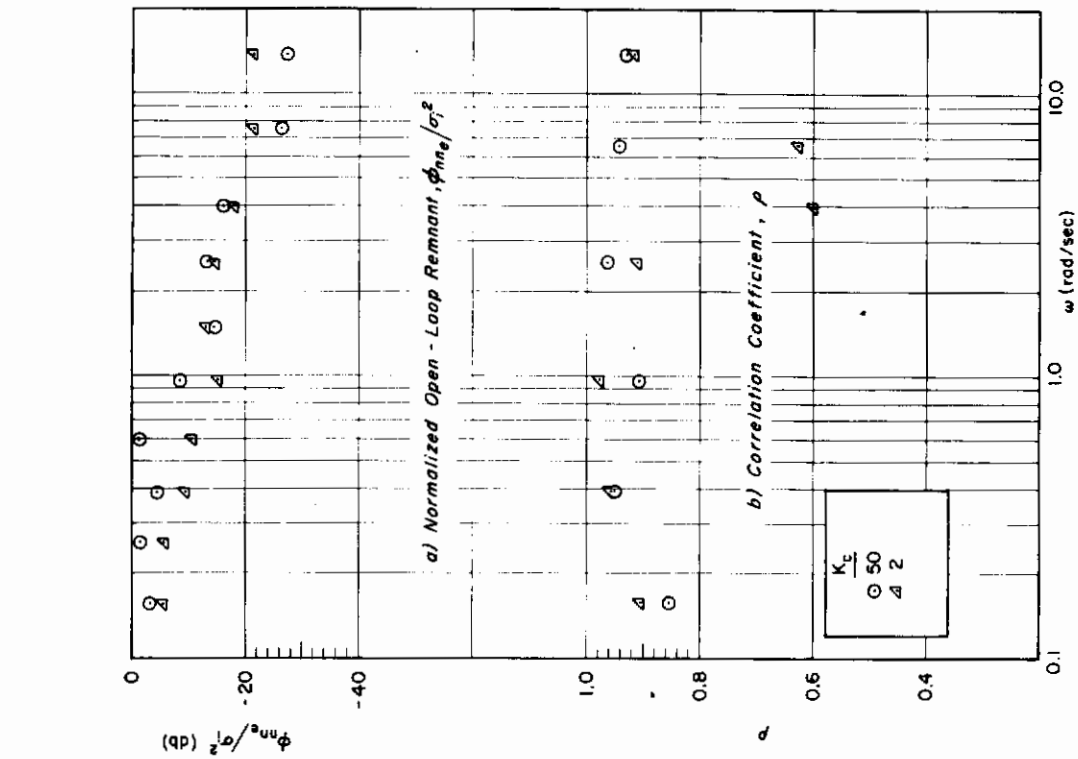

Figure 59. Effect of K_c Variation on Remnant; $Y_c = K_c/(j\omega)^2$, $\omega_1 = 2.5$, Pilot 8

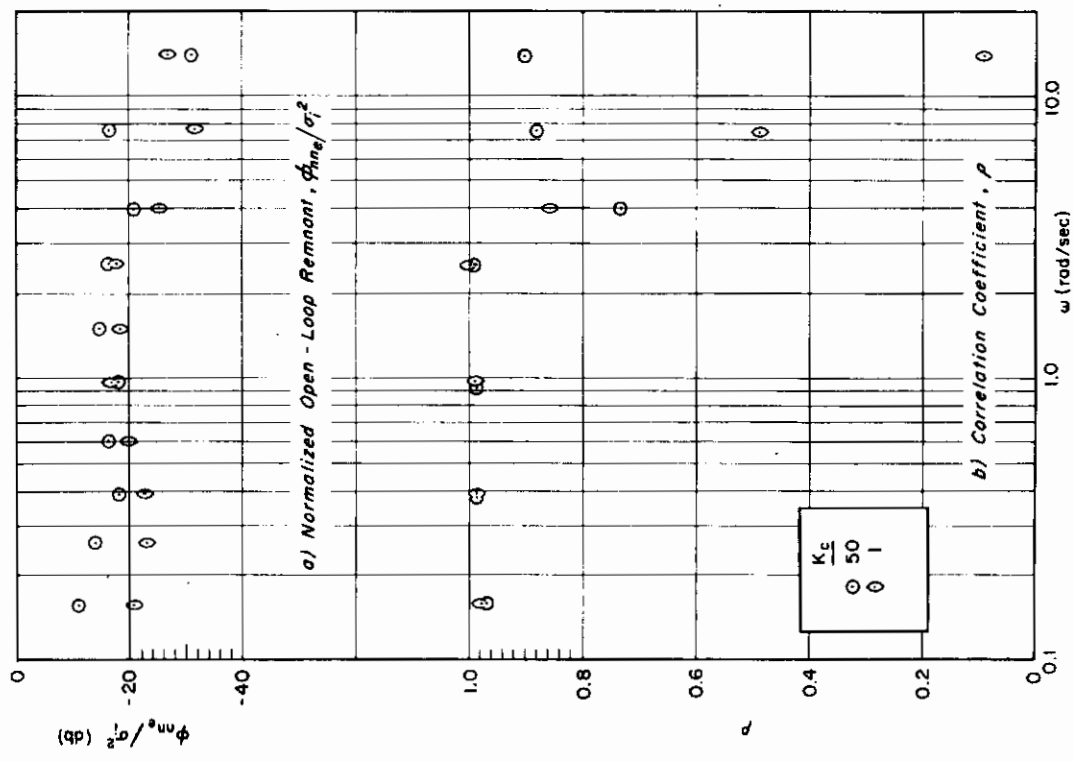

Figure 58. Effect of K_c Variation on Remnant; $Y_c = K_c/j\omega$, $\omega_1 = 2.5$, Pilot 8

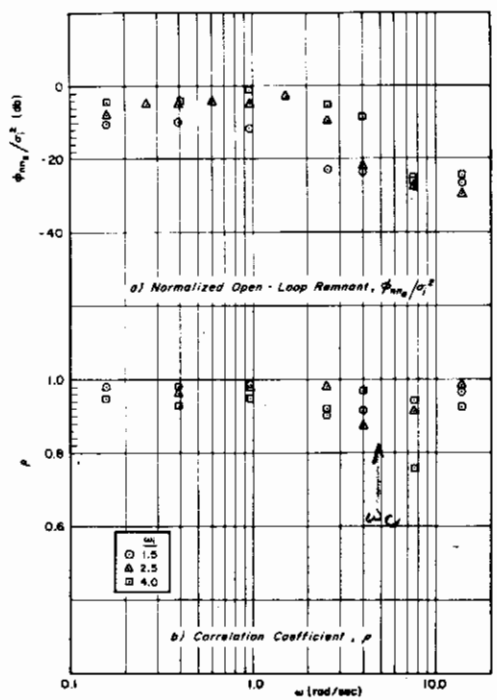

Figure 60. Effect of ω_i Variation on Remnant; $Y_c = 6/j\omega$, Pilot 7

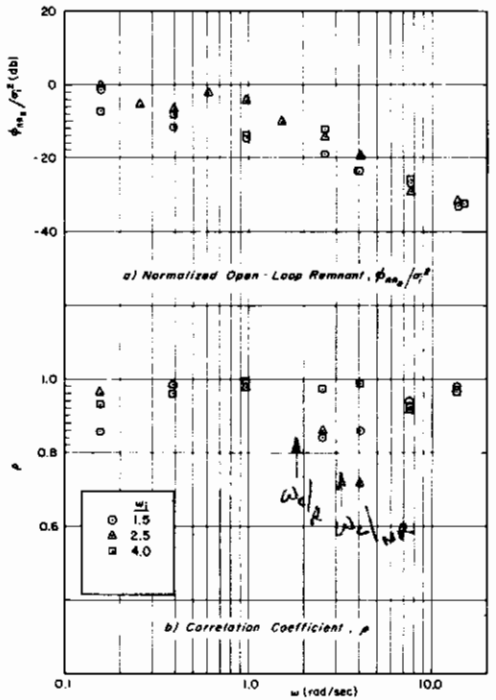

Figure 61. Effect of ω_i Variation on Remnant; $Y_c = 5/(j\omega)^2$, Pilot 2

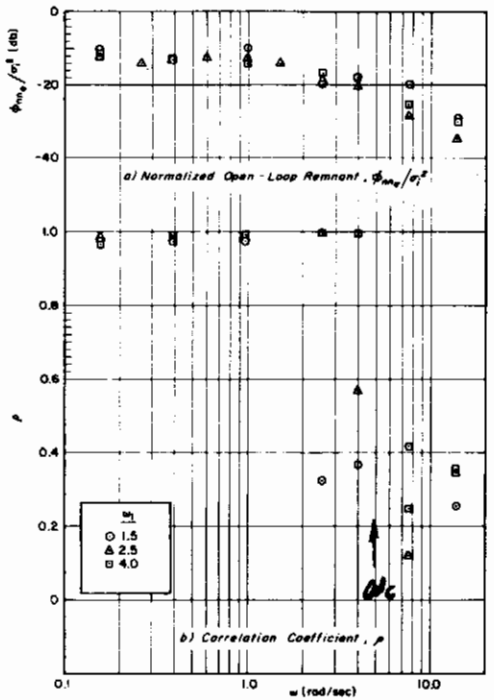

Figure 62. Effect of ω_i Variation on Remnant; $Y_c = 5/(j\omega - 2)$, Pilot 3

3. Effect of Controlled Element Variation on Remnant

The Pilot 8 data presented previously in Figs. 58 and 59 were seen there to be dependent on controlled element gain for the two controlled elements considered. To determine the effect of controlled element per se, these data were averaged for each controlled element, and the averages obtained are compared in Fig. 63. When data from other pilots are added to those of Pilot 8, as in Fig. 64, it is seen that the major effect of variation on the remnant is as much intersubject as inter-controlled-element.

An exceptionally interesting and crucial example of a more substantial remnant variation due to controlled element changes is shown in Fig. 65. Here the two limiting cases, $1/T = 0$ and 1.5, for the critical controlled element, $Y_c = 2.5/j\omega(j\omega - 1/T)$, are shown. The remnant for $1/T = 0$ is considerably less than that for $1/T = 1.5$, while the correlation coefficient varies in an opposite fashion. The $1/T = 1.5$ critical case, in fact, has the lowest correlation coefficients of the entire experimental series. These low ρ's indicate a good deal of describing function time variation in the course of the run. As noted previously, the pilots were often on the verge of losing control. It will be recalled from Fig. 34 that the amplitude ratio was quite tightly held, whereas the phase exhibited wide run-to-run variations. These data, taken in context with those of Fig. 65, are very strong evidence indeed that describing function time variations are a major remnant contributor.

D. AMPLITUDE DISTRIBUTIONS OF SIGNALS IN THE LOOP

One can attempt further insights into the origin of the remnant by examining the amplitude distribution for c(t) and e(t) for the runs listed in Table VII. Since i(t) has a nearly Gaussian distribution, a non-Gaussian distribution at c or, more unexpectedly, at e would indicate a strong source of nonlinear behavior and a possible basis for remnant generation. The amplitude distribution functions were examined as follows.

The data on the runs listed in Table VII were sampled once per second for a total of 240 observations for each quantity considered, i.e.,

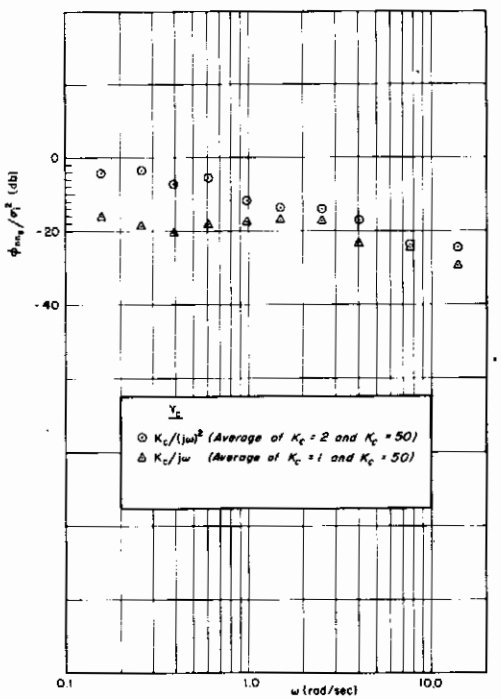

Figure 63. Effect of Y_c Variation on Remnant; $Y_c = K_c/j\omega$, $\omega_i = 2.5$, Pilot 8

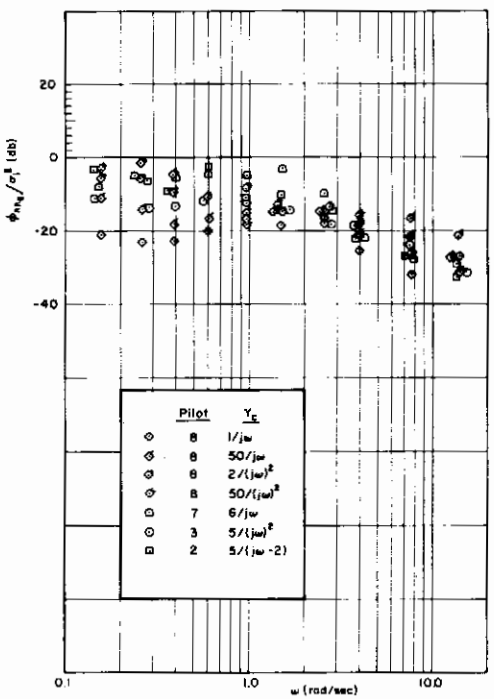

Figure 64. Effect of Y_c and Pilot Variations on Remnant; $\omega_i = 2.5$

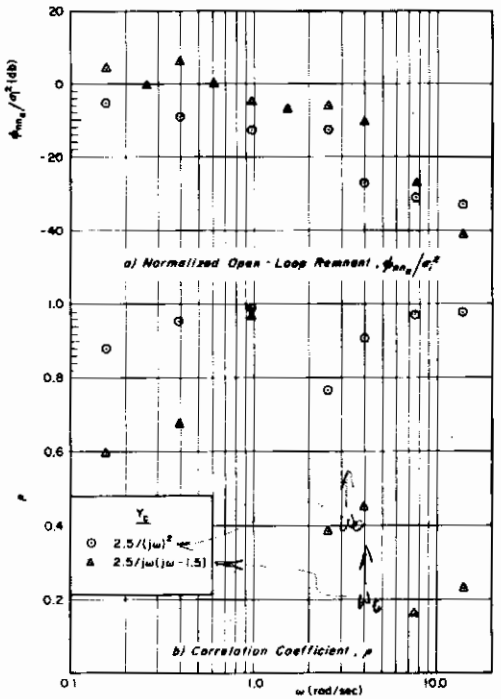

Figure 65. Effect of Y_c Variation on Remnant; $Y_c = K_c/j\omega(j\omega - 1/T)$, $\omega_i = 1.5$, 1/4", Pilot 5

either c(t) or e(t). The mean and variance were then computed for each data set. Since the first eight deciles for the standardized variable x/σ_x in a normal distribution are $x/\sigma_x = \pm 0.25, \pm 0.53, \pm 0.83$, and ± 1.28, multiplying these standard values by the measured σ_x and adding the mean value defines the actual bounds for all ten deciles. Everything not included within $x/\sigma_x = \pm 1.28$ is in the plus or minus last decile. If the data were Gaussian, an equal number of data points would be found in each decile. Because the actual data are not necessarily Gaussian, the subdivisions are not necessarily decile for the actual data. Such possible differences between expected and observed values provide the basis for a chi-squared test (Ref. 23) for goodness of fit. Using this test (for goodness of fit between expected and observed data in each decile), at the 0.05 level (Ref. 23) six c(t) distributions and one e(t) distribution were determined to be non-Gaussian.

In order to approximate a probability density function from these data, bar graphs were created such that the amplitude of each bar was the relative frequency (number of measured points within the decile divided by the total number of points) divided by the width of the decile. This approximate distribution is symmetrical about $c/\sigma_c = 0$ or $e/\sigma_e = 0$, and has eight amplitude bars since the amplitudes of the last two deciles become zero because their widths are infinite.

The amplitude distributions shown in Figs. 66b, f, and g are all Gaussian as indicated by the chi-squared test — a somewhat surprising result by the look of the distributions. All figures except Fig. 66d are measurements of c(t); Fig. 66d is the one e(t) distribution that was not Gaussian. The numerical coding on each element of Fig. 66 represents pilot, controlled element, and ω_i, in that order.

From visual observation of tracking records and subjects, we can assert that two kinds of control action are likely to be major causes of non-Gaussian output behavior. One is an occasional tendency for bang-bang-like limit-to-limit control activity. The other is a tendency to control controlled elements similar to $Y_c = K_c/(j\omega)^2$ by output pulses having areas roughly proportional to the stimulus. Idealized bang-bang action will result in bimodal distributions wherein the relative frequeneies

are large at either extreme. The pulsing behavior also results in distributions with a relatively large proportion of amplitudes near the fringes, although intermediate amplitudes are also likely to be present. Several distributions shown in Fig. 66 are compatible with this pulse-like activity, although these distribution plots are at best only roughly indicative of possibilities.

Of all the non-Gaussian output amplitude distributions, the strongest indication of bimodal operation is shown in Fig. 66a for Pilot 2 $\left[K_c/(j\omega)^2,\ \omega_i = 1.5\right]$. Further evidence of nonlinear operation is seen in the low value for ρ_a^2 of 0.35 for this condition (see Table VII). As the input cutoff frequency is increased, ρ_a^2 becomes larger, 0.50 for $\omega_i = 2.5$ and 0.69 for $\omega_i = 4.0$. At the same time the amplitude distribution becomes more nearly Gaussian, showing much less tendency for bimodal behavior (Figs. 66b and c). The results of the chi-squared tests for $\omega_i = 2.5$ and 4.0 indicated a Gaussian distribution for $\omega_i = 2.5$ but not for $\omega_i = 4.0$, which is contrary to what would be expected. The wider input bandwidth should require a greater number of small corrections by the operator, which would force him to exhibit a more linear characteristic. However, the failure of the chi-squared test to verify the expected behavior in this case is not serious, since the number of classes on which it was based was small. The chi-squared test becomes more sensitive as the number of classes on which it is based is increased. No large difference between the distributions for $\omega_i = 2.5$ and 4.0 is evident from Figs. 66b and c.

The effect of controlled element gain on the tracking behavior of Pilot 8 is illustrated in Figs. 66e and f for $K_c/(j\omega)^2$ and in Figs. 66g and h for $K_c/j\omega$. It is interesting to note that a non-Gaussian output is produced by the operator for the small value of K_c when controlling $K_c/(j\omega)^2$, and for the large value of K_c when controlling $K_c/j\omega$. However, there is a distinct difference in the shape of the distributions for these cases. Figure 66h $(K_c/j\omega)$ indicates some degree of bimodal operation, whereas Fig. 66f $\left[K_c/(j\omega)^2\right]$ shows no indication at all. Reference to the ρ_a^2 values given in Table VII shows a much lower value for large values of K_c for both controlled elements than for small values of K_c.

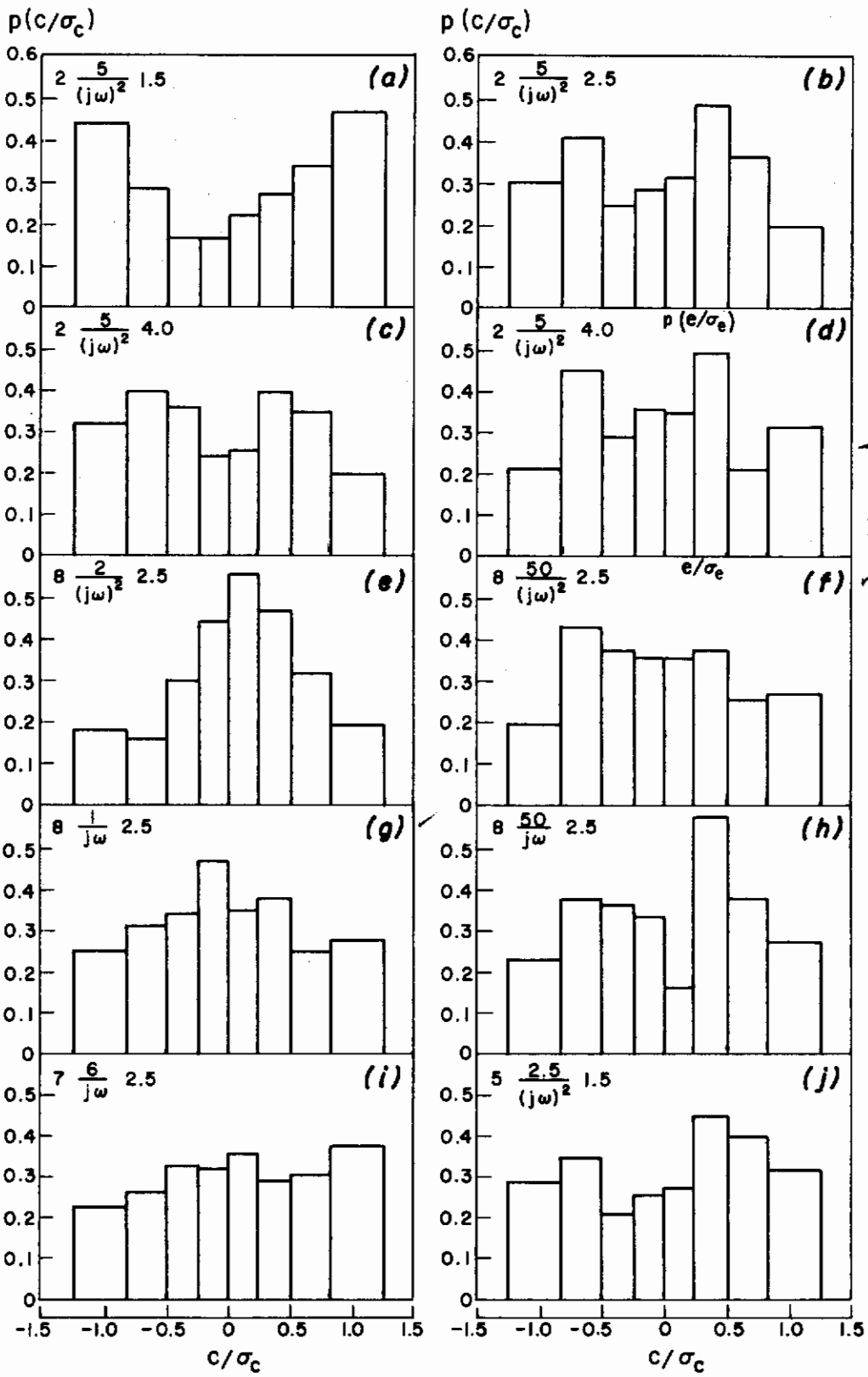

Figure 66. Amplitude Distributions

Thus, while the large values of K_c generally result in increased remnant, the amplitude distribution of the remnant does not necessarily become non-Gaussian.

II. OUTPUT POWER SPECTRAL DENSITIES

Still another way to investigate remnant sources is to examine $\Phi_{cc}(\omega)$ in great detail. There have been repeated suggestions that the remnant can be explained by means of a model which includes certain pronounced nonlinearities (e.g., Ref. 36) or by means of a model which includes a nearly periodic sampler (Refs. 5, 6, and 60). These suggestions, if followed through, place requirements on what is to be expected in the spectrum of the operator's output.

To some extent the expectations depend on the analytical description of the forcing function, i.e., whether $\Phi_{ii}(\omega)$ should be considered as it really is — a sum of deterministic sinusoids — or as an equivalent to a random process. Either presumption may have merit, depending on the problem at hand, and sometimes the results desired are insensitive to the viewpoint taken. Here, however, a potential conflict does exist — the type of output power spectrum due to operator nonlinear or sampling actions will be quite different, depending on whether the forcing function spectra are a series of lines or continuous in nature. To avoid any such confusion, the only spectral data examined here will be for single runs. The appropriate forcing function description will then be as a series of line spectra.

With the line spectrum forcing function, nonlinearities in the operator would be expected to result in output spectrum peaks which are harmonically related to the forcing function frequencies. Constant-rate sampling on the part of the operator will also tend to produce recurring peaks and valleys in the output spectrum. If the sampler is precisely periodic at a frequency ω_s, output spectral lines would be expected at frequencies $\omega_n \pm m\omega_s$, $m = 0, 1, 2, 3, \cdots$. Slight variations in sampling rate over a measurement run would tend to slur the lines into peaks.

A search for peaks of either or both natures was undertaken by a painstaking spectral analysis of several output spectra from ω_1 up to

40 rad/sec. Figures 67 – 69 show a survey conducted for a pure gain controlled element. Pilots 2, 6, and 3 were examined for $Y_c = K_c = 1$, 5, and 10, respectively. These data show evidence neither for sampling nor for nonlinear behavior.*

To determine if higher levels of forcing function power at high frequencies would modify the above results, the forcing function was changed from the augmented rectangular form to a pure rectangular shape wherein each sinusoid in the forcing function had the same amplitude. The resulting forcing function spectra are referred to as R14 (R = rectangular, 14 rad/sec = approximate bandwidth). Figure 70 indicates that this change in forcing function spectral shape fails to evoke any indication of sampling or nonlinear behavior.

Because the pilot sometimes appears to exert control by means of a pulsing motion when $Y_c = K_c/(j\omega)^2$ (e.g., Pilot 2 in Fig. 66), the output spectral density for some of these cases was examined for conditions which might make the presence of output sampling more likely. Figures 71, 72, and 73 are for Pilots 2, 7, and 8 controlling ω_i = 1.5, 1/2" for $Y_c = K_c/(j\omega)^2$ with K_c = 5, 5, and 10, respectively. Again there is no evidence for either sampling or strong nonlinear behavior.

In summary, the evidence presented in this section strongly indicates that neither periodic sampling nor nonlinear transfer characteristics are dominant remnant sources. Although Section D presented some amplitude distribution data tending to support a pulsing type of control action for certain $K_c/(j\omega)^2$ cases, this does not appear to result in substantial remnant relative to other sources. So much for what the remnant is not. However, enough data and interpretation have already been presented to indicate that the major source of remnant is nonstationary behavior during measurement runs; and to tend to isolate the major kind of non-steady activity as a time-varying phase shift.

*The scale is such that 1.0 in^2/rad/sec on the graph is zero db. The tape noise level is indicated by a broken line.

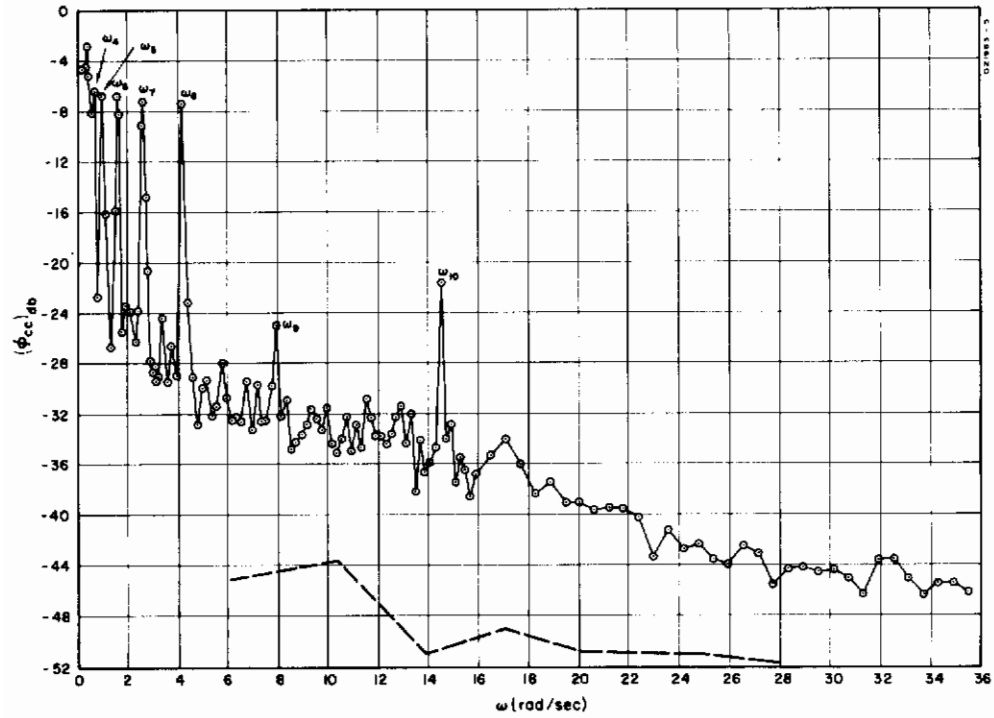

Figure 67. Output Power Spectrum; $Y_c = K_c = 1$, $\omega_i = 4$, 1"
Pilot 2

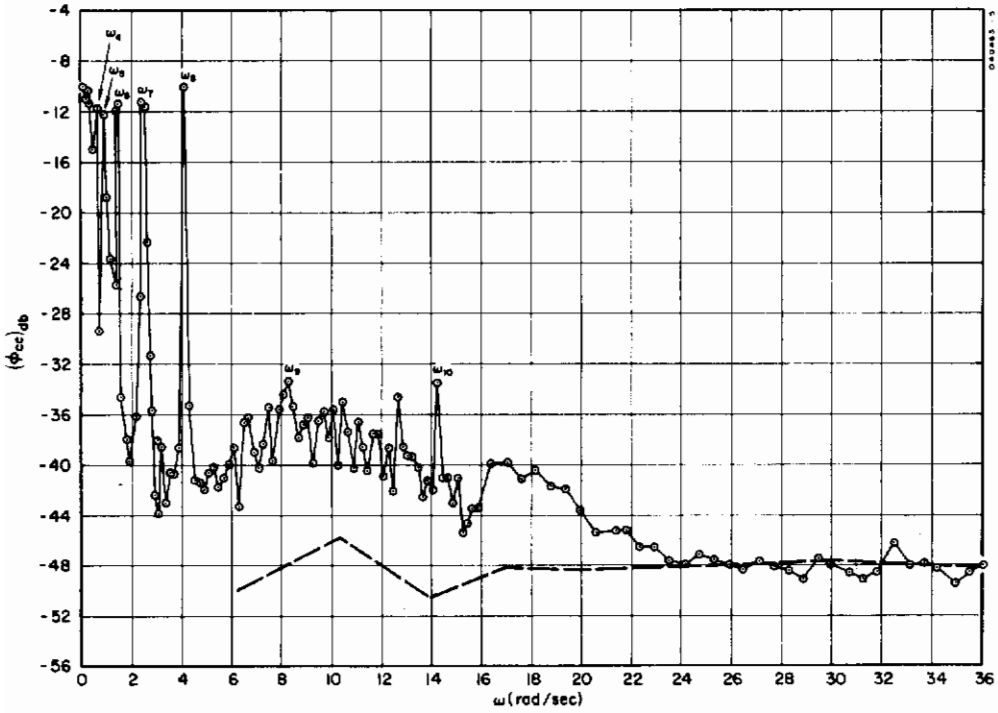

Figure 68. Output Power Spectrum; $Y_c = K_c = 5$, $\omega_i = 4$, 1"
Pilot 6

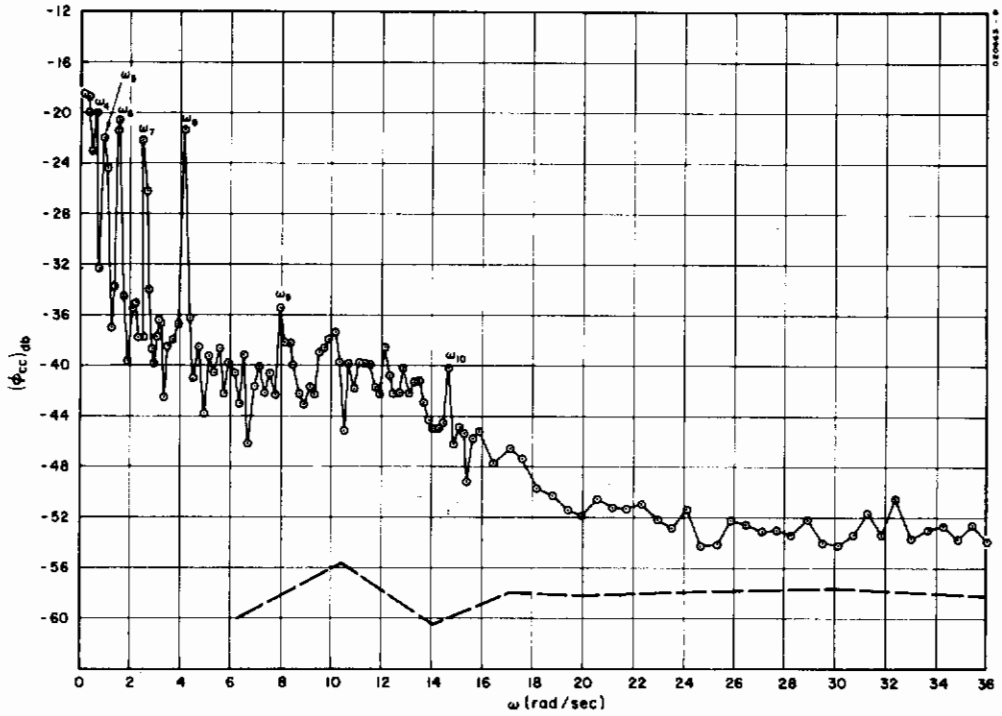

Figure 69. Output Power Spectrum; $Y_c = K_c = 10$, $\omega_i = 4$, 1"
Pilot 3

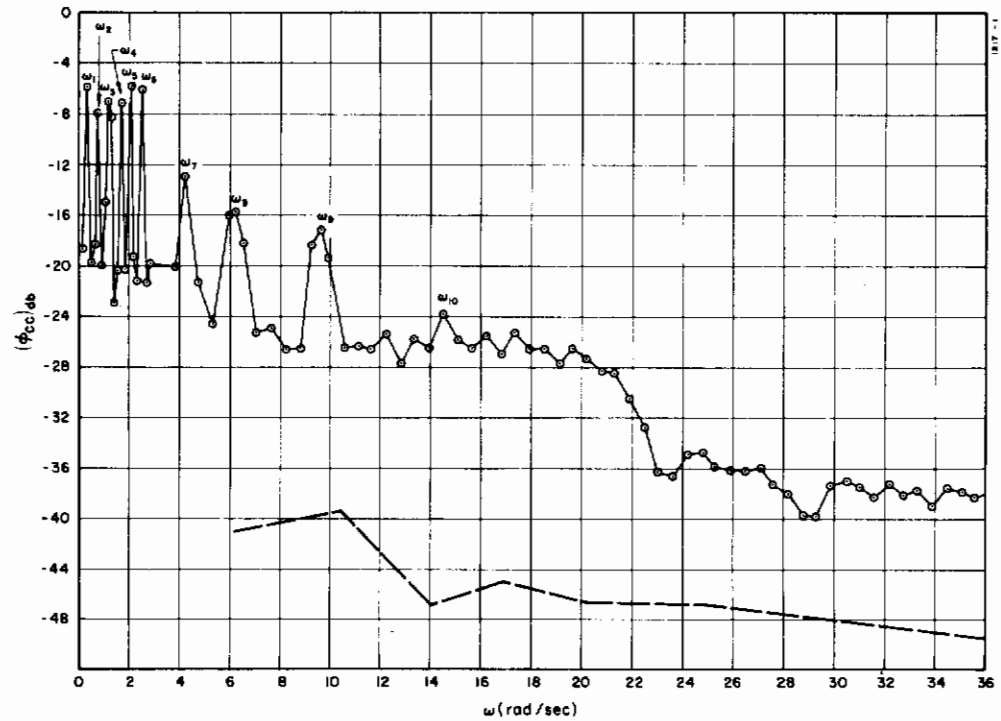

Figure 70. Output Power Spectrum; $Y_c = K_c = 1$, R14, 1"
Pilot 1

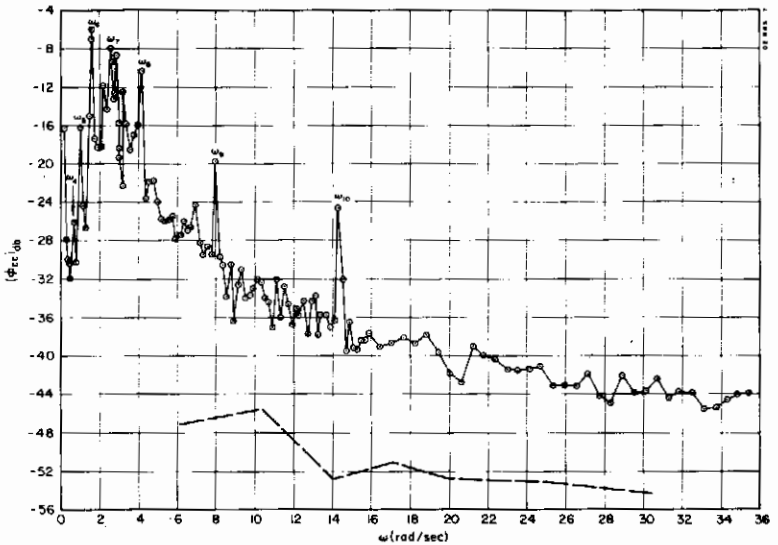

Figure 71. Output Power Spectrum;
$Y_c = 5/(j\omega)^2$, $\omega_i = 1.5$, 1/2"
Pilot 2

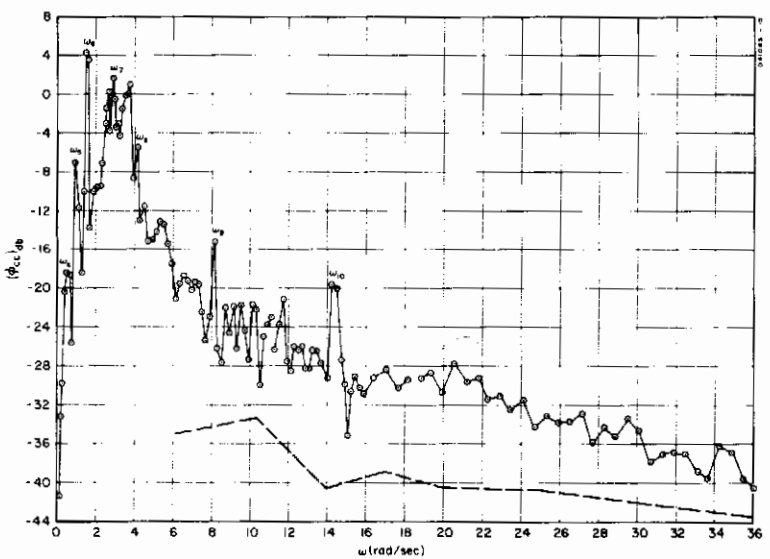

Figure 72. Output Power Spectrum;
$Y_c = 5/(j\omega)^2$, $\omega_i = 1.5$, 1/2"
Pilot 7

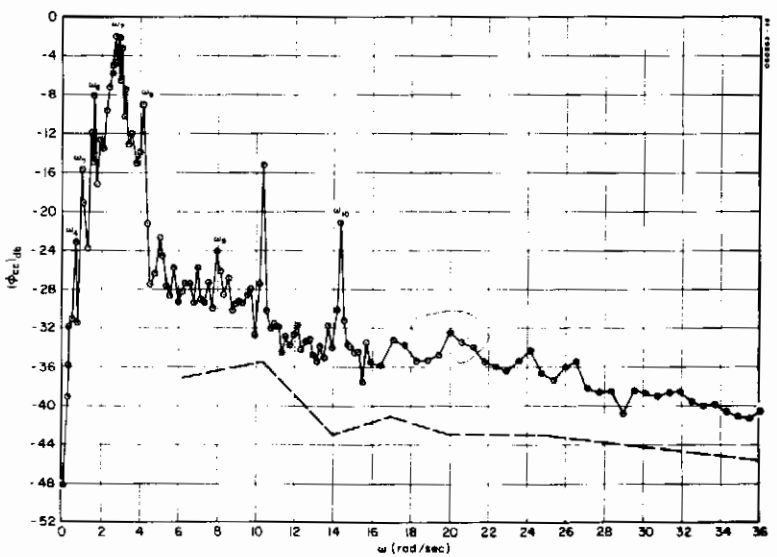

Figure 73. Output Power Spectrum;
$Y_c = 10/(j\omega)^2$, $\omega_i = 1.5$, 1/2"
Pilot 8

CHAPTER VII

INTERPRETATION AND ANALYTICAL APPROXIMATIONS FOR DESCRIBING FUNCTION AND PERFORMANCE DATA

A. INTRODUCTION

The describing function data of Figs. 41 – 44 contain the quasi-linear transfer characteristics of the human pilot for the experimental situations examined. The dependence of the operator's transfer characteristics on the forcing function and controlled element task variables is explicitly revealed by comparisons between these data. For the experimental conditions considered we can qualitatively describe the trends, features, differences, similarities, etc., exhibited by the data for and across the several conditions. Such a qualitative description provides on a verbal level, with some generalization, the information explicitly exhibited numerically by the data themselves. This procedure has already been used in the chapters presenting the describing function data and will be invoked again later.

Qualitative description, while necessary, does not provide a sufficient basis for the abstractions needed to achieve simplification and generality. This can best be accomplished using quantitative models which in some sense or other approximate the actual data. When the experimental results are approximated by analytical models, the numerical values of the model parameters serve as quantitative measures of the experimental data. Then we can develop some "laws" of operation for the approximate analytical models in which the variations in these parameter values exhibit trends similar to those observed experimentally. In this way verbal description is reduced to simple quantitatively expressed characterizations. To the extent that the analytical model approximates the actual data and is reasonably simple in form, we may obtain much greater insight into the "laws" which actually govern the operator's behavior. To achieve this end we shall evolve in this chapter some simple analytical models for the data of Figs. 41 – 44.

The purposes which the analytical models are intended to serve include:

1. Characterization of past observations for fixed experimental conditions with simple analytical forms, thereby achieving economies in description of the experimental data

2. Quantitative description of experimentally observed trends in terms of analytical relationships between model parameters and task variables

3. Establishment of the basis for a rationale which can be used to better "understand" the ways in which the pilot behaves as a control system component

4. Provision of a basis for quantitative extrapolation, thereby making possible the prediction of pilot behavior in novel situations

With these purposes in mind, turn next to the possible types of models which might be used to characterize the data. Clearly, a highly desirable feature would be some form in which a minimum number of parameters are capable of representing the phenomena selected for emphasis in that particular model. Equally important is the desire that the particular model form be one which is analytically simple and tractable. These desires can conceivably conflict with the requirement that the analytical model be reasonably descriptive of the data. Fortunately, both desires and requirements can be met by using describing function forms made up largely of ratios of rational polynomials with the addition of a transport lag (pure time delay) term. The use of such analytical models for human operator describing function description has been extensively discussed and applied elsewhere (e.g., Refs. 13, 34, and 53) and, in fact, the existing analytical-verbal model is of precisely this nature. Our major task, therefore, is to examine the data presented here using such forms rather than to justify the particular variety of form selected.

In the following sections analytical models shall be derived by curve-fitting the experimental describing function data. In the process three basic levels of approximation shall be used. At the first level

are extremely simple models which exhibit characteristics similar to the actual data in the crossover region. The forms used amount to the crossover model, i.e.,

$$Y_pY_c \doteq \frac{\omega_c e^{-j\omega\tau_e}}{j\omega} \tag{68}$$

When both ω_c and τ_e are allowed to vary, this equation has enough flexibility to characterize the basic crossover region trends for the $K_c/j\omega$ and $K_c/(j\omega)^2$ data. With somewhat less accuracy it is also suitable for the $K_c/(j\omega-2)$ cases. With this first model the variations of paramount importance are those of τ_e and ω_c with controlled element and forcing function bandwidth. In the course of the discussion, Adjustment Rules 4b (system phase margin) and 5b ($\omega_c - \omega_i$ dependence) will be modified.

Modified versions of the crossover model are more appropriate to systems involving extensive pilot lead and/or those having controlled element dynamics with break points in the general crossover region. These include such open-loop describing functions as

$$Y_pY_c \doteq \frac{(K_pK_c)\left[\frac{\omega_c}{K_pK_c}\, j\omega + 1\right]e^{-j\omega\tau_e}}{(j\omega)^2} \tag{69}$$

for $Y_c = K_c/(j\omega)^2$;

$$Y_pY_c \doteq \frac{(K_pK_c)\left[\frac{\omega_c}{K_pK_c}\, j\omega + 1\right]e^{-j\omega\tau_e}}{j\omega(j\omega - 1/T)} \tag{70}$$

for $Y_c = K_c/j\omega(j\omega - 1/T)$; and

$$Y_pY_c \doteq \frac{K_pK_c e^{-j\omega\tau_e}}{(j\omega - 1/T)} \tag{71}$$

for $Y_c = K_c/(j\omega - 1/T)$. These direct extensions of crossover models are the simplest forms possible which are compatible with even a gross characterization of the data over the measurement bandwidth.

Both the crossover model and its direct extensions fail to account for the low frequency phase lags. These are handled by refining the extended crossover model to include a catchall increment to the low frequency phase.

With the extended crossover model, all of the major trends supported by several data points over a portion of the measurement bandwidth are described reasonably well. There are, however, certain isolated data points which require further explanation or which can serve as a basis for further elaboration. These isolated points occur at the extremes of the measurement bandwidth, where data variability tends to be largest. However, for the $Y_c = K_c/(j\omega - 2)$ case the constraining nature of the controlled element dynamics acts to keep the variability low, so these data offer admirable possibilities for further elaboration and refinement. This is accomplished using "precision fits" for the data which support the so-called precision model. This most refined model is the only one which has a basic form which is not necessarily restricted to use over only a finite bandwidth, i.e., it satisfies physical limitations as ω approaches zero or infinity while characterizing the data exceptionally well over the measurement band.

The three basic levels of model precision introduced here will be discussed in the three immediately following sections. As a final preview to help keep things straight for the reader, a total of five actual model types are used. These are summarized below with a listing of the parameters which are allowed to vary in order to fit the data for a given Y_c.

Crossover Models

$$Y_pY_c \doteq \frac{\omega_c e^{-j\omega\tau_e}}{j\omega} \quad , \quad \omega_c,\ \tau_e \text{ variable} \tag{72}$$

$$Y_pY_c \doteq \frac{\bar{\omega}_c e^{-j\omega\tau_e}}{j\omega} \quad , \quad \tau_e \text{ variable} \tag{73}$$

Extended Crossover Models

First Approximation:

$$Y_p \doteq K_p \left(\frac{T_L j\omega + 1}{T_I j\omega + 1}\right) e^{-j\omega\tau_e} \quad ; \quad K_p,\ T_L,\ T_I,\ \tau_e \text{ variable} \qquad (74)$$

Second Approximation:

$$Y_p \doteq K_p \left(\frac{T_L j\omega + 1}{T_I j\omega + 1}\right) e^{-j(\omega\tau_e + \alpha/\omega)} \quad ; \quad K_p,\ T_L,\ T_I,\ \tau_e,\ \alpha \text{ variable} \qquad (75)$$

Precision Model

$$Y_p \doteq K_p e^{-j\omega\tau_d} \left(\frac{T_L j\omega + 1}{T_I j\omega + 1}\right)\left(\frac{T_K j\omega + 1}{T_K' j\omega + 1}\right) \frac{1}{\left(T_{N_1} j\omega + 1\right)\left[\left(\frac{j\omega}{\omega_N}\right)^2 + \frac{2\zeta_N j\omega}{\omega_N} + 1\right]} \qquad (76)$$

The final section of the chapter discusses the mean-squared error performance measure, crossover frequency regression, and related aspects of the data. In this section the nature of the gain, i.e., crossover frequency, and phase margin adjustments and their relationships with average performance are explored in terms of the crossover model.

B. THE CROSSOVER MODEL

Visual examination of the data shown in Figs. 48–50 indicates that, to a first order at least, the crossover model discussed in connection with Eq 10 is likely to have a fair range of applicability. As noted when it was introduced, the model would appear to be a better description of amplitude ratio than of phase characteristics. Also, the amplitude ratio for $Y_c = K_c/(j\omega - 2)$ tends to be somewhat flatter than −20 db/decade. Still, the elementary crossover model is adequate to describe key trends in the crossover region using only ω_c and τ_e as parameters.

Although the basic Y_pY_c approximate form is the same for all these data, the numerical values of crossover frequency and τ_e are not. In order to separate the effects of the two task variables, Y_c and ω_i, a perturbation treatment is appropriate. For

$$Y_pY_c = \frac{\omega_c e^{-j\omega\tau_e}}{j\omega} \tag{77}$$

the crossover frequency is, of course, ω_c and the phase margin is

$$\varphi_M = \frac{\pi}{2} - \tau_e\omega_c \tag{78}$$

If τ_e and ω_c are now divided into two components, one depending on Y_c alone and the other on ω_i and Y_c, then

$$\omega_c(Y_c, \omega_i) = \omega_{c_o}(Y_c) + \Delta\omega_c(\omega_i, Y_c) \tag{79}$$

$$\tau_e(Y_c, \omega_i) = \tau_o(Y_c) - \Delta\tau(\omega_i, Y_c) \tag{80}$$

The "o" subscript in Eqs 79 and 80 indicates values taken when $\omega_i = 0$. Using these equations with the phase margin expression, and assuming that the product $\Delta\omega_c\Delta\tau$ will be negligible, the phase margin becomes

$$\varphi_M \doteq \frac{\pi}{2} - \tau_o\omega_{c_o} + \omega_{c_o}\Delta\tau - \tau_o\Delta\omega_c \tag{81}$$

An important consideration in carrying this development further is the value of the phase margin when $\omega_i = 0$. The phase margin data presented in Fig. 46a indicate a trend toward zero phase margin as ω_i decreases. Although this trend to the origin can only be demonstrated directly for $\omega_i \neq 0$, it is a common observation that signals circulate throughout the manual control loop without any forcing function as long as the operator is in active control. In the absence of other inputs or disturbances, the presence of these signals implies an on-the-average condition of

zero phase margin. So, both the direct and indirect evidence indicates that phase margin is zero when ω_i is zero. Because ω_{c_o} and τ_o are equal, by definition, to ω_c and τ_e, respectively, for $\omega_i = 0$, then the phase margin for this case becomes

$$\varphi_M = \frac{\pi}{2} - \tau_o \omega_{c_o} = 0 \tag{82}$$

or

$$\tau_o = \frac{\pi}{2\omega_{c_o}} \tag{83}$$

Equation 83 indicates that τ_o and ω_{c_o} are not independent entities, and that only one need be specified. Since these quantities are the only ones in Eqs 79 and 80 which depend on the controlled element alone, either ω_{c_o} or τ_o must be used to subsume controlled element differences as represented in the crossover model if $\Delta\omega_c$ and $\Delta\tau$ variations with Y_c are small.

When the above considerations are taken into account, the phase margin expression simplifies to

$$\varphi_M \doteq \omega_{c_o}\Delta\tau - \tau_o\Delta\omega_c \tag{84}$$

or

$$\Delta\tau \doteq \frac{\varphi_M + \tau_o\Delta\omega_c}{\omega_{c_o}} \tag{85}$$

The nature of the variations of $\Delta\omega_c$ and $\Delta\tau$ with ω_i and controlled element, and the variation of ω_{c_o} or τ_o with controlled element, can be explored using crossover frequency and phase margin data extracted from Figs. 48–50. These are presented in Table VIII. Included in the table are data for $Y_c = K_c$ tests which are not documented in detail in this report although they are indicated in the experimental plan of Fig. 27b. For these tests only three subjects with a total of six runs per forcing function condition were available.

The crossover frequency is plotted as a function of ω_i in Fig. 74. There is a slight increase in ω_c with ω_i which, as already noted in Chapter V, deviates from mean values by only 5 percent or so (with the exception of $Y_c = K_c$). For the purposes of this model we shall consider

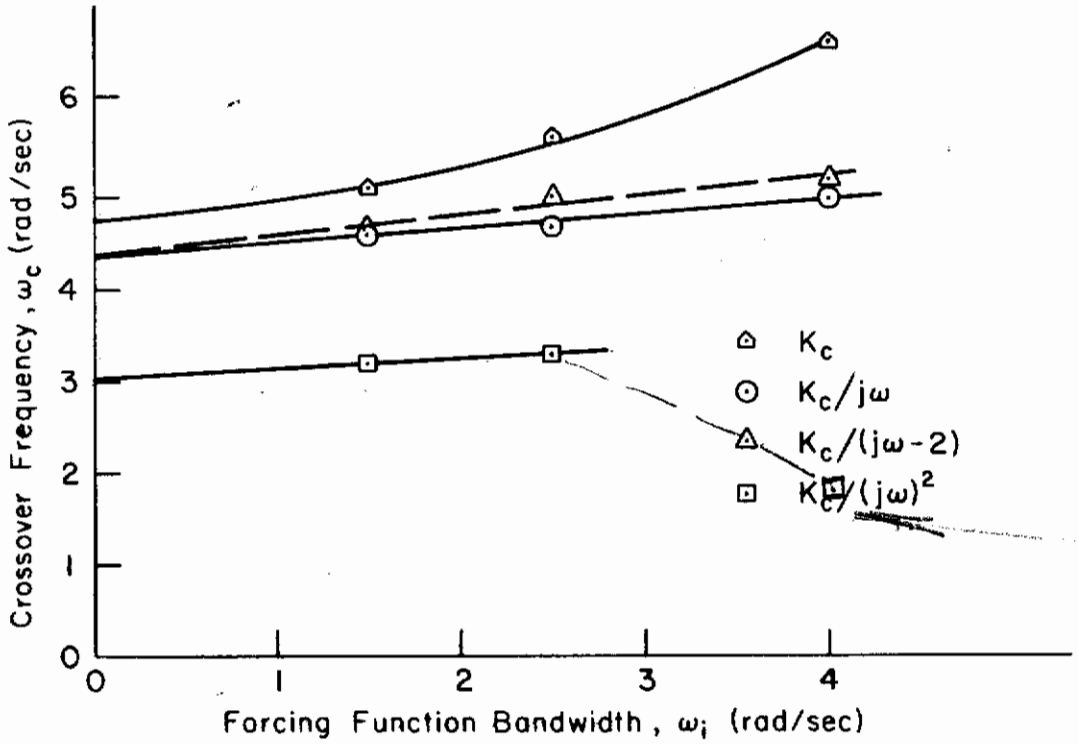

Figure 74. Variations of Crossover Frequency with Forcing Function Bandwidth

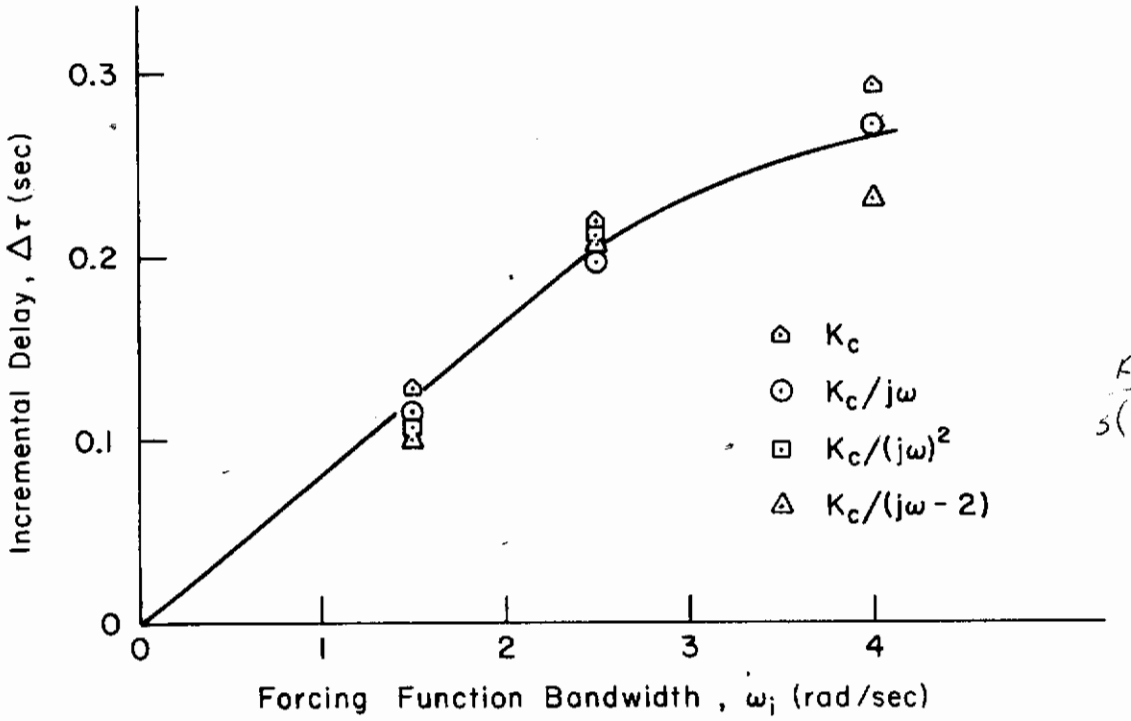

Figure 75. Dependence of Incremental Time Delay on Forcing Function Bandwidth

TABLE VIII

PHASE MARGINS AND CROSSOVER FREQUENCIES

Y_c	ω_i = 1.5 rad/sec		ω_i = 2.5 rad/sec		ω_i = 4.0 rad/sec	
	φ_M (rad)	ω_c (rad/sec)	φ_M (rad)	ω_c (rad/sec)	φ_M (rad)	ω_c (rad/sec)
K_c	0.51	5.1	0.75	5.7	0.75	6.7
$K_c/j\omega$	0.42	4.6	0.73	4.7	0.94	5.0
$K_c/(j\omega - 2)$	0.35	4.6	0.66	5.0	0.70	5.2
$K_c/(j\omega)^2$	0.26	3.2	0.51	3.3	0.73*	1.8*

*Regressive

the actual variation indicated by the data. This will change the $\omega_c - \omega_i$ adjustment rule slightly, although to a somewhat lower level of approximation the adjustment rule is adequate as it now stands.

One of the primary purposes of Fig. 74 is to obtain an estimate of ω_{c_o}. For $K_c/j\omega$, $K_c/(j\omega - 2)$, and $K_c/(j\omega)^2$ this is done by fairing straight lines through the data and extrapolating to $\omega_i = 0$. For $Y_c = K_c$ a straight-line extrapolation would result in an ω_{c_o} less than that for either $Y_c = K_c/j\omega$ or $K_c/(j\omega - 2)$. Because all of the existing data points for $Y_c = K_c$ are larger than those for the other controlled elements such an extrapolation does not appear warranted, so the $Y_c = K_c$ points are connected with a curve which for low ω_i is roughly parallel to the curves for the other controlled elements. The ω_{c_o} and associated τ_o values are given in Table IX. This table also contains a recapitulation of the averaged crossover frequency, $\bar{\omega}_c$, from Fig. 45a. When ω_{c_o} is subtracted from the ω_c values given in Table VIII, the resulting $\Delta\omega_c$ data points coalesce fairly well when plotted versus ω_i. As can be appreciated from an examination of Fig. 74, the major deviation from this is $Y_c = K_c$. The $\Delta\omega_c$ data appear to be substantially independent of controlled element, and a linear fit is adequate (except for the larger

TABLE IX

SUMMARY OF τ_o AND ω_{c_o}

Y_c	τ_o (sec)	ω_{c_o} (rad/sec)	$\bar{\omega}_c$ (rad/sec)
K_c	0.33	4.8	5.8
$K_c/j\omega$	0.36	4.4	4.75
$K_c/(j\omega - 1/T)$	0.36	4.4	4.9
$K_c/(j\omega)^2$	0.51	3.0	3.25

ω_i data for $Y_c = K_c$). This is given approximately by

$$\Delta\omega_c(\omega_i) \doteq 0.18\omega_i \tag{86}$$

Sufficient information is now available to compute the incremental effective delay, $\Delta\tau$, using Eq 85. The result is presented in Fig. 75, which shows a remarkable lack of dependence of $\Delta\tau$ on controlled element. In the low forcing-function-bandwidth linear range,

$$\Delta\tau(\omega_i) \doteq 0.08\omega_i \tag{87}$$

This reduction in effective time delay as forcing function bandwidth is increased is the principal factor involved in the phase margin increase. A very similar result is obtained if the crossover frequency is presumed constant, with a value given by $\bar{\omega}_c$, although the $\Delta\tau$ data points obtained for $\omega_i = 4$ rad/sec exhibit a wider spread than that shown in Fig. 75.

In summary, the basic trends revealed by the simple crossover model include an increase in the phase margin as forcing function bandwidth is increased, which is accomplished by a reduction of the high frequency lag characteristics subsumed in τ_e. A small part of this reduction in effective time delay is used to increase crossover frequency, although

this can be considered a second-order effect. Both changes are in a direction which tends to compensate for the increase in mean-squared error due to increases in forcing function bandwidth——a topic covered in detail in Section F. Finally, in the simple crossover model the effect of controlled element is totally given by τ_o or, alternatively, by ω_{c_o}.

C. THE EXTENDED CROSSOVER MODEL

The simplified crossover model discussed above is deficient in several respects. First, for the controlled elements with nonzero poles the open-loop describing function in the region of crossover tends to be somewhat less than −20 db/decade. For these cases the data are better fitted with open-loop describing functions which contain the controlled element dynamics explicitly. Second, the second-order controlled elements require lead equalization. This is implicit in the crossover model, but for more refined models should be made explicit. When these two major deficiencies in the simplified crossover model are corrected, the open-loop describing function models are adequate to describe most of the closed-loop system characteristics.

The extreme phase lags at low frequencies usually do not substantially affect the closed-loop characteristics because magnitude $|Y_pY_c|$ is much greater than unity at the frequencies where the lags are present. However, the ubiquitous nature of the low frequency phase lags, and their occasional importance on closed-loop dynamics, demands attention. This is accomplished here by adding a catchall increment to the low frequency phase which takes into account dynamics having amplitude ratio break points below, or in the lowest frequency portion of, the measurement bandwidth. The basis for this approximation derives from considering that the low frequency phase lag is due to an equal number of lags and leads having break points generally below the lower measurement frequencies. Thus, for M leads and lags occurring at $1/T_{lead_i}$ and $1/T_{lag_i}$ the phase will be

$$\Delta\varphi_{low} = \sum_{i=1}^{M} \tan^{-1} T_{lead_i}\omega - \sum_{i=1}^{M} \tan^{-1} T_{lag_i}\omega \qquad (88)$$

When all of the break points occur below the measurement bandwidth, the phase angle within the measurement bandwidth will be approximately

$$\Delta\varphi_{low} \doteq \sum_{i=1}^{M} \left(\frac{\pi}{2} - \frac{1}{\omega T_{lead}}\right)_i - \sum_{i=1}^{M} \left(\frac{\pi}{2} - \frac{1}{\omega T_{lag}}\right)_i$$

$$\doteq \frac{1}{\omega} \sum_{i=1}^{M} \left(\frac{1}{T_{lag}} - \frac{1}{T_{lead}}\right)_i \qquad (89)$$

$$\doteq \frac{\alpha}{\omega}$$

where $$\alpha = \sum_{i=1}^{M} \left(\frac{1}{T_{lag}} - \frac{1}{T_{lead}}\right)_i \qquad (90)$$

The effective time constant $1/\alpha$ describes the effect within the measurement band of leads and lags below measurement frequencies. In this sense it is analogous to τ_e, which lumps high frequency phenomena into a simple low frequency approximation suitable within the measurement bandwidth. In the describing function the low frequency term is represented as $e^{-j\alpha/\omega}$.

In the following the various open-loop describing functions are curve-fitted in two ways which differ only in whether or not they include the low frequency phase correction. To restrict somewhat the total number of parameters varied for a given controlled element form, the crossover frequencies are held to be invariant with ω_i for the $Y_c = K_c/j\omega$, $K_c/(j\omega - 2)$, and $K_c/(j\omega)^2$ (with the exception of the regressive $\omega_i = 4.0$) cases. The second-order diverging controlled element, $K_c/j\omega(j\omega - 1/T)$, situations amount to a special set in which ω_c is not constant. Consequently, the first three controlled elements and the second-order diverging case are separately treated below as two grand families.

1. Extended Crossover Models for $Y_c = K_c/j\omega$, $K_c/(j\omega - 2)$, and $K_c/(j\omega)^2$

Examination of the averaged Y_pY_c data of Figs. 48-50 reveals the following general trends:

a. Crossover frequency is nearly independent of ω_i (see Fig. 45a)

b. Phase margin is nearly proportional to ω_i (see Fig. 46a)

c. The incremental low frequency phase lag generally increases with ω_i

Two exceptions to these generalizations need to be noted. One is the $\omega_i = 4.0$ regressive case for $Y_c = K_c/(j\omega)^2$ and the other is the ordering of the low frequency phase lag for $Y_c = K_c/j\omega$, where the $\omega_i = 4.0$ condition has less lag than the other two ω_i conditions. With these noted exceptions, the trends listed are exhibited by the analytical models.

a. $Y_c = K_c/j\omega$. The simplest models are those for $K_c/j\omega$. The appropriate first and second approximation forms for the analytical models are:

$$\text{First approximation:} \quad Y_p Y_c \doteq \frac{\bar{\omega}_c e^{-j\omega\tau_e}}{j\omega} \tag{91}$$

$$\text{Second approximation:} \quad Y_p Y_c \doteq \frac{\bar{\omega}_c e^{-j(\omega\tau_e + \alpha/\omega)}}{j\omega} \tag{92}$$

The first approximation model is identical in form to the crossover model, except that ω_c is presumed to be the constant value of $\bar{\omega}_c$. The general adequacy of these models is graphically illustrated by Figs. 76a through 76c. The constants are summarized in Table X. Note here that $\bar{\tau}_o$, which is given by $\pi/2\bar{\omega}_c$, corresponds to the value of τ_e that would be present for $\omega_i = 0$.

TABLE X

SUMMARY OF DESCRIBING FUNCTION CONSTANTS FOR $Y_c = K_c/j\omega$

$\bar{\omega}_c = 4.75$ rad/sec ; $\bar{\tau}_o = 0.33$ sec

ω_i	φ_M		τ_e	α	$\frac{\Delta\tau_e}{(\bar{\tau}_o - \tau_e)}$
	deg	rad	sec	rad/sec	sec
1.5	24	0.42	0.24	0.14	0.088
2.5	42	0.73	0.18	0.11	0.15
4.0	56	0.98	0.12	0.20	0.21

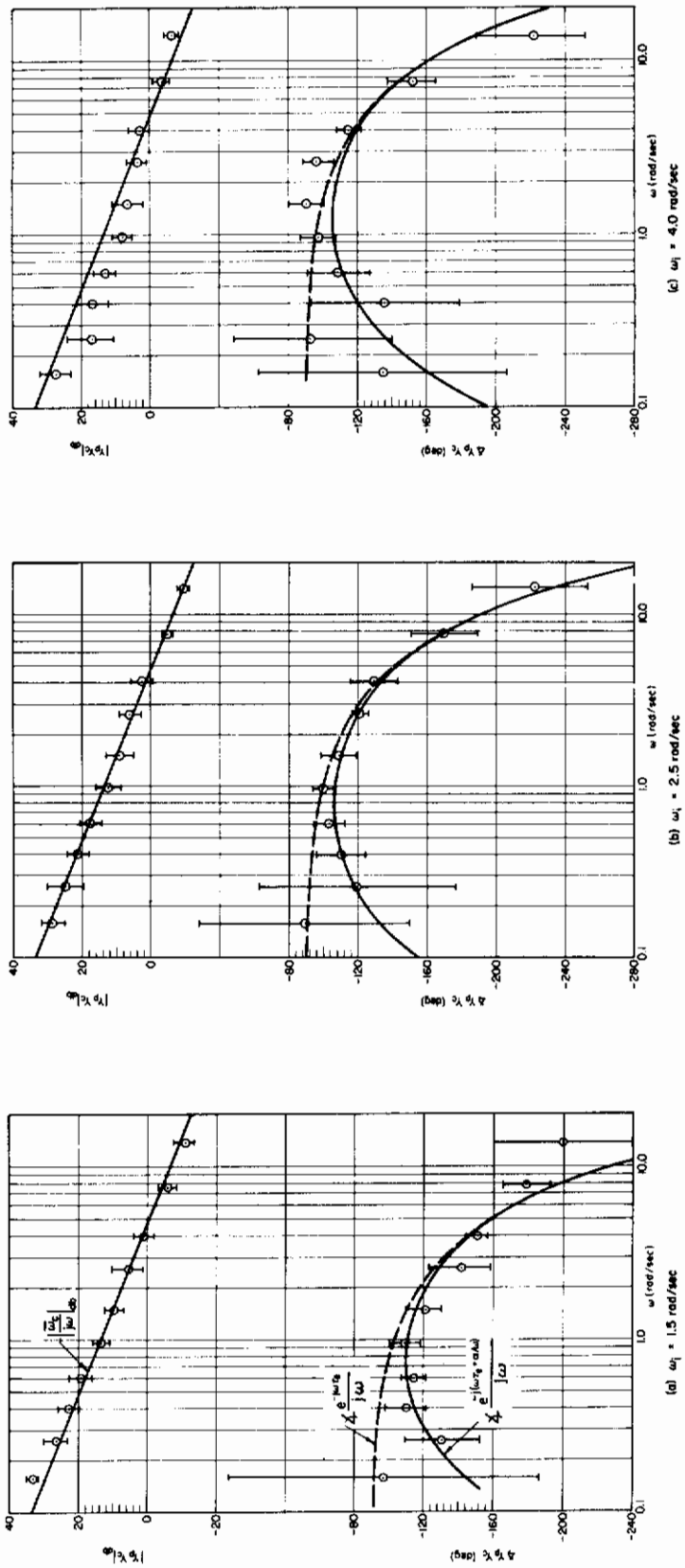

Figure 76. Extended Crossover Models for $Y_c = K_c/j\omega$

b. $Y_c = K_c/(j\omega - 2)$. The first and second approximation analytical model forms for $Y_c = K_c/(j\omega - 2)$ are:

$$\text{First approximation:} \qquad Y_p Y_c \doteq \frac{-Ke^{-j\omega\tau_e}}{(-j\omega/2 + 1)} \tag{93}$$

$$\text{Second approximation:} \qquad Y_p Y_c \doteq \frac{-Ke^{-j(\omega\tau_e + \alpha/\omega)}}{(-j\omega/2 + 1)} \tag{94}$$

where K is the total open-loop D.C. gain. Figures 77a through 77c illustrate these fits, which, together with the analytical model data, are summarized in Table XI.

TABLE XI

SUMMARY OF DESCRIBING FUNCTION CONSTANTS FOR $Y_c = K_c/(j\omega - 2)$
$\bar{\omega}_c = 4.9$ rad/sec

ω_i	φ_M		τ_e	K	α	$\Delta\tau_e$ $(\bar{\tau}_o - \tau_e)$
	deg	rad	sec		rad/sec	sec
1.5	24.0	0.42	0.16	2.65	0.2	0.086
2.5	33.0	0.58	0.13	2.65	0.19	0.12
4.0	39.0	0.68	0.10	2.65	0.18	0.14

For this case, $\bar{\tau}_o$ will be given by

$$\bar{\tau}_o = \frac{1}{\bar{\omega}_c} \tan^{-1} \frac{\bar{\omega}_c}{2} \tag{95}$$

$$= 0.24 \text{ sec}$$

As can be appreciated by examining Fig. 77, the extended model is quite adequate to describe all of the data except for the highest and lowest frequency amplitude ratio points for all three ω_i values. These discrepancies can be corrected by adding a high frequency lead and some lags and a low frequency lag-lead, while making appropriate modifications to τ_e and α. For instance, α is reduced to zero by adding the low frequency lag-lead pair $(T_K j\omega + 1)/(T'_K j\omega + 1)$ to the describing function form.

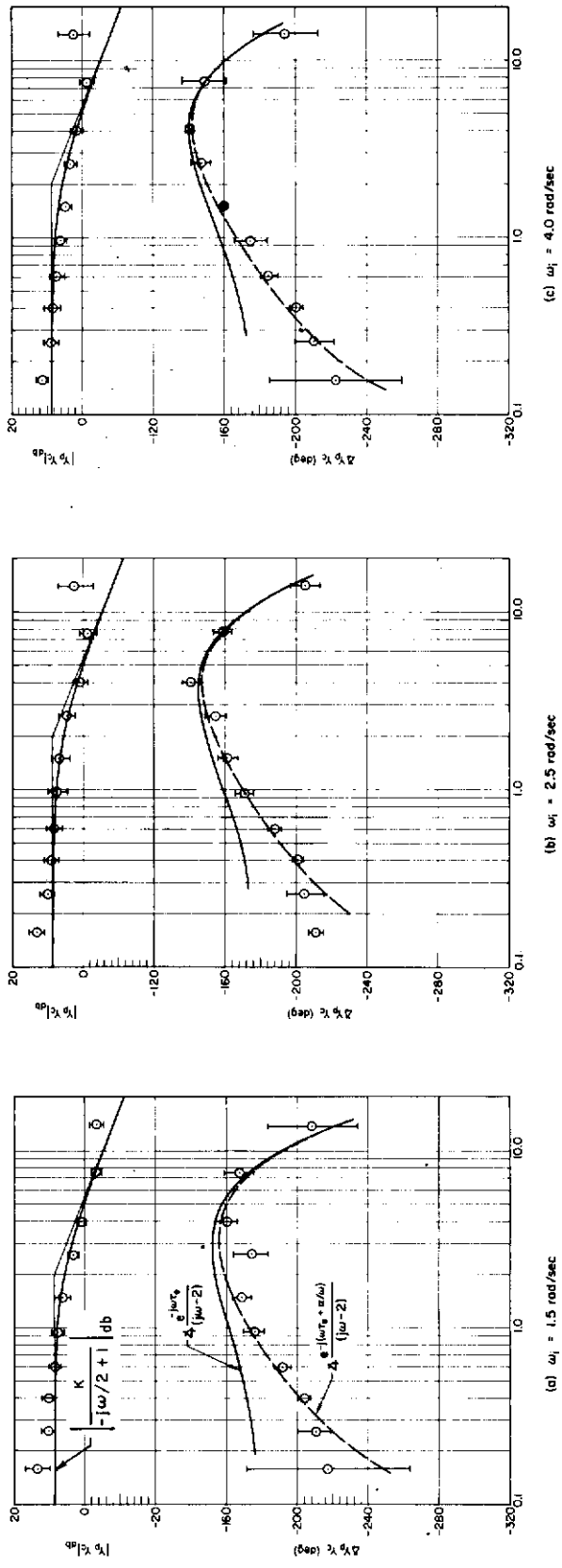

Figure 77. Extended Crossover Models for $Y_c = K_c/(j\omega - 2)$

Considerations such as these are used in the next section to develop a precision model.

c. $Y_c = K_c/(j\omega)^2$. The two forms for $Y_c = K_c/(j\omega)^2$ are:

First approximation:
$$Y_p Y_c \doteq \frac{\bar{\omega}_c e^{-j\omega\tau_e}}{j\omega} \tag{96}$$

Second approximation:
$$Y_p Y_c \doteq \frac{(\bar{\omega}_c/T_L)(T_L j\omega + 1)e^{-j(\omega\tau_e + \alpha/\omega)}}{(j\omega)^2} \tag{97}$$

Just as with $Y_c = K_c/j\omega$, the first approximation fits are similar to the simple crossover model, but with crossover frequency held constant at $\bar{\omega}_c$.

As a prelude to the final fitting procedure for the second approximation form, a large number of variations were used at the low frequency end. A comparison of these for the three ω_i conditions indicated that an excellent case could be made for a nearly constant T_L having a value of 5 sec or greater. In Figs. 78a through 78c the minimum value is used. Table XII summarizes all the data for $Y_c = K_c/(j\omega)^2$ models.

TABLE XII

SUMMARY OF DESCRIBING FUNCTION CONSTANTS FOR $Y_c = K_c/(j\omega)^2$

$\bar{\omega}_c = 3.25$ rad/sec ; $\bar{\tau}_o = 0.483$ sec

ω_i	ω_c	φ_M		τ_e	T_L	α	$\Delta\tau_e$ $(\bar{\tau}_o - \tau_e)$
		deg	rad			rad/sec	sec
1.5	3.25	16.0	0.279	0.385	5	0.2	0.098
2.5	3.25	25.5	0.445	0.335	5	0.333	0.148
4.0	1.8	42.0	0.733	0.260	5	0.533	0.223

d. Summary Data. The key variations of effective time delay, τ_e, with forcing function bandwidth, ω_i, are shown in Fig. 79. The trends shown are generally compatible with those that would be exhibited if the simple crossover model data were presented in a similar way. This can

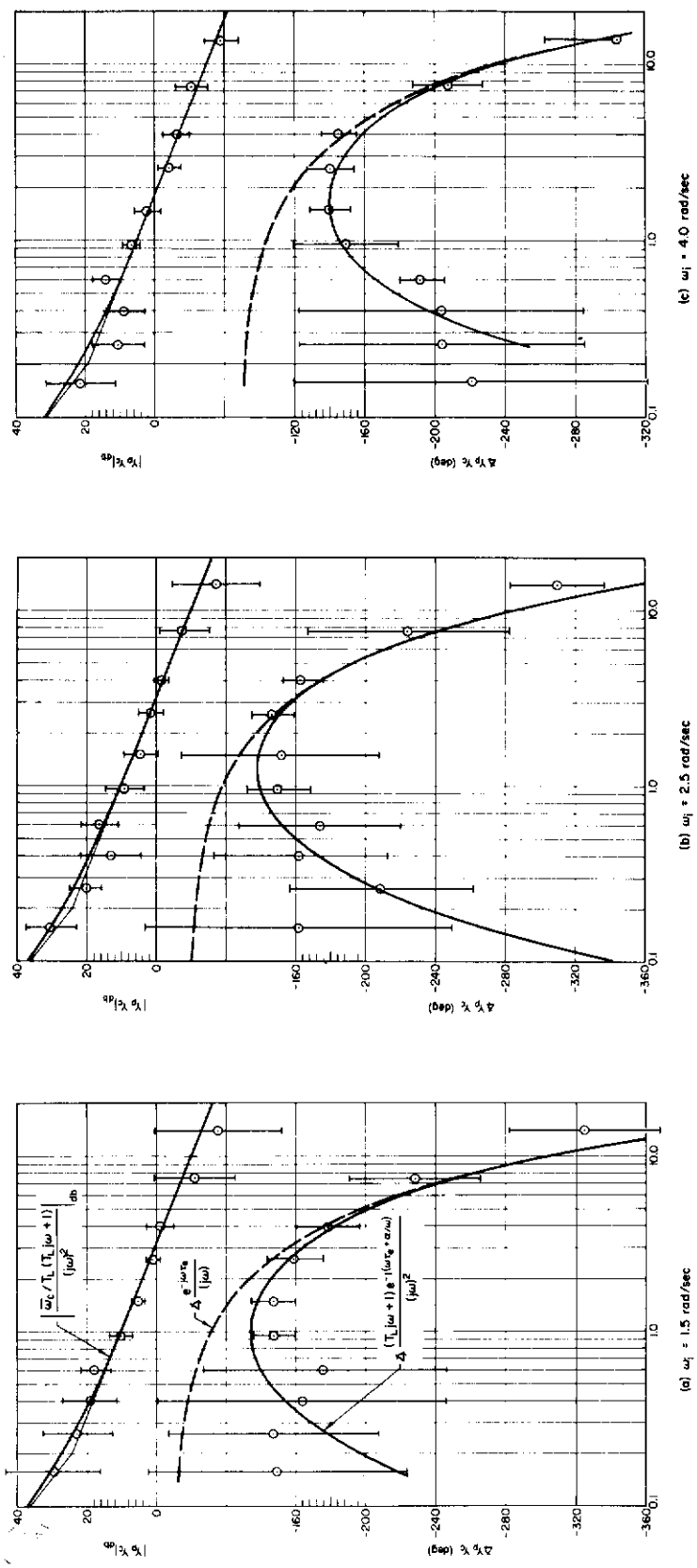

Figure 78. Extended Crossover Models for $Y_c = K_c/(j\omega)^2$

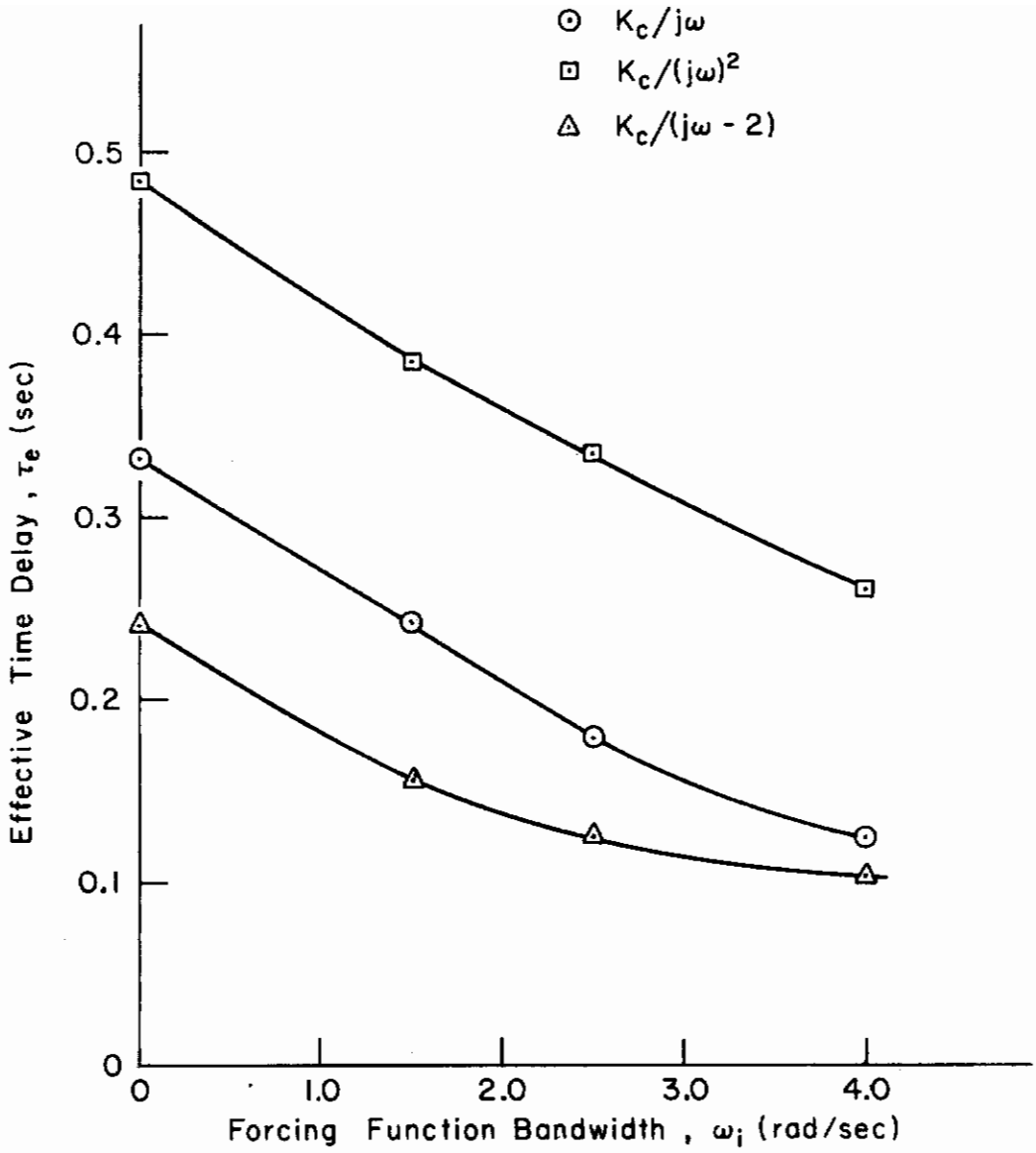

Figure 79. Variations of Effective Time Delays with Forcing Function Bandwidth (ω_i = 0 points are extrapolations)

perhaps best be appreciated by comparing the variation of the incremental time delay for the simple crossover model with forcing function bandwidth shown in Fig. 75 with the similar plot, Fig. 80, made for the extended models. The major differences between these stem from the absence of the correction for crossover frequency increase with ω_i in Fig. 80. In this respect the simple crossover model results are superior to those of the extended versions. If the decreasing slope tendency which is especially evident for the $K_c/(j\omega - 2)$ controlled element is to be taken seriously, an asymptotic lower level for τ_e would be indicated. This would appear to have a value somewhere near 0.1 sec or less.

The variation of the incremental low frequency phase lag measured by α with forcing function bandwidth is shown in Fig. 81. Two limiting cases appear. For the highly constrained $K_c/(j\omega - 2)$ condition, α is substantially independent of forcing function bandwidth. At the other extreme, for $Y_c = K_c/(j\omega)^2$, α is approximately proportional to ω_i. The simple integrator controlled element has a trend of α versus ω_i which ranges between the two extremes. The low frequency incremental phase lag has no precedent in the existing analytical–verbal model. However, it is necessary to recall that such terms are not new. They have appeared before and were carefully considered in Ref. 34 before being thrown out as major effects. At least one of these "reasons" (i.e., that the points were inconclusive due to variability in computational problems) is no longer as strong as it once was. Other "reasons" such as the relatively inconsequential nature of the low frequency phase lags in terms of closed-loop characteristics are still pertinent for some controlled elements, but not all.

Both the variation or the lack thereof of the low frequency incremental phase lag and the effective time delay with forcing function bandwidth are major experimental facts which must be explained in any adequate model of the human operator. This has been accomplished in another phase of the research program, of which this report documents a portion, although it is beyond our present scope. It turns out that essentially all the variations noted are compatible with a variable-gain adaptive model of the neuromuscular system which, in turn, is generally compatible with the known physiological characteristics of the same system.

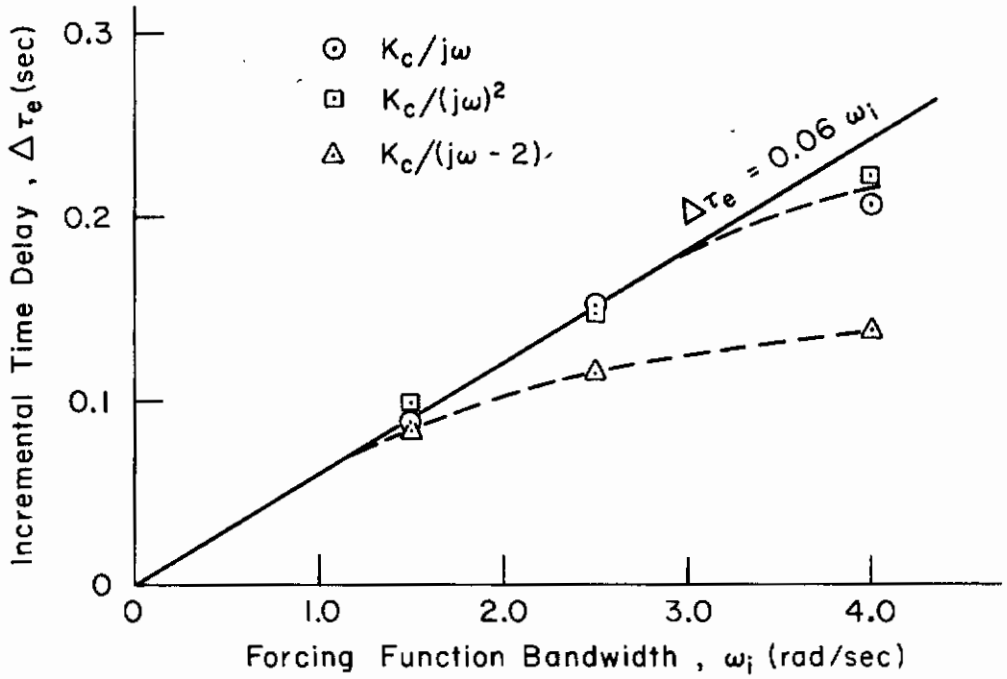

Figure 80. Dependence of Incremental Time Delay on Forcing Function Bandwidth

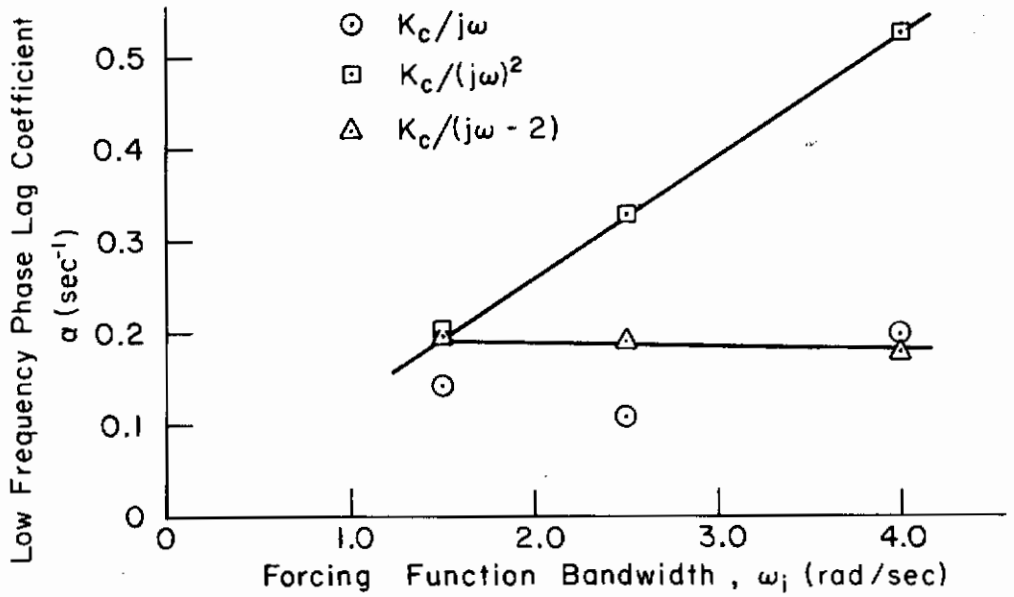

Figure 81. Variations of Low Frequency Incremental Phase Lag with Forcing Function Bandwidth

2. Extended Crossover Models for $Y_c = K_c/j\omega(j\omega - 1/T)$

Examination of Fig. 44 and its comparison with the pre-experiment analyses shown in Figs. 6 and 9 indicates that a minimum form for the open-loop describing function should be

$$Y_pY_c = \frac{K_pK_c(T_Lj\omega + 1)e^{-j\omega\tau_e}}{j\omega(j\omega - 1/T)} \tag{98}$$

Suitable parameters can be selected in this form such that the amplitude ratio is reasonably well described over the measurement band, while the phase is accurately characterized only in the region of crossover. In fact, some of these data absolutely require the low frequency phase lag correction in order to be fitted at all well, even at frequencies near crossover. Consequently, the more refined second approximation form,

$$Y_pY_c = \frac{K_pK_c(T_Lj\omega + 1)e^{-j(\omega\tau_e + \alpha/\omega)}}{j\omega(j\omega - 1/T)} \tag{99}$$

will be used at the outset.

From comparison of the several plots it is noted that the major trends are:

a. ω_c increases with $1/T$ (see Fig. 45b)

b. Phase margin is generally very low and decreases as $1/T$ increases (see Fig. 46b)

c. The low frequency phase lag increases with an increase in $1/T$

As a consequence of the first of these trends, τ_e will decrease as $1/T$ increases, up to the point where control is lost.

Just as with the $Y_c = K_c/(j\omega)^2$ case, a large number of variations were tried in fitting the low frequency data. As it turned out, the lead time constant, T_L, can be considered independent of $1/T$, with a value of about 5 sec. Then α and τ_e will carry the primary variation with controlled element change. The actual curve fits are given in Figs. 82a through 82d and tabulated in Table XIII. The use of α alone to

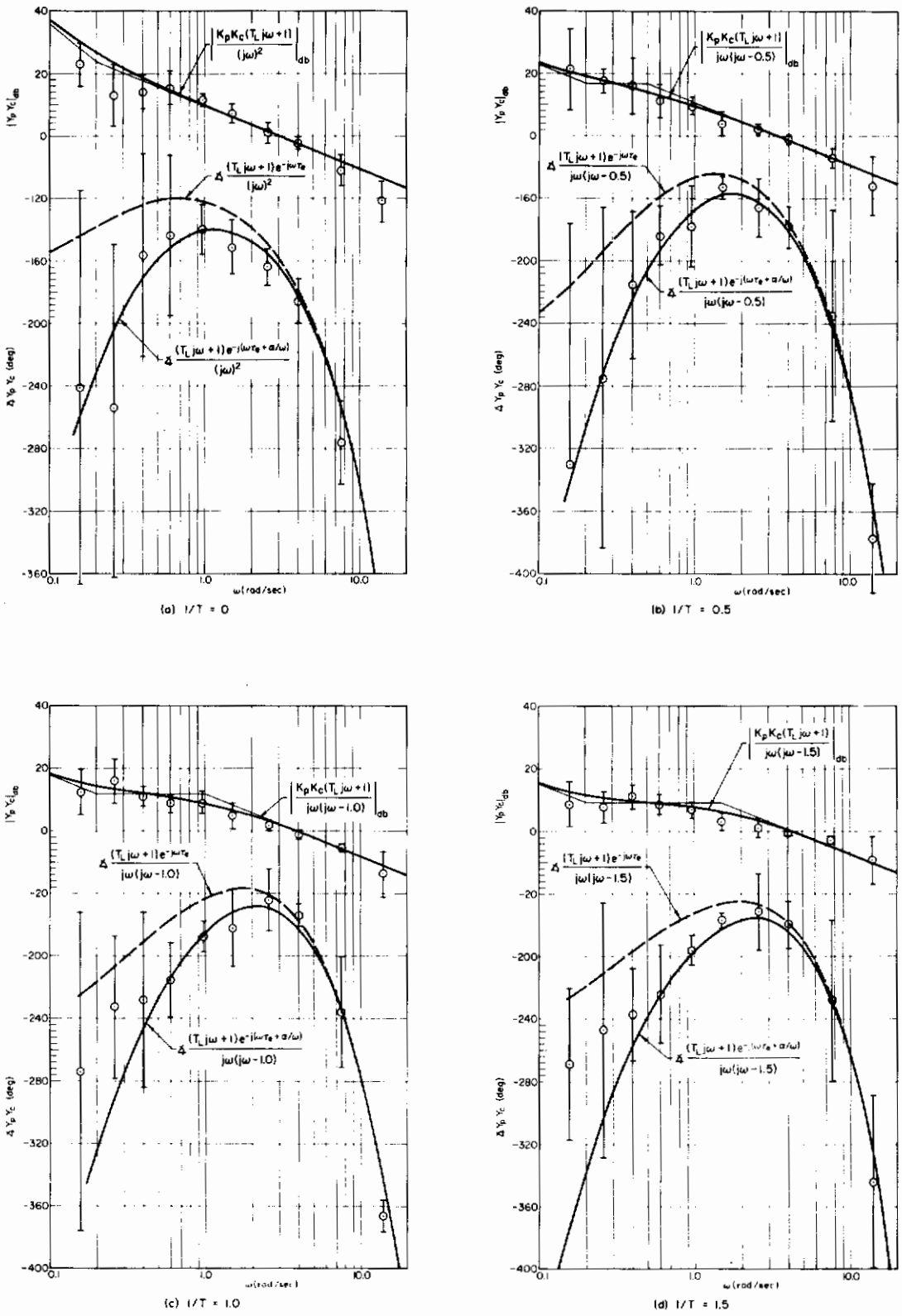

Figure 82. Extended Crossover Models for $Y_c = K_c/j\omega(j\omega - 1/T)$, $\omega_i = 1.5$

approximate effects which are probably due to a low frequency lag-lead has a tendency to overestimate the low frequency phase lag at the very lowest frequencies of measurement. This is especially noticeable in Figs. 82c and 82d. The effect can, of course, be eliminated by using the lag-lead instead of α, with the consequent addition of another parameter.

TABLE XIII

SUMMARY OF DESCRIBING FUNCTION CONSTANTS
FOR $Y_c = K_c/j\omega(j\omega - 1/T)$, $\omega_1 = 1.5$

$1/T$	ω_c	Φ_M		T_L	τ_e	α
rad/sec	rad/sec	deg	rad	sec	sec	rad/sec
0.0	3.0	10	0.17	5	0.37	0.32
0.5	3.4	10	0.17	5	0.33	0.34
1.0	3.7	7	0.12	5	0.31	0.37
1.5	4.0	0	0.0	5	0.29	0.40

As can best be appreciated by examining Fig. 83, the increase in low frequency phase lag and decrease in effective time delay behave in essentially a parallel fashion as the controlled element divergence is increased. In fact, it is evident that the conflict between the low frequency phase lag and the high frequency phase decrease accompanying τ_e decreases is the significant factor in the pilot's ability to control diverging controlled elements. Here, because of the intimate connection between τ_e and α, the τ_e decrease can only be effective as long as its effect is not overpowered by the incremental low frequency phase lag. The source of the close tie between τ_e and α again involves the details of the neuromuscular subsystem, and hence is again beyond our current scope.

D. PRECISION MODEL

In its most refined version, the extended crossover model given by

$$Y_p \doteq K_p\left(\frac{T_L j\omega + 1}{T_I j\omega + 1}\right)e^{-j(\omega\tau_e + \alpha/\omega)} \qquad (100)$$

$$Y_c = \frac{K_c}{j\omega(j\omega - 1/T)}$$

$\omega_i = 1.5$

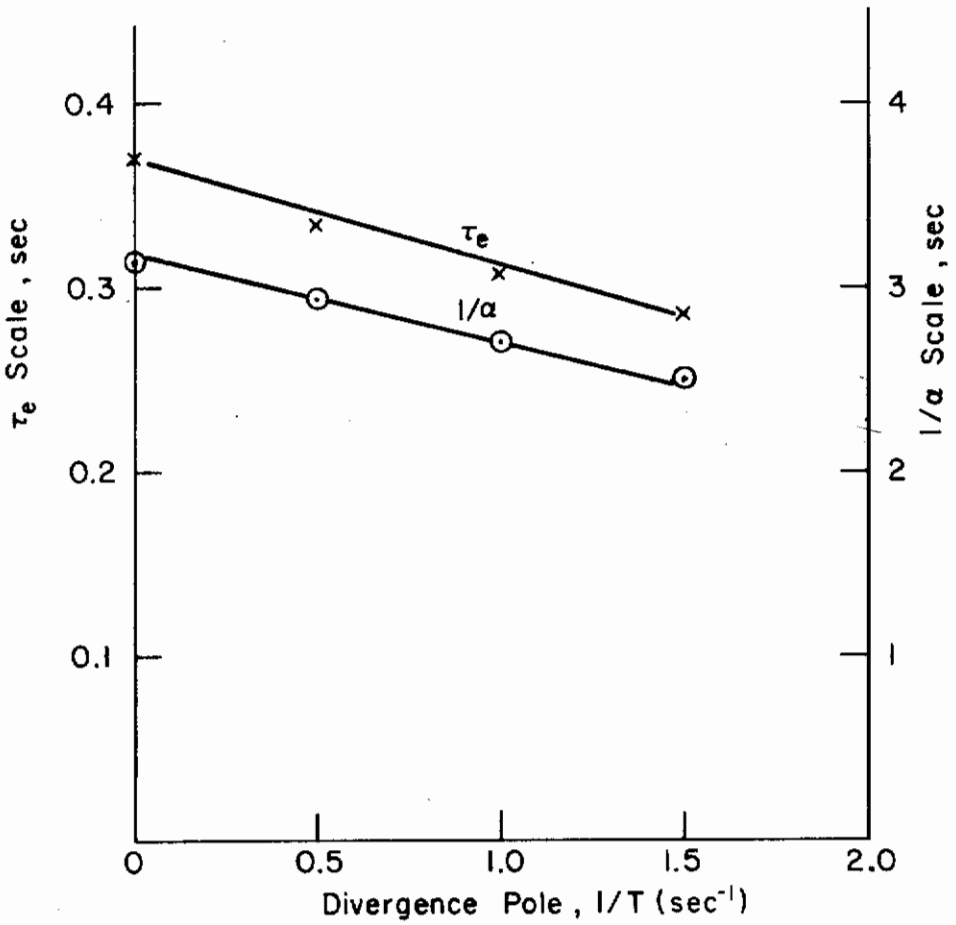

Figure 83. Variation of Effective Time Delay and Low Frequency Incremental Phase Lag with $1/T$ for $Y_c = K_c/j\omega(j\omega - 1/T)$

is sufficient to characterize almost all the data for all the controlled elements tested. Exceptions occur at very low and very high frequencies. For instance, in the discussion completed just above, values of α based on the lower variability mid-frequency and low frequency data tend to overestimate the phase lag at the very lowest frequencies. Also, for the $Y_c = K_c/(j\omega - 2)$ data the very lowest and very highest amplitude ratio points are not compatible with curve fits using the extended crossover model alone. These deviations between data and model offer opportunities for model extension.

A more subtle defect of the extended crossover model of Eq 100 is the possible confusion resulting when this form is used at frequencies for which it was never intended. Neither of the exponential term's components can be extrapolated beyond the measurement band without the possibility of conceptual error. It must always be remembered that the $e^{-j(\alpha/\omega)}$ term represents lags and leads having break points below or in the lowest portion of the measurement bandwidth; and similarly that at least part of the $e^{-j\omega\tau_e}$ includes the low frequency effects of leads and lags having break points above or in the highest regions of the measurement band. Thus, extrapolation of Eq 100 either to very low frequencies where the phase will tend to minus infinity or to very high frequencies where the amplitude ratio approaches a constant is unwarranted.

The primary intent of this section is to take advantage of the additional scope offered for model extension by the data which are not quite characterized by the refined crossover models while also removing the subtle limiting frequency difficulties of the extended form. To do this a precision model which contains many more components is formulated. Most of these additional components have break points outside the measurement bandwidth which must be estimated by their often small effects within this band. Consequently, only the lowest variability data available are appropriate for use as an initial data base in model elaboration. For this reason the precision model developments here will use only the exceptionally low variability data obtained for the highly constraining $K_c/(j\omega - 2)$ controlled element.

Even with these rather remarkable data, the development of a precision model can be only academic unless a good deal of additional information is considered in the model construction process. When this is done, however, the precision model evolved is compatible not only with the data of the current program, but with the other findings introduced into the structure as well.

The model development process can best be described as a sequence of operations, each based on one or more fundamental considerations. Each of the steps included are detailed below.

1. As a minimum to replace the α and to better fit the lowest frequency amplitude ratio data, a lag–lead form is indicated wherein the lead is just within the measurement band and the lag occurs at much lower frequencies. Careful consideration of the $|Y_p|/K_p$ data at low frequencies for the three forcing function cases indicates that these are nearly identical. This feature is also reflected by the values previously found for α, which are essentially the same for all three conditions. Therefore, the lead–lag added will be the same for all three forcing function conditions. This very low frequency lag–lead has no amplitude ratio and negligible phase effect at the higher frequencies, so the break points can be determined independently of other parameters. The values selected are:

$$\left(\frac{T_K j\omega + 1}{T'_K j\omega + 1}\right) = \left(\frac{\frac{j\omega}{0.3} + 1}{\frac{j\omega}{0.05} + 1}\right) \qquad (101)$$

2. Data and interpretations from this and other experimental programs have increased our knowledge of the dynamics of the neuromuscular system. As already noted several times, the details of these are beyond the present scope, but two findings related to the precision model development task are:

   a. A fairly complete description of the high frequency neuromuscular system dynamics requires a third-order system, i.e.,

$$\frac{1}{\left(T_{N_1} j\omega + 1\right)\left[\left(\frac{j\omega}{\omega_N}\right)^2 + \frac{2\zeta_N}{\omega_N} j\omega + 1\right]}$$

All these terms are shown in Eq 1. Their presence there was based largely on high frequency neuromuscular system dynamics as revealed by the dynamic portion of step response data. More fundamentally,

the third-order form constitutes a minimal analytical description of the muscle impulse response.

b. The effective neuromuscular system high frequency lag,

$$T_N \doteq T_{N_1} + \frac{2\zeta_N}{\omega_N} \tag{102}$$

tends to vary in the same fashion as α. In this instance, for $Y_c = K_c/(j\omega - 2)$, α is constant with ω_i. Therefore, T_N will also be essentially constant.

3. For the data being considered, the components of the effective time delay, τ_e, will be

$$\tau_e \doteq \tau + T_{N_1} + \frac{2\zeta_N}{\omega_N} - T_L \doteq (\tau + T_N) - T_L \tag{103}$$

The pure time delay, τ, is due to latencies in the visual process, delays due to neural conduction and coding, etc. Accordingly, its value is not likely to change with forcing function bandwidth. Thus, for these $Y_c = K_c/(j\omega - 2)$ data the term $\tau + T_N$ will be independent of the forcing function bandwidth. In Eq 103 this leaves the lead, T_L, which is generally adjustable, as the likely source for the observed changes in τ_e with ω_i.

4. Minimum values of $1/T_L$ can be found by considering that:

a. The mid-frequency regions for the $|Y_p|/K_p$ data are the same for all ω_i, thereby indicating that $1/T_L$ influences only the two highest frequency amplitude ratio data points.

b. Because the neuromuscular system dynamics do not change with ω_i in this particular case, the departure of the highest frequency amplitude ratio point (ω_n = 13.8 rad/sec) from the partial amplitude ratio curve fit (which includes the lead, T_L, but excludes the neuromuscular system lags) should be the same for all three forcing function conditions. With only a small amount of cut-and-try, lead values can be found which are compatible with these factors. These are:

ω_i	$\left[\frac{1}{T_L}\right]_{min}$	$T_{L_{max}}$	τ_e	$\tau_e + T_L$
1.5	13.0	0.077	0.156	0.233
2.5	9.0	0.111	0.125	0.236
4.0	7.8	0.128	0.104	0.232

Note that $\tau_e + T_L$ is essentially a constant, as is required if $\tau + T_N$ is to be invariant with ω_i.

5. At this point the third-order neuromuscular and pure time delay effects must be estimated from their influence on about five or six phase points and two amplitude ratio points. A unique determination of these parameters is not to be expected, but good fits which are generally compatible with associated data can be found. As a first step, the pure time delay, τ, can be estimated from physiological data. Its components include:*

Flash stimulus, shortest path to cortex.....	0.04 to 0.07 sec
Conduction within the cortex to convergence center of visual, proprioceptive, and kinesthetic information to formulate motor output	0.005 sec
Cortex to spinal cord.....	0.01 to 0.015 sec
Spinal cord to periphery (via alpha motoneurons).....	0.005 to 0.01 sec
	0.06 to 0.10 sec

For the present data a value of 0.09 sec shall be used. This is selected because it is near the upper end of the range given above and, incidentally, because it worked somewhat better than other values within this range in the cut-and-try fitting efforts.

6. The residual amplitude ratio and phase left over when the terms thus far considered are removed from the data are shown in Fig. 84. These data are to be fitted with

$$\frac{1}{\left(T_{N_1} j\omega + 1\right)\left[\left(\frac{j\omega}{\omega_N}\right)^2 + \frac{2\zeta_N}{\omega_N} j\omega + 1\right]}$$

After considerable cut-and-try, representative numerical values were determined to be

$$\frac{1}{\left(\frac{j\omega}{10} + 1\right)\left[\left(\frac{j\omega}{16.5}\right)^2 + \frac{2(0.12)}{16.5} j\omega + 1\right]}$$

These correlate reasonably well with representative third-order system approximations which characterize the so-called dynamic portion of the step response (see Ref. 34) for $Y_c = K_c$.

*Personal communication—Dr. George Moore, Asst. Prof. of Physiology, UCLA Medical School.

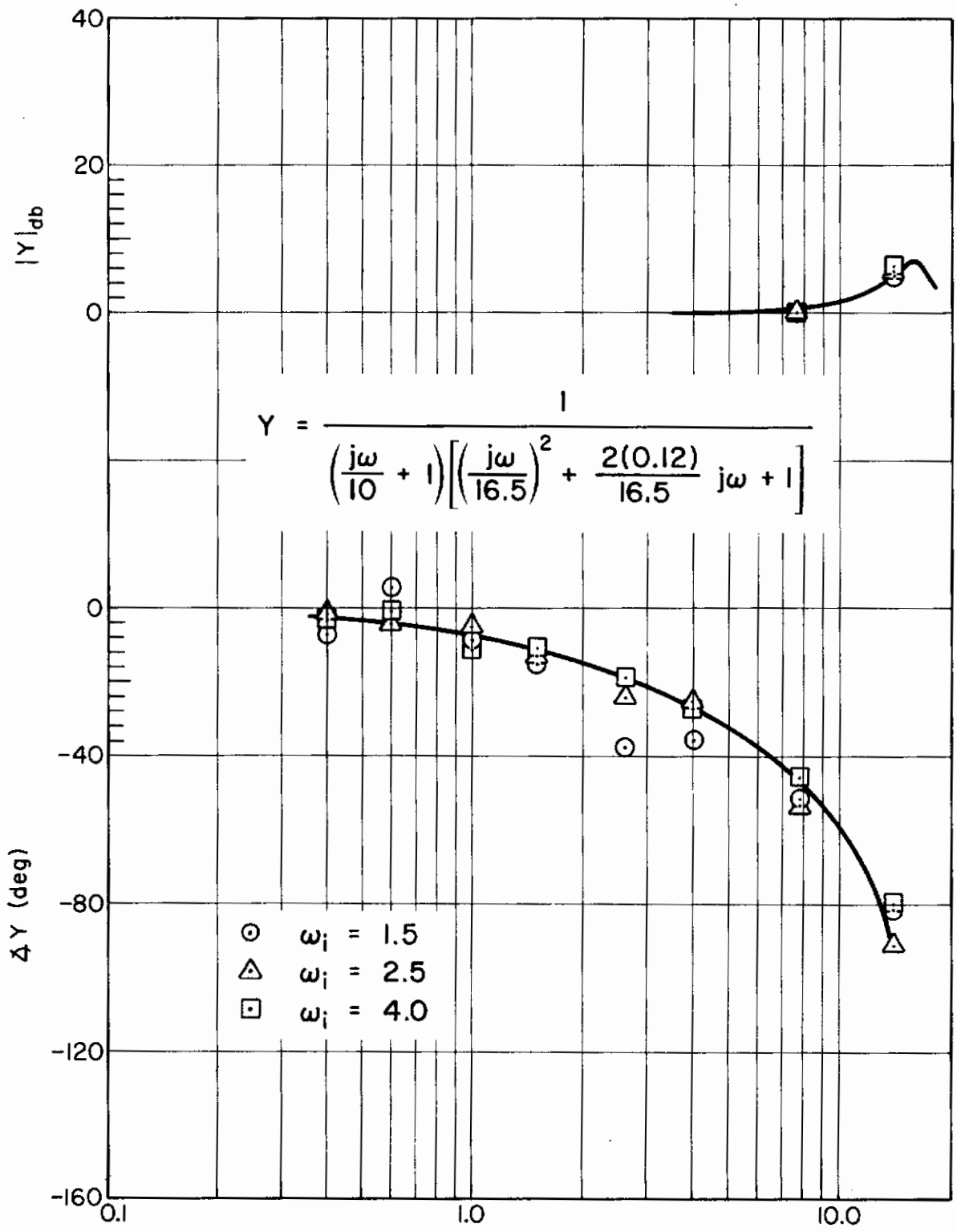

Figure 84. Residual Amplitude Ratio and Phase Giving High Frequency Neuromuscular System Characteristics for $Y_c = K_c/(j\omega - 2)$

The final forms found to fit the three ω_i cases for $Y_c = K_c/(j\omega - 2)$ are

$$Y_p = \begin{Bmatrix} 28.2 \\ (29\ db) \\ 31.6 \\ (30\ db) \\ 25.1 \\ (28\ db) \end{Bmatrix} \left\{ \begin{matrix} \frac{j\omega}{13}+1 \\ \\ \frac{j\omega}{9}+1 \\ \\ \frac{j\omega}{7.8}+1 \end{matrix} \right\} \left(\frac{\frac{j\omega}{0.3}+1}{\frac{j\omega}{0.05}+1} \right) \frac{e^{-0.09j\omega}}{\left(\frac{j\omega}{10}+1\right)\left[\left(\frac{j\omega}{16.5}\right)^2 + \frac{2(0.12)}{16.5}\, j\omega + 1\right]} \tag{104}$$

for $\omega_i = 1.5$, 2.5, and 4.0, respectively. The over-all merit of this detailed precision model can be judged from Figs. 85a through 85c, which present the data and the precision model forms of Eq 104. The general adequacy of these curve fits is exceptionally good evidence for the extension of the general model form shown in Eq 1 to that given by

$$Y_p = K_p \left(\frac{T_L j\omega + 1}{T_I j\omega + 1} \right) \left(\frac{T_K j\omega + 1}{T_K' j\omega + 1} \right) \frac{e^{-j\omega\tau}}{\left(T_{N_1} j\omega + 1\right)\left[\left(\frac{j\omega}{\omega_N}\right)^2 + \frac{2\zeta_N}{\omega_N}\, j\omega + 1\right]} \tag{105}$$

In this more general model the gain and equalization terms are identical to those previously used, whereas the neuromuscular system characteristics have been expanded by the addition of the low frequency lag-lead.

An interesting aspect of the precision model is its reduction of pure time delay terms to minimum or near-minimum values. All the high frequency leads and lags which were previously lumped into low frequency approximations represented by $e^{-j\omega\tau_e}$ have now been removed, leaving only the bare bones of a pure time delay which is compatible with that expected on physiological grounds.

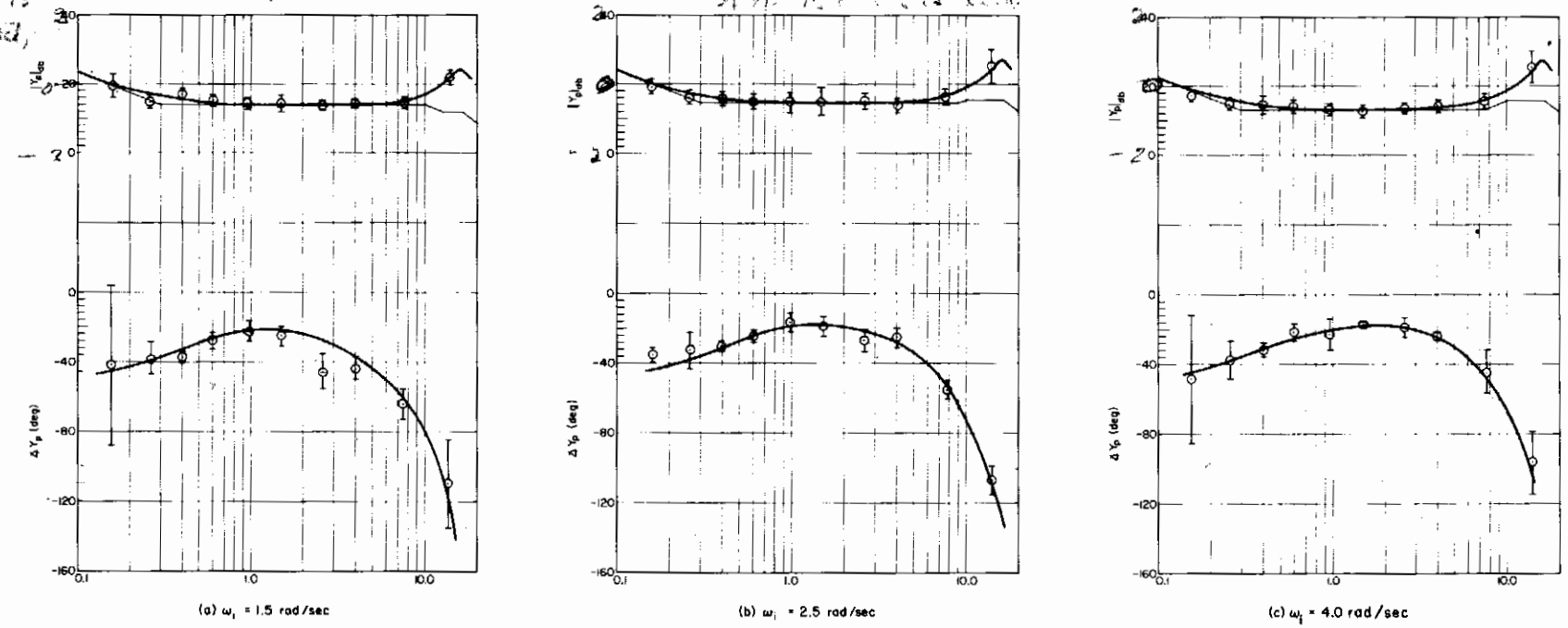

Figure 85. Comparison of Precision Model with Data for $Y_c = K_c/(j\omega - 2)$

E. ω_c REGRESSION, PERFORMANCE MEASURES, AND τ_e TRAJECTORIES

In this section some of the adjustments revealed by the describing function data will be rationalized in terms of the simple normalized mean-squared-error models derived in Chapter III.

1. ω_c Regression

The first topic is that of ω_c regression. This phenomenon was first noticed in Elkind's rectangular forcing function spectra data. Most of these had open-loop describing function characteristics reasonably compatible with those given in Eq 10, so the normalized mean-squared-error model of Eq 35 forms an appropriate analytical framework with which to "explain" these data and the ω_c regression phenomenon.

In Table XIV are presented data based on Elkind's original results, Ref. 13. The normalized mean-squared error is only that component which has frequencies within the forcing function bandwidth. This is a close approximation to $\overline{e_I^2}/\sigma_I^2$. Because the rectangular forcing function spectra used by Elkind had no power in the region of crossover, the crossover frequency for the lower forcing function bandwidths was not directly measurable. However, extrapolation of the available low frequency describing

TABLE XIV

NORMALIZED MEAN-SQUARED-ERROR DATA
DERIVED FROM ELKIND'S $Y_c = 1$ EXPERIMENTS

FORCING FUNCTION	ω_i (rad/sec)	$\left[\frac{\overline{e^2}}{\sigma_i^2}\right]_{\omega_i}$	ω_c (rad/sec)	$\overline{\tau}_o\omega_c$	$\overline{\tau}_o\omega_i$	$\frac{\omega_i^2}{3\omega_c^2}$
R.16	1.0	0.0081	7.6	1.57	0.21	0.0058
R.24	1.5	0.011	7.6	1.57	0.31	0.013
R.40	2.5	0.041	7.6	1.57	0.52	0.036
R.64	4.0	0.098	7.6	1.57	0.83	0.092
R.96	6.0	0.51	6.3	1.30	1.24	0.30
R1.6	10.0	1.16	2.0	0.414	2.07	

function data to the crossover region reveals that the ω_c was probably the same for all of these cases (this extrapolation was, in fact, the primary justification for Adjustment Rule 5b). Elkind's B-6 forcing function spectra can be used to estimate a likely crossover frequency for the lower ω_i data. This is the basis of the 7.6 rad/sec shown for R.16 through R.64 (see Fig. 29). The $\overline{\tau}_o$ corresponding to this crossover frequency, when it is considered as an $\overline{\omega}_c$, is 0.21 sec. The rest of the data in Table XIV follows directly. Figure 86 shows the data from Table XIV superimposed on the normalized mean-squared error versus normalized crossover frequency families. This plot actually involves three quantities, i.e., $\overline{e_i^2}/\sigma_i^2$, $\overline{\tau}_o\omega_c$, and $\overline{\tau}_o\omega_i$ (the constant $\overline{\tau}_o$ is a normalizing parameter). The actual variation being illustrated is $\overline{e_i^2}/\sigma_i^2$ versus ω_c (normalized), with ω_i (normalized) as a parameter. The data are entered on the plot using the first two as abscissa and ordinate. The arrow leading from each data point has its head at the appropriate $\overline{\tau}_o\omega_i$. Thus, the R.96 data, for instance, show a normalized mean-squared error of 0.51 versus normalized crossover of 1.30 with the arrowhead touching a family $\overline{\tau}_o\omega_i = 1.24$. If the arrow lengths were zero, the experimental data would coincide precisely with all three parameters of the plot.

The approximately constant crossover, low forcing function bandwidth data and the R1.6 large Φ_{ii} bandwidth point all correspond quite closely to the theoretical. The lower ω_i data are also compatible with minimization of the mean-squared error, whereas the high ω_i point (R1.6) illustrates the ω_c regression. The R.96 data point departs a good deal from the idealization. This too is as it should be, for the open-loop describing function here is transitionary and departs considerably from the simple -20 db/decade constant-slope amplitude ratio. This data point could have been left off the plot for this reason; instead, it is entered to indicate how closely the theoretical $\omega_i < 0.8\omega_c$ condition is likely to apply.

In the present program only one condition resulted in an ω_c regression. This was for $Y_c = K_c/(j\omega)^2$, $\omega_i = 4.0$ (see Fig. 45a). The idealized mean-squared-error plot of Fig. 11 (or Fig. 86) is, unfortunately, not as quantitatively appropriate for the $Y_c = K_c/(j\omega)^2$ data as it is for the $Y_c = K_c$ or $K_c/j\omega$ cases because the open-loop phase differs drastically

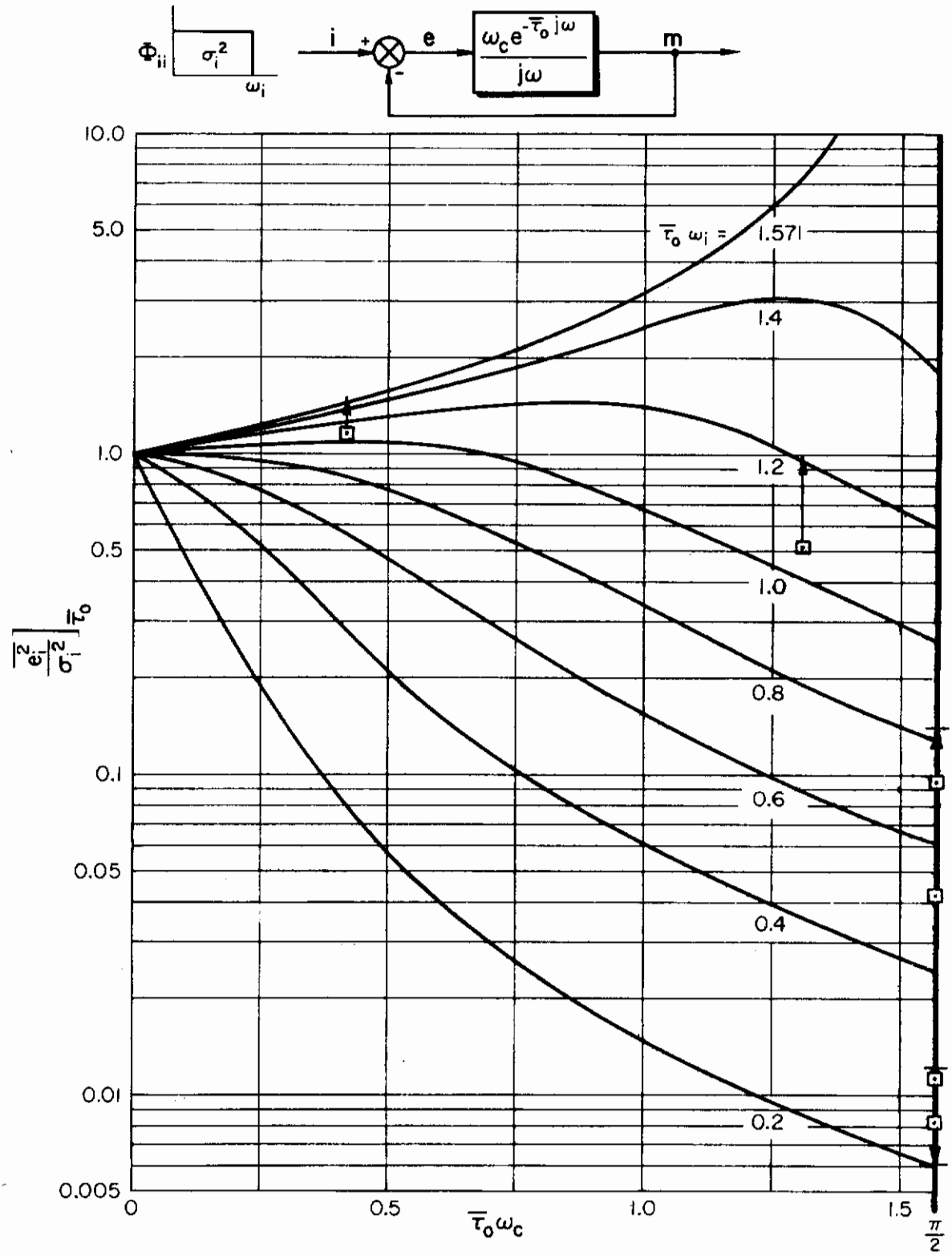

Figure 86. Elkind's Data Superimposed on Mean-Squared Error: Crossover Frequency Plot

from that presumed in the theoretical calculations. Still, the actual data bear a qualitative resemblance to the theoretical behavior, i.e., ω_c is essentially constant for low forcing function bandwidths, and the crossover regresses when ω_i approaches this ω_c value.

2. Performance Measures

In Section C of Chapter III estimates of the trend of normalized mean-squared error with ω_i were made presuming the crossover model of Eq 10. These estimates can now be compared with the actual results. The predictions were made in terms of the mean-squared-error component due to the forcing function alone, so only that portion will be considered here.

Included in the data for Elkind's $Y_c = 1$ experiments summarized in Table XIV are predicted mean-squared errors based on the one-third law (Eq 37). These predictions are compared with the actual data in Fig. 87. The correlation between the theory and experiment indicated in this figure is quite satisfactory.

Similar data based on the $Y_c = K_c/j\omega$ series reported here are presented in Fig. 88. Three types of correlations are shown. The first, similar to that already shown for Elkind's data, is with the one-third law. For the second correlation, denoted in Fig. 88 as $\overline{e_i^2}/\sigma_i^2\big]_{\text{continuous}}$, the idealized data of Fig. 11 are used for the predicted values. The "continuous" subscript here refers to the continuous nature of the forcing function's rectangular power spectral density used in the calculations leading to Fig. 11. In the actual experimental series the forcing function was composed of discrete sinusoids rather than continuous functions. This makes a small difference in the normalized mean-squared-error prediction, as is shown by the third correlation given in Fig. 88, i.e., the actual normalized mean-squared error compared with $\overline{e_i^2}/\sigma_i^2\big]_{\text{discrete}}$. Estimates made on all three bases compare favorably with the actual results achieved.

For the final comparison of estimated versus actual performance measures, the $Y_c = K_c/(j\omega)^2$ situations shall be examined. Figure 89 presents correlations for this case which parallel those given in Fig. 88 for the single-integrator controlled element. Here the correlation is by

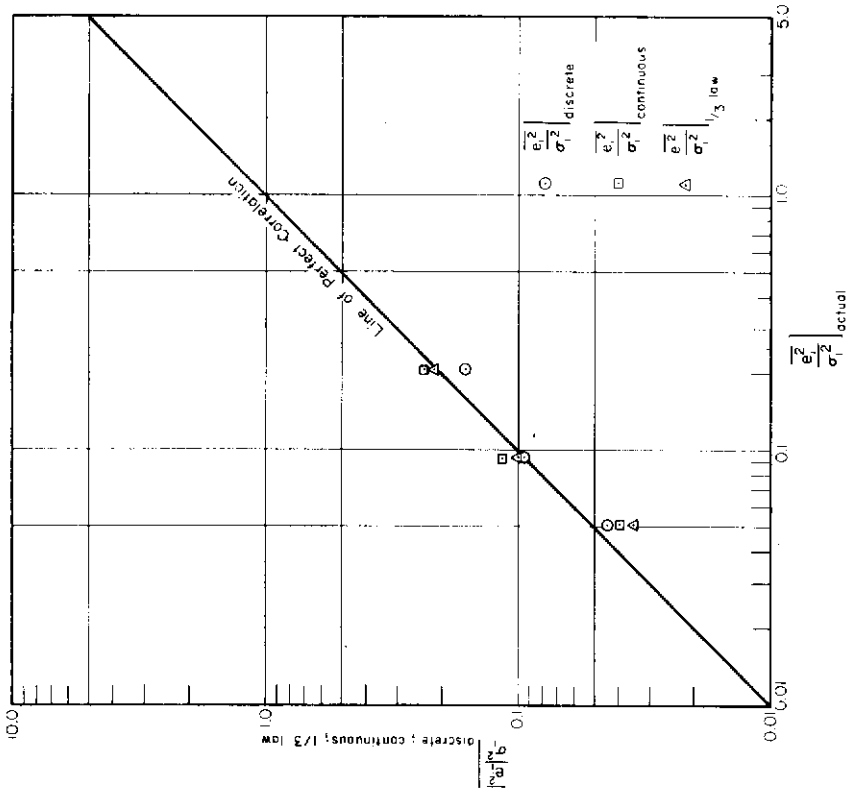

Figure 88. Comparison of Actual Mean-Squared Error with Estimated Values Based on Various Assumptions, $Y_c = K_c/j\omega$.

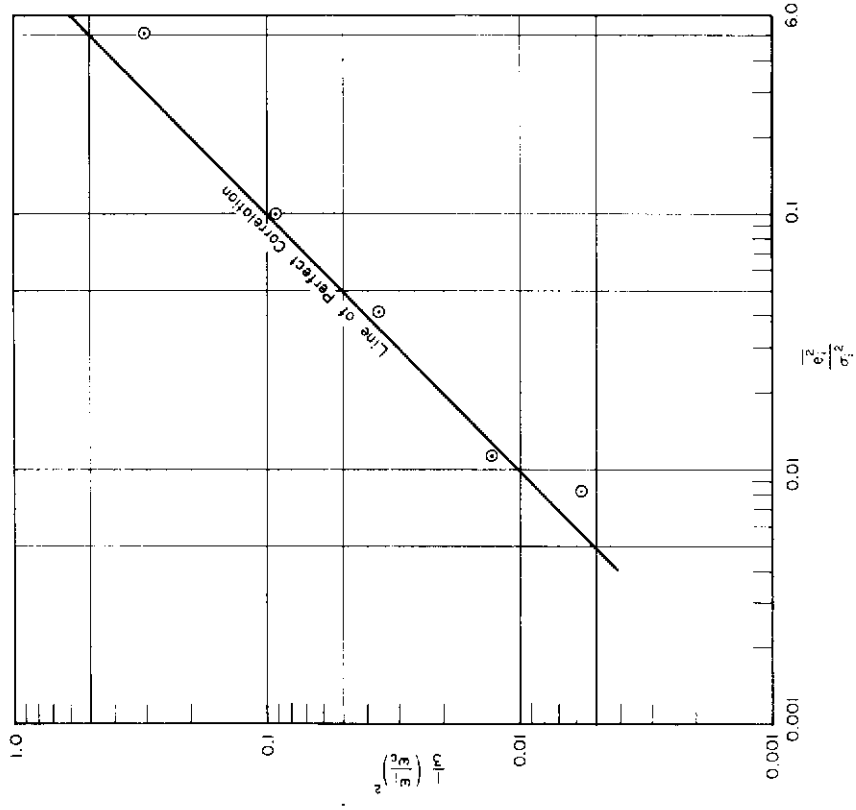

Figure 87. Comparison of Actual Mean-Squared Error with One-Third Law Estimates, $Y_c = K_c$

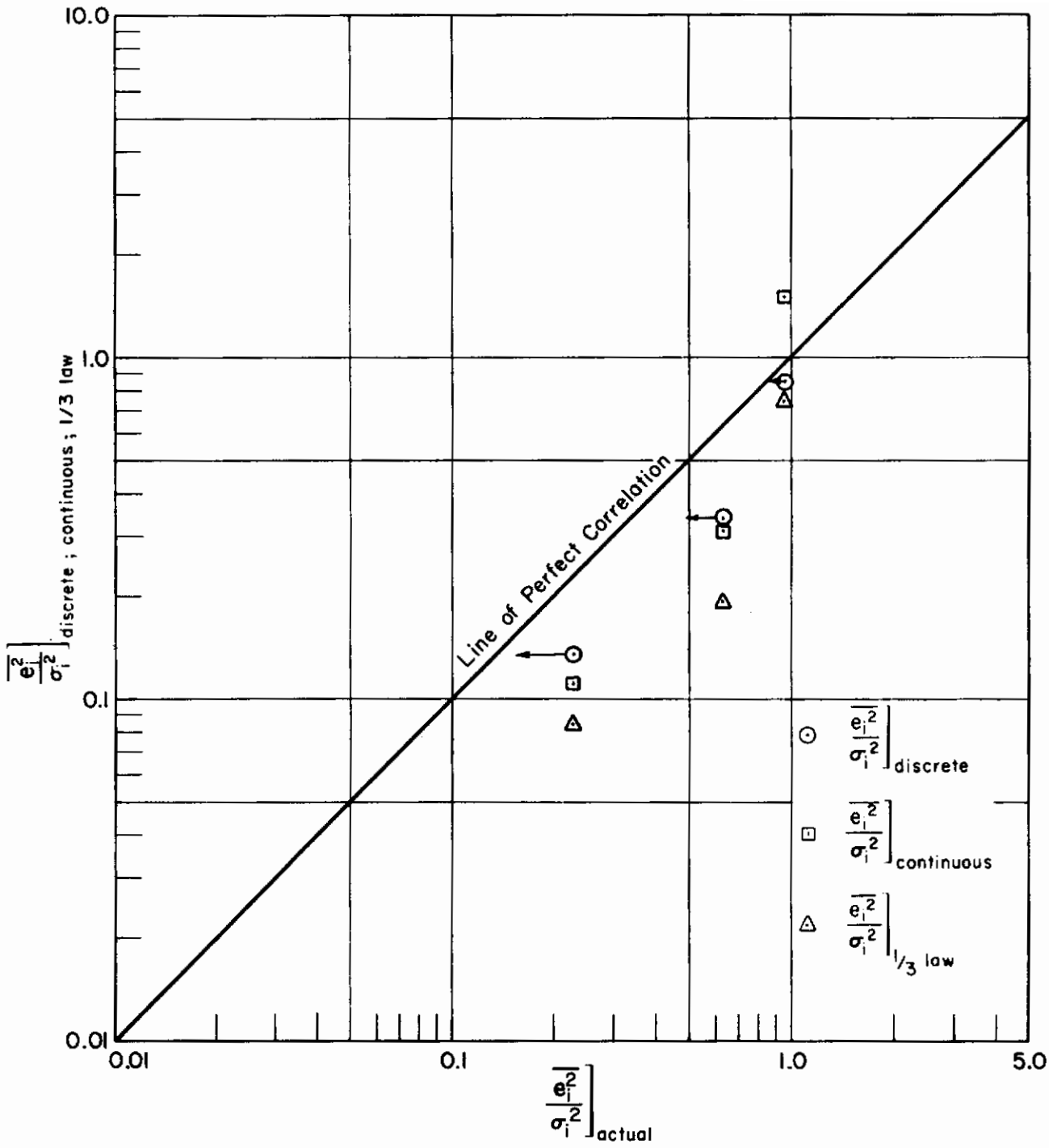

Figure 89. Comparison of Actual Mean-Squared Error with Estimated Values Based on Various Assumptions, $Y_c = K_c/(j\omega)^2$

no means as good as that for the two previous cases examined. The primary reason for this is the departure of the actual open-loop phase angle from that of the simple crossover model. To illustrate the magnitude of this effect, calculations of $\overline{e_i^2/\sigma_i^2}\Big]_{\text{discrete}}$ were made in which the phase for only the highest frequency point within the large amplitude portion of the forcing function was changed from its actual value to one compatible with the simple crossover model. This solitary modification would change the $\overline{e_i^2/\sigma_i^2}\Big]_{\text{discrete}}$ points to the locations indicated by the arrowheads in Fig. 89. These points would be considered very good correlation indeed, so they imply that even the one-third law could be used for the $Y_c = K_c/(j\omega)^2$ case with simply-applied special corrections.

The data correlations given above show how well the one-third law works even though the actual forcing function and $Y_p Y_c$ differ considerably from the idealized model on which the law is based. This implies that lower limit values of steady-state performance, i.e., normalized mean-squared error due to forcing function, can be estimated using extremely simple idealizations for conditions where the crossover model is a reasonable approximation. The main source of difficulty in such an estimation procedure is in the determination of the crossover frequency. For this task, the techniques illustrated in Chapter III can be used, with the τ_e values modified to be consonant with the new data of this report. The discussion above has bypassed any problems of ω_c estimation by considering trends only, and by using experimentally determined values of ω_c.

3. τ_e Trajectories and Phase Margin Adjustment

The connection of performance measures and mean-squared-error minimization with crossover frequency is but half the story of the crossover model adjustment. The other parameter involved is the adjustment of τ_e or its exact equivalent for the crossover model, the phase margin. An appreciation for the possible rationale behind this adjustment can be obtained by considering Fig. 90, which is a crossplot of Fig. 11. In this figure the abscissa is the effective time delay, τ_e, normalized by the mean crossover frequency, $\bar{\omega}_c$. The families shown are for constant forcing function bandwidth, ω_1, also normalized by $\bar{\omega}_c$. Thus, the variation being illustrated

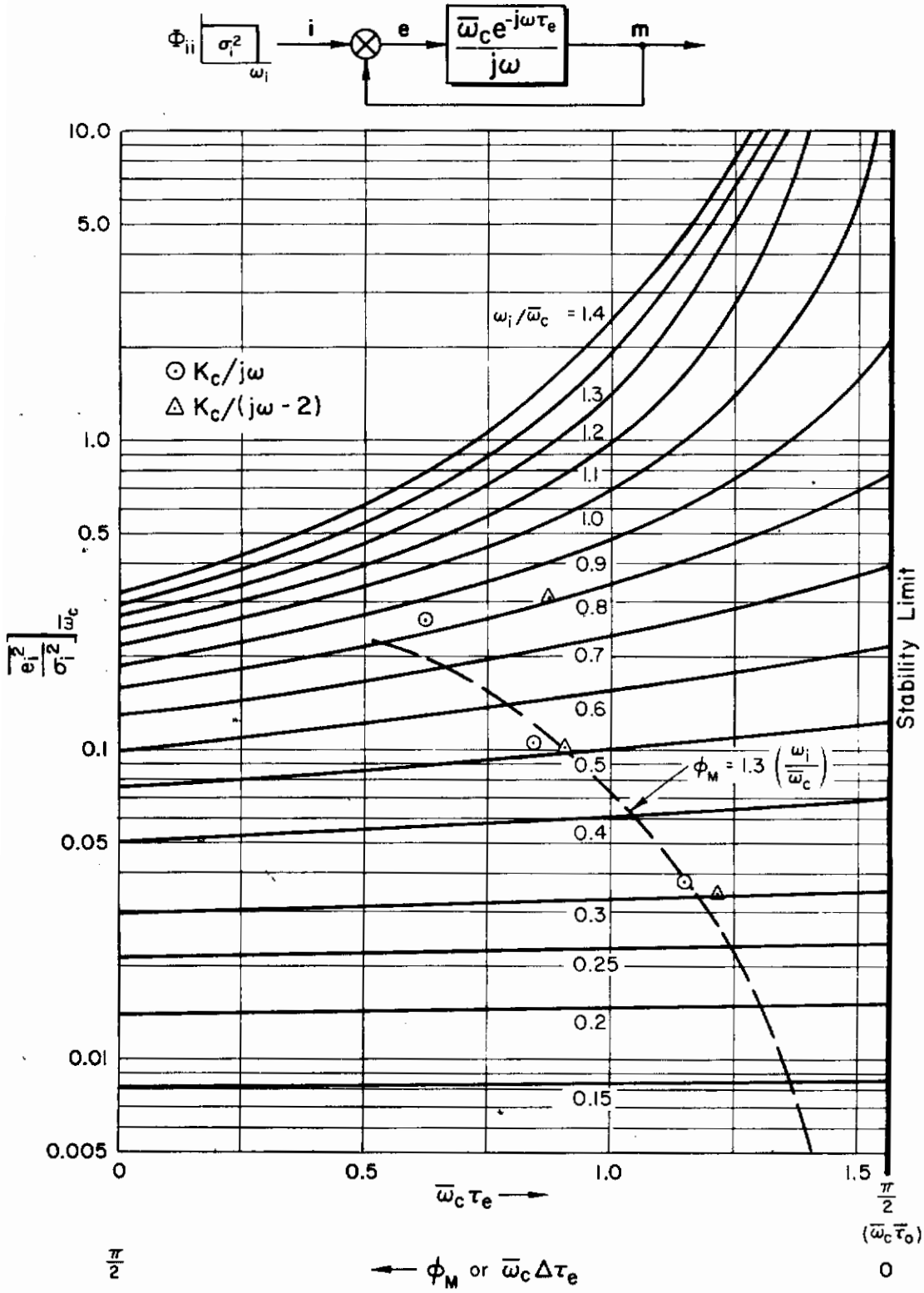

Figure 90. Pilot Optimization Adjustments of Time Delay for $Y_c = K_c/j\omega$ and $Y_c = K_c/(j\omega - 2)$

here is $\overline{e_i^2}/\sigma_i^2$ versus τ_e (normalized) with ω_i (normalized) as a parameter. On this basis Fig. 90 can be thought of as a section of a hypersurface for which Fig. 11 is another section. It will be observed that for small values of normalized mean-squared error the $\omega_i/\overline{\omega}_c$ family lines are nearly horizontal, indicating that normalized mean-squared error is nearly independent of τ_e. This region corresponds to $\omega_i/\overline{\omega}_c$ values for which the one-third law is an adequate approximation to the normalized mean-squared error. As forcing function bandwidth is increased, the $\omega_i/\overline{\omega}_c$ families tilt toward the left and the mean-squared error becomes a much stronger function of the time delay. The minimum mean-squared error, which always corresponds to $\tau_e = 0$, becomes a much sharper minimum as $\omega_i/\overline{\omega}_c$ increases.

For the human controller with random forcing functions, τ_e can never become zero, but the τ_e data do show distinct reductions as functions of ω_i. The nature of this adjustment in terms of the theoretical mean-squared error versus $\overline{\omega}_c\tau_e$ plot is illustrated by the data superimposed on the theoretical gridwork of Fig. 90. The data used for this purpose are for $Y_c = K_c/j\omega$ and $K_c/(j\omega - 2)$. These cases were selected because they correspond most closely to the simple crossover model. The actual data points are entered on the plot using the phase margin and $\omega_i/\overline{\omega}_c$. The nature of a linear phase margin variation with ω_i is, in these coordinates, indicated by the $\Phi_M = 1.3(\omega_i/\overline{\omega}_c)$ curve shown. A phase margin adjustment of this kind places sufficient emphasis on phase margin increase with ω_i to assure that the system with time delay has a mean-squared error reasonably close to the physically unrealizable absolute minimum for $\tau = 0$. The human operator approximates this adjustment for $\omega_i/\overline{\omega}_c \leq 0.5$, but tends to fall off somewhat for larger values, although phase margin still increases.

An alternative view to the same adjustments noted above can be developed using the sketch of Fig. 91. This figure shows the open-loop and the closed-loop error/input transfer functions for a feedback system based on the simple crossover model. The maximum amplitude ratio of the error/input transfer function is very nearly the departure at the break point, which coincides with the crossover frequency, ω_c. As noted in the plot, this is a function of the phase margin alone, and for small phase margins the peak magnitude

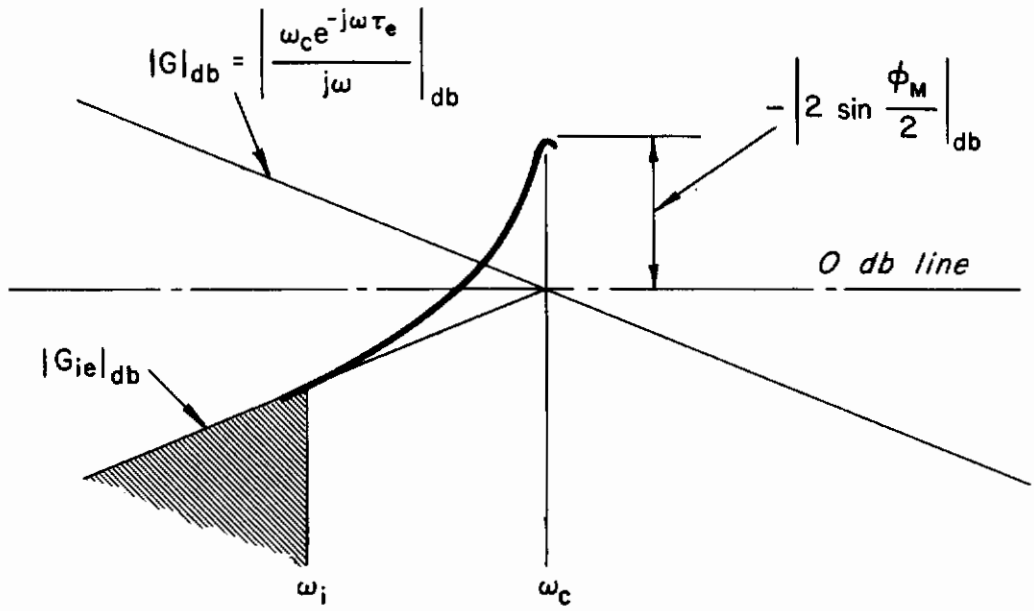

Figure 91. Sketch of Closed-Loop Error/Forcing Function Transfer Function for System Based on Simple Crossover Model

is approximately equal to the phase margin in db. Now consider a rectangular forcing function spectrum with bandwidth ω_i. The resulting system mean-squared error will be proportional to the area under the crosshatched portion of the G_{ie} amplitude ratio curve when this is transformed to linear units and squared. When ω_i is small compared with ω_c, the actual and asymptotic $|G_{ie}|_{db}$ curves are nearly coincident. Under these circumstances any peaking effect at ω_c due to small phase margins has very very little effect on the mean-squared error. This is the region wherein the one-third law applies. As ω_i gets closer to ω_c, the effect of the amplitude ratio departure from the asymptotes becomes more significant. Thus, the appropriate adjustment as ω_i/ω_c becomes larger is for the phase margin to be increased, thereby decreasing the peak and the positive departure of the actual curve from the asymptote, and hence the rms error.

CHAPTER VIII

GENERAL SUMMARY AND CONCLUSIONS

It will be recalled from Chapter II that the primary purposes of the experimental series were the validation of the existing analytical–verbal model and the extension of this model in accuracy and detail. The experimental data analyses and interpretations reported here have accomplished these purposes and, in addition, have revealed many other facets of human pilot dynamics. The total effort can be conveniently summarized under four major headings: (1) The Data in General; (2) Status of the Existing Analytical–Verbal Describing Function Model; (3) Extensions to the Analytical–Verbal Describing Function Model; (4) Status of Remnant Data. Conclusions of this program relating to these topics are summarized in outline and tabular form below. The ranges of known validity are restricted, of course, by the limits inherent in the data and analyses presented earlier.

A. THE DATA IN GENERAL

1. General Nature. The data accumulated have shown consistent, repeatable results which can be fitted into and/or extend the general context of past results and theories derived therefrom.

2. Tie-In. The data taken for $Y_c = 1$ are close enough to Elkind's to constitute our tie-in with past data and to enable his data to be considered as a subset of ours.

3. Quasi-Linearity. Conventional quasi-linear constant-coefficient describing function models can be evolved to characterize the data. The primary variables which fix the conditions for quasi-linearity in this study are controlled element and forcing function.

4. σ_i Independence. There is no evidence of nonlinear dependence of the describing function measurement on forcing function amplitude.

5. Selective Variability. Human controllers exhibit a remarkable capacity to suppress all sources of variability and to operate with high

repeatability and intersubject uniformity in frequency regions where it is necessary, e.g., at crossover or over wider frequency bands in the control of conditionally stable systems. In other frequency bands where variations in pilot dynamics do not materially affect closed-loop performance, there is much more intra- and interpilot variability, and pilots exhibit individual styles.

6. **Normality of Describing Function Data.** Both amplitude ratio and phase data appear to be distributed in a Gaussian manner.

7. **Time-Varying Behavior.** In general, pilot dynamic characteristics are reasonably stationary over the measurement run lengths as indicated by the typical ρ ranges over the main power portion of the forcing function bandwidth given below for $\omega_i = 2.5$.

Y_c	ρ Range
$K_c/j\omega$	0.97 – 0.99
$K_c/(j\omega - 2)$	0.99 –
$K_c/(j\omega)^2$	0.85 – 0.98

a. Selective variability. There is more time variation in frequency ranges wherein variability is relatively unimportant to closed-loop performance than over more crucial frequency ranges.

b. Task complexity, ω_i. Stationarity decreases as ω_i increases (e.g., a change in ρ from 0.98 to 0.93 as ω_i changes from 1.5 to 4.0 for $Y_c = K_c/j\omega$). This effect is not so pronounced when the controlled element is made more constraining, e.g., $Y_c = K_c/(j\omega - 2)$.

c. Task complexity, Y_c. As the controlled element dynamics become more difficult to control, the time variation of the pilot's dynamics increases substantially. In this sense, ρ could conceivably be used as a measure of task difficulty.

B. STATUS OF THE EXISTING (CIRCA 1960) ANALYTICAL-VERBAL DESCRIBING FUNCTION MODEL

1. In almost all cases the general describing function form

$$Y_p \doteq \frac{K_p e^{-j\omega\tau_e}(T_L j\omega + 1)}{(T_I j\omega + 1)(T_N j\omega + 1)} \tag{106}$$

can be suitably adjusted to provide a satisfactory description for crossover region characteristics.

2. There is striking evidence that for a variety of forcing functions and controlled elements the slope of $Y_p Y_c$ at crossover is -20 db/decade. Under these conditions the model of Eq 106, when taken in company with the controlled element dynamics, reduces to the especially simple form

$$Y_p Y_c \doteq \frac{\omega_c e^{-j\omega\tau_e}}{j\omega} \tag{107}$$

where

$$\begin{aligned} \omega_c &\doteq \omega_{c_o} + 0.18\,\omega_i \\ \tau_e &\doteq \tau_o - 0.08\,\omega_i \\ \tau_o &= \pi/2\omega_{c_o} \end{aligned} \tag{108}$$

Values of τ_o for conditions other than those tested can be estimated using the data given below and interpolation based on the slope of $|Y_c|_{db}$ over the likely crossover region.

Y_c	$\left[\frac{d\lvert Y_c\rvert_{db}}{d \ln \omega}\right]_{\omega=\omega_c}$ (db/decade)	τ_o (sec)
K_c	0	0.33
$K_c/j\omega$	−20	0.36
$K_c/(j\omega)^2$	−40	0.52

3. For $Y_c = K_c/j\omega$, $K_c/(j\omega)^2$, $K_c/(j\omega - 2)$, and $K_c/j\omega(j\omega - 1/T)$, which constitute critical experiments for the circa 1960 analytical-verbal model, the data obtained support a priori predictions based on this model as to Y_p form. Pre-experiment estimates of crossover frequencies were properly ordered and reasonably accurate, although generally somewhat higher than the experimentally determined values.

4. $\overline{e_i^2}$ performance measure trends based on the crossover model for $Y_c = K_c$ and $K_c/j\omega$ are supported by the experimental data.

5. The essentially constant crossover frequency for $\omega_i < 0.8\omega_c$ and the phenomenon of ω_c regression for $\omega_i > 0.8\omega_c$ can be explained using the crossover model of Eq 107 and the presumption that the pilot tends to minimize the mean-squared tracking error.

6. The adjustment rules for the existing analytical-verbal model are generally adequate, although Adjustment Rules 4b (**Parameter Adjustment** – system phase margin) and 5b and 5c ($\omega_c - \omega_i$ **Independence** and ω_c **Regression**) require minor modifications in the nature of refinements (see below). In terms of the adjustment rules the major impact of the experimental program has been to validate with concrete data those "rules" which had previously been based primarily on extrapolations and rationalization. In this sense all of the rules given in Chapter II, with the modifications noted below, are now solidly based on experiment.

C. EXTENSIONS TO THE ANALYTICAL-VERBAL DESCRIBING FUNCTION MODEL

1. Adjustment Rules

a. Adjustment Rule 4b should now be stated as:

"System phase margin, ϕ_M, is directly proportional to ω_i, the forcing function bandwidth, for values of ω_i less than about 2.0 rad/sec. The strong effect of forcing function bandwidth on the phase margin is associated with the variation of T_N with the same task variable."

b. A new adjustment rule, 4c, should be added:

"Equalization time constants T_L or T_I, when form selection requires $1/T_L$ or $1/T_I \ll \omega_c$, will be adjusted such that low frequency response will be essentially insensitive to slight changes in T_L or T_I ($\omega_i \ll \omega_c$).

c. Adjustment Rules 5b and 5c should now be restated as:

5b. **$\omega_c - \omega_i$ Independence:** System crossover frequency depends only slightly on forcing function bandwidth for $\omega_i < 0.8\ \omega_{c_o}$ (ω_{c_o} is that value of ω_c adopted for $\omega_i \ll \omega_c$).

5c. **ω_c Regression:** When ω_i nears or becomes greater than $0.8\,\omega_{c_o}$, the crossover frequency regresses to values much lower than ω_{c_o}.

2. Low Frequency Phase Lags. A lagging phase angle at low frequencies appears in all the data. The general low frequency describing function form of Eq 106 is not suitable at the lower frequencies. To adequately characterize the data it must be modified to

$$Y_p \doteq \frac{K_p e^{-j(\omega\tau + \alpha/\omega)}(T_L j\omega + 1)}{(T_I j\omega + 1)(T_N j\omega + 1)} \qquad (109)$$

The parameter α added here is a "high frequency" approximation to low frequency leads and lags occurring below the measurement bandwidth. In higher order approximations to the low frequency phase lag, a lag–lead largely outside the bandwidth of the measurements is usually adequate. α increases both with ω_i and with controlled element order, except for the constraining controlled element, $Y_c = K_c/(j\omega - 2)$. Although not described in this report, the nature of α and its variations can be explained by properties of the neuromuscular system.

3. Input-Adaptive Neuromuscular Characteristics. The first-order lag, T_N, approximation to the high frequency neuromuscular system dynamics is input adaptive. Its decrease is ordinarily the basis for the variation of τ_e with ω_i indicated by Eq 108 [the data for $Y_c = K_c/(j\omega - 2)$ are an exception to this statement].

4. Higher Order Neuromuscular Lags. The previous strong evidence for a third-order neuromuscular lag has now been added to by describing function measurements. These lags replace essentially all of the residual previously assigned to a τ_e or to a τ and T_N in more approximate models. The net effective lag, $T_{N_1} + 2\zeta_N/\omega_N$, is essentially equal to the first-order approximation, T_N, and is variable with ω_i in a similar fashion.

5. **Residual τ.** The third-order neuromuscular system plus a pure time delay of about 0.09 sec are adequate descriptors of the high frequency describing function data. The pure time delay is of the same order of magnitude as neural delays in the visual modality, i.e., latencies in the visual process plus conduction delays, etc.

6. **General Describing Function Form.** The most general describing function model form, replacing Eq 1, is given by

(110)

$$Y_p = K_p K_T \left[\frac{a_T}{\sigma_T}\right] e^{-j\omega\tau} \left(\frac{T_L j\omega + 1}{T_I j\omega + 1}\right) \left\{ \left(\frac{T_K j\omega + 1}{T_K' j\omega + 1}\right) \left[\frac{1}{\left(T_{N_1} j\omega + 1\right)\left[\left(\frac{j\omega}{\omega_N}\right)^2 + \frac{2\zeta_N}{\omega_N} j\omega + 1\right]} \right] \right\}$$

The major elements of complication introduced in this precision model are those in the braces. These all arise from the neuromuscular system, which has both very high and very low frequency effects. For almost all practical cases Eq 110 can be simplified to Eq 106 or even Eq 107. When the controlled element is such as to make the system conditionally stable, Eq 109 should be used for safety's sake, since the low frequency phase lag can be important for this kind of system.

D. STATUS OF REMNANT DATA

1. Values of the remnant computed at the forcing function frequencies generally fit a smooth curve through values measured between and above forcing function frequencies. This indicates that the power spectral density of the remnant is generally continuous and that line spectra indicating periodicities are absent.

2. At very low frequencies the remnant data for a wide variety of controlled elements coalesce best when all the remnant is reflected to the pilot's input.

3. Remnant increases with controlled element gain, with forcing function bandwidth, and with control order. For extreme controlled element forms such as $Y_c = K_c/j\omega(j\omega - 1.5)$ the remnant increases

greatly, primarily because of the pilot's time-varying behavior induced by his attempts to retain control over this drastically unstable controlled element.

4. Some evidence for pulsing behavior in control of second-order controlled elements is present from output amplitude distributions. These indicate a tendency for the pilot's output to be pulse areas roughly proportional to the stimulus amplitude.

5. Careful examination of the output power spectral density indicated no evidence for periodic sampling or significant nonlinear behavior.

6. Partly by process of elimination and partly by direct evidence, it appears that the major source of remnant is nonstationary pilot behavior, i.e., time-varying components in the effective time delay and gain. For the second-order controlled elements the pulsing nature of the pilot's output contributes an additional remnant source.

REFERENCES

1. Ashkenas, I. L., and D. T. McRuer, The Determination of Lateral Handling Quality Requirements from Airframe/Human-Pilot System Studies, WADC-TR-59-135, June 1959.

2. Ashkenas, I. L., and D. T. McRuer, "A Theory of Handling Qualities Derived from Pilot-Vehicle System Considerations," Aerospace Eng., Vol. 21, No. 2, Feb. 1962, pp. 60, 61, 83-102.

3. Ashkenas, I. L., and T. S. Durand, "Simulator and Analytical Studies of Fundamental Longitudinal Control Problems in Carrier Approach," AIAA Simulation for Aerospace Flight Conference, A Volume of Technical Papers Presented Aug. 26-28, 1963, Columbus, Ohio, AIAA, New York, 1963, pp. 16-34.

4. Ashkenas, I. L., H. R. Jex, and D. T. McRuer, Pilot-Induced Oscillations: Their Cause and Analysis, Northrop Corporation, Norair Division, Rept. NOR 64-143 (Systems Technology, Inc., TR-239-2), 20 June 1964.

5. Bekey, G. A., An Investigation of Sampled Data Models of the Human Operator in a Control System, ASD-TDR-62-36, Feb. 1962.

6. Bekey, G. A., "The Human Operator as a Sampled-Data System," IRE Trans., Vol. HFE-3, No. 2, Sept. 1962, pp. 43-51.

7. Bode, H. W., Network Analysis and Feedback Amplifier Design, D. Van Nostrand Co., New York, 1945.

8. Cromwell, C. H., and I. L. Ashkenas, A Systems Analysis of Longitudinal Piloted Control in Carrier Approach, Systems Technology, Inc., TR-124-1, June 1962.

9. Donner Scientific Division Manual 9496, Instruction Manual, Model 3605 Power Spectral Analyzer, Oct. 1961.

10. Donner Scientific Division Rept. D-061-23, Engineering Test Report, Model 3605 Power Spectral Analyzer, Nov. 1961.

11. Durand, T. S., and H. R. Jex, Handling Qualities in Single-Loop Roll Tracking Tasks: Theory and Simulator Experiments, ASD-TDR-62-507, Nov. 1962.

12. Durand, T. S., and G. L. Teper, An Analysis of Terminal Flight Path Control in Carrier Landings, Systems Technology, Inc., TR-137-1, Aug. 1964.

13. Elkind, J. I., Characteristics of Simple Manual Control Systems, MIT, Lincoln Laboratory, TR-111, 6 Apr. 1956.

14. Elkind, J. I., "A Survey of the Development of Models for the Human Controller," Guidance and Control—II, ed. R. C. Langford and C. J. Mundo (Progress in Astronautics and Aeronautics, Vol. 13) Academic Press, New York, June 1964, pp. 623–643.

15. Elkind, J. I., and D. L. Darley, "The Normality of Signals and Describing Function Measurements of Simple Manual Control Systems," IEEE Trans., Vol. HFE-4, No. 1, Sept. 1963, pp. 52–55.

16. Ferrick, K. A., and R. A. Peters, Operation and Maintenance Manual, Watthour Meter Analyzer, Systems Technology, Inc., TM-115-1, Mar. 1962.

17. Frost, G. G., An Application of a Dynamic Pilot-Model to System Design, ASD-TN-61-57, Apr. 1961.

18. Goodyear Aircraft Corporation Rept. GER-4750, Human Dynamic Study, Apr. 8, 1952.

19. Goodyear Aircraft Corporation Rept. GER-6726, Investigation of Control "Feel" Effects on the Dynamics of a Piloted Aircraft System, Apr. 25, 1955.

20. Goss, C. M. (ed.), Gray's Anatomy of the Human Body (26th ed.), Lea and Febiger, Philadelphia, 1954.

21. Graham, D., and D. McRuer, Analysis of Nonlinear Control Systems, John Wiley and Sons, New York, 1961.

22. Greenwood, I. A., Jr., J. V. Holdam, Jr., and D. MacRae, Jr., Electronic Instruments, McGraw-Hill Book Co., New York, 1948.

23. Hald, A., Statistical Theory with Engineering Applications, John Wiley and Sons, New York, 1952.

24. Hall, I. A. M., Effects of Controlled Element on the Human Pilot, WADC-TR-57-509, Aug. 1958.

25. Hall, I. A. M., "Study of the Human Pilot as a Servo-Element," J. Royal Aeron. Society, Vol. 67, No. 630, June 1963, pp. 351–360.

26. James, H. M., N. B. Nichols, and R. S. Phillips, Theory of Servomechanisms, McGraw-Hill Book Co., New York, 1947.

27. Jex, H. R., and C. H. Cromwell, Theoretical and Experimental Investigation of Some New Longitudinal Handling Quality Parameters, ASD-TR-61-26, Mar. 1961.

28. Krendel, E. S., and D. T. McRuer, "A Servomechanisms Approach to Skill Development," J. Franklin Inst., Vol. 269, No. 1, Jan. 1960, pp. 24–42.

29. Krendel, E. S., and G. H. Barnes, Interim Report on Human Frequency Response Studies, WADC-TR-54-370, June 1954.

30. Krendel, E. S., and W. C. Reisener, Preliminary Human Dynamics Measurements, Franklin Institute Laboratories STI-FIL Rept. 4, Sept. 1962.

31. Leonard, T. E., "Optimizing Linear Dynamics for Human-Operated Systems by Minimizing the Mean Square Tracking Error," IRE WESCON Convention Record, Vol. 4, Part 4, 1960, pp. 57–62.

32. Licklider, J. C. R., "Quasi-Linear Operator Models in the Study of Manual Tracking," Developments in Mathematical Psychology, ed. R. Duncan Luce, The Free Press of Glencoe, Ill., 1960, pp. 169–279.

33. Loller, T. E., and J. Matous, "Observed Pilot–Vehicle Loop-Closure Characteristics for Hovering Aircraft Control," IEEE Trans., Vol. HFE-4, No. 1, Sept. 1963, pp. 60–63.

34. McRuer, D. T., and E. S. Krendel, Dynamic Response of Human Operators, WADC-TR-56-524, Oct. 1957.

35. McRuer, D. T., and E. S. Krendel, "The Human Operator as a Servo System Element," J. Franklin Inst., Vol. 267, No. 5, May 1959, pp. 381–403; No. 6, June 1959, pp. 511–536.

36. McRuer, D. T., I. L. Ashkenas, and C. L. Guerre, A Systems Analysis View of Longitudinal Flying Qualities, WADD-TR-60-43, Jan. 1960.

37. McRuer, D. T., and E. S. Krendel, "The Man–Machine System Concept," Proc. IRE, Vol. 50, No. 5, May 1962, pp. 1117–1123.

38. McRuer, D. T., and D. Graham, "Pilot–Vehicle Control System Analysis," Guidance and Control — II, ed. R. C. Langford and C. J. Mundo (Progress in Astronautics and Aeronautics, Vol. 13), Academic Press, New York, June 1964, pp.

39. McRuer, D. T., Unified Analysis of Linear Feedback Systems, ASD-TR-61-118, Mar. 1961.

40. McRuer, D. T., Some Statistical Properties of Time Functions Composed of Sinusoids, Systems Technology, Inc., TM-80, 9 Mar. 1961.

41. Magdaleno, R. E., WHM Analyzer Finite Run Length Errors, Systems Technology, Inc., TM-84, 8 Mar. 1961.

42. Magdaleno, R. E., Sampling Behavior for the Human Operator, Systems Technology, Inc., TM-115-4, 27 July 1962.

43. Muckler, F. A., and R. W. Obermayer, The Use of Man in Booster Guidance and Control, AIAA Paper 63-312, Aug. 1963. (Also published as NASA CR-81, July 1964.)

44. Peters, R. A., Test Report, Watthour Meter Analyzer, Systems Technology, Inc., TM-115-2, Mar. 1962.

45. Peters, R. A., Test Report, D-C Analog Combined Power and Cross Spectrum Analyzer, Systems Technology, Inc., TM-106, 8 Dec. 1961.

46. Reisener, W. C., Equipment Tests and Calibration, Franklin Institute Laboratories STI-FIL Rept. 3, June 1962.

47. Russell, Lindsay, Characteristics of the Human as a Linear Servo-Element, Master's thesis, MIT, Dept. of Electrical Eng., May 18, 1951.

48. Sadoff, M., Effects of High Sustained Acceleration on Pilots' Performance and Dynamic Response, NASA TN D-2067, July 1964.

49. Sadoff, M., The Effects of Longitudinal Control-System Dynamics on Pilot Opinion and Response Characteristics as Determined from Flight Tests and from Ground Simulator Studies, NASA Memo 10-1-58A, Oct. 1958.

50. Seckel, E., I. A. M. Hall, D. T. McRuer, and D. H. Weir, Human Pilot Dynamic Response in Flight and Simulator, WADC-TR-57-520, Oct. 1957.

51. Seltzer, L. J., and D. T. McRuer, Survey of Analog Cross Spectral Analyzers, WADC-TR-59-241, Dec. 1959.

52. Senders, J. W., Survey of Human Dynamics Data and a Sample Application, WADC-TR-59-712, Nov. 1959.

53. Sheridan, T. B., "The Human Operator in Control Instrumentation," Progress in Control Engineering, Vol. I, ed. R. H. Macmillan, T. J. Higgins, and P. Naslin, Academic Press, New York, 1962, pp. 141–187.

54. Slack, M., "The Probability Distribution of Sinusoidal Oscillations Combined in Random Noise," Jour. IEE (London), Vol. 93, Pt. III, 1945.

55. Smith, R. H., "On the Limits of Manual Control," IEEE Trans., Vol. HFE-4, No. 1, Sept. 1963, pp. 56–59.

56. Stapleford, R. L., D. E. Johnston, G. L. Teper, and D. H. Weir, A Method for Evaluating the Lateral-Directional Handling Qualities of a Supersonic Transport in the Landing Approach and Assessing Competing Augmentation Systems, Systems Technology, Inc., TR-131-1, Dec. 1963.

57. Systems Technology, Inc., D-C Analog Combined Power and Cross-Spectrum Analyzer, Design Specification for, Specification 115-1, 27 Feb. 1961.

58. Taylor, L. W., Jr., Analysis of a Pilot-Airplane Lateral Instability Experienced with the X-15 Airplane, NASA TN D-1059, Nov. 1961.

59. Tustin, A., "The Nature of the Operator's Response in Manual Control and Its Implications for Controller Design," J. IEEE, Vol. 94, Part IIA, No. 2, 1947.

60. Ward, J. R., The Dynamics of a Human Operator in a Control System—A Study Based on the Hypothesis of Intermittency, Ph.D. dissertation, University of Sydney, Australia, May 1958.

Unclassified
Security Classification

DOCUMENT CONTROL DATA - R&D

(Security classification of title, body of abstract and indexing annotation must be entered when the overall report is classified)

1. ORIGINATING ACTIVITY (Corporate author) Systems Technology, Inc., Hawthorne, Calif. The Franklin Institute, Philadelphia, Pa.	2a. REPORT SECURITY CLASSIFICATION Unclassified 2b. GROUP N/A

3. REPORT TITLE

HUMAN PILOT DYNAMICS IN COMPENSATORY SYSTEMS

4. DESCRIPTIVE NOTES (Type of report and inclusive dates)

Final Report

5. AUTHOR(S) (Last name, first name, initial)

McRuer, D. T.
Graham, Dunstan
Krendel, Ezra
Reisener, William, Jr.

6. REPORT DATE	7a. TOTAL NO. OF PAGES	7b. NO. OF REFS
July 1965	194	60

8a. CONTRACT OR GRANT NO.	9a. ORIGINATOR'S REPORT NUMBER(S)
AF33(616)-7501 b. PROJECT NO. 8219 c. Task 821905 d.	AFFDL TR 65-15 9b. OTHER REPORT NO(S) (Any other numbers that may be assigned this report) None

10. AVAILABILITY/LIMITATION NOTICES

Qualified requestors may obtain copies of this report from DDC.

11. SUPPLEMENTARY NOTES	12. SPONSORING MILITARY ACTIVITY
None	AFFDL (FDCC) Wright-Patterson AFB, Ohio

13. ABSTRACT

The description of human pilot dynamic characteristics in mathematical terms compatible with flight control engineering practice is an essential prerequisite to the analytical treatment of manual vehicular control systems. The enormously adaptive nature of the human pilot makes such a description exceedingly difficult to obtain, although a quasi-linear model with parameters which vary with the system task variables had been successfully applied to many flight situations. The primary purposes of the experimental series reported are the validation of the existing quasi-linear pilot model, and the extension of this model in accuracy and detail.

DD FORM 1 JAN 64 1473

Unclassified
Security Classification

Unclassified
Security Classification

14. KEY WORDS	LINK A		LINK B		LINK C	
	ROLE	WT	ROLE	WT	ROLE	WT
Human Response						
Manual Control Systems						
Human Engineering						
Aircraft Handling Qualities						
Flight Control Systems						

INSTRUCTIONS

1. ORIGINATING ACTIVITY: Enter the name and address of the contractor, subcontractor, grantee, Department of Defense activity or other organization *(corporate author)* issuing the report.

2a. REPORT SECURITY CLASSIFICATION: Enter the overall security classification of the report. Indicate whether "Restricted Data" is included. Marking is to be in accordance with appropriate security regulations.

2b. GROUP: Automatic downgrading is specified in DoD Directive 5200.10 and Armed Forces Industrial Manual. Enter the group number. Also, when applicable, show that optional markings have been used for Group 3 and Group 4 as authorized.

3. REPORT TITLE: Enter the complete report title in all capital letters. Titles in all cases should be unclassified. If a meaningful title cannot be selected without classification, show title classification in all capitals in parenthesis immediately following the title.

4. DESCRIPTIVE NOTES: If appropriate, enter the type of report, e.g., interim, progress, summary, annual, or final. Give the inclusive dates when a specific reporting period is covered.

5. AUTHOR(S): Enter the name(s) of author(s) as shown on or in the report. Enter last name, first name, middle initial. If military, show rank and branch of service. The name of the principal author is an absolute minimum requirement.

6. REPORT DATE: Enter the date of the report as day, month, year; or month, year. If more than one date appears on the report, use date of publication.

7a. TOTAL NUMBER OF PAGES: The total page count should follow normal pagination procedures, i.e., enter the number of pages containing information.

7b. NUMBER OF REFERENCES: Enter the total number of references cited in the report.

8a. CONTRACT OR GRANT NUMBER: If appropriate, enter the applicable number of the contract or grant under which the report was written.

8b, 8c, & 8d. PROJECT NUMBER: Enter the appropriate military department identification, such as project number, subproject number, system numbers, task number, etc.

9a. ORIGINATOR'S REPORT NUMBER(S): Enter the official report number by which the document will be identified and controlled by the originating activity. This number must be unique to this report.

9b. OTHER REPORT NUMBER(S): If the report has been assigned any other report numbers *(either by the originator or by the sponsor)*, also enter this number(s).

10. AVAILABILITY/LIMITATION NOTICES: Enter any limitations on further dissemination of the report, other than those imposed by security classification, using standard statements such as:

(1) "Qualified requesters may obtain copies of this report from DDC."

(2) "Foreign announcement and dissemination of this report by DDC is not authorized."

(3) "U. S. Government agencies may obtain copies of this report directly from DDC. Other qualified DDC users shall request through _____."

(4) "U. S. military agencies may obtain copies of this report directly from DDC. Other qualified users shall request through _____."

(5) "All distribution of this report is controlled. Qualified DDC users shall request through _____."

If the report has been furnished to the Office of Technical Services, Department of Commerce, for sale to the public, indicate this fact and enter the price, if known.

11. SUPPLEMENTARY NOTES: Use for additional explanatory notes.

12. SPONSORING MILITARY ACTIVITY: Enter the name of the departmental project office or laboratory sponsoring *(paying for)* the research and development. Include address.

13. ABSTRACT: Enter an abstract giving a brief and factual summary of the document indicative of the report, even though it may also appear elsewhere in the body of the technical report. If additional space is required, a continuation sheet shall be attached.

It is highly desirable that the abstract of classified reports be unclassified. Each paragraph of the abstract shall end with an indication of the military security classification of the information in the paragraph, represented as *(TS), (S), (C), or (U)*.

There is no limitation on the length of the abstract. However, the suggested length is from 150 to 225 words.

14. KEY WORDS: Key words are technically meaningful terms or short phrases that characterize a report and may be used as index entries for cataloging the report. Key words must be selected so that no security classification is required. Identifiers, such as equipment model designation, trade name, military project code name, geographic location, may be used as key words but will be followed by an indication of technical context. The assignment of links, rules, and weights is optional.

Unclassified
Security Classification